Abstract

The topics discussed within this thesis are varied, but focus primarily on the unique reactivities and structural diversity which can be obtained when alkali metal reagents are combined with divalent magnesium and zinc mixtures.

In chapter two, a family of homometallic anthracenolate complexes were synthesised by reaction of either mixed-metal or monometallic bases with tricyclic ketone anthrone. When an alkali metal is present in the initial base (in combination with magnesium or zinc or alone), dimers of formulation [(donor)·M(C$_{14}$H$_9$O)]$_2$ (donor = TMEDA when M= Li or Na and donor = PMDETA when M=K) were isolated. When [(TMEDA)·Bu$_2$Mg] or [(TMEDA)·Et$_2$Zn] were reacted with anthrone, monomers of formulation [(TMEDA)·Mg(C$_{14}$H$_9$O)(^{n}Bu)] and [(TMEDA)·Zn(C$_{14}$H$_9$O)(Et)] respectively were obtained, and characterized fully in both solid state and solution. In the zinc complex, a TMEDA resonance exhibiting dynamic behaviour within the ^{1}H NMR spectrum was investigated by variable temperature techniques.

The zincates [(TMEDA)Na·(μ-TMP)(μ-^{t}Bu)Zn(^{t}Bu)] **2a** and [(TMEDA)Na·(μ-HMDS)(μ-^{t}Bu)Zn(^{t}Bu)] were found to facilitate alkylation of both fluorenone and 2-benzoylpyridine in the unusual 6 position with respect to the oxygen atom, allowing crystallization of these 1, 6- adducts (when **2a** was utilized). Use of [(TMEDA)Na·(μ-HMDS)(μ-^{t}Bu)Zn(^{t}Bu)] gave structural evidence of both 1, 2- and 1, 6- addition products in the reaction with 2-benzoylpyridine. After aqueous workup of these mixtures, ring *tert*-butylated products and the corresponding tertiary alcohol were produced, and separated by chromatography column. When the zincate [(TMEDA)·Na(μ-TMP)(μ-Et)Zn(Et)] was reacted with fluorenone, a hexameric dimer (Na-9-Et-9*H*-Fluoren-9-olate)$_6$ was structurally characterized. The zincate **2a** was also found to act as a single electron transfer reagent towards chalcone, resulting in a novel homocoupling product.

The chemistry of potassium magnesiates in arene deprotonation and inverse crown formation was studied, in terms of both the active basic species and in new reactivities. The species [KMg(TMP)$_2$Bu]$_x$ was crystallized as a tetrameric, hexameric and polymeric aggregate, and found by a variety of NMR spectroscopic techniques to be the active base in formation of hexameric inverse crown complexes. It was then used to form a new inverse crown via deprotonation of naphthalene at the 2-position, trapping 6

monometallated units within a 24 membered $[KNMgN]_6$ ring. A new ferrocenophane $[\{Fe\text{-}(C_5H_4)\}_2\{K_2Mg_3(TMP)_2(THF)_2(toluene)_2\}]$ was generated by reacting $[KMg(TMP)_2Bu]_x$ with ferrocene at reflux temperature. Two new polymeric species of consititution $[KMg(TMP)(CH_2SiMe_3)_2]_\infty$ and $[(Tol.)KMg(TMP)(CH_2SiMe_3)_2]_\infty$ were also crystallized.

Acknowledgements

I have left this part until last, as I believe it to be both the easiest and most difficult section to write within a document which details my accumulated efforts of the past three and a half years. Easy because I have met and worked with so many wonderful people throughout this time, and difficult because most of them I will see little of, if ever, in the future. I would first like to begin with my boss, Charlie O'Hara, kind and helpful almost to a fault, without whom I doubt I could ever have managed to complete this PhD. He allowed me to have and implement my own ideas whilst also working on his, and even allowed me to write this thesis in my own way, two things I am most grateful for, and which not many supervisors would have suffered. I honestly don't believe I could have asked for one better.

Next to thank would be the other two bosses Eva and Rab, who together make up our unique three-in-one lab collective, both skilled and different in their own right, both contributing in no small way to my progress throughout the years. In fact, had it not been for choosing Eva as my final year project supervisor, I should never have ended up in R-526 in the first place, something I will remain ever thankful for. Next in line are the Research Fellows and Post-Docs, lab leaders and occasional ball-busters, who've helped keep the whole operation going. Jan and Pablo, some of my oldest lab-mates, I would thank for solving my crystal structures and countless Friday pints, both whom I loved working with and whose leaving the group I felt very keenly. I'd also like to thank Stuart for the same reasons (but he's still here), but I have no idea how he still has such a fine head of grey hair left after all his stress in the past year and a bit. Some man.

Next I'd like to thank my oldest PhD mates, all just starting (or finishing) when I was a plucky young final year. Vicky, the lab pitbull, was sweet and severe in equal measure, and helped me hone my skills. Ben Conway, the other Ben, always good for a laugh but definitely couldn't take a joke! Liam, who could sometimes seem a bit serious, was always there to help when you needed it, a good Celtic man, and the most stylish chemist I ever met. Gemma, fellow O'Hara, who I wrongly believed was quiet, proved me wrong once and for all in LA when she screamed for eight straight hours in the theme park. She was the lab cleaning fairy, meticulous and always good for a chat. I could write a separate appendix about Ross, but all I can say is he was one of the most helpful, genuine, wholly inappropriate and unique individuals I have ever encountered, and missed by everyone who knew him. Perhaps the biggest loss for me in the lab was

Publications and conference presentations

Publications

1.) "*Structural elucidation of homometallic anthracenolates synthsised via deprotonative metallation of anthrone.*" W. Clegg, B. J. Fleming, P. Garcia-Alvarez, L. M. Hogg, A. R. Kennedy, J. Klett, A. J. Martinez-Martinez, R. E. Mulvey, L. Russo and C. T. O'Hara, *Dalton Trans.*, **2013**, *42*, 2512.

2.) "*Synthesis and structural elucidation of a rare example of a tris(amido) potassium magnesiate.*" B. J. Fleming, P. Garcia-Alvarez, E. Keating, A. R. Kennedy, C. T. O'Hara, *Inorg. Chim. Acta*, **2012**, *384*, 154.

3.) "*Single electron transfer (SET) activity of the dialkyl-amido zincate [(TMEDA)·Na(μ-TMP)(μ-^{t}Bu)Zn(^{t}Bu)] towards TEMPO and chalcone.*" D. R. Armstrong, L. Balloch, J. J. Crawford, B. J. Fleming, L. M. Hogg, A. R. Kennedy, J. Klett, R. E. Mulvey, C. T. O'Hara, S. A. Orr and S. D. Robertson, *Chem. Commun.*, **2012**, *48*, 1541.

4.) "*Remote functionalization via sodium alkylamidozincate intermediates: access to unusual fluorenone and pyridyl ketone reactivity patterns.*" J. J. Crawford, B. J. Fleming, A. R. Kennedy, J. Klett, C. T. O'Hara and S. A. Orr, *Chem. Commun.*, **2011**, *47*, 3772.

Conference Presentations

1.) *Ring, ring, ring: Reactions of organo-alkali metal and alkali metal ates with tricyclic ketones.* Ben Fleming and Charles T. O'Hara. Poster presentation at 44th Universities of Scotland Inorganic Conference (USIC), Durham University, 8th July 2010.

2.) *Ring, ring, ring: Reactions of organo-alkali metal and alkali metal ates with tricyclic ketones.* Ben Fleming, Alan R. Kennedy, Charles T. O'Hara and Samantha Orr. Poster presentation at Pacifichem, Hawaii, 16th December 2010.

3.) *Alkali-metal zincates: Beyond deprotonation*. Ben Fleming and Charles T. O'Hara. Oral presentation at West Brewery, 29th June 2011.

4.) *Alkali-metal zincates: Beyond deprotonation*. Ben Fleming and Charles T. O'Hara. Oral presentation at the 45th Universities of Scotland Inorganic Conference (USIC), Glasgow University, 21st July 2011.

5.) *Exploring inverse crown precursors, leading to the rational synthesis of new inverse crown complexes*. Ben Fleming and Charles T. O'Hara. Poster presentation at 46th Universities of Scotland Inorganic Conference (USIC), University of St. Andrews, 29th August 2012.

Numbered compounds

2a	**[(TMEDA)Na(μ-TMP)(μ-^{t}Bu)Zn(^{t}Bu)]**
2b	**[(TMEDA)·Na(OC$_{14}$H$_9$)]$_2$**
2c	**[(TMEDA)·Li(OC$_{14}$H$_9$)]$_2$**
2d	**[(PMDETA)·K(OC$_{14}$H$_9$)]$_2$**
2e	**[(TMEDA)·Mg(^{n}Bu)(C$_{14}$H$_9$O)]**
2f	**[(TMEDA)·Zn(Et)(C$_{14}$H$_9$O)]**
3a	**[(TMEDA)·Na{μ-OC(Ph)(4-^{t}Bu-C$_6$H$_5$)}(μ-TMP)Zn(^{t}Bu)]**
3b	**[(TMEDA)·Na{μ-OC(Ph)(4-^{t}Bu-C$_6$H$_4$)}(μ-TMP)Zn(^{t}Bu)]**
3c	**[(TMEDA)·Na{μ-OC(Ph)(4-^{t}Bu-C$_6$H$_4$)}(μ-HMDS)Zn(^{t}Bu)]**
3d	**[(TMEDA)·Na{μ-OC(Ph)(4-^{t}Bu-C$_5$NH$_4$)}(μ-TMP)Zn(^{t}Bu)]**
3e	**[(TMEDA)·Na{μ-OC(Ph)(4-^{t}Bu-C$_5$NH$_4$)}(μ-TMP)Zn(^{t}Bu)] and**
	[(TMEDA)·Na{μ-OC(^{t}Bu)(Ph)(C$_5$NH$_5$)}(μ-TMP)Zn(^{t}Bu)]
3f	**[(Na-9-Et-9H-Fluoren-9-olate)$_6$]**
4a	**[(TMEDA).Na(μ-^{n}Bu)(μ-TMP)Mg(TMP)]**
4b	**[{(THF)$_6$·Na}$^+${(THF)·Mg(o-carborane)$_3$}$^-$]**
4c	**[{(^{t}Bu)$_3$Zn$_3$(m-carborane)$_3$}$^{3-}${(THF)$_6$·Li$_3$}$^+$]**
4d	**[(TMEDA)·Na(μ-TMP)(μ-TEMPO)Zn(^{t}Bu)]**
4e	**[(TMEDA)·Na(μ-TEMPO)$_2$Zn(^{t}Bu)]**
4f	**[(TMEDA)·{Na(μ-TMP)Zn(^{t}Bu)}$_2$(μ-OCPhCH=CHPhCHPhCH=CPh-μ-O)]**
4g	**[(TMEDA).Na(μ-DTBN)$_2$Zn(^{t}Bu)]**
4h	**[(PMDETA)·K(μ-NPh$_2$)Mg(THF)(NPh$_2$)$_2$]**
4i	**[(TMEDA)Na·(μ-TMP)(μ-Ph)Zn(Ph)]**
5a	**[Na(μ-HMDS)$_2$Mg(^{n}Bu)]$_\infty$**
5b	**[NaMg(μ-TMP)$_2$(^{n}Bu)]$_\infty$**
5c	**[Na$_4$Mg$_2$(TMP)$_6$(C$_6$H$_4$)]**
5d	**[KMg(μ-HMDS)$_2$(^{n}Bu)]$_\infty$**

5e $[KMg(TMP)_2(C_6H_5)]_6$

5f $[KMg(TMP)_2(^nBu)]_\infty$

5g $[KMg(TMP)_2(^nBu)]_4$

5h $[KMg(TMP)_2(^nBu)]_6$

5i $[\{Fe\text{-}(C_5H_4)\}_2\{K_2Mg_3(TMP)_2(THF)_2(Toluene)_2\}]$

5j $[KMg(TMP)_2(C_{10}H_7)]_6$

5k $[KMg(CH_2SiMe_3)_2(TMP)]_\infty$

5l $[(Toluene) \cdot KMg(CH_2SiMe_3)_2(TMP)]_\infty$

List of Abbreviations

TMP	2, 2, 6, 6 – tetramethylpiperidide
TMEDA	N, N, N', N' – tetramethylethylenediamine
THF	Tetrahydrofuran
r.t.	Room temperature
R	Alkyl
M	Metal
Me	Methyl
Mes	Mesityl
PMDETA	N, N, N', N'', N''- pentamethyldiethylenetriamine
^{n}Bu	n-butyl
^{t}Bu	t-butyl
eq.	Equivalents
HMDS	1, 1, 1, 3, 3, 3 – hexamethyldisilazide
^{i}Pr	isopropyl
Ph	Phenyl
Et_2O	Diethyl ether
Et	Ethyl
Py	Pyridine
COSY	Correlation spectroscopy
DOSY	Diffusion-ordered spectroscopy
DFT	Density functional theory
DA	Diisopropylamide
D_2O	Deuterated water
C_6D_{12}	Deuterated cyclohexane
C_6D_6	Deuterated benzene
d^8-THF	Deuterated THF
d^8-Tol.	Deuterated toluene

Me. Cy.	Methylcyclohexane
AMMM	Alkali-Metal-Mediated Metallation
AMMZn	Alkali-Metal-Mediated Zincation
AMMMg	Alkali-Metal-Mediated Magnesiation
LICKOR	Lochmann-Schlosser Superbase
ppm	Parts per million
TM	Transition Metal
NMR	Nuclear Magnetic Resonance
HSQC	Heteronuclear Single Quantum Coherence
ICE	Inverse Crown Ether
2-Bzp.	2-Benzoylpyridine
N-Boc	*n*-butyl oxycarbamate
Me$_6$-TREN	[tris(N, N – dimethyl-2-aminoethyl)amine]
SET	Single electron transfer
DTBN	Di-tert-butyl nitroxide
TEMPO	(2, 2, 6, 6- Tetramethylpiperidenyl) oxyl
S. M.	Starting material

Table of contents

1. Introduction: History of s-block & zinc organometallic chemistry

1.1 Organolithium Reagents

Of all synthetic strategies devised for tailoring and functionalising molecules, metallation is among the most useful and universally practised, whereby a comparatively inert carbon - hydrogen bond is converted to a more reactive, and consequently more useful, carbon − metal bond. In achieving this end, organolithium reagents have shown themselves as invaluable,[1] owing to the highly reactive nature of the polar lithium carbon bond. Their solubility in both hydrocarbon and ethereal solvents adds to the attractiveness for their employment in syntheses from bench to industrial scale. These reagents are also less reactive than their analogous sodium and potassium counterparts, and although known to attack both solvents and themselves,[2] these unwanted effects can often be controlled by use of sub-ambient temperatures.

First prepared by Schlenk and Holtz in 1917,[3] these early syntheses involved reaction of metallic lithium with dialkyl or diaryl mercury compounds, a process which grew quickly out of favour due to mercury's inherent toxicity. Great progress in this area emerged from research conducted by Zeigler and Colonius,[4] whereby lithium metal was instead reacted with organic halides to provide the corresponding alkyllithium compound.

After more than a century of pioneering research, the formation of organolithium compounds is most commonly achieved by the following four methods:

Deprotonation:- involves lithium-hydrogen exchange, a process strongly favoured at sites adjacent to heteroatoms for intramolecular coordination, or sites α- to an electron withdrawing group. Lithiation of hydrocarbons is a sluggish process in molecules bereft of such features **[Figure 1(a)]**.

Lithium-halogen exchange:- can be described as an equilibrium process, preferentially forming the less basic organolithium reagent with release of the corresponding organohalide [**Figure 1(b)**].

1

Reductive Lithiation:- involves the reaction of two equivalents of lithium metal with a single equivalent of an alkyl halide. This process is favoured by formation of the LiX salt, due to its high lattice energy. This process, whilst attractive, is complicated by the potential of the newly formed organolithium reagent to attack unreacted starting material, forming undesired coupling products [**Figure 1(c)**].

Carbolithiation:- involves insertion of an alkyllithium reagent into an unsaturated C=C double bond. This process is understandably of limited synthetic potential, and is fraught with potential difficulties, such as further reaction of organolithium product with unreacted starting material [**Figure 1(d)**].
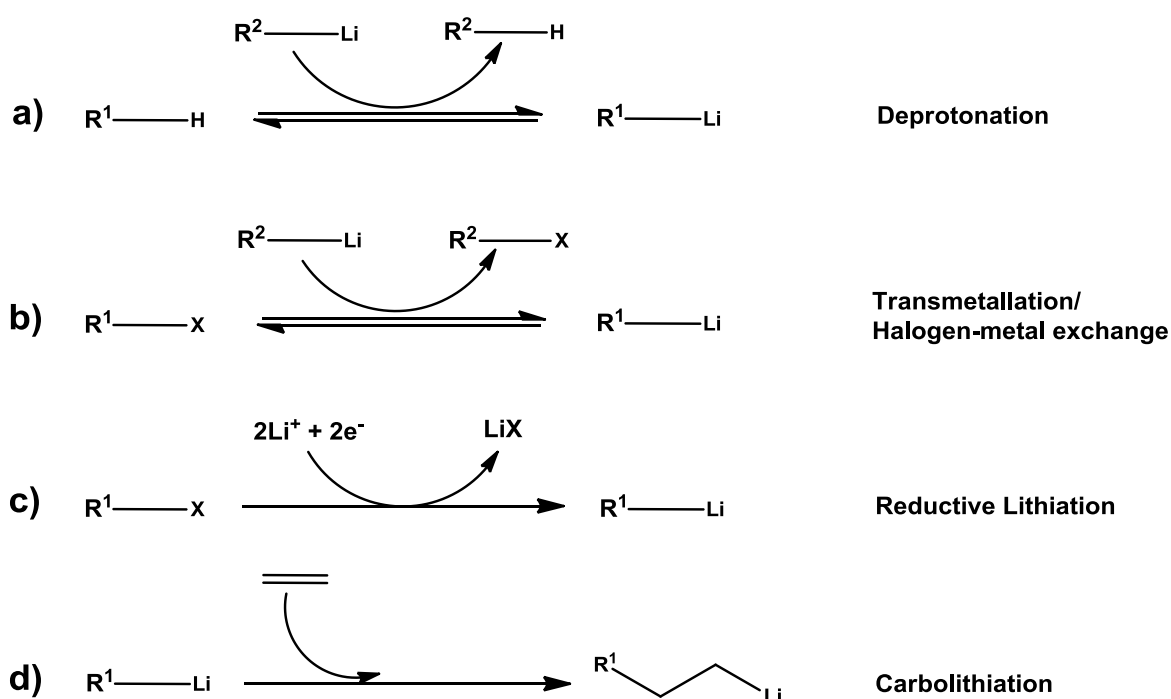
Fig. 1.1

When considering the behaviour of these species in solution, one cannot succumb to the beguiling simplicity of a diagram. In truth these organolithiums never exist as monomeric species. Due to the highly electron deficient nature of the lithium centre, greater stability than that afforded by a single carbanionic ligand is required; thus these organolithiums inevitably aggregate to maximise electrostatic interactions.[5] In hydrocarbon solvents, EtLi and ^{n}BuLi adopt a hexameric arrangement, with the more basic ^{t}BuLi forming a tetramer preferentially due to the increased steric bulk of the

carbanion. These aggregation states can however be influenced by solvent effects. In solvents where a coordinating heteroatom is present e.g. Et$_2$O or THF, the extra electron density previously provided by incorporation of more carbanionic ligands is now imparted by coordination of these atoms to the electron deficient lithium. This allows the organolithium reagent to deaggregate to a state more entropically favoured. Whilst in THF for instance,[6] EtLi, ^{n}BuLi and MeLi retain the aggregation states previously adopted in hydrocarbon solvent, ^{t}BuLi has its aggregation reduced to that of a dimer. This aggregation can be lowered further by utilising the coordinating power of an amine or more strongly coordinating ethereal solvent, with simultaneous enhancement of reactivity.[7] The amine most commonly employed to this end is TMEDA (*N*, *N*, *N'*, *N'*-tetramethylethylenediamine).

These coordinating solvents can even be utilised to achieve enantioselectivity in synthesis. Use for instance of the chiral amide (-)-sparteine can effect deprotonation with subsequent quenching yielding the desired product. In this example, the Boc-protected benzylamine derivative is lithiated α to the N by *n*-BuLi-(-)-sparteine, furnishes the desired product in levels of good enantiomeric excess (**Scheme 1.1**). [8]
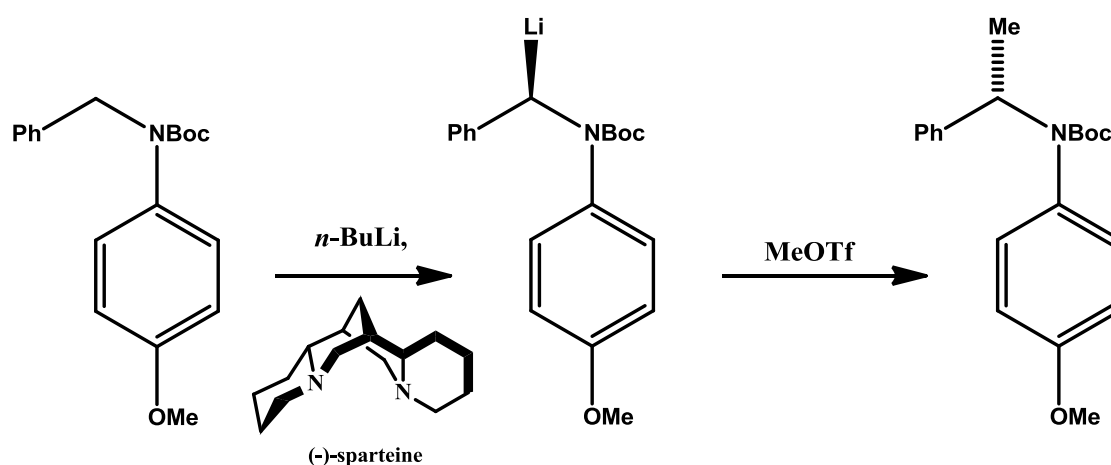
Scheme 1: Enantioselective deprotonation of benzylamine derivative.

This example serves to emphasise the range of applications enjoyed by organolithium reagents, a success paid homage to by their continued worldwide interest. High reactivity and sometimes unpredictable selectivity have however curbed their potential to an extent, paving the way for a new era of metallating agents, both highly reactive and selective.

1.2 **Organosodium Reagents**

Following seminal work in the preparation of ethyl derivatives of tin, lead and mercury by Buckton in 1859, [9] he postulated "whether sodium is capable of displacing ethyl from mercuric ethyl."[9b, c] He noted in his reaction of elemental sodium with diethylmercury, the formation of a grey material exhibiting "spontaneous combustibility in a marked degree." He correctly hypothesised the initial formation of ethyl sodium and subsequent thermal decomposition into a NaMg amalgam and the respective gases ethane and ethene. These experiments, although not pursued by Buckton, represented the first preparation of an organosodium compound. Almost half a century would expire before these highly reactive species were utilised in synthetic transformations. Schorigin found that EtNa prepared *in situ* by the same combination of Et_2Hg and Na (except this time carried out in Et_2O solution), could be then reacted successfully with several electrophiles and quenched to give the respective products of addition.[10]
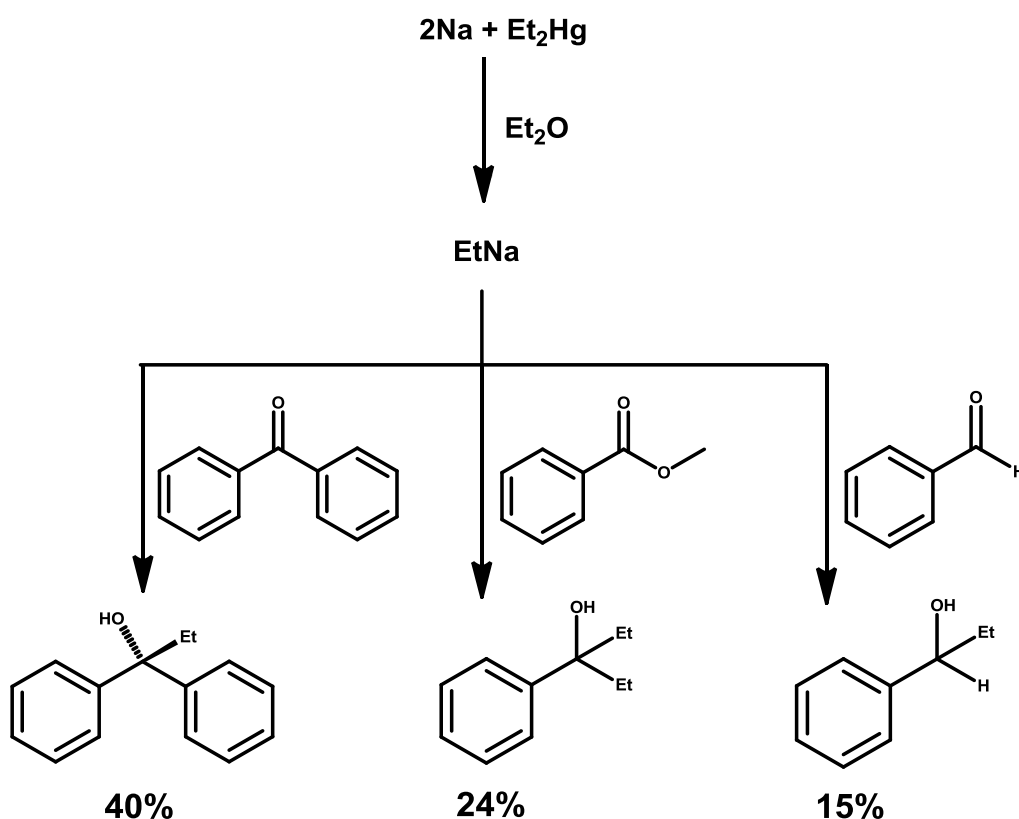
Fig. 1.2: Formation of ethylsodium and subsequent addition reactions

He deduced the low yields of some of these reactions was a consequence of competitive side reaction of the organosodium reagent with the ethereal solvent, an effect now

known to be extremely common in reactions involving such highly reactive species. A curious observation, pertinent to all proceeding research on the subject of deprotonative metallation chemistry, came about when Schorigin exchanged Et_2O for benzene in an attempt to curb these unwanted side reactions. He discovered upon reaction of ethyl sodium with the carbon dioxide in benzene medium, the presence of benzoic acid after aqueous work up.[11] He proposed rightly that benzene had been metallated by the ethyl sodium reagent. It was not until later, however, that the pioneering work of Gilman,[12] Morton[13] and many others,[14] was to prove the generality and effectiveness of sodium alkyls in deprotonating weak organic acids.

As a consequence of their limited solubility in hydrocarbon solvents, structural data of unsolvated sodium alkyl complexes is very rare,[15] although several representative examples of alkylsodium reagents stabilised by donors THF and TMEDA do exist.[16] One such rare example of a donor free alkyl sodium species is that of "$NaCH_2SiMe_3$", characterised by Hevia *et al.*[17] (**Figure 1.3**)
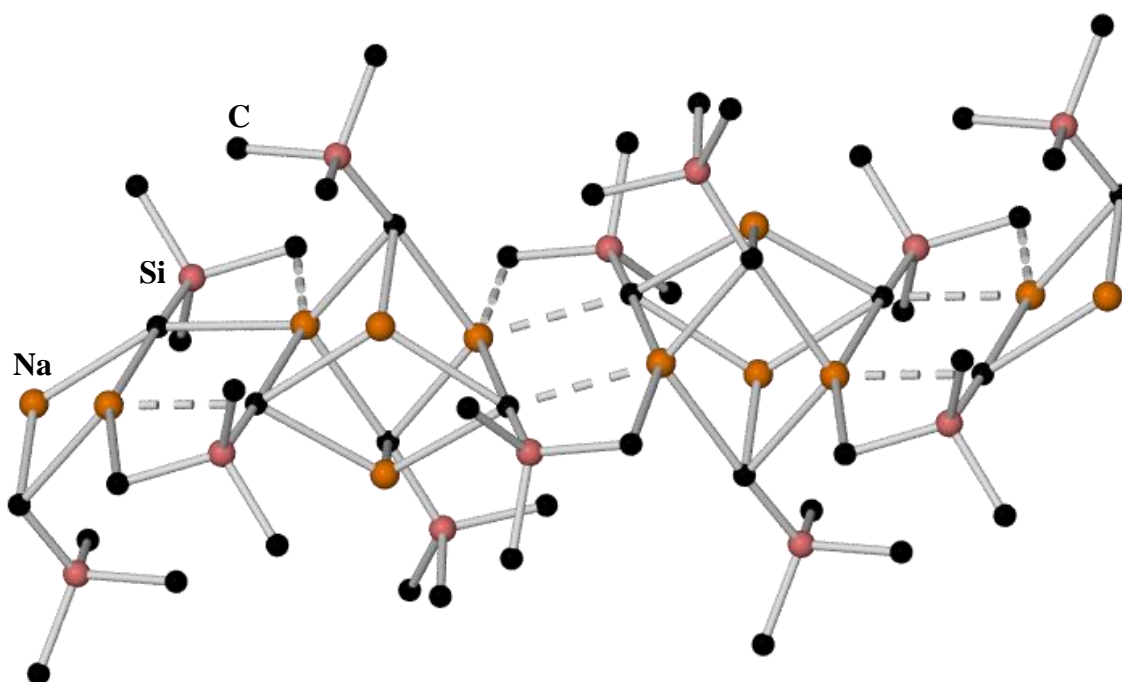
Fig. 1.3: Molecular structure of the alkylsodium polymer $[NaCH_2SiMe_3]_\infty$

This structure can be considered as a polymer of tetramers, each repeating unit a distorted Na_4 tetrahedron, with a CH_2SiMe_3 anion capping each face. It is noteworthy that this structure compares nicely in form to those of several classical organolithium reagents in the solid state.[18]

Another class of sodium reagents which have enjoyed much attention both fundamentally and from a more practical standpoint are the sodium amides. These structures, also essentially ionic in nature, often require strong donors such as TMEDA and PMDETA to break down and solubilise them, a fact likewise reflected in the abundance of examples characterised structurally when compared to their unsolvated precursors. Three such examples do exist however, of unsolvated Na amide complexes, most notably NaTMP[19] (a cyclic trimer) and two polymorphs of NaHMDS (a linear chain polymer[20] and a cyclic trimer[21]). (**Figure 1.4**).
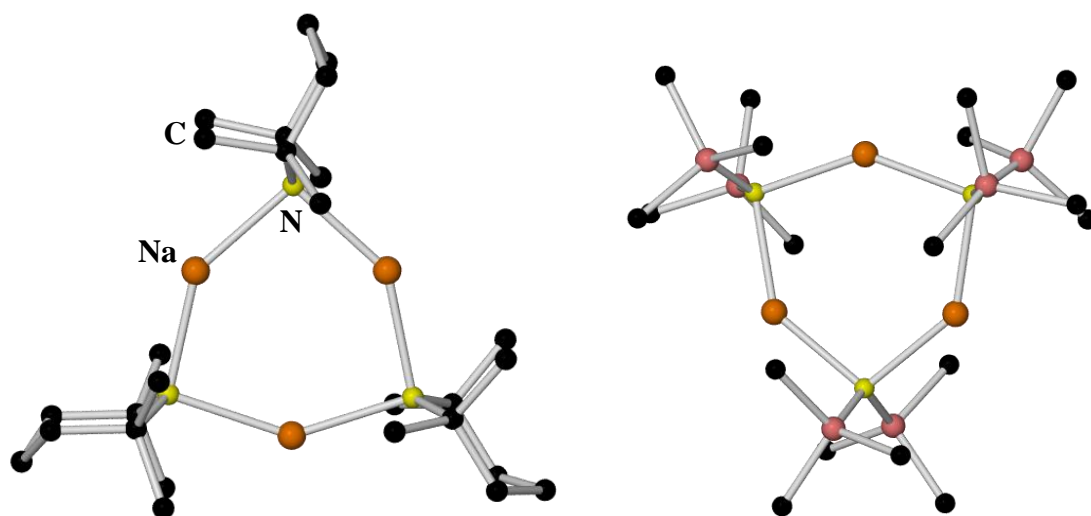
Fig. 1.4: Left: NaTMP trimer; Right: NaHMDS trimer

Each of these species when solvated by TMEDA, to form discrete dimeric species exhibiting planar Na-N-Na-N cores.[22]

1.3 Organopotassium Reagents

As a consequence of an inherent reactivity some orders of magnitude greater than both their lithium and sodium counterparts and their more ionic, salt-like nature,[23] relatively little structural information is known about organopotassium reagents, with only three examples of truly unsolvated potassium alkyl species (*i.e.* without even arene coordination) crystallographically characterised (**Figure 1.5**). [24] It is perhaps unsurprising that all known examples of both sodium and potassium alkyls in the solid state are polymeric in nature, considering their pronounced insolubility in hydrocarbon media.
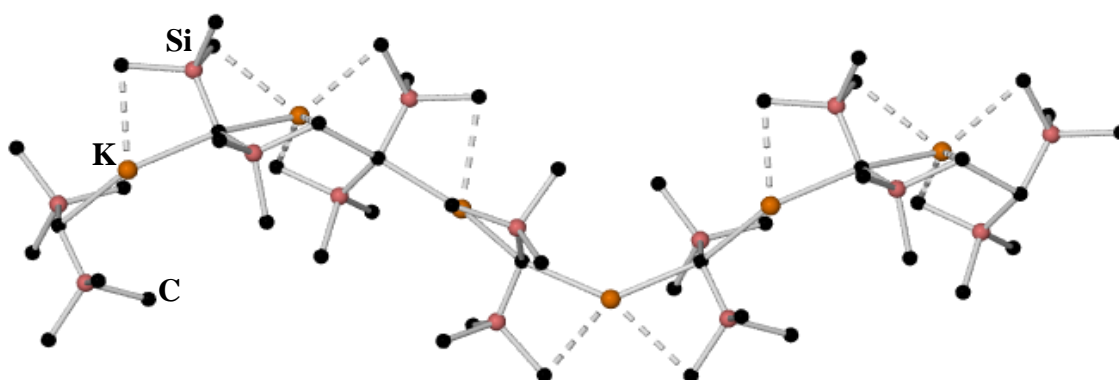
Fig. 1.5: A rare example of an unsolvated potassium alkyl complex $[K(CHSiMe_3)_2]_\infty$

Any structural information pertaining to the potassium analogue of the previously described $[NaCH_2SiMe_3]_\infty$ species[17] remains, unfortunately, elusive. This particular potassium reagent has been utilised to great effect by the Mulvey group at Strathclyde as a source of potassium in routinely forming mixed-metal compounds,[25] owing both to its incredibly reactive nature, but greatly enhanced stability in the solid state, compared to butylpotassium used by this group previously. This extra stability under inert atmosphere allows its storage within a glove box for a period of months with no appreciable degradation, a stability it owes to an absence of β hydrogen atoms on the ligand. This species when combined with equimolar equivalents of the tridentate Lewis base PMDETA in hexane solution, was found crystallographically to exist as a polymer (despite the incorporation of a Lewis base), though this time each potassium atom is bound η^3 to the N atoms of the PMDETA ligand.[26] It was also discovered on turning to the bidentate TMEDA, deaggregation of the presumed polymer occurred, forming an open tetrameric species, with only three of the K atoms capped by a TMEDA ligand (**Figure 1.6**).
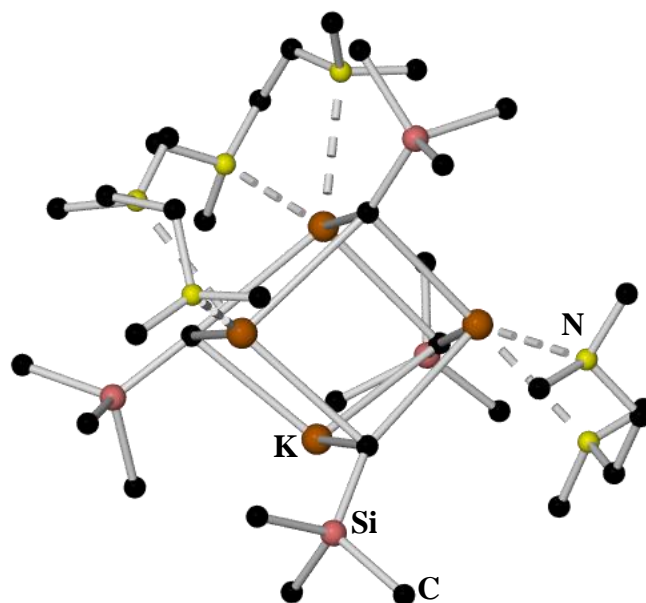
Fig. 1.6: Molecular structure of the TMEDA solvated alkylpotassium [(TMEDA)$_3$(KCH$_2$SiMe$_3$)$_4$].

This paucity of structural information surrounding organopotassium reagents is paralleled by a similar lack of their employment in deprotonative metallation reactions. In a point neatly surmised by Schlosser he notes the folly in supposing the marked increase in reactivity of alkylpotassium reagents, compared to their organolithium counterparts, should give in turn both the greatest selectivity and yield of metallation product.[27] It is known, for instance, that in the absence of a donor, alkylpotassiums are able to deprotonate benzene, whereas alkyllithiums are not.[28] *n*-butylpotassium has also been proven as an effective agent of Brønsted basicity towards both cyclic and acyclic ethers at subambient temperatures.[29] So effective in fact is *n*-butylpotassium in performing this latter metallation that it decomposes immediately in THF solution, even at -100°C. It is precisely the duplicitous nature of these organopotassium reagents that has prohibited their more extensive use: greatly enhanced reactivity, but too great for any real selectivity or control. This fact prompted a thorough investigation into whether their edge could be tempered and made more controllable, more selective, by combination with other metals in bimetallic superbasic mixtures.

In the case of monometallic amido-potassium species crystallographically characterised, only KHMDS has been achieved in the absence of a donor molecule.[30] Perhaps counterintuitively, this species exists as a dimer, whereas its related lithium and sodium

counterparts form cyclic trimers, despite the smaller coordination spheres of the respective metals. This could be perhaps explained in part by the propensity of potassium on many occasions[31] to form strong agostic contacts to the methyl groups of the TMS moiety. The closest K-C contacts to the methyl groups in $(KHMDS)_2$ are 3.34 and 3.47 Å, indicative of significant interactions. These bond distances, though more distended, compare favourably with those of the related mixed polymer $[\{Me_3Si)_2NLi\}\{Me_3Si)_2NK\}]$,[31a] with smallest K-C agostic interactions of 3.14(13) and 3.34(13) Å.

1.4 Organozinc Reagents

Although only recently considered again as useful tools in synthesis, organozinc reagents have been known for a long time. Possessors of the first metal-carbon σ-bond, Frankland in 1849[32] synthesised both diethyl and dimethyl zinc via a process of heating metallic zinc with both ethyl and methyl iodide respectively in a sealed tube:

$$2RI + 2Zn \rightarrow 2RZnI \qquad (1.1)$$

Until only last year, the structures of these earliest organometallic ancestors were unknown, before elucidation by Steiner *et al* revealed that they were essentially linear geometries in the solid state.[33] Their discovery more than 150 years ago led incidentally to the birth of organometallic chemistry, these compounds still being used routinely today, such is their usefulness in synthesis.

One of the reasons that organozinc compounds fell into obscurity from the end of the nineteenth century up to the latter portion of the twentieth, was the discovery and application of Grignard (RMgX) and alkyllithium reagents (RLi). Due to the more polarised character of the Mg-C and Li-C bonds compared with those of zinc, these exhibited far higher reactivities and allowed many transformations to be carried out more easily. The "renaissance" of organozinc reagents in research came about paradoxically, because of their comparatively unreactive nature. These "softer" organozincs often display both greater selectivity in synthesis and increased functional group tolerance, proving useful agents for metallating in positions not previously possible.

The unique stability of zinc is imparted by its filled d shell, lending properties uncharacteristic of the first row transition metals. In this respect it is more akin to magnesium, its chemistry mostly influenced by an s^2 valence shell. Its ability to form

stable +2 oxidation states and strong σ bonds with carbon help establish these two as chemical cousins rather than the distant neighbours suggested by their placement in the Periodic Table. The greatest difference between the two is the obviously increased electronegativity of zinc, bestowing greater covalent character to zinc carbon bonds, making them stronger and shorter.

Though perhaps with the exception of zinc amides (containing a more polarised Zn-N bond), organozinc reagents have shown themselves as consistently poor agents of deprotonative metallation. Their greatest synthetic attributes over the past century or so have proven to be in mediating many nucleophilic additions, Reformatsky type reactions,[34] and playing an essential part in the development of Negishi cross-couplings, one of the most versatile and universally practised methods of C-C bond formation.[35] Diphenylzinc has proven, under catalytic conditions, an effective aryl nucleophile towards a variety of heterocycles, aldehydes and ketones. Interestingly, it has even shown itself capable of effecting epoxide polymerisation in water (a solvent ordinarily completely incompatible with main group/zinc organometallics),[36] compared to the correspondingly more reactive phenyllithium,[37] requiring hexane to carry out such reactions.

1.5 Organomagnesium Reagents

Like zinc, organomagnesium reagents are also amongst the earliest known classes of organometallic compounds. Charged with the task of optimising what is now referred to as the Barbier reaction,[38] early synthesis by Grignard involved combination of a ketone, methyl iodide and magnesium metal, facilitating nucleophilic addition across the carbonyl group and generation of a tertiary alcohol on work up, whilst still keeping intact a remote C=C bond within the molecule:
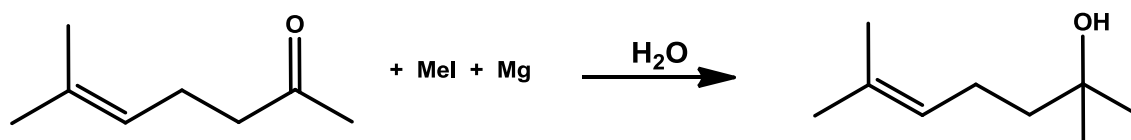
Scheme 1.2: The Barbier reaction, whereby MeI and Mg metal are added to a ketone, generating a tertiary alcohol.

From this Grignard deduced that an intermediate of formulation RMgX could be present, and found that in ethereal solvents addition of magnesium metal to alkyl halides did indeed give compounds of this type, with insertion of the metal into the R-X bond. Isolation of this intermediate followed by addition to the ketone provided increased yields of the final alcohol[39]compared to simultaneous addition of all components. These results marked Grignard for greatness, their worth measured finally by achievement of Chemistry's ultimate accolade *viz.* his award of the Nobel Prize in Chemistry in 1912.

The structure of these Grignard reagents though would be a matter of continual debate for decades after their discovery. The discrete structure represented as RMgX was disproved and instead a more polarised form proposed as $[R^-(MgX)^+]$,[40] compounded by the existence of what is now called the Schlenk equilibrium (eqn. 1):

$$2\ \mathbf{RMgX} \rightleftharpoons \mathbf{R_2Mg} + \mathbf{MgX_2} \qquad (1.2)$$

The actual structure of these species in solution is a matter of some complexity, as they "depend on the nature of R, the nature of X, the properties of the coordinating solvent, concentration and temperature."[41] With appropriate advances made in X-ray crystallography, the eventual structural elucidation of both phenylmagnesium bromide and ethylmagnesium bromide (both solvated by diethyl ether) was achieved in 1963,[42] proving unequivocally their existence as discrete monomers in the solid state *i.e.*, each magnesium bound to both the alkyl group and halide, satisfied further by two molecules of diethyl ether; structures in marked contrast to those proposed some five decades previously by both Grignard and Baeyer/Villiger.[43]

Although more reactive than their organozinc counterparts, these organomagnesium compounds showed themselves able to be improved. It was found that by the addition of LiCl to these Grignard reagents, their reaction rates were drastically increased.[44] Outstripping their predecessors in both reactivity and functional group tolerance, these so called "Turbo Grignards" were found to perform magnesium-halogen excahange with ease on a large range of heterocycles. Magnesium reagents exhibiting the formula $R_2NMgCl \cdot LiCl$ (turbo-Hauser base) were found to perform especially well in the area of deprotonative metallation.[45] For example, Knochel in 2006 utilised the turbo Hauser base $TMPMgCl \cdot LiCl$[46] (**Figure 1.7**) to such an end, magnesiating (among a wide

breadth of heterocycles) pyrimidine derivatives with great control in regioselectivity (**Scheme 1.3**).[45b]
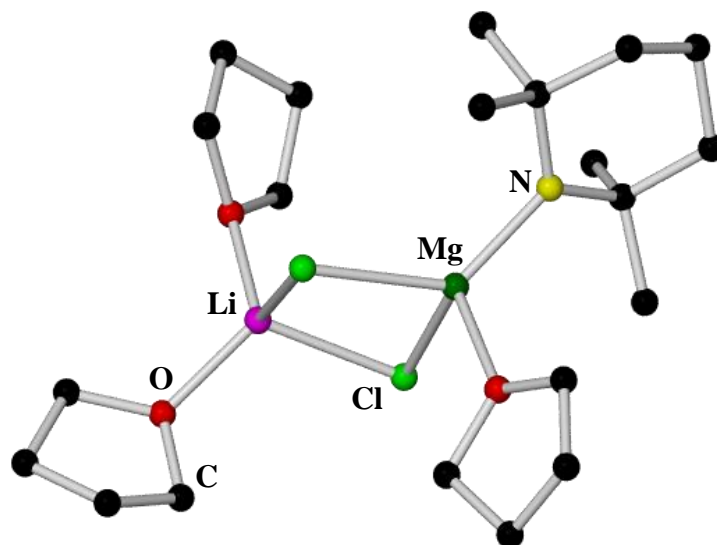
Fig. 1.7: Structure of Turbo-Hauser base TMPMgCl.LiCl
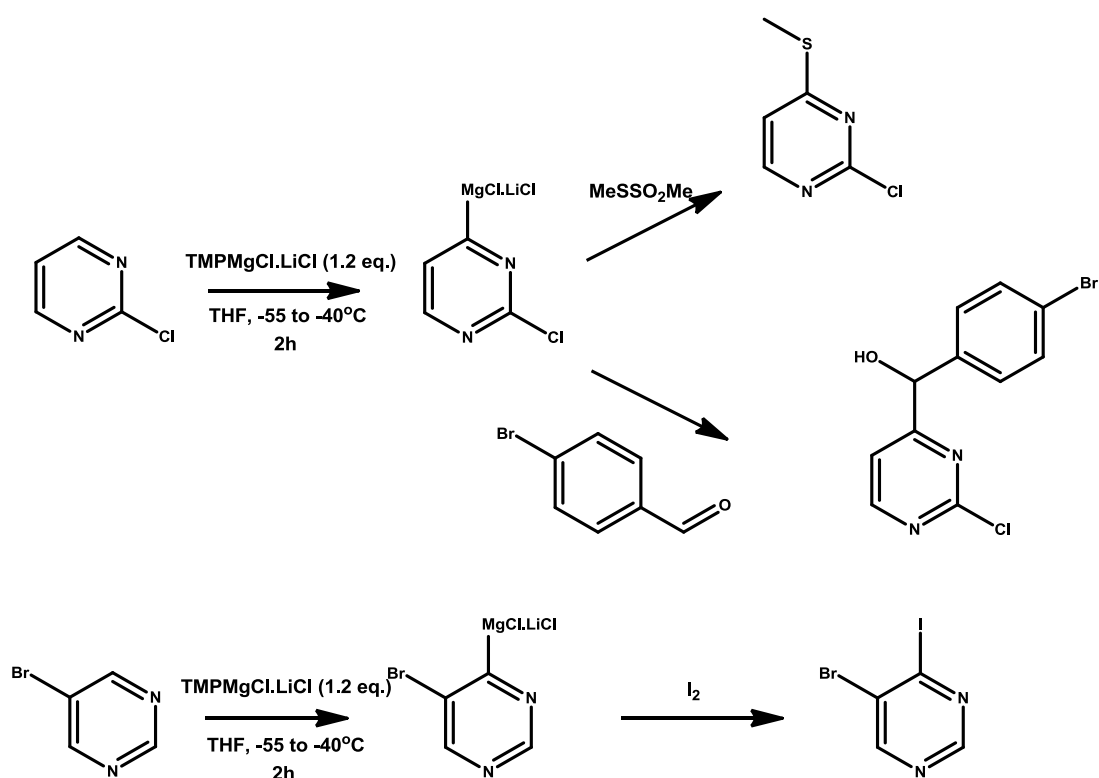
Scheme 1.3: Pyrimidine magnesiation and electrophilic[45b] quenching, with the deprotonation step carried out by the turbo Hauser base, taking place between the N heteroatom and the Br functionality.

The obvious disadvantage to utilising these systems, with reagents such as TMPMgCl, TMPMgCl.LiCl or LiTMP for example, is that each has only one basic TMP arm able to participate in deprotonative metallation reactions. In 1989, Easton developed a bis-amido magnesium species, basic enough to carry out double deprotonations of functionalised aromatic species, namely $Mg(TMP)_2$,[47] synthesised as a clear solution on refluxing di-*n*-butylmagnesium with two equivalents of TMP(H). He found that on reaction of excess base with the disubstituted *N, N*-diethylterephthalamide, heated to reflux in THF for 2 hours, double deprotonation had occurred, *ortho* to each of the amide functionalities. Further reaction with CO_2 and CH_2N_2 gave the product of double esterification in 87% yield (**Scheme 1.4**). Easton rationalised this superiority in dideprotonation over using two equivalents of LiTMP with the same substrate, in that the initial *ortho* lithiation results in a Li-C bond too polarised, thereby deactivating the remaining ring positions towards a second deprotonation, in marked contrast to the more covalent nature of the Mg-C bond. As an aside it is also interesting to note that in the same paper they reacted $Mg(TMP)_2$ with an arene bearing an ester functionality, which are known to be especially prone to nucleophilic attack by more traditional organolithium reagents.
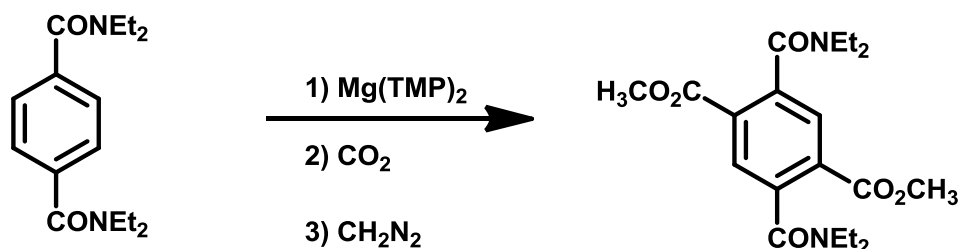
Scheme 1.4: Dideprotonation by $Mg(TMP)_2$ and esterification

More recently, $Mg(TMP)_2$ has also been used to good effect in the *ortho* metallation of a variety of boron substituted benzenes, also managing to trap and crystallographically characterise one such species.[48] Unfortunately, to date the solid state structure of $Mg(TMP)_2$ is unknown, although both related $Zn(TMP)_2$[49] and $Cd(TMP)_2$[50] exist as (essentially identical) discrete liner monomeric species.
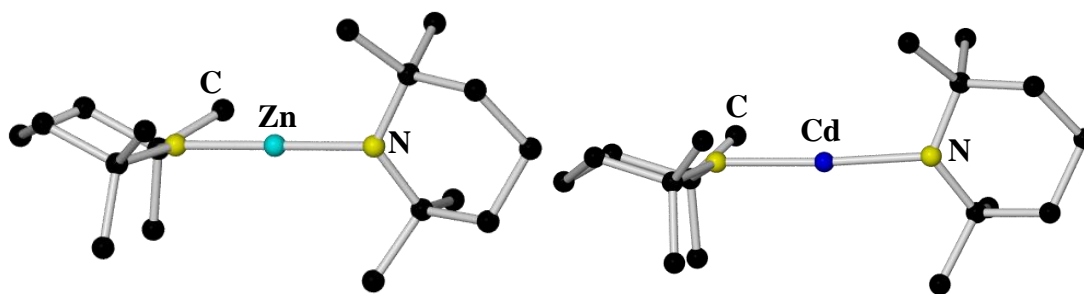
Fig 1.8: Molecular structures of monomeric Zn(TMP)$_2$ right and Cd(TMP)$_2$ left.

1.6 Synergic metallators and "ate" chemistry

Having limited the preceding discussions to essentially unimetallic reagents, it seemed apt to introduce the area of mixed metal and superbasic chemistry beginning with unimetallic superbases. Despite the fact that basic species of this type were discovered after their heterogeneous counterparts, it is appropriate to discuss them as a preface, owing to their arguably less complex nature. In a 1993 review,[51] Caubère remarks on the nature and definition of the term "superbase," surmising succinctly that the term should apply only "to bases resulting from a mixture of two (or more) bases leading to new basic species possessing inherent new properties." In his own research, Caubère would develop a complex unimetallic superbase of composition "BuLi-Me$_2$N(CH$_2$)$_2$OLi", which showed on reaction with 2-methoxypyridine significant C-6 metallation,[52] as opposed to the usual C-2 azomethine addition usually observed when this substrate is reacted with traditional alkyllithium reagents.[53] Indeed, to circumvent unwanted nucleophilic addition to these electron deficient pyridine rings, secondary lithium amides are often employed, though significant conversion usually requires a large excess of base. The Caubère reagent enjoys the dual advantage of near stoichiometric deprotonation and simultaneous suppression of the nucleophilic addition reaction.

Arguably the first, or at least most famous, bimetallic superbase to enjoy any synthetic applicability is that produced by a 1:1 combination of *n*-butyllithium and potassium *tert*-butoxide, devised by Lochmann[54] and Schlosser.[55] This base is often called the "LICKOR" superbase, with the "LIC" portion referring to the alkyllithium, and the "KOR" the appropriate potassium alkoxide. What was discovered was an intermediate reactivity between organolithium and organopotassium reagents, in effect boosting the reactivity of the organolithium, whilst tempering their inherent nucleophilicity, and proving itself an exclusive agent of deprotonation. This powerful reagent has proven

itself capable of deprotonating a wide range of weakly acidic organic substrates, such as benzene[55] (by comparison, *n*-BuLi requires TMEDA to achieve this),[56] various alkenes,[57] dienes[58] and allyl thioethers.[59] Indeed, such is its effectiveness in these transformations, that a superbasic approach was devised to achieve the target drug Ibuprofen, through three sequential metallations from the starting material *para*-xylene, metallating in each instance the least hindered benzylic site.[60]
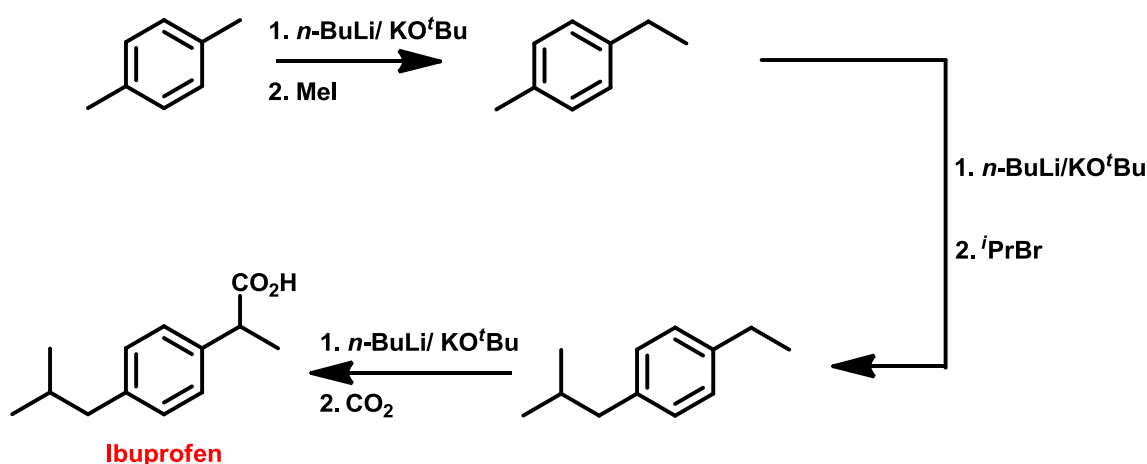
Scheme 1.5: Sequential 3-step superbase metallation and quenching to form ibuprofen.

The main drawbacks to this extremely potent superbase, is the necessity of cryogenic temperatures, and their somewhat limited selectivity, the other side of the reactivity coin. Unfortunately to date, no structure of the "LICKOR" superbase has never been characterised, meaning the exact nature of the base is still elusive, probably due to the co-existence of a large number of different aggregates in solution.

In a more recent Li/K superbase development, O'Shea has shown that combination of LiTMP with KO*t*Bu can effect a large number of lateral metallations preferentially over sites on the aromatic ring.[61] Much like with the naming of the "LICKOR" base, an acronym has been coined to describe this type of chemistry, a term O'Shea has called "LiNK" chemistry, made up of Li, N and K representing those respective elements. The observations in his reactions with various toluenes of different substitution pattern, each with the same OMOM (methoxymethylether) appendage, showed conclusively that the LiTMP/KO*t*Bu combination gave selective benzylic metallation, whereas by comparison the "LICKOR" superbase showed invariable preference for ring deprotonation.[62]
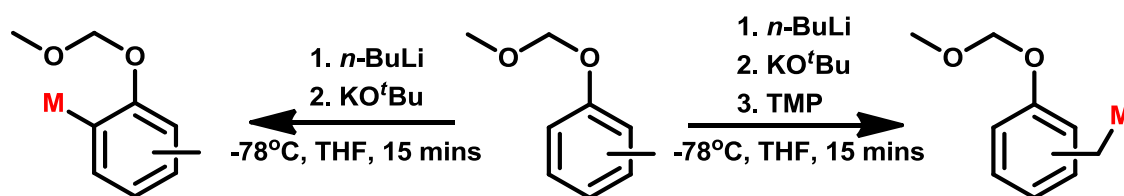
Scheme 1.6: LiCKOR vs. LiNK metallation of MOMO substituted toluenes

Although none of these reagents have ever been structurally characterised, one such representative example of a model superbase does exist, namely the mixed Li-Primary amide/K alkoxide $[\{^{t}BuN(H)\}_4(^{t}BuO)_4Li_4K_4.(C_6H_6)_n]$,[63] exhibiting two core Li-N-Li-N rings fused to two K-O-K-O rings, each set perpendicular to the other. This example stands as the first bona-fide example of a superbase used experimentally in metallation.
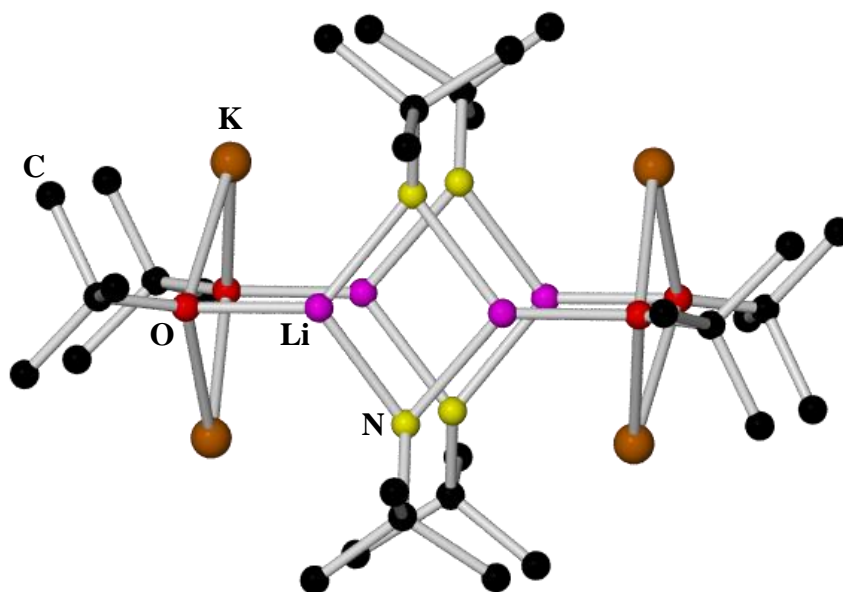
Fig 1.9: Structure of superbasic $[\{^{t}BuN(H)\}_4(^{t}BuO)_4Li_4K_4.(C_6H_6)_n]$

In 1979, Lochmann used this base to prove that combination of the primary lithium amide $^{t}BuN(H)Li$ with $KO^{t}Bu$ achieved toluene deprotonation in the methyl position,[64] a feat the parent lithium amide could not achieve alone, further proved by direct dissolution of the complex isolated by Mulvey in benzene and subsequent reaction with toluene. Although of limited synthetic worth outwith these two complementary studies, this novel structure still serves as direct evidence of the cooperative effects of the metals and consequent reactivity increase achieved by these superbasic mixtures.

1.7 Alkali-metal mediated Zincation

Though a fairly modern field of chemistry for application and use, the synthesis of the first "ate" compound, a phrase coined by Wittig almost a century later, was performed by Wanklyn in 1858,[65] namely the complex Et_3ZnNa. These compounds, displaying higher reactivity than traditional alkylzinc species (ZnR_2)[66] (due to the reactivity imparted by the presence of more electropositive alkali metals and greater number of anionic ligands surrounding zinc) were of great importance to synthetic chemists.

Their use has been extended from compounds of limited synthetic worth to fundamental reagents in many cornerstone reactions and transformations, such as metal-halogen exchange [67] (their first synthetic use),[68] nucleophilic addition[69] and deprotonation reactions.[68]

It has been shown that lithium zincates, for example, can take on the general formulae $LiZnR_3$ and Li_2ZnR_4,[70] and that within this formulation an accepted subdivision exists where they can be described as "contacted ion pairs" (*e.g.* $LiZnR_3$), where a bridging ligand exists between both metals, or " separated ion pairs" (*e.g.* $Li^+ZnR_3^-$),[71] where the alkali metal is solvated by the solvent, forming the cation, and the zinc coordinated to the anionic ligands, constituting the anionic portion of the neutral molecule. Indeed, the first structure of an unsolvated lithium zincate (tetraalkyl) was published by Weiss in 1968, exhibiting the formula $Li_2[ZnMe_4]$.[72]

Some novel examples have shown that the alkylzinc component cannot functionalise or operate in the same fashion alone as it does co-complexed with the alkali metal and *vice- versa*, giving rise to the concept of "synergy"; that their action of operation depends on their togetherness. In effect, the zinc is bolstered by the contribution of the more electropositive Li, Na etc. This complementary action has been described therefore as "alkali-metal-mediated zincation",[71] the combination of group 1 organometallic reactivity with organozinc selectivity.

Citing an example, whereby the synergic deprotonation of toluene was carried out using such a mixed metal reagent, Scheme 3 shows the effects of attempting to metallate toluene first with NaTMP and TMEDA together, then with $^tBu_2Zn$ and TMEDA together, the latter producing no reaction and the former carrying out lateral metallation exclusively.[73]

A further reaction was the carried out reacting toluene with the bimetallic dialkyl(amido) base [(TMEDA)Na(^{t}Bu)(TMP)Zn(^{t}Bu)](**1**) (**Figure 1.10**). Interestingly, direct zincation occurred on the ring at *meta-* and *para-* positions (64.5% and 35.5%) respectively, not at the more thermodynamically favoured methyl position. (**Figure 1.11**):
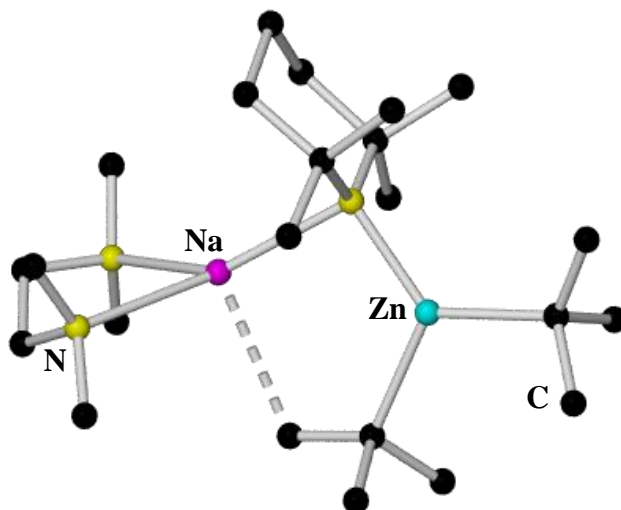
Fig. 1.10: Molecular structure of the sodium zincate [(TMEDA)·Na(^{t}Bu)(TMP)Zn(^{t}Bu)] (H atoms omitted for clarity).
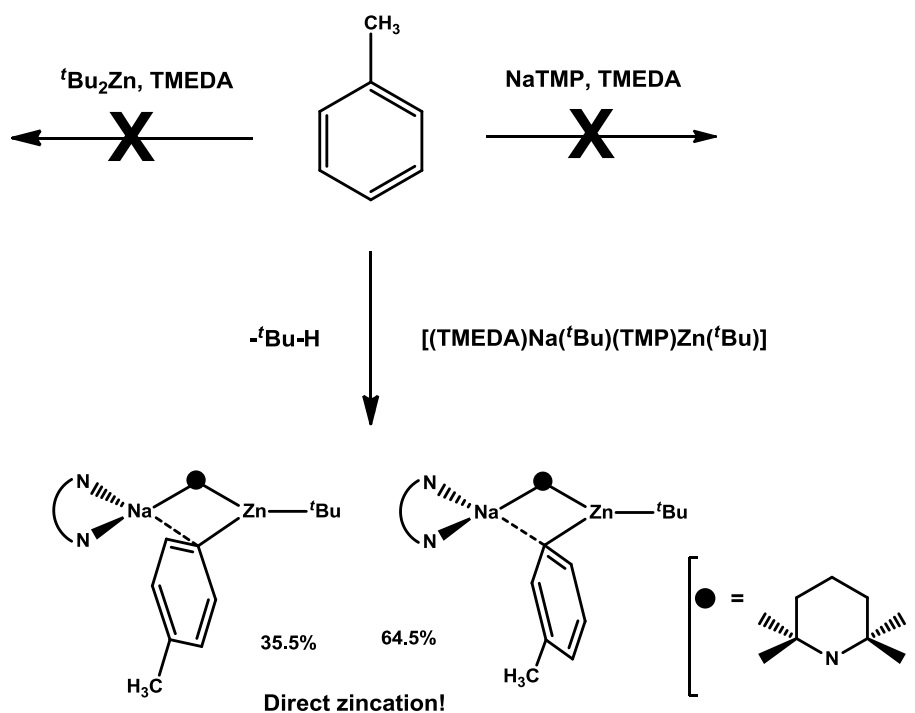
Fig. 1.11: Direct zincation of toluene**.**

In 2008, Hevia *et al* reported a series of experiments, where the reactivity of lithium zincates as deprotonative reagents for the sterically demanding ketone 2, 4, 6-trimethylacetophenone to produce the corresponding enolates is compared with the reactivity of homometallic Zn(TMP)$_2$ on its own with the same substrate. [73]

Thus, tris(amido)zincate LiZn(TMP)$_3$ was prepared *in situ* by reacting three molar equivalents of LiTMP with ZnCl$_2$. Trimethylacetophenone was then added in the presence of TMEDA, then without, producing in each case a single different product, both characterised crystallographically (**Figure 1.12**).
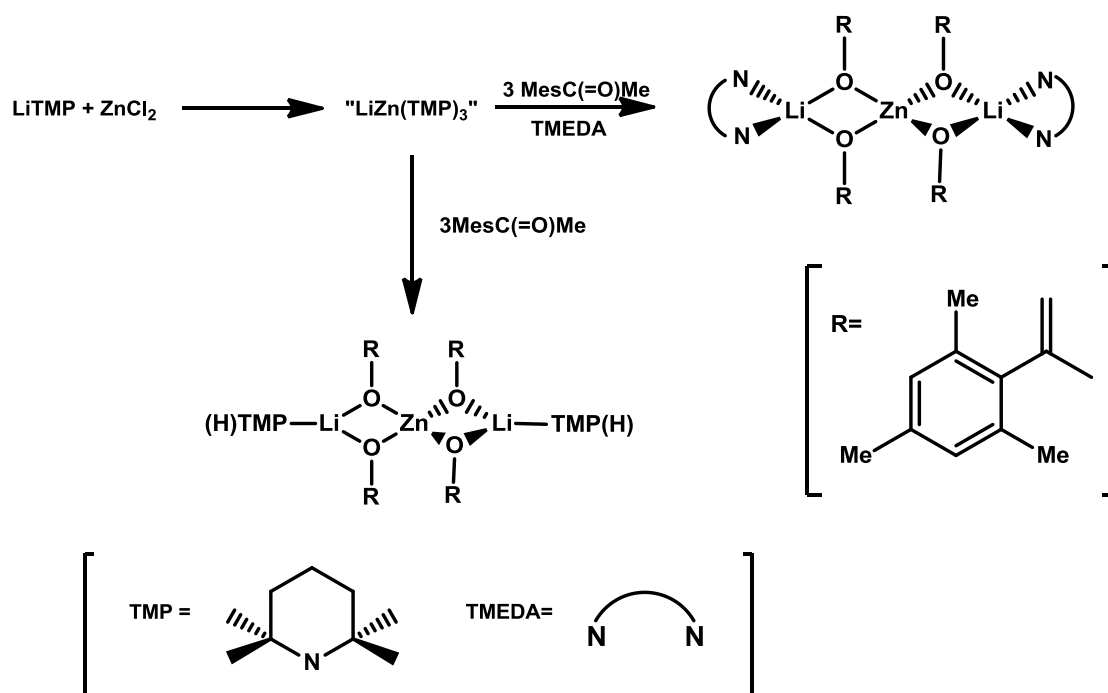
Fig. 1.12: Reaction of LiZn(TMP)$_3$ with 2, 4, 6-acetophenone.

Interestingly, mixed metal compounds are obtained in both cases where the ketone has been metallated at the CH$_3$ position, even in the absence of the chelating ligand TMEDA.

Altering the conditions, LiTMP was reacted with dimethylzinc in the presence of TMEDA to produce the corresponding dialkyl amido zincate [(TMEDA)LiZn(TMP)Me$_2$], with only one basic "TMP arm". This when reacted with the ketone, affording a lithium enolate species as shown in **Figure 1.12,** a consequence of the disproportionation of the mixed metal compound [(TMEDA)Li(OR)ZnMe$_2$].

A final reaction containing the "zinc only" bis- amido species Zn(TMP)$_2$ with the same ketone in the presence of TMEDA afforded the monomeric zinc enolate product. Both reactions are depicted in the following scheme (**Figure 1.13**).
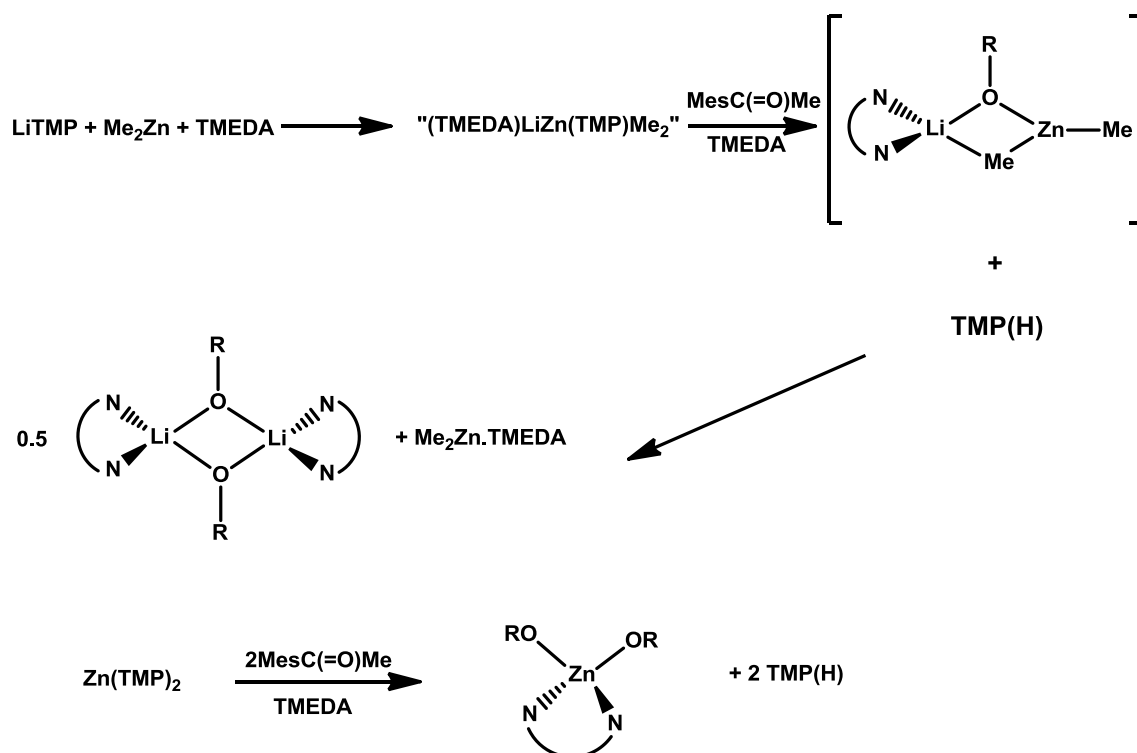
Fig. 1.13: Reaction of Zn(TMP)$_2$ and "(TMEDA)LiZn(TMP)Me$_2$" with

2, 4, 6 -acetophenone

These reactions highlight the wealth and diversity of different products that can be obtained from the deprotonation of the same ketone via slight alterations in the reagents used i.e., two mixed-metal enolate compounds with lithium atoms coordinated to different neutral ligands (TMEDA or TMP(H)), and two single metal compounds, containing only lithium (dimeric) and zinc (monomeric) respectively.

In the same study, theoretical experiments were carried out following the production of Zn(OR)$_2$ via two different reagents: the dialkyl zinc species ZnEt$_2$, and the diamido species Zn(TMP)$_2$. Figure 4 illustrates the progress of both reactions, with ZnEt$_2$ shown in blue, and Zn(TMP)$_2$ in green:
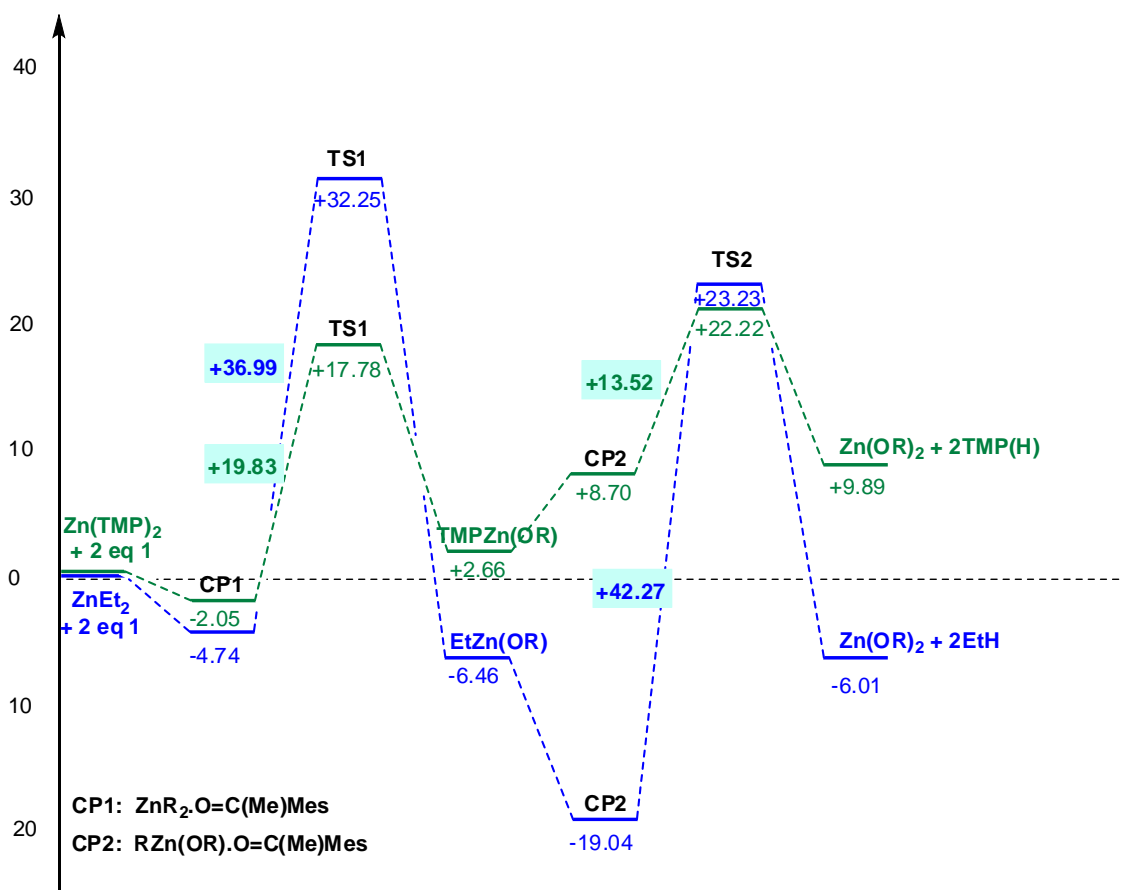
Fig. 1.14: Energetics of the reaction of two equivalents of acetophenone with both Zn(TMP)$_2$ and ZnEt$_2$. Energy changes given in kcal/mol.

Following the reaction, we see that the final Zn(OR)$_2$ product obtained by the dialkyl species, is exothermic (-ve. ΔE), and is the more thermodynamically stable of the two. However, note that in achieving first the intermediate alkoxide species TMPZn(OR), the massive activation energy (E$_{act}$) difference between both possible routes to reach the first transition state (19.83 kcal mol^{-1} for Zn(TMP)$_2$ *c.f.* 36.99 kcal mol^{-1} with ZnEt$_2$). Again, the second activation energy difference is much greater (13.52 kcal/mol for Zn(TMP)$_2$ *c.f.*, 42.27 kcal mol^{-1} for ZnEt$_2$). On this basis, we can see that although thermodynamically the route described in blue seems favourable when considering the final product, the energy barriers involved are too great, and kinetically the formation of the enolate achieved far more easily via the Zn(TMP)$_2$. This example proves conclusively the increased kinetic reactivity of Zn-N bonds compared to the kinetic retardation of Zn-C bonds and thus provides a fitting place for amido-zinc reagents in synthesis.

An important study highlighting the use of such zincates in deprotonation whilst preserving and keeping potentially reactive functional groups intact was undertaken by

Kondo *et al* in 1999. They first synthesised a lithium zincate via the co-complexation reaction of Li(TMP) with di-*tert*-butylzinc to form the heteroleptic zincate di-*tert*-butyl(tetramethylpiperidino)zincate (**Figure 1.15).**[74]
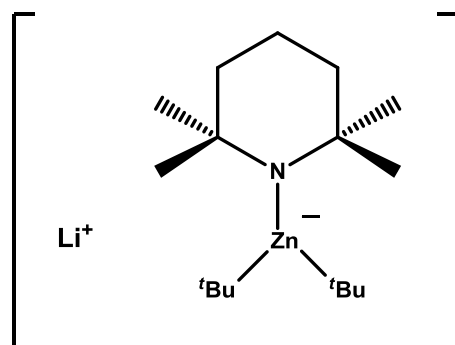
Fig. 1.15: ChemDraw representation of Li(TMP)Zn^{t}Bu$_2$

They then reacted this new zincate with a series of functionalised arenes, observing the products of Zn-H exchange at the *ortho*-position in each case, followed by treatment with I$_2$ to produce the corresponding iodo derivatives (**Scheme 1.7**).

1a) R=CO$_2$Me
1b) R=CO$_2$Et
1c) R=CO$_2$^{i}Pr
1d) R=CO$_2$^{t}Bu
2) R=CON^{i}Pr
3) R=CN

4) R=(Me, Et, ^{i}Pr ^{t}Bu) 73-99%

5) 95%

6) E=(I, CH(OH)Ph) 92-96%
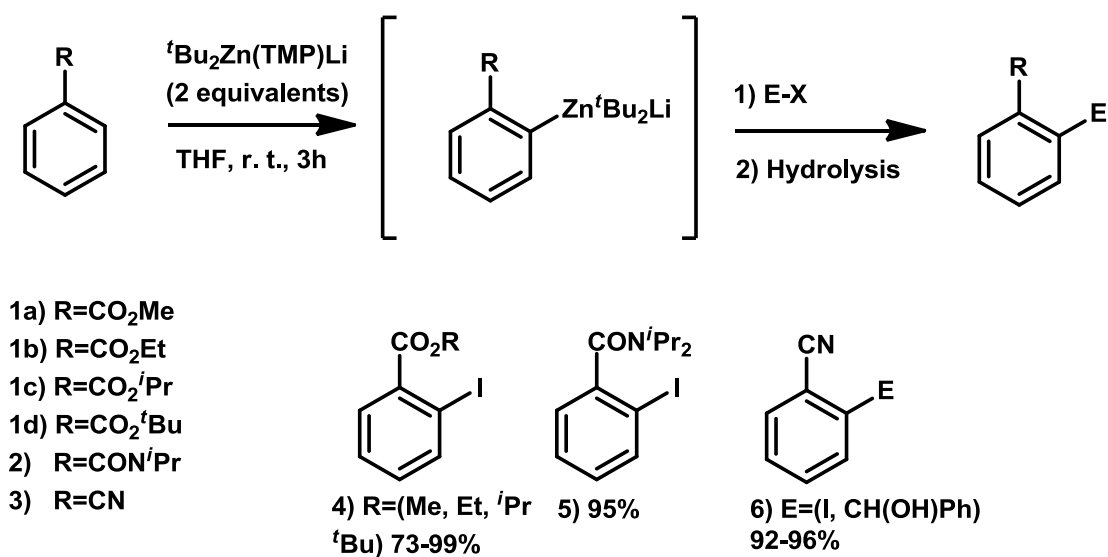
Scheme 1.7: Reaction of a series of functionalised arenes with ^{t}Bu$_2$Zn(TMP)Li.

As shown in **Scheme 1.7**, these substrates can be deprotonated at room temperature, very mild compared to the conditions which are generally required for alkyllithium bases. Often these reactions must be performed at -78°C (or lower) in order to avoid side reactions. It serves too as a concise example of the functional group tolerance exhibited by these new zincates, carrying out metallation at the correct position without alteration of the rather sensitive functional group R.

As shown by these examples, the synthetic worth of these bimetallic reagents is unquestionable, a notion attested to by the marked increase in their worldwide interest since Kondo's discovery [Note however, that the most efficient transformations in metal-hydrogen deprotonative metallations occur with zincates exhibiting the formulation $MZn(NR_2)R'_2$ (Where M=Li or Na, R= alkyl and NR_2=secondary amide)].

This can be rationalised by the inherent carbophilicity of Zn *i.e.* in compounds of the formulae ZnR_2, $MZnR_3$ (where R= alkyl group e.g., Et, ^{t}Bu, Ph etc). Indeed, these reagents were used to greatest effect in metal-halogen exchange,[67] owing to their "softness", and proved rather ineffective in deprotonations. These Zn-C compounds are kinetically retarded,[66] and have thus proved reluctant to react as bases. For instance, Uchiyama reported recently the use of the tetraorganozincate ^{t}Bu$_4$ZnLi$_2$ as a highly chemoselective reagent for just such a Zn-X exchange (X = halogen).[74b] He reacted this species with (4-iodophenol)methanol at room temperature to prepare the relevant product of zinc-halogen exchange, then reacted this with several electrophiles under similar, very mild reaction conditions to attain a number of different products, shown in the following scheme (**Scheme 1.8**), leaving the acidic OH functionality intact. In addition, the same mixed-metal reagent can be used as an initiator in the polymerisation of acrylamide in protic solvents such as MeOH or even water!
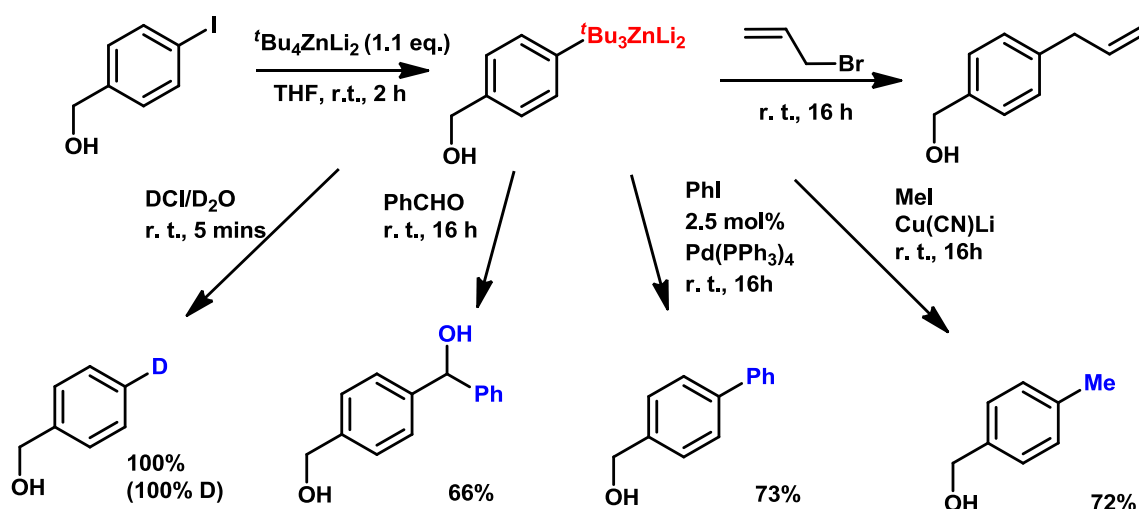
Scheme 1.8: Reaction of aryliodides with tetrabutyl dilithiumzinc and subsequent electrophilic trapping reaction.

By comparison, Zn-N bonds are much more kinetically reactive, so employment of amido ligands e.g. TMP, HMDS (hexamethyldisilazide) and DA (diisopropylamide) allow deprotonative metallation to occur far more readily. The three ligands mentioned above have in fact been quoted as the most synthetically useful amides worldwide.[71]

1.8 Alkali-Metal Mediated Magnesiation (AMMM)

Along with the aforementioned zincates, magnesiates can be counted amongst the forerunners of modern organometallic chemistry. A seminal paper was published by Wittig in 1951,[75] in which alongside an analogous "zincate" example, he reported an "ate" complex of formulation $LiMgPh_3$, produced by combination of the two homometallic species, namely Ph_2Mg and PhLi. Unique reactivities of this new chemical class were observed when this tris-alkyl "ate" complex was reacted with benzalacetophenone. They observed predominantly the 1, 4- addition product, contrasting markedly with the 1, 2- adduct formed on reaction with monometallic PhLi alone.[75]
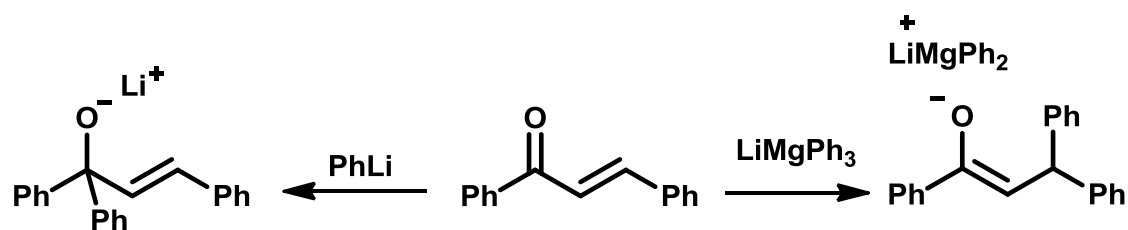
Scheme 1.9: Differing modes of addition towards benzalacetophenone by both PhLi and $LiMgPh_3$.

As mentioned previously, this enhanced or often very different chemistry observed in "ate" complexes can be accounted for at least in part by the increased number of anionic ligands surrounding the metals.[76] Like their zinc counterparts, these organomagnesiates can also adopt a tetraorganic formulation i.e. M_2MgR_4. A recent publication highlights the synthetic utility of bases exhibiting both forms, by their facile deprotonation of various arenes, prior to functionalization. Arenes bearing *ortho*-directing substituents were reacted with either $LiMgBu_3$ or Li_2MgBu_4, followed by trapping with various electrophiles, or utilised in cross-coupling reactions (**Scheme 1.10**).[77] It is noteworthy that the heteroarylmagnesiate species participate readily in these palladium-catalysed

cross-coupling reactions without the need of a transmetallation step, which is required when an aryllithium is utilised.
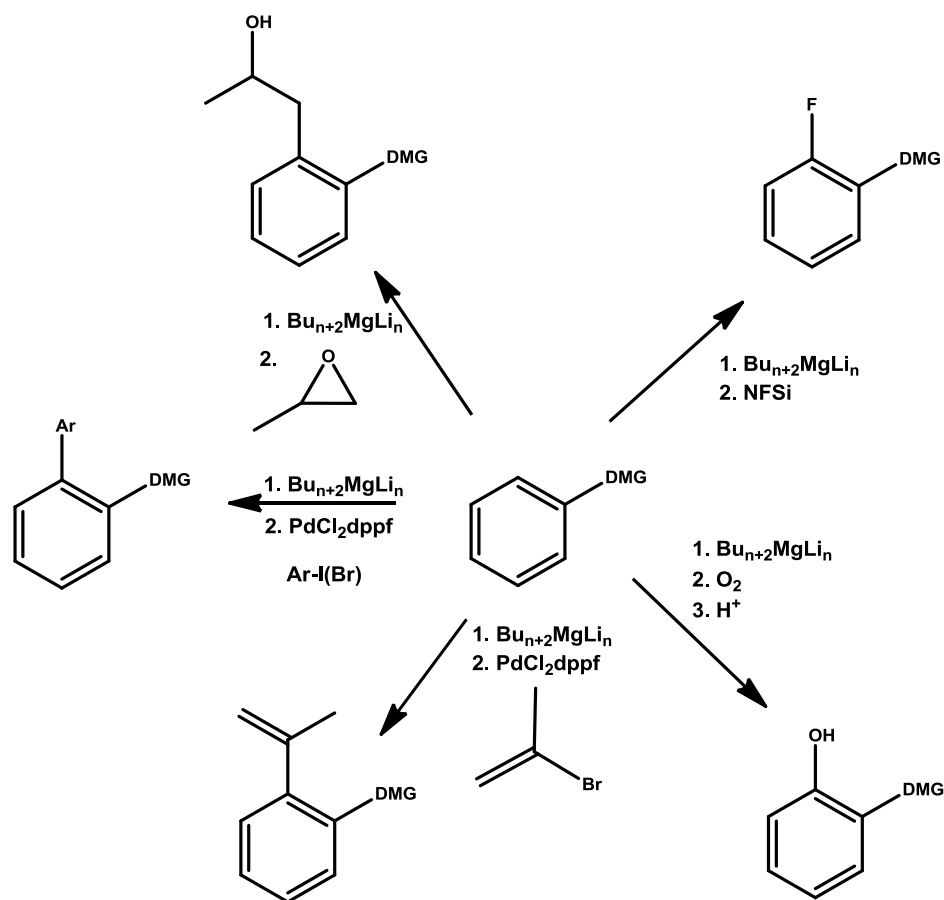
Scheme 1.10: Arene deprotonation by alkyllithium magnesiates followed by electrophilic quenching.

In 1999, a tris-amido lithium magnesiate complex was prepared utilising the sterically demanding amine hexamethyldisilazane [HMDS(H)] $LiMg(HMDS)_3$.donor (where donor = THF or pyridine). Removal of the donor solvent however allowed retention of this structural motif, rationalised by bending of two of the methyl groups of the HMDS ligand towards the lithium, which is now far more exposed following loss of the dative bond formed by the donor. This in itself was an unexpected result, soon to be overshadowed by the consequences of an attempted repetition.

Formation of the donor free complex mentioned above had not occurred, but instead an unusual oxygen containing species $[Li_2Mg_2\{N(SiMe_3)_2\}_4(O_2)_x(O)_y]$ had crystallised preferentially, despite the lack of any oxygen containing reagents being employed and the utilisation of stringent inert atmosphere techniques.[78] This species was crystallised time and again in low yields (1-5 %). An attempt to synthesise this species rationally

was undertaken, whereby atmospheric oxygen was deliberately introduced and the solution stirred for four days. Generation of the desired product was achieved, in a yield increased five-fold (24%); this result however could not provide unequivocally the origin of this serendipitous oxygen, whether molecular oxygen or water.[79]
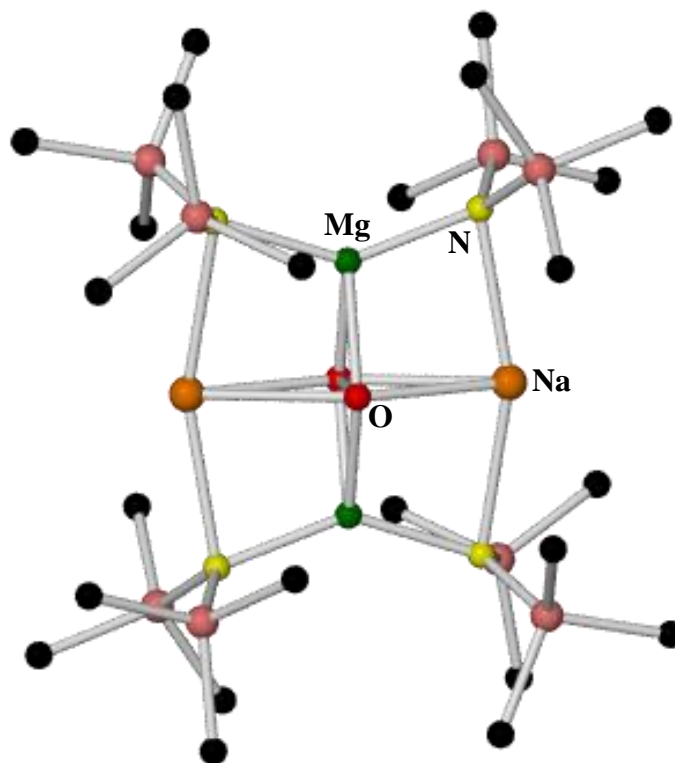
Fig. 1.16: Molecular structure of the inverse crown ether molecule [Li$_2$Mg$_2$\{N(SiMe$_3$)$_2$\}$_4$(O$_2$)$_x$(O)$_y$].

This surprising structure contains an eight membered ring at its core, with Li and Mg alternately bridged by an N atom of the HMDS ligand. Neutrality is achieved by the encapsulated oxo or peroxo species at the ring's core. In order to contextualise the importance and novelty of this complex, it is befitting that a comparison should be made with traditional crown ether complexes, whose chemistry has been known for some time.[80] These host-guest complexes typically operate by the stabilisation of a central metal (electron poor) by Lewis basic oxygen atoms held fixed within a macrocyclic framework.
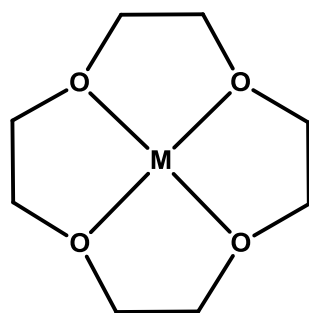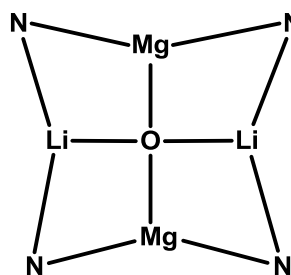
12-crown-4 complex   **LiMgHMDS**

Fig. 1.17: Simplified crown and inverse crown ether motifs.

The obvious likeness between both motifs brings to the fore an equally glaring disparity. Whilst the traditional crown ether complex plays anionic host to cationic guest, the opposite part played by the Li/Mg containing species thus engendered the moniker "inverse crown ether". It seemed fitting then to explore the generality of this reaction, whether it should be considered an anomaly, mere fluke, or its potential extended to a system of synthetic worth. Fortunately, employment of other utility amides such as the even more sterically demanding TMP in place of HMDS, proved beyond doubt that formation of inverse crown ether complexes bearing different amides was not only possible but could be performed routinely.[81] Changing the alkali metal to either potassium or sodium also proved feasible,[81-82] with the respective congeners prepared via the same synthetic route as the first example.

This mixed metal system was not however resigned in playing host to oxo guests alone. Indeed, more excitingly, it was found that by reacting BuNa, $^{n}Bu_2Mg$ and $^{i}Pr_2NH$ in a 1:1:3 ratio (forming a putative basic intermediate of suggested formulation ["NaMg($^{i}Pr_2N)_3$"] with ferrocene at reflux temperature for fifteen minutes, an unprecedented fourfold deprotonation of ferrocene had occurred, two magnesiations taking place on each Cp ring.[83]
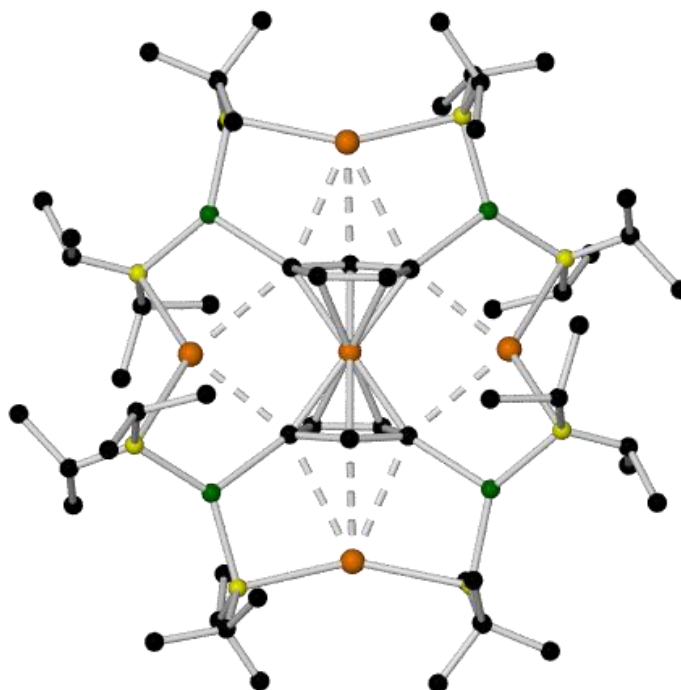
Fig. 1.18: Fourfold deprotonation of ferrocene by sodium magnesiate base.

Ordinarily, traditional alkyllithium reagents (in the presence of donor ligands) can strip either one or two protons from the ferrocenyl scaffold, depending on the stoichiometry employed.[84] In this instance however, ordinary rules of basicity have been circumvented, with a polymetallic framework bearing an overall 4^+ charge, encapsulating a formally 4^- ferrocenyl tetraanion, a situation allowed by both the stable steric encapsulation of the cyclic amido crown, and the large number of complimentary Mg-σ and Na-π interactions providing unique stability to what could be intuitively considered an unstable system.[85] Proof that metallocene tetrametallation and encapsulation of this type is a fairly general reaction was afforded when this same magnesiate base, under identical conditions, was reacted with the heavier group 8 analogues ruthenocene and osmocene, forming a homologous series.[86]

Prepared in the same fashion, this $^{i}Pr_2N^-$ containing magnesiate can also give rise to another intriguing inverse crown product. When heated at reflux temperature in the presence of toluene for one hour, two hydride anions are trapped within the inverse crown cavity, producing an unexpected complex, the formation of which they rationalise in terms of a β-hydride elimination pathway (**Scheme 1.11**).[87]
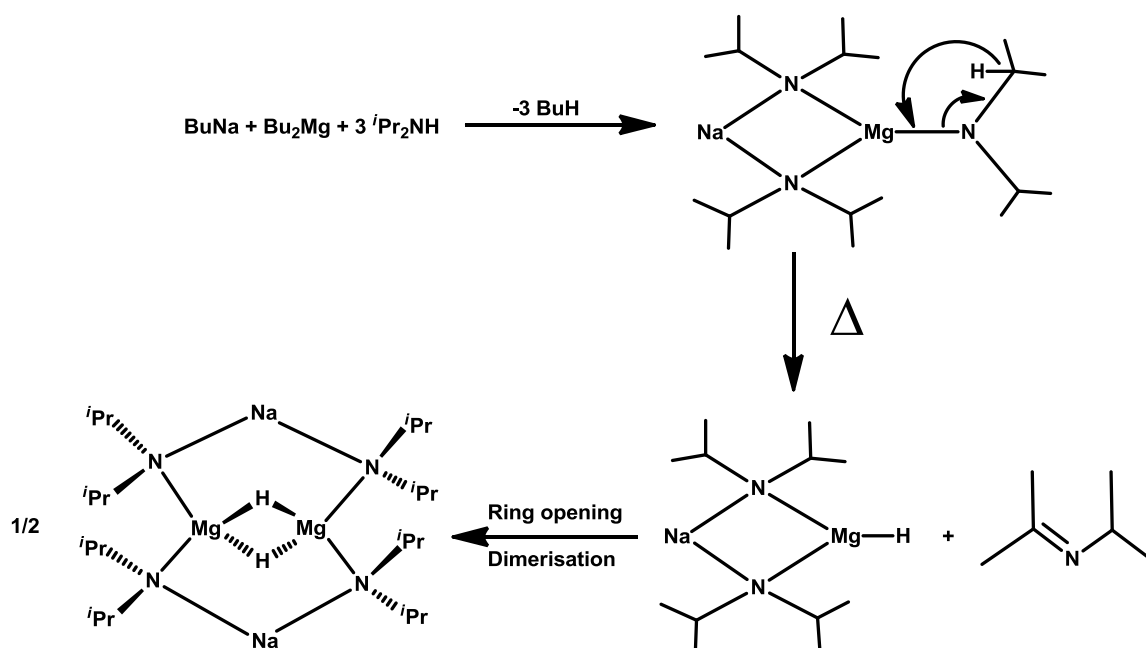
Scheme 1.11: Formation of sodium magnesiate followed by β-hydride elimination, ring opening and dimerization to form hydride encapsulated inverse crown.

It has been shown then that these magnesiates can affect unusual regioselectivities and exhibit great structural control. Recent studies have revealed arguably the most impressive example of magnesiate chemistry to date when reacted with the cyclic ether THF (tetrahydrofuran).[88] Since time immemorial (in chemistry terms at least) organometallic chemists have been plagued by decomposition of this solvent, omnipresent in both industry and academia. Reactive organometallic species deprotonate at the α carbon adjacent to the oxygen heteroatom, inducing spontaneous ether cleavage via reverse [3 + 2] cycloaddition to form ethene and the corresponding metal enolate.[89] A recent publication has shown that trapping at room temperature of this highly reactive anion can be achieved by the bisalkyl monoamido zincate [(TMEDA)·Na(μ-TMP)(μ-CH$_2$SiMe$_3$)Zn(CH$_2$SiMe$_3$)] in a process termed "synergic sedation".[90] By contrast the more reactive magnesiate species [(TMEDA)·Na(μ-TMP)(μ-CH$_2$SiMe$_3$)Mg(TMP)] does indeed induce ether cleavage on stoichiometric addition, breaking six of the thirteen bonds within the THF molecule. Such molecular destruction should not ordinarily merit celebration, but remarkably, each part of the fragmented molecule is trapped and stabilised to such an extent that they are isolable in crystalline form.

It is assumed that both C-O bonds are broken initially and an assumed oxide dianion (O^{2-}) liberated. This species is trapped within the familiar guest-host environment of an inverse crown previously described, surrounded by an eight membered ring of alternating Na and Mg atoms, bridged by the N atoms of TMP. Within the remaining portion of the THF molecule, four C-H bonds are broken, giving rise to the formation of a butadiene dianion of *s-trans* orientation. Both anionic ends of this butadiene fragment are stabilised by bimetallic caps, bound to the magnesium atom, which is in turn bound to two TMP N atoms, one terminal and one bridging. Completing this bimetallic cap is the Na atom, chelated by TMEDA and bridged to the Mg by the N atom of the TMP. The molar ratio of these products was found in practice to be approximately 50:50, following near quantitative conversion.
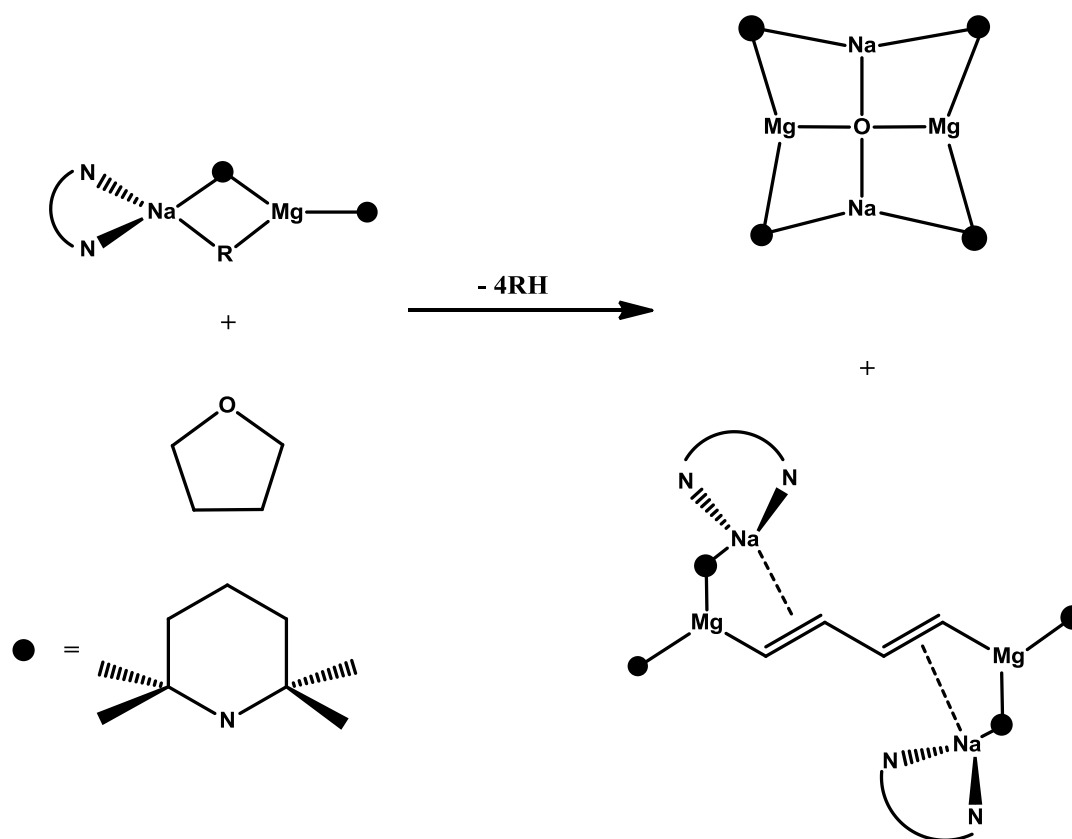
Fig. 1.19: THF cleavage and capture of anionic fragments by the reaction of a sodium magnesiate with THF.

This "cleave and capture" approach compliments nicely the sedation employed by the related sodium zincate in that each allows highly reactive intermediates to be studied. They represent to date the most spectacular display of intermediate trapping achieved by these bimetallic bases, placing them at the forefront of pioneering research into metallation.

Clearly these new synergic bimetallic reagents are capable of chemistry the depth and diversity of which has been hitherto only glimpsed at. What began as a niche, a novelty, has shown in itself true synthetic presence, establishing through years of research and painstaking design a host of unique reagents, capable not only of mediating many challenging and otherwise impossible molecular syntheses, but also of probing our fundamental understanding of organometallic behaviour. And though perhaps professionally unbecoming, what inorganic synthetic chemist does not delight in the elegance of the structures wrought by these reagents, brought from crystalline obscurity to corporeal form, inspiring us on screen and paper. It is our aim then to explore further the capabilities of these reagents, and test their mettle against many important and otherwise unstudied substrates in the field of bimetallic chemistry, forming the basis of this project.

2. <u>Structural elucidation and characterisation of a homometallic anthracenolate family</u>

2.1 Introduction

Aromatic ketones are of fundamental importance in nature, found in a full gamut of natural products.[91] They also provide the frameworks of many other important molecules within the fields of polymer science and photoelectric devices.[92] Therefore, functionalization of aromatic ketones is of great significance to the synthetic chemist. Following the success of these previous examples, we have now turned our attention towards the related tricyclic ketone anthrone,[93] another molecule providing the skeleton of many natural products,[94] appearing in the biological production of hepatocarcinogens.[95] It is also used routinely in determining carbohydrate concentration.[96] The only structural difference between this molecule and benzophenone is that an sp^3-hybridised methylene CH_2 bridge connects the two phenyl rings (**Figure 2.1**).
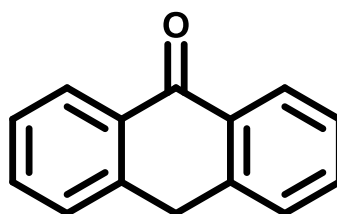
Fig. 2.1: ChemDraw representation of anthrone.

We decided to investigate the reactivity of [(TMEDA)·Na(μ-TMP)(^{t}Bu)Zn(^{t}Bu)] **2a** with anthrone to determine what effect this compositional/structural change (new bridging methylene centre) has on its activity (**2a** was prepared via the known literature method and dissolved in hexane).[97] An equimolar quantity of anthrone was added, causing an immediate pale yellow to bright red colour change. Cooling the solution to −27°C yielded a crop of yellow crystals (55%), confirmed by both X-ray crystallographic and NMR spectroscopic analysis as the sodium dimer [(TMEDA)·Na(OC$_{14}$H$_9$)]$_2$ **2b** (**Figure 2.2**). Complex **2b** was also prepared rationally by combining an equimolar mixture of *n*-butylsodium, anthrone and TMEDA in hexane solution. This monometallic approach was then exploited to prepare the corresponding lithium and potassium congeners. By altering the organo-alkali metal reagent to *n*-butyllithium or trimethylsilylmethylpotassium in hexane solution, the homobimetallic complexes [(donor)·M(OC$_{14}$H$_9$)]$_2$ **2c** (M = Li, donor = TMEDA) and **2d** (M = K, donor

= PMDETA) respectively can be prepared rationally. On treating the cyclic ketone with an equimolar amount of hydrocarbon solutions of di-n-butylmagnesium or diethylzinc and TMEDA, the heteroleptic monomeric TMEDA-solvates [(TMEDA)·Mg^{n}Bu(OC$_{14}$H$_9$)] **2e** and [(TMEDA)·ZnEt(OC$_{14}$H$_9$)] **2f** were forthcoming. In all of these reactions anthrone has been deprotonated at the acidic "CH$_2$ centre". This is not surprising, considering that anthrone undergoes a keto-enol tautomerisation akin to phenol, rendering the hydrogen atoms highly acidic (pK$_a$ in aqueous solution is 10[98] *e.g.*, comparable to that of ArOH =8-11[99]).

2.2   Synthesis of [(TMEDA)·Na(OC$_{14}$H$_9$)]$_2$ 2b

Despite initially starting from sodium zincate **2a** [or indeed the related magnesiate complex {(TMEDA)·Na(TMP)(^{n}Bu)Mg(TMP)}][100], the reaction with anthrone yields a homometallic sodium product. This suggests that, in these reactions, **2b** is a product of fragmentation (**Scheme 2.1**). Despite several efforts, a mixed-metal complex containing an anthronyl/anthracenolate anion could not be obtained, which is rather surprising considering reactivity studies with benzophenone and fluorenone (discussed in depth in Chapter 3) with **2a** generally produce mixed-metal species. This is perhaps best accounted for by focusing on several different electronic considerations which may be at play in this reaction. It is envisaged that the deprotonation of anthrone by the zincate (or magnesiate) TMP arm (as evidenced by the presence of TMP(H) in the reaction filtrate) generates an anthracenolate anion. Presumably a putative ate complex which contains a Na-O-Zn (or -Mg) bridge is formed. Due to the fact that a bulky TMP anion is not present, it is presumed that dimerisation is favourable, maximising ionic Na-O interactions, whilst retaining the same number of Zn-C (or Mg-C) bonds, at the expense of losing a Zn-O or Mg-O interaction. This situation satisfies the strong oxophilicity of sodium and strong carbophilicity of zinc. **Figure 2.2** shows the molecular structure of **2b,** as derived from a crystal structure of **2b**.toluene, along with its pertinent structural dimensions.
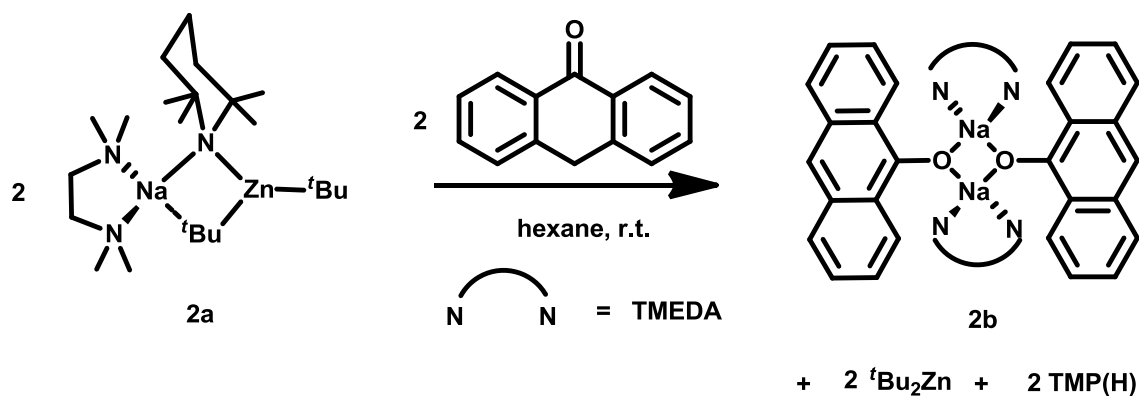
Scheme 2.1: Possible formation of **2b** from **2a** and anthrone via a fragmentation mechanism.

2.2.1   X-ray crystallographic studies of 2b

It consists of a central four-membered, crystallographically non-centrosymmetric ring, made up of alternating Na and O atoms, with each Na atom chelated by a TMEDA ligand, rendering the geometry of each distorted tetrahedral (sum of angles around Na1 = 661.26° and Na2 = 661.82°). The Na-O bond lengths exhibited by this structure [*i.e.*, Na1-O1 2.235(3), Na1-O2 2.215(3), Na2-O1 2.226(3), Na2-O2 2.238(3) Å] are essentially uniform.
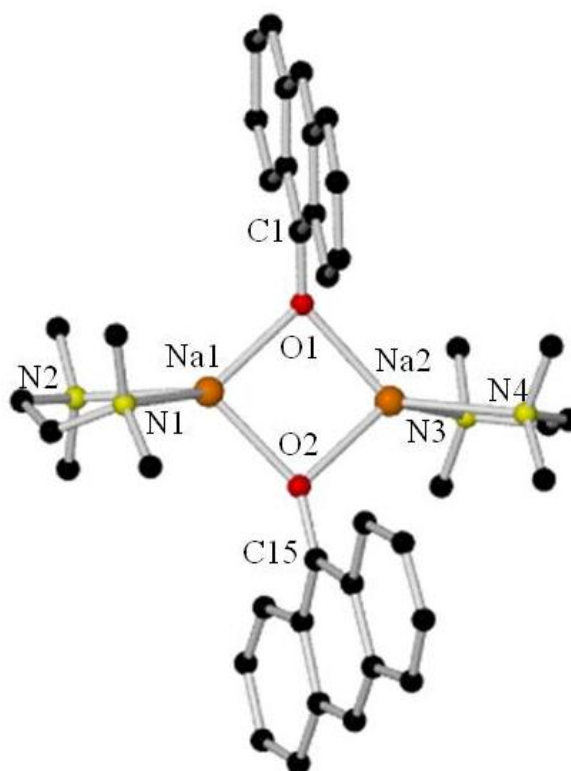
Fig. 2.2: Molecular structure of **2b**. Hydrogen atoms and the disordered component have been omitted for clarity. Selected bond distances (Å) and bond angles (°): Na1-O1 2.235(3), Na1-O2 2.215(3), Na2-O1 2.226(3), Na2-O2 2.238(3), Na1-N1 2.421(3), Na1-N2 2.471(3), Na2-N3 2.457(3), Na2-N4 2.459(4), Na1-O1-Na2 89.94(9), Na1-O2-Na2 90.17(10), O1-Na1-O2 89.84(10), O1-Na2-O2 89.46(10), O2-Na1-N2 127.88(12), O2-Na1-N1 110.13(11), O2-Na2-N3 125.31(12), O2-Na2-N4 117.76(12), O1-Na2-N3 120.40(11), O1-Na2-N4 131.91(13), O1-Na1-N1 131.56(12), O1-Na1-N2 124.79(11), N1-Na1-N2 77.06(11), N3-Na2-N4,77.04(12), Na1-O1-C1 124.7(15), Na1-O2-C15 146.5(2), Na2-O1-C1 137.0(15), Na2-O2-C15 123.2(2).

2.3   Synthesis of [(TMEDA)·Li(OC$_{14}$H$_9$)]$_2$ 2c

Generation of a bimetallic anthracenolate species containing both sodium and either magnesium or zinc has thus far not proved possible via this methodology. Moving to the smaller alkali metal Li, a test reaction was carried out first by generation of the bimetallic base [(TMEDA)·Li(μ-TMP)(μ-Et)Zn(Et)][101], followed by subsequent reaction with anthrone. As previously observed with sodium zincates and magnesiates, fragmentation occurred to produce a lithium anthracenolato dimer [(TMEDA)·Li(OC$_{14}$H$_9$)]$_2$ **2c** and diethylzinc. This former complex was then synthesised rationally by reacting ^{n}BuLi with anthrone in the presence of stoichiometric TMEDA.

Interestingly enough, in previous work conducted by Saá,[102] when the reaction of two molar equivalents of ^{t}BuLi with a single equivalent of anthrone was carried out in tetrahydropyran, subsequent quenching with dimethyldisulfide and aqueous workup furnished the 1-(methylthio)anthrone product in good yields (**Scheme 2.2**). In this instance the first equivalent of lithiating agent forms the OLi salt as observed in our own research, whilst the second performs a ring deprotonation at the 1-position of the anthrone molecule. With the more acidic CH_2 site no longer available for metallation, the OLi portion of the molecule acts as an effective *ortho* directing group.
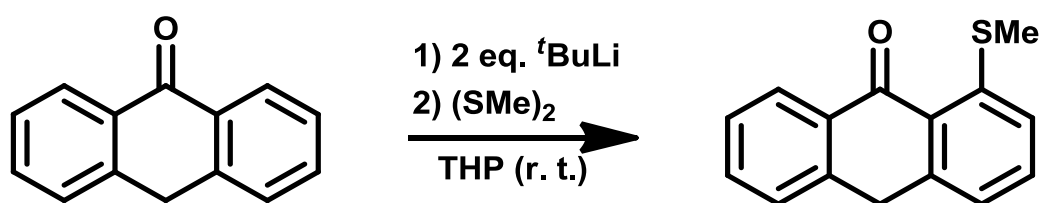
Scheme 2.2: Reaction of anthrone with ^{t}BuLi (1:2) and electrophilic quenching.

The solid state structure of **2c** was determined as a toluene solvate. The molecular structure is shown in **Figure 2.3**. However, the structure features disorder in all of its organic components and so structural discussion is limited to noting that the core structural features are all similar to those of the sodium analogue **2b**.
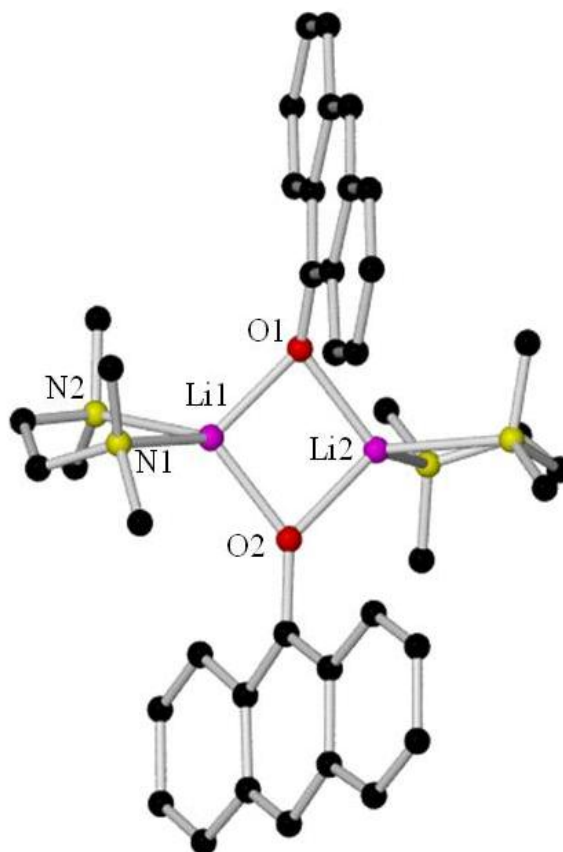
Fig. 2.3: Structure of Li anthracenolate [(TMEDA)·Li(OC$_{14}$H$_9$)]$_2$ **2c**.

2.4   Preparation of [(PMDETA)·K(OC$_{14}$H$_9$)]$_2$ 2d

The influence of the heavier alkali metal potassium on structural control is well documented in the literature.[63, 103] One such striking example occurs in the different coordination modes exhibited by the homologous series Li, Na and K monomeric complexes bearing identical ligand sets.[104] Complexes of the benzyl ligand (PhCH$_2^-$) with each of these metals, solvated by the tetradentate ligand Me$_6$-TREN [tris(N, N − dimethyl-2-aminoethyl)amine][105] were prepared. In the case of the lithium example, the Li atom sits almost coplanar with the ring, exhibiting nigh exclusive σ coordination, and virtually no interaction with the phenyl ring (Li-C$_{ipso}$ distance 3.467(3) Å; Li-C$_\alpha$ distance 2.352(3) Å). Moving to the heavier potassium analogue, a remarkable structural difference was noted. As with the previous Li example, the K was five-coordinate, but this time sat immediately above the face of the phenyl ring, exhibiting almost exclusively π interactions, with no appreciable localisation of the negative charge in the carbananion (K-C$_{ipso}$ distance 3.098(4) Å; K-C$_\alpha$ distance 3.893(4) Å). Even with potassium's considerably larger coordination sphere (Ionic radii of Li$^+$ = 0.90

Å, K$^+$ = 1.52 Å) we can see that its M-C$_{ipso}$ bond is shorter by 0.369 Å, and its proximity to the other ring carbons even more pronounced.

Fig. 2.4: Comparison of Li and K bonding in complexes with identical ligand sets.

Therefore it seemed interesting to probe whether potassium could effect a different structural motif to that produced by the lighter group 1 metals. Owing to the apparently unfavoured formation of heterobimetallic anthracenolate species, we utilised in this instance KCH$_2$SiMe$_3$, solvated by the tridentate donor PMDETA. As before, only deprotonation at the bridging CH$_2$ position is observed, generating the dimeric potassium anthracenolate species.
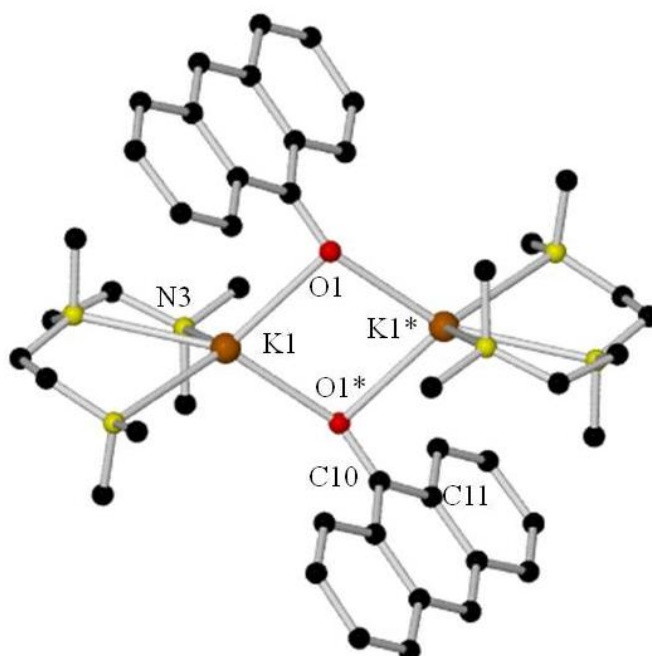
Fig. 2.5: Molecular structure of **2d**. Hydrogen atoms and disordered components have been omitted for clarity. Selected bond distances (Å) and bond angles (°): K1-O1

2.678(12), K1-O1* 2.568(10), O1*-C10 1.288(17), K1-N3 2.831(16), K1-O1-K1* 98.72(4), O1-K1-O* 81.28(4), K1-O1*-C10 152.73(11), K1*-O1*-C10 97.82(10).

2.4.1   X-ray crystallographic studies and structural comparison of 2b, 2c and 2d

A difference between the structure of **2d** and its Li and Na congeners, is that whereas for the lighter metals the anthracenolate ring systems are roughly equidistant between the metal centres of the dimer, in **2d** each anthracenolate ligand is distinctly displaced towards a K centre. This results in a geometry where the K centre displays some features of π-bonding to both atoms of the C-O unit rather than simple bonding to the O atom alone (**Figure 2.6**). This is shown both by the M-O-C angles (minimum 97.77(9), 123.2(2) and 129.3(12)° for K, Na and Li species respectively) and by the differences between the M-O and M-C distances (K-C is 3.124(2) Å, which is only 0.447 Å longer than the K-O bond. The equivalent differences for the much smaller Na and Li species are much larger at approximately 0.909 and 1.145 Å).

When we compare this difference in angles to that found in **2b** and **2c**, a pattern emerges. The mean difference in C-O-Li angles is only 5.03°, the smaller coordination sphere of lithium remaining contented with only its formal heteroatom interactions for stability. This difference in mean angles is increased on moving to the heavier Na congener (17.8°), whose greater steric capacity for engaging in π-arene interactions is well documented.[31c, 68, 106] These differences in angles are greatly magnified, however, in the above potassium example (54.91°). The anthracenolate unit tilts upwards towards a K atom, maximising these stabilising interactions. In turning toward one K atom, the anthracenolate unit concomitantly moves away from the other to give a wide angle of 152.73(11)° (**Figure 2.6**).
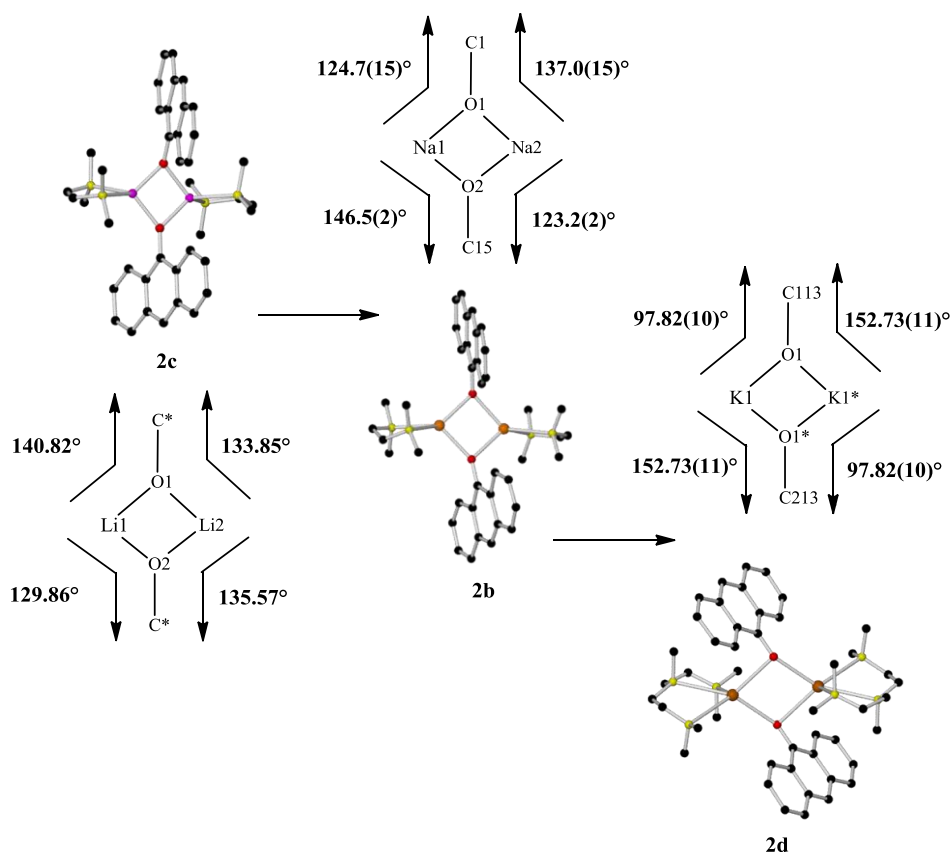
Fig. 2.6: Pictorial representation of decreasing M-O-C angles (C* used in lithium example to account for mean Li-O-C angles of the components of disorder).

Having established that the highly acidic methylene centre is the prime influence for the outcome of this reaction, we have been unable to achieve generation of a heterobimetallic anthracenolate species via the methodologies employed to date. Deprotonation invariably occurs at this position, with fragmentation proving the most favourable outcome. The most electropositive metal, that is the alkali metal, binds strongly to the O atom of the deprotonated anthrone unit, followed ultimately by amine solvation and dimerisation, yielding stable, isolable compounds.

2.5 Preparation and X-ray crystallographic studies of [(TMEDA)·Mg(^{n}Bu)(C$_{14}$H$_9$O)] 2e

In order to access homometallic M^{2+} species, we next synthesised a magnesium anthracenolate complex, by reacting equimolar amounts of anthrone and ^{n}Bu$_2$Mg in the presence of TMEDA. Structural elucidation of crystalline material isolated from this reaction revealed that a heteroleptic magnesium anthracenolate

[TMEDA·Mg(^{n}Bu)(C$_{14}$H$_9$O)] **2e** had been produced.
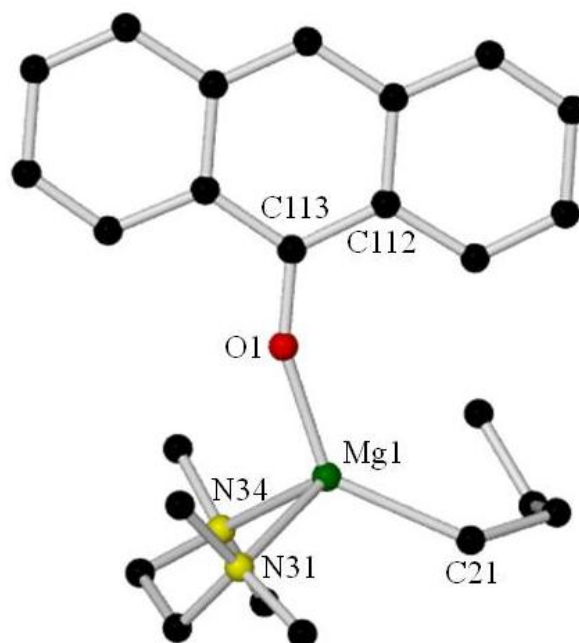
Fig. 2.7: Molecular structure of **2e**. Hydrogen atoms have been omitted for clarity. Selected bond distances (Å) and bond angles (°): Mg1-O1 1.890(4), Mg1-C21 2.130(5), Mg1-N31 2.182(4), Mg1-N34 2.193(4), Mg1-O1-C113 156.38(3), O1-Mg1-C21 132.08(18), N31-Mg1-N34 83.97(15), O1-Mg-N31 102.39(16), O1-Mg1-N34 104.46(17), C21-Mg1-N31 115.93(19), C21-Mg1-N34 107.06(18).

The crystal structure of **2e**, in contrast to the dimeric compounds previously observed, is monomeric (**Figure 2.7**). A single *n*-Bu arm had deprotonated the anthrone, with butane gas formation driving the reaction, whilst the second *n*-Bu arm remains metal-bound. Magnesium's coordination sphere is completed by binding to the phenolic oxygen of the anthracenolate anion and to the two N atoms of TMEDA. The Mg atom adopts a severly distorted tetrahedral arrangement [O1-Mg1-C21 132.08(18), O1-Mg1-N31 102.39(16), O1-Mg1-N34 104.46(17), C21-Mg1-N1 115.93(19), C21-Mg1-N34 107.06(18), N31-Mg1-N34 83.97(15)], forming short, strong contacts to both the O atom [1.890(4) Å] and the C atom [2.130(5) Å] of the *n*-Bu group. The sum of these internal angles is 645.89°, with the greatest deviation from true tetrahedral occurring in the N31-Mg1-N34 angle (Δ 25.53°). A magnesium anthracenolate complex [(2,6-^{i}Pr$_2$C$_6$H$_3$-BIAN)Mg(OC$_{14}$H$_9$)(THF)$_2$] (where 2,6-^{i}Pr$_2$C$_6$H$_3$-BIAN is 1,2-bis[(2,6-diisopropylphenyl)imino]acenaphthene) has been previously characterised (**Figure 2.8**). The Mg-O bond in this complex [1.889(4) Å] is essentially identical in length to its

counterpart in **2e**.
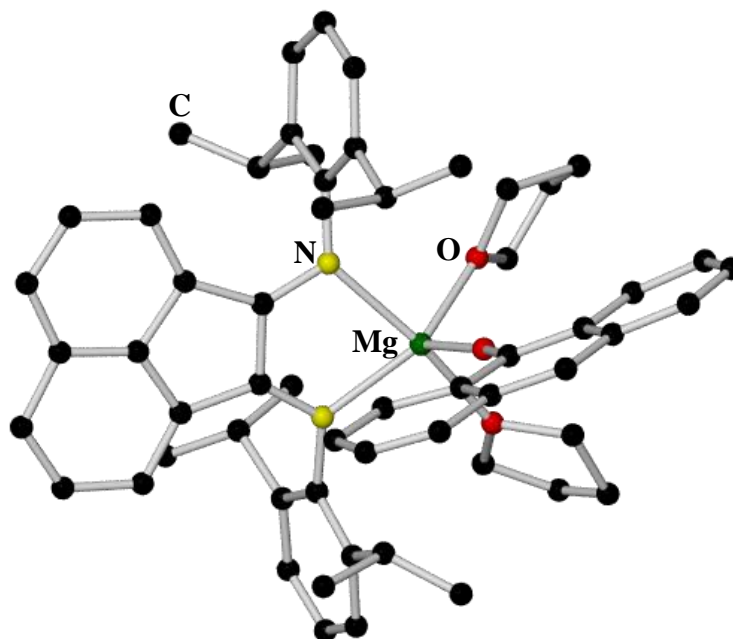
Fig. 2.8: Sturcture of magnesium anthracenolate complex [(2,6-^{i}Pr$_2$C$_6$H$_3$-
BIAN)Mg(OC$_{14}$H$_9$)(THF)$_2$].

2.6   Preparation   and   X-ray   crystallographic   studies   of [(TMEDA)·Zn(Et)(C$_{14}$H$_9$O)] 2f

Zinc-carbon bonds, generally stable owing to their highly covalent and consequently kinetically retarded nature, make alkylzinc reagents poor mediators of deprotonation. However, their basicity can be enhanced by the presence of a donor, such as TMEDA. With this in mind, we reacted Et$_2$Zn with anthrone in the presence of TMEDA to produce heteroleptic [(TMEDA)·Zn(Et)(C$_{14}$H$_9$O)] **2f**.

X-ray crystallographic data of **2f** revealed that even the ordinarily weak base [(TMEDA)·Et$_2$Zn] had deprotonated the anthrone unit, losing ethane, and forming a Zn-O bond [1.925(12) Å]. In this transformation, zinc has retained one ethyl arm, and the metal's coordination sphere is completed by a chelating molecule of TMEDA, rendering its geometry distorted tetrahedral [N31-Zn-N34 85.17(5), N34-Zn-C21 113.06(6), N34-Zn-O1 97.48(5), N31-Zn-O1 96.21(5), N31-Zn-C21 114.99(6), O1-Zn-C21 137.14(6)], the sum of these internal angles being 644.05°, with the greatest deviation from tetrahedral (Δ 27.64°) occurring in the O1-Zn-C21 angle. As with the previous magnesium example, this zinc anthacenolate **2f** exists as a monomer.
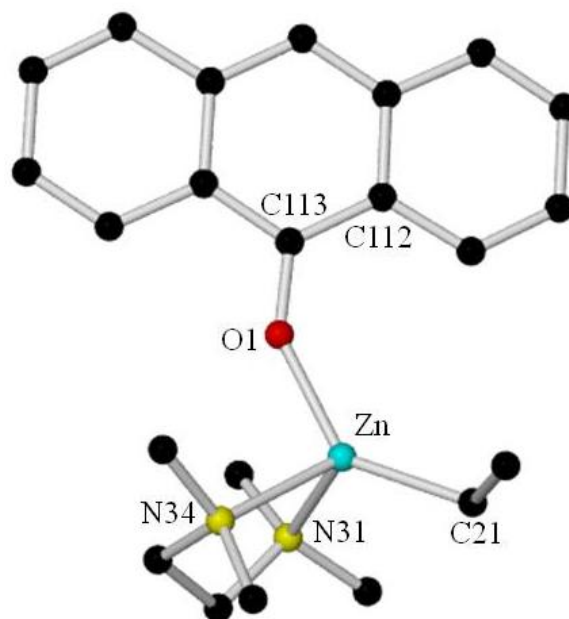
Fig. 2.9: Molecular structure of **2f**. Hydrogen atoms have been omitted for clarity. Selected bond distances (Å) and bond angles (°): Zn-O1 1.924(12), Zn-C21 1.988(17), Zn-N31 2.144(13), Zn-N34 2.173(13), N31-Zn-N34 85.17(5), N34-Zn-C21 113.06(6), N34-Zn-O1 97.48(5), N31-Zn-O1 96.21(5), N31-Zn-C21 114.99(6), Zn-O1-C113 147.48(11).

2.7   NMR spectroscopic studies of complex 2b

The good solubility of complexes **2b-2f** in C_6D_6 solution allowed multinuclear NMR spectroscopic studies (^{1}H and ^{13}C) to be conducted. These spectra suggest the solution structures of the alkali metal anthracenolate salts (**2b-2d**) are simple and match well with their respective solid-state structures. For instance, focusing on **2b**, the methyl signals of the TMEDA ligand appear as a singlet integrating to 12 H atoms, at 1.43 ppm, followed closely by the TMEDA CH_2 H atoms at 1.29 ppm. Both these resonances appear markedly upfield compared to the respective H atoms of the 'free' TMEDA ligand (2.12 and 2.36 ppm respectively). Five signals attributed to the aromatic H atoms anthracenolate ligand are also evident. A doublet appears furthest downfield, indicative of the C_1 protons (**Figure 2.11**) at a value of 9.04 ppm. A second doublet represents the hydrogen atoms attached to the C_4 carbons, at a chemical shift of 8.05 ppm. A singlet representing the single unique H atom C_5 at 7.67 ppm and the final almost equivalent resonances corresponding to the four C_2/C_3 protons are observed as triplets at 7.42 ppm and 7.47 ppm respectively, completing the ^{1}H NMR spectrum.
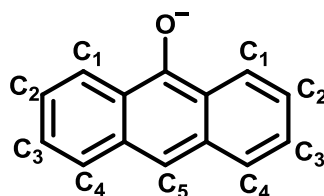
Fig. 2.10: Numbering of the anthracenolate anion
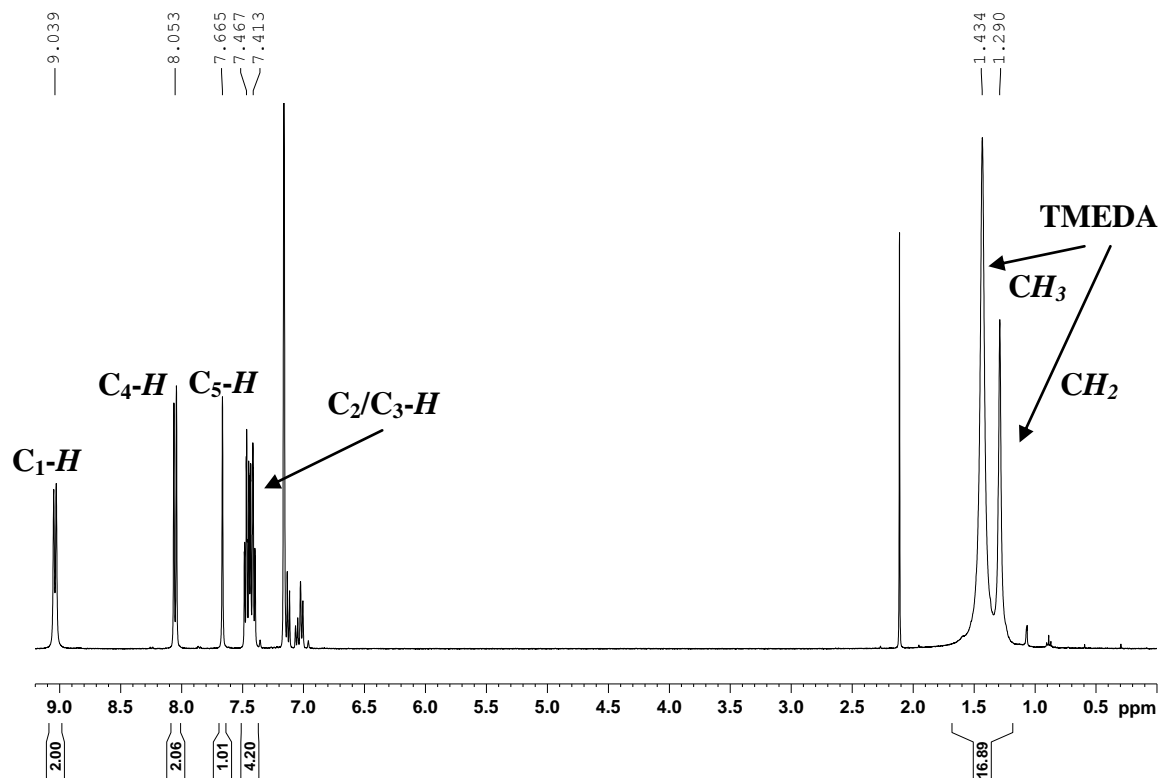
Fig. 2.11: ^{1}H NMR spectrum of compound **2b** in C_6D_6 solution.

The ^{13}C NMR spectrum (**Figure 2.12**) of **2b** is in good agreement with that of the ^{1}H NMR spectrum. Moving around the ring we observe first a shift at 124.6 ppm, corresponding to the atom C_1, followed by shifts of 120.0 and 125.6 ppm for atoms C_2 and C_3 respectively, followed by the most significantly downfield shifted C_4 atom, with a resonance at 129.0 ppm. Located in a unique position between both rings, the somewhat anomalously placed C_5 atom exhibits a pronounced upfield resonance of 106.3 ppm. Counterpointing this signal is the C-O resonance, located by comparison at a value 135.9 ppm. The values for the TMEDA ligand resonances appear at 56.5 (CH_2) and 44.9 (CH_3) ppm.
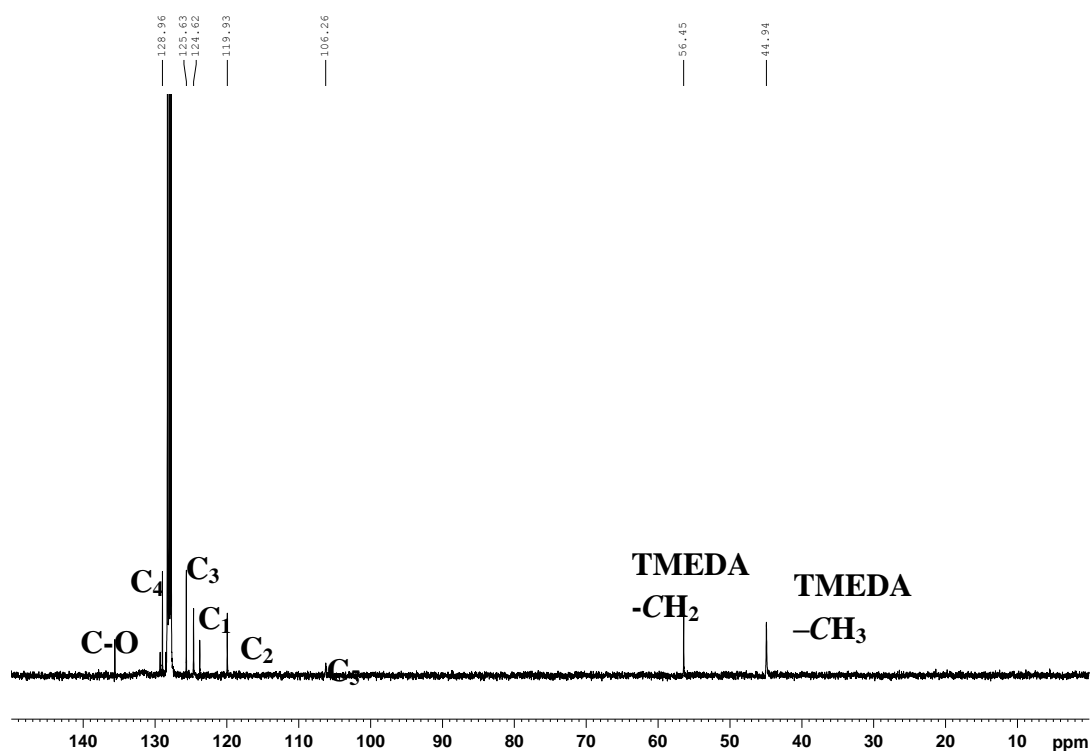
Fig. 2.12: ^{13}C NMR spectrum of compound **2b** in C_6D_6 solution.

The relationship between both the ^1H and ^{13}C aromatic signals for **2b** can be observed more clearly by its 2D HSQC spectrum (**Figure 2.13**).
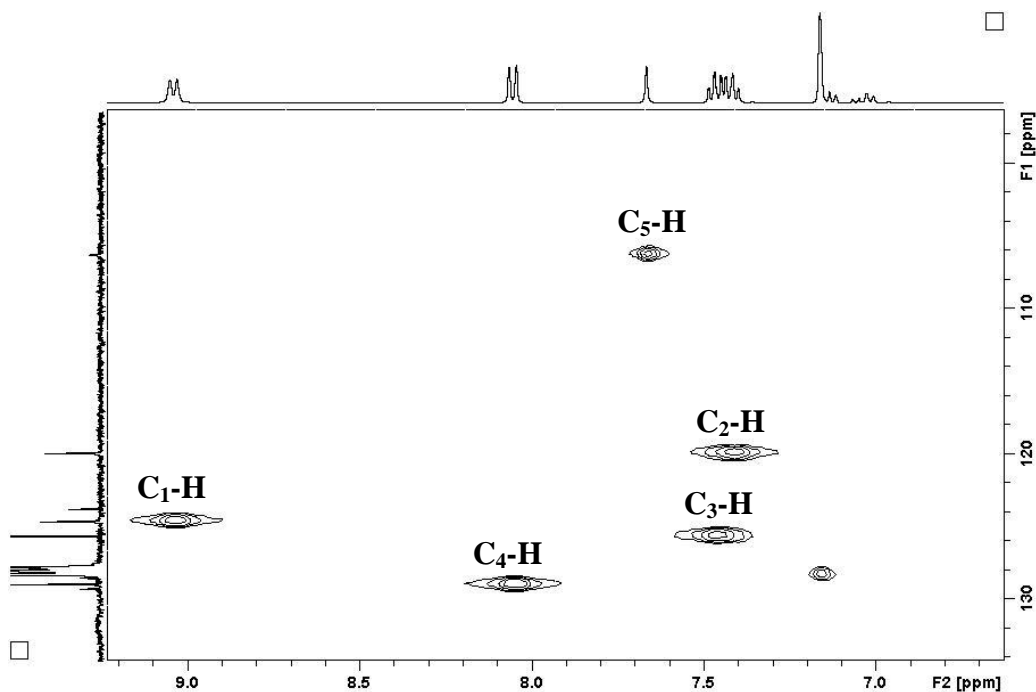
Fig. 2.13: HSQC (^1H, ^{13}C) spectrum of **2b** in C_6D_6 solution (Expanded aromatic region).

45

2.8   NMR spectroscopic studies of complex 2d

The ^{1}H and ^{13}C NMR shifts for **2c** and **2d** essentially mirror those of **2b**. Complex **2d**, being slightly less soluble in C_6D_6 was also studied in d_8-THF solution, mirroring the spectra seen previously (signals are amplified), and with inevitable displacement of the PMDETA ligand and total upfield shift of the resonances associated with the aromatic portion of the molecule, a consquence of new predominating THF coordination (**Figure 2.14**). Beginning with the signal at C_1, it appears to exhibit in the ^{1}H spectrum the most significantly downfield shifted resonance, with a doublet at a value of 8.66 ppm. Moving around the ring, the signals C_2 and C_5 appear as overlapping and virtually coincident, at value of 6.94 and 6.91 ppm respectively. The signals at C_3 and C_4 appear at values of 7.13 and 7.58 ppm, as triplets and doublets respeciely. The remaining signals are attributed to the (now free) PMDETA ligand [2.42 (4H, t, CH_2-PMDETA), 2.30 (4H, t, CH_2-PMDETA), 2.15 (12H, s, CH_3-PMDETA(outer)), 2.19 (3H, s, CH_3-PMDETA(central))].
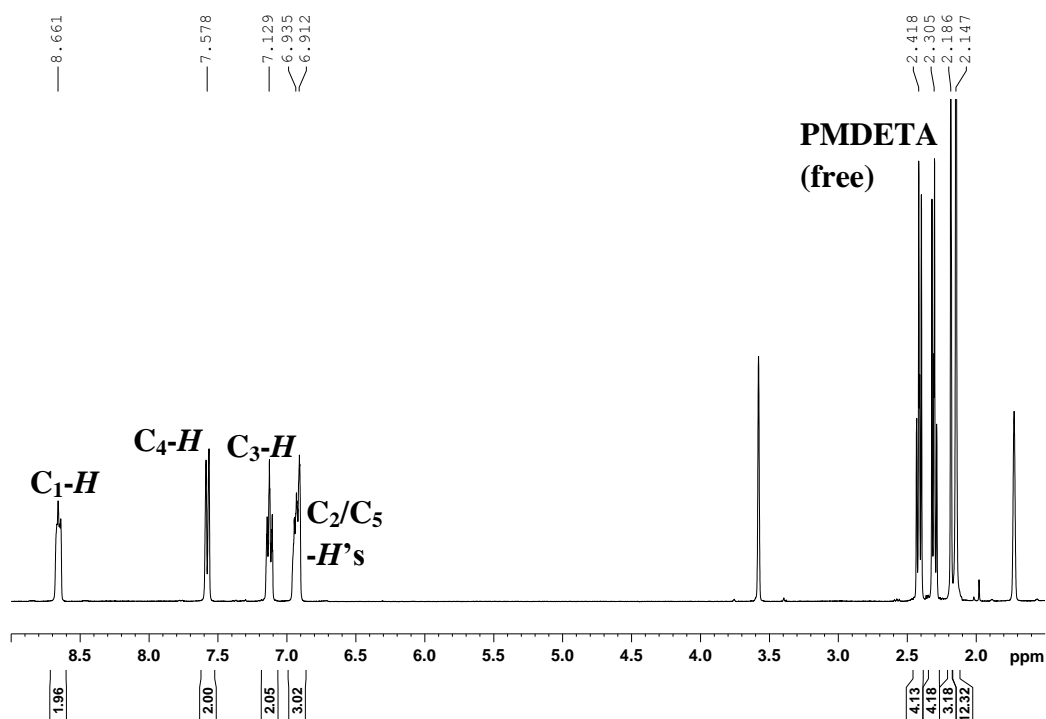
Figure 2.14: Compound **2d** in d_8-THF solution.

The data for each complex **2b-2f** show that reaction of anthrone with an organometallic base results in consequent aromatisation, as evidenced by the significant change in both

the ^{1}H and ^{13}C NMR chemical shifts associated with anthrone *versus* the anthracenolate ligands [most pronounced at C_5 (**Figure 2.12**): In **2b**, respective ^{1}H and ^{13}C NMR shifts are 7.67 and 106.3 ppm, compared with CH_2 in anthrone (3.55 and 32.0 ppm)].

2.9   NMR spectroscopic studies of complex 2e

In the Mg monomer **2e**, detailed solution studies by ^{1}H NMR spectroscopy appear to suggest that the structure is fluxional. The aromatic region follows the same integration pattern as that observed for **2b**-**2d**, with five distinct chemical environments. The resonances associated with the TMEDA ligand are markedly broader than those observed in the previous examples, possibly indicating that the ligand is subject to dynamic exchange. The other notable exception in this spectrum is the inclusion of the *n*Bu arm, still attached to the Mg, giving rise to four sets of signals. The triplet corresponding to the Mg-CH_2 appears furthest upfield at a value of 0.14 ppm, followed by multiplets at 1.86 ppm and 2.18 ppm, which can be attributed to the remaining CH_2's of the butyl group. The final CH_3 signal appears as a triplet at a value of 1.33 ppm.
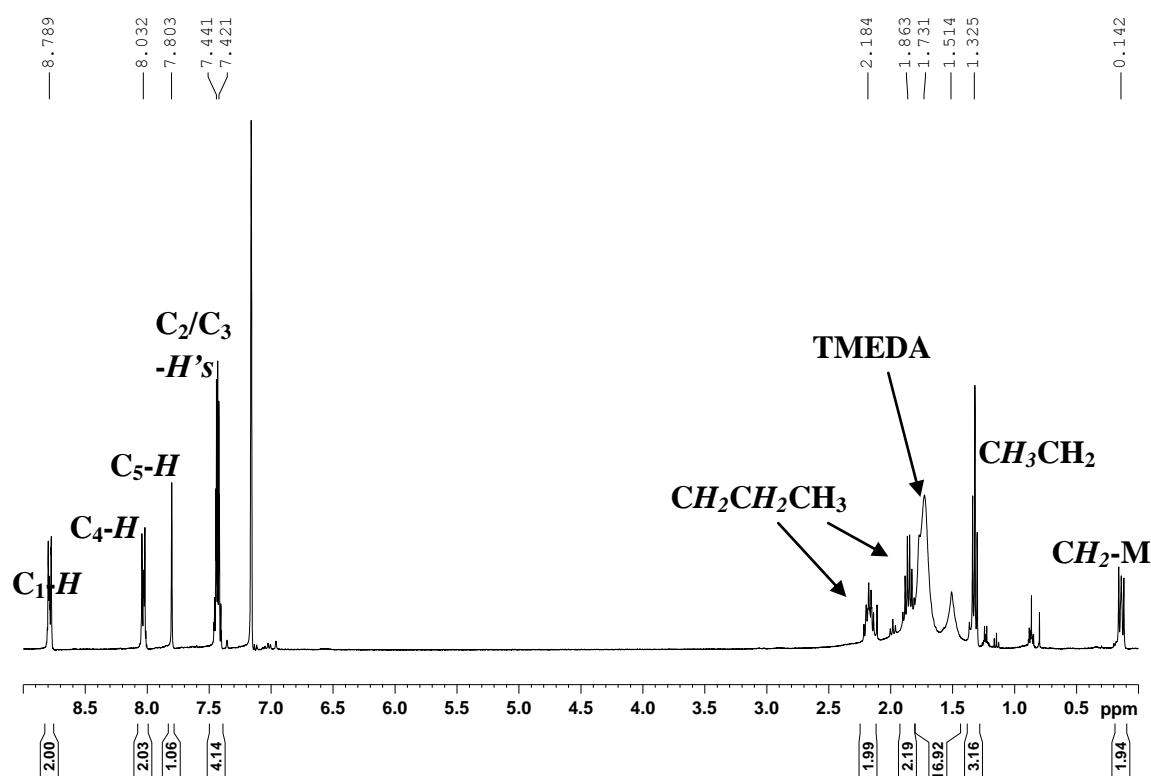
Fig. 2.15: ^{1}H NMR spectrum of compound **2e** in C_6D_6 solution.

2.10   NMR spectroscopic studies of complex 2f at room temperature

The previously mentioned fluxional behaviour of the TMEDA ligand at room temperature is more evident in the solution structure of **2f**. Turning to the aliphatic region, two markedly broad overlapping signals at 1.78 ppm are observed for TMEDA, instead of the usual two distinct signals (**Figure 2.16**). Dynamic TMEDA behaviour of this kind had been previously noted in four-coordinate zinc alkoxide complexes before. In 2010, Hevia *et al* reacted zinc species of the type (TMEDA)ZnR$_2$ (R=Me, Et, ^{t}Bu) with 2, 2, 2 –trifluoroacetophenone, affording carbonyl addition products of the respective R group (**Scheme 2.3**).[107]
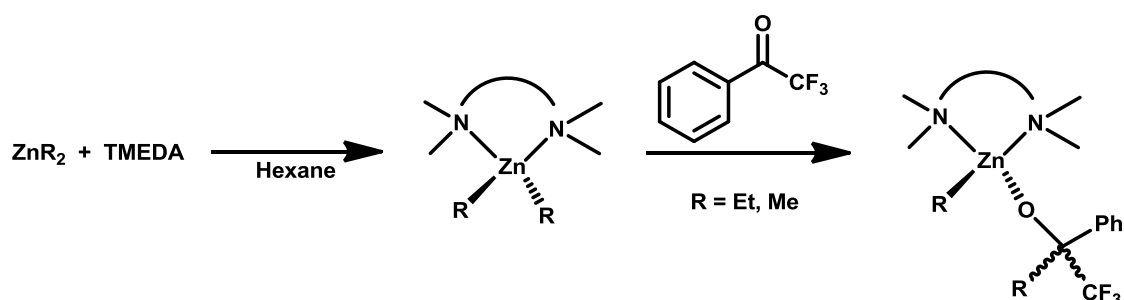
Scheme 2.3: Addition of TMEDA.ZnR$_2$ to trifluoroacetophenone.

NMR spectroscopic analysis at room temperature of the methyl adduct revealed a broad hump, attributed to the TMEDA, a coalescence of all resonances. At high temperature (80°C) the usual 12:4 ratio for methyl and ethyl groups respectively was achieved. They noted however that as you decreased the temperature of the sample to -35°C, the TMEDA split up into 8 signals, showing each methyl group as spectroscopically distinct and different, and similarly each of the four protons residing on the ethyl backbone as distinct multiplets.
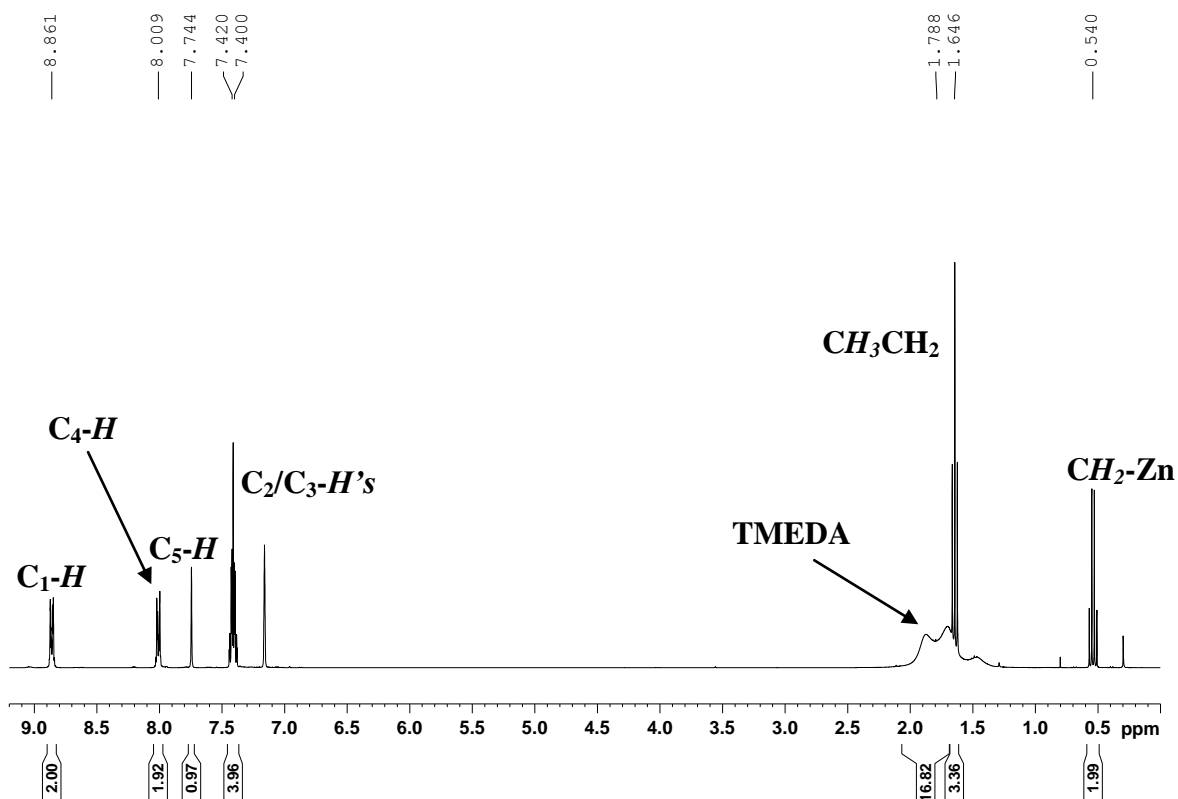
Fig. 2.16: ^{1}H NMR spectrum of compound **2f** in C_6D_6 solution.

2.10.1 Variable temperature NMR spectroscopic studies of complex 2f

In order to probe our own sample **2f** further and better understand the behaviour of the TMEDA ligand, variable-temperature NMR spectroscopic studies were undertaken, over the range of 353 K to 223K (in 10K increments). At higher temperatures (from 313 to 353K) TMEDA appears in its usual two environments in a 12:4 Me:CH_2 ratio, indicating that two distinct chemical environments for the CH_2 (four H atoms) and CH_3 (twelve H atoms) are observed. On lowering the temperature, the resonances gradually broaden and at 303K only one resonance is discernible presumably due to hindered, slow rotation of the TMEDA ligand.
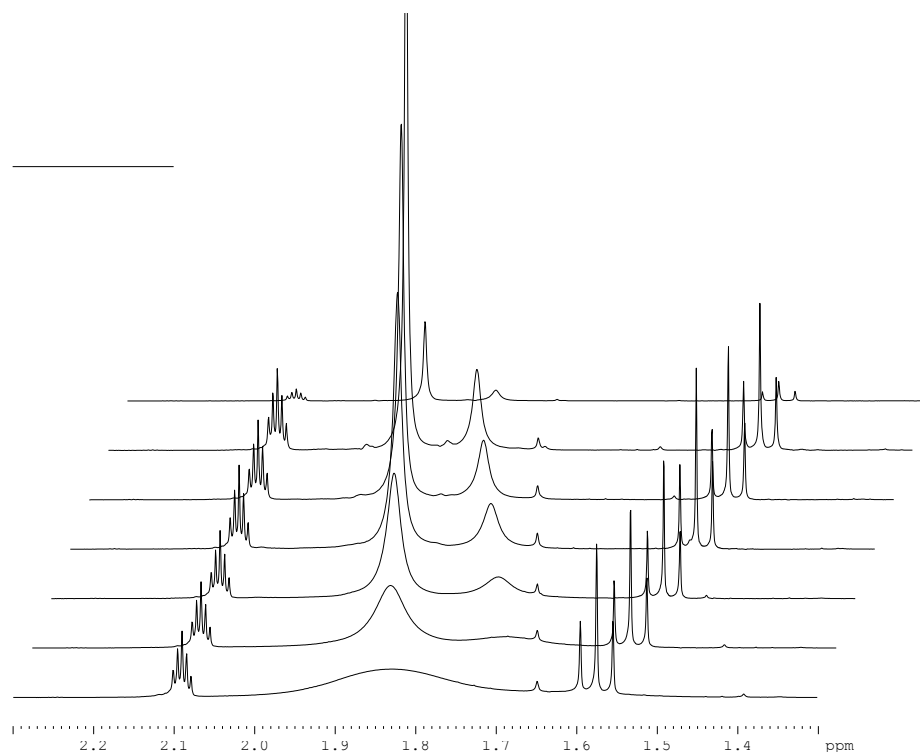
Fig. 2.17: Variable temperature ^{1}H NMR study of **2f** in d_8-tol. Between temperature range 353 K (top spectrum)-293 K (bottom spectrum).

At temperatures below 293K, the signals appear to sharpen again; however, two new resonances appear. These four resonances correspond to two distinct methyl, and two distinct methylene-CH_2 groups. As a consequence, the TMEDA ligand appears to the mimic the situation observed in the solid state. To elaborate, at 283K, a broad resonance at 1.47 ppm is clearly visible, assigned to a CH_2 group. The TMEDA methyl signals have now split into two singlets (1.90 and 1.69 ppm), each integrating to six H atoms. The most upfield of these methyl resonances overlaps with the second CH_2 resonance (1.74 ppm). As the temperature is gradually decreased, the appearance of the resonances associated with the CH_2 groups is more pronounced. The TMEDA CH_3 and CH_2 resonances all drift upfield as the temperature is decreased from 283K. The other resonance (attributed to CH_3CH_2Zn) experiences a marked downfield shift from 1.61 (at 303K) to 1.78 (at 223K).

50
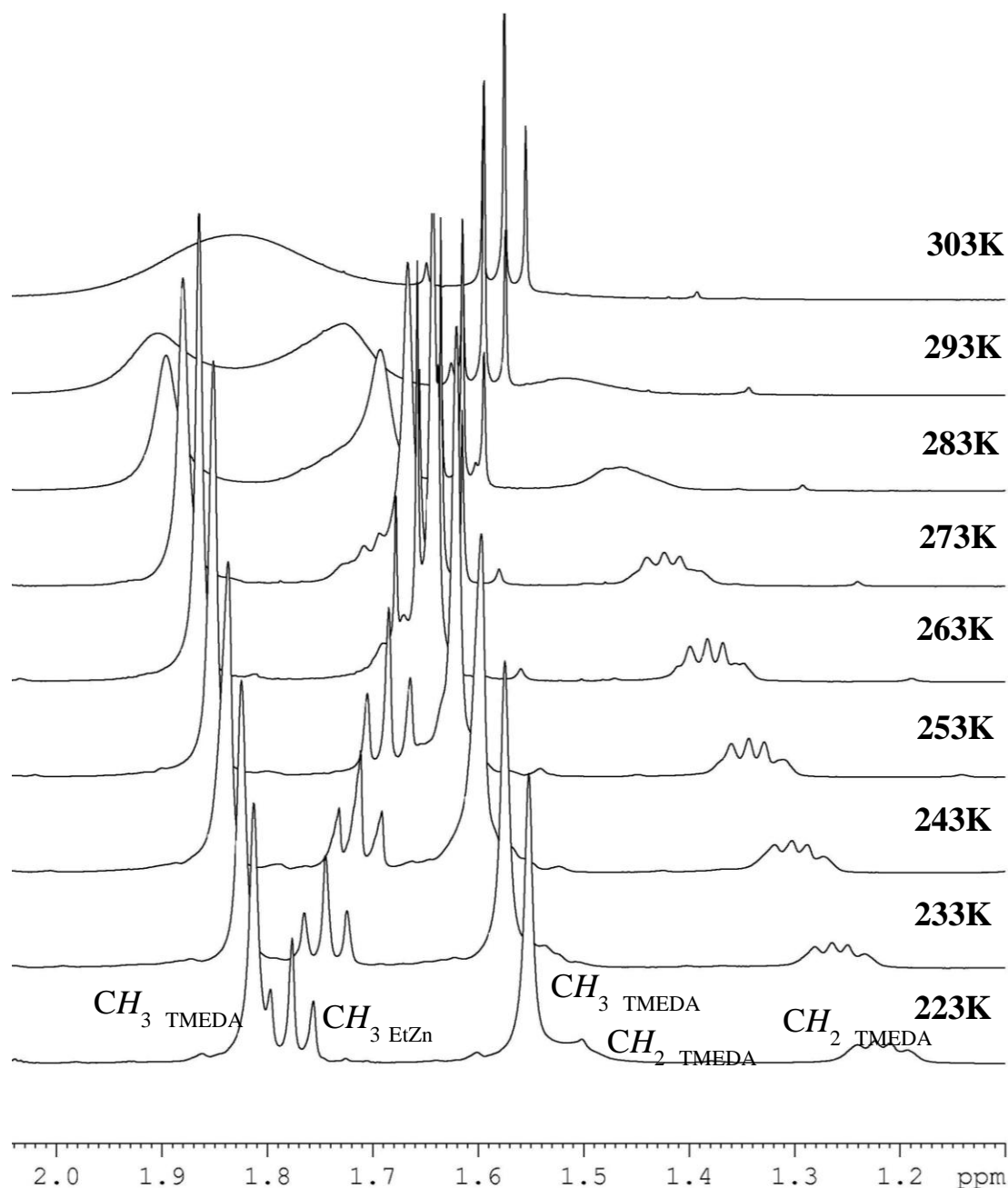
Fig. 2.18: Variable Temperature ^{1}H NMR study of **2f** in d$_8$-tol (temperature range 223-303 K).

Having seen in the past how the zincate [(TMEDA)·Na(μ-TMP)(μ-^{t}Bu)Zn(^{t}Bu)] could anomalously add a ^{t}Bu group to the six position of benzophenone (with respect to the oxygen atom) in hexane at room temperature, this result was deemed an ideal starting point to probe the generality of this type of alkylation, otherwise unachievable unless carried out by the more aggressive ^{t}BuLi in THF at -100°C. The tricyclic ketone anthrone was first selected, containing a position of enhanced acidity (*i.e.* sp^{3} centre between phenyl rings) and this reacted the same sodium zincate. The dimeric species

51

[(TMEDA)$_2$·Na$_2$(C$_{14}$H$_9$O)$_2$] was isolated invariably, containing only sodium, a product proposed to occur via a CH$_2$ deprotonation and subsequent fragmentation pathway, and which could be produced rationally by the reaction of (TMEDA)·BuNa with anthrone. A number of different sodium zincate and magnesiate combinations were then reacted with our ketone, but discovered in every instance only the homometallic sodium dimer could be crystallographically characterized. The analogous lithium and potassium zincates [(TMEDA)·Li(μ-TMP)(μ-Et)Zn(Et)] and [(PMDETA)·K(μ-TMP)(μ-^{t}Bu)Zn(^{t}Bu)] were then utilised under identical conditions, but in each instance the sodium situation was directly mimicked, forming time and again the respective homodimers [(TMEDA)$_2$·Li$_2$(C$_{14}$H$_9$O)$_2$] and [(PMDETA)$_2$·K$_2$(C$_{14}$H$_9$O)$_2$]. In order to ascertain whether zinc or magnesium containing anthracenolates were achievable, the comparitively weak monometallic bases (TMEDA)·Mg^{n}Bu$_2$ and (TMEDA)·ZnEt$_2$ were employed, and noted that deprotonation in the same position by a single basic arm had occurred, allowing us to isolate the monomeric species [(TMEDA)·Mg(C$_{14}$H$_9$O)(^{n}Bu)] and [(TMEDA)·Zn(C$_{14}$H$_9$O)(Et)]. In the duration of this project, we were unable to obtain a mixed metal species containing the anthracenolate anion, but the complexes produced have provided a platform for further studies, which could include reactions of different stoichiometries, different temperatures, or even indirect formation of mixed metal species by addition of a homometallic alkali metal reagent (*e.g.* BuLi, NaTMP) to either a magnesium or zinc monomer. Since a position of such enhanced acidity exists with anthrone, it is perhaps unlikely that addition could take place preferentially over deprotonation in a 1:1 reaction, but a systematic study of different stoichiometries could reveal either polymetallation or dual addition/metallation modes of reactivity as plausible outcomes, both of which these bimetallic reagents have shown themselves able to carry out in the past.

3. Accessing unusual substitution patterns of fluorenone and 2-benzoylpyridine *via* sodium alkylamidozincate intermediates

3.1   Introduction

Arguably the simplest, yet indispensible member of the diarylketone family is benzophenone (Ph$_2$C=O), which, although in itself it has shown worth as a building block for many important organic molecules, alone it functions as an important photosensitizer,[108] photoinitiator[109] and additive in packaging etc. Functionalization of this species then is an object of real importance to the synthetic chemist. Due to the polarised nature of the carbonyl group, reactions of benzophenone with traditional organometallic reagents more often than not yield products dictated by the electronics of the molecule i.e., addition products, as benzophenone containins no H atoms of enhanced acidity. In 2001, for instance, Richey utilised several organolithiums to this effect (even reaction with functionalised benzophenones), and subsequent quenching with H$_2$O furnished only alcohols born of 1, 2 – addition products (**Figure 3.1**).[110]

	X	Y
a	H	H
b	H	Me
c	H	CF$_3$
d	F	H
e	Cl	H
f	H	Cl
g	OMe	H
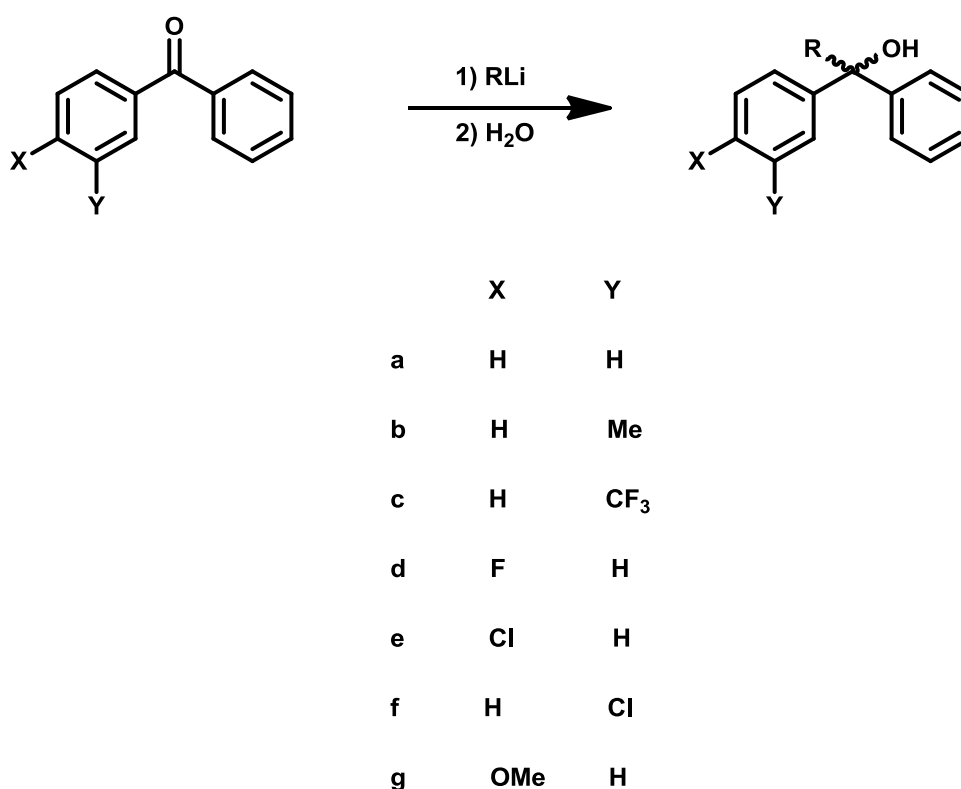
Fig. 3.1: Alkyl addition and electrophilic quenching of benzophenone derivatives.

Even formation of these 1, 2- adducts and subsequent tertiary alcohol formation is not so trivial a task. To this end, alongside alkyllithium reagents, alkylzincs and Grignard reagents are often put to use, though again not without complications. Dialkylzinc reagents alone can be generally ignored as without the inclusion of a common ligating group such as TMEDA, their inherently poor reactivity negates any kind of chemical usefulness in achieving such an addition.[111] Focusing instead on both alkyllithium and Grignard reagents, their comparatively reactive natures give rise to competitive reactions and thus associated side products. Included in these are formation of the desired adducts, and side products generated by both β-hydride transfer of alkyl groups and unwanted aldol reactions (**Figure 3.2**).[112]
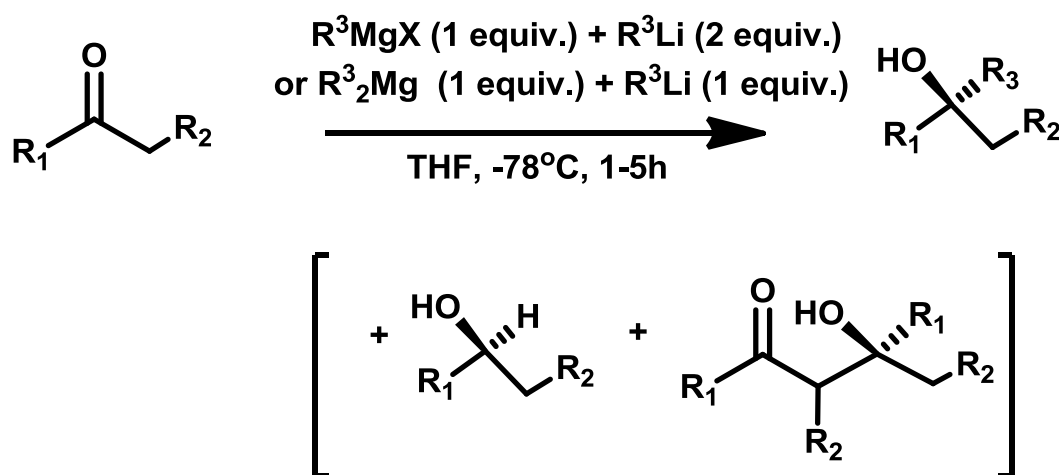
Fig. 3.2: Ketone alkylation with alkyllithium and magnesium species

It has been recently proved possible however to circumvent such products by complimentary addition of excess LiCl to the Grignard reagents, thus facilitating alkylation of ketones smoothly whilst simultaneously minimising side product formation; a process achieved by formation of so called "Turbo-Grignard" reagents.[113]

Whilst the strongly polarised C=O bond present in benzophenone does indeed make 1, 2 addition the most likely position of attack with traditional alkyllithiums and Grignard reagents, there have been several notable exceptions.

3.1.2 Alkylation of benzophenone by [(TMEDA)·Na(^{t}Bu)(TMP)Zn(^{t}Bu)]

Recent developments, although precipitating great improvements in yields and reaction rates for alkylations of cyclic ketones, have done little to overcome the draw of the strongly electrophilic carbonyl carbon. One such example, prepared by Mulvey *et al* in 2005 provides just such an atypical example, whereby benzophenone is alkylated directly in a 1, 6 - fashion.[114] Previously mentioned as a powerful deprotonating agent, able also to participate in metal-halogen exchange, the scope of the synergic base [(TMEDA)·Na(^{t}Bu)(TMP)Zn(^{t}Bu)] **2a** was extended to participate in nucleophilic additions. **3a** was prepared first by suspension of 1 mmol BuNa (0.08g) in 10 ml hexane, to which was added an equimolar amount of TMP(H) (0.17 ml). This was then stirred for approximately one hour, forming NaTMP with concomitant release of butane gas. In a second Schlenk tube, ^{t}Bu$_2$Zn (1mmol, 0.18g) was likewise dissolved in hexane solution, then added via cannula into the first Schlenk tube. A single equivalent of TMEDA (1 mmol, 0.15 ml) was added, and subsequently stirred for approximately 30 minutes, completing the base. Upon reaction of molar equivalents of both benzophenone and the sodium zincate, the corresponding enolate of a 1, 6- adduct (**Figure 3.3**) was trapped and stabilised in an isolable crystalline yield of 60%.
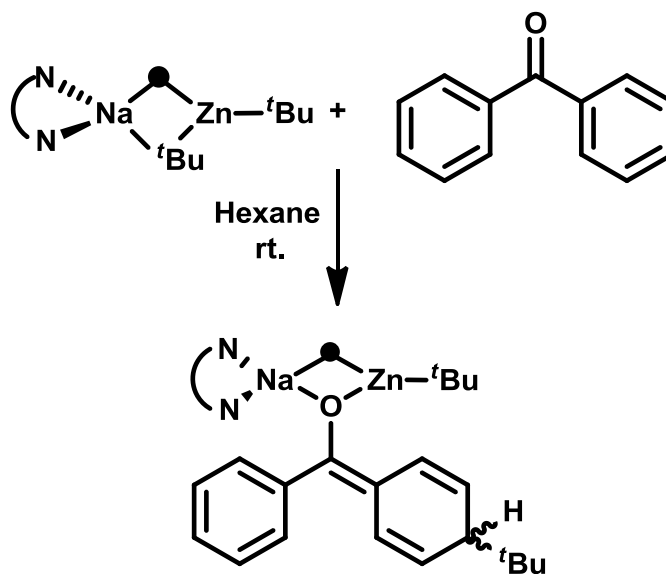
Fig. 3.3: Formation of 1, 6 – adduct **3a** by reaction of **2a** with benzophenone.
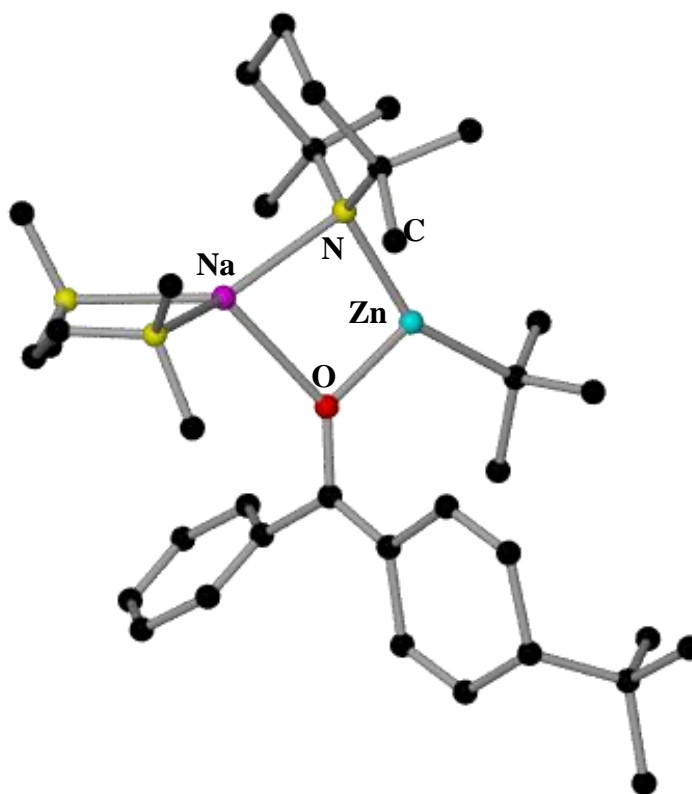
Fig. 3.4: Molecular structure of **3a** (H atoms have been omitted for clarity).

Rationale for this apparent anomaly is placed on the fact that the substituted phenyl ring lies towards the ^{t}Bu-Zn-O portion of the molecule, sterically less demanding than the region bearing Na and TMEDA. Selectivity such as this seems unique in these bimetallic systems, as "the participation of two distinct metals leads naturally to an asymmetry within structures/ transition states that can influence (at best, dictate) the selectivity of nucleophilic addition."

3.1.3   Functionalization of fluorenone

With the potential then for these bimetallic reagents as architects of nucleophilic addition cemented, the task was undertaken to probe the generality of this reaction, and find to what extent this effect could be replicated when applied to other cyclic ketones. Having systematically explored the reactivity of our bimetallic bases with the tricyclic ketone anthrone, we turned our attention to a related substrate, namely 9-fluorenone.
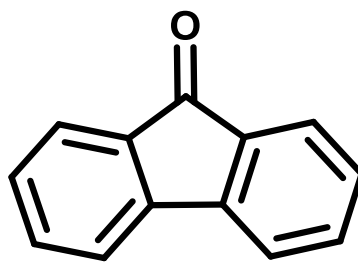
Fig. 3.5: 9-fluorenone

This substrate shares more chemical similarities to benzophenone than anthrone, the only real structural difference being a C-C bond linking both phenyl rings where previously there was none, creating a central five membered ring. This has the effect of keeping each ring held rigid, hindering any opportunity for rotation and forcing planarity. The fluorenone unit presents itself as the core structure for many important organic molecules, such as the natural products dengibsin and dengibsinin.[115] Fluorenone related drugs have also shown themselves as exhibiting potent anti-malarial[116] and anti-tumour properties.[117]

Synthesis of functionalised fluorenones has presented itself as synthetically challenging, with present syntheses almost all involving functionalising prior to ring cyclization, often requiring multiple steps. A recent study undertaken by Cheng *et al*, involves the reaction of aromatic aldoxime ethers with aryl halides. Initially, these reactions involve C-H activation facilitated by a palladium catalyst, followed by oxidative Heck cyclization to yield the final fluorenone derivatives (**Scheme 3.1**). It has also been shown that functionalised fluorenones can be synthesised beginning with the parent biaryls, then using an intramolecular Friedel-Crafts acylation, the desired compound formed.[118] Snieckus and co-workers have also produced a number of fluorenone deriatives via their directed metallation methodologies.[119]

Previously reported syntheses involved some prior functionalization and final cyclization to achieve a final product, with none, to the best of our knowledge, involving direct functionalization of the parent fluorenone molecule, which can be purchased cheaply from many chemical suppliers. In achieving this we sought to utilise the same methodology effective in alkylating benzopheneone.
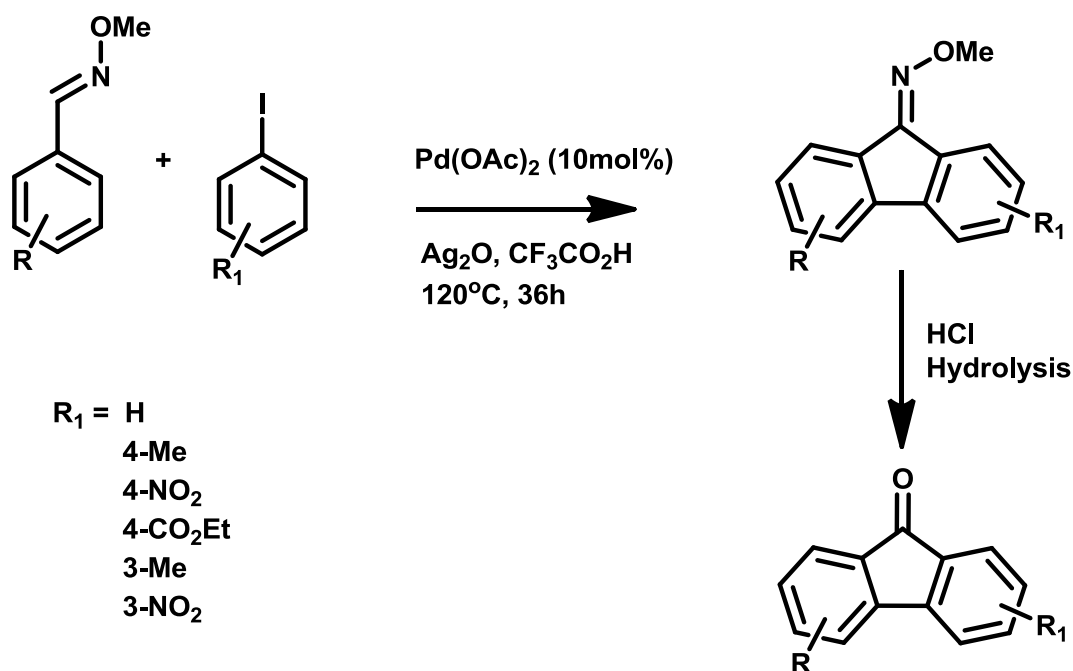
Scheme 3.1: Oxidative Heck cyclization and oxidation.

3.2   Reactivity of 2a towards fluorenone

A stoichiometric amount of 9-fluorenone was reacted with the synergic base **2a** at room temperature and left stirring in hexane for 30 minutes. After removal of a small amount of solvent *in vacuo* the remaining deep red solution was placed overnight in the freezer, yielding a small crop of yellow crystals. Structural elucidation of this compound revealed not a product of deprotonation but addition. The 1, 6- adduct observed for benzophenone also occurred for fluorenone (**Figure 3.6**).

3.3   Crystallographic   studies   of   [TMEDA.Na{μ-OC(Ph)(4-^{t}Bu-C$_6$H$_4$)}(μ-TMP)Zn(^{t}Bu)] 3b

The sodium zincate has added across fluorenone in a 1, 6- fashion, whereby the O atom of the new enolate system is sandwiched between the Na and Zn atoms, and a ^{t}Bu group has been transferred to C3 (labelled C20 in **Figure 3.6**) of the fluorenone group, forming a new C-C bond and causing disruption of aromaticity in the fluorenone unit. The enolate anion is bound in turn to both Na and Zn atoms, bridged doubly by this and the N atom of the TMP, forming what can be roughly described as a near planar four element ring comprising four different atoms. The sum of the internal angles totals 359.93°. The Zn exists in a trigonal planar coordination, with the remaining ^{t}Bu group

still bound to it at a short distance of 1.995(3) Å. The backbone of the original zincate is still essentially intact, orientated in a near perpendicular fashion to the fluorenone portion of the molecule. The C-O bond in moving from double to single bond character has elongated to 1.32(3) Å (typically 1.23 Å for carbonyl compounds), a value in good agreement with the analogous benzophenone example (1.34 Å).
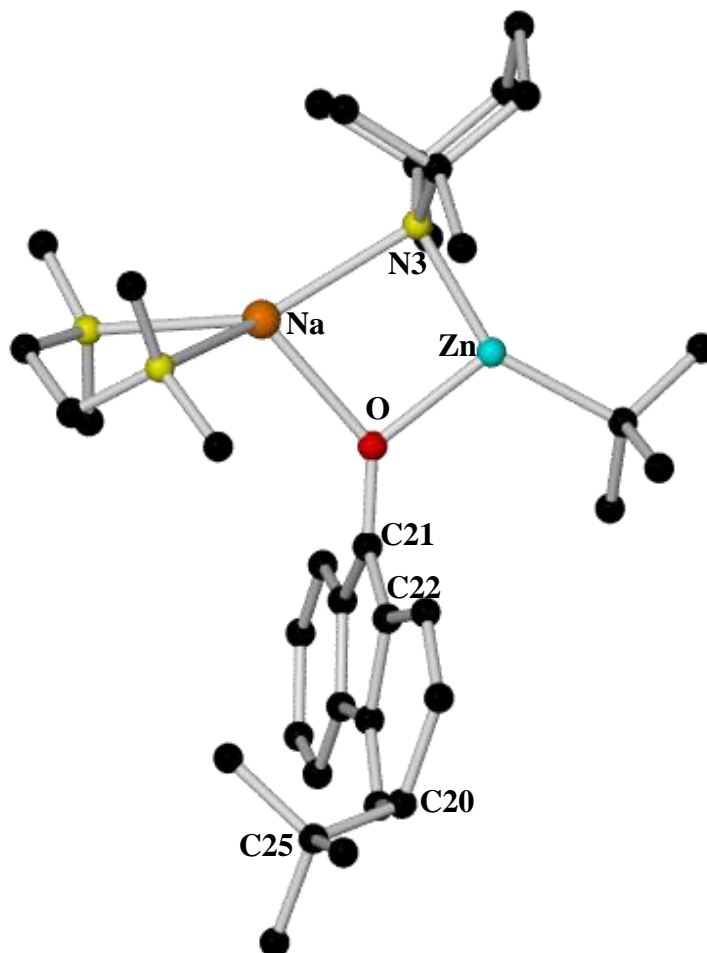
Fig. 3.6: Molecular structure of [TMEDA.Na{μ-OC(Ph)(4-^{t}Bu-C$_6$H$_4$)}(μ-TMP)Zn(^{t}Bu)] **3b**.

An important structural difference between the two is the effect of the C-C bond joining both phenyl rings. In **3a**, the rings are puckered following disruption of aromaticity. The ring facing the O-Na-N portion of the molecule *i.e.*, the most sterically encumbered part is orientated towards the Na atom, maximising the number of stabilising π interactions. In the fluorenone example, planarity is retained [deviations of C23, C24, C25 and C26 from the plane defined by the five C atoms of the central ring are 0.168(6), 0.183(7), ⁻0.089(7) and ⁻0.014(6) Å respectively], and both rings orientated almost perpendicular

to the Na-O-N-Zn ring. The plane of the fluorenyl ligand in **3b** adopts a perpendicular stance between the two metal centres [dihedral angle between NaNZnO ring plane and that of the 5-membered ring is 82.95(9)°], thus not favouring one metal over the other. The crystalline material also revealed the ^{t}Bu group attached to the ring to point in a single direction *i.e.*, a stereocentre is generated. The ^{t}Bu group protrudes from its adjoining sp^3 carbon on the sodium side of the molecule and the loss of aromaticity in the six-atom ring is evident due to the alternate short and long bond distances [C21–C22, 1.375(4); C22–C23, 1.442(4); C23–C24, 1.353(4); C24–C25, 1.523(5); C25–C26, 1.516(5); C26–C27, 1.335(4); C27–C28, 1.473(4) Å] consistent with localized C–C bonding. The unsubstituted ring of fluorenone remains aromatic as gauged by the similarity of the C29–C210, C210–C211 and C211–C212 bond distances [range 1.377(4)–1.386(4) Å]. The Na-O distance is 0.22 Å longer than the corresponding Zn-O distance, accounted for by the larger Na atom size.

	Bond length (Å)		Bond angle (°)
Na - N3	**2.442(3)**	**Na-N3-Zn**	**90.19(10)**
Na - O	**2.242(2)**	**N3-Zn-O**	**96.75(9)**
Zn-N3	**1.951(2)**	**Na-O-Zn**	**94.49(9)**
Zn-C1	**1.995(3)**	**N3-Na-O**	**78.5(8)**
Zn-O	**2.018(2)**	**C1-Zn-N3**	**148.4(13)**
C21-O	**1.316(3)**	**C1-Zn-O**	**114.81(12)**
C21-C22	**1.374(4)**	**N3-Na-N41**	**133.5(11)**
C25-C20	**1.544(5)**	**N44-Na-N3**	**141.72(10)**

Table 3.1: Selected bond lengths and angles for compound **3b**.

3.4   NMR spectroscopic studies of 3b

Characterisation of this species in solution was achieved by a variety of NMR spectroscopic techniques. The ^{1}H NMR spectrum in C_6D_6 revealed that the solid state structure appeared to be retained in solution.
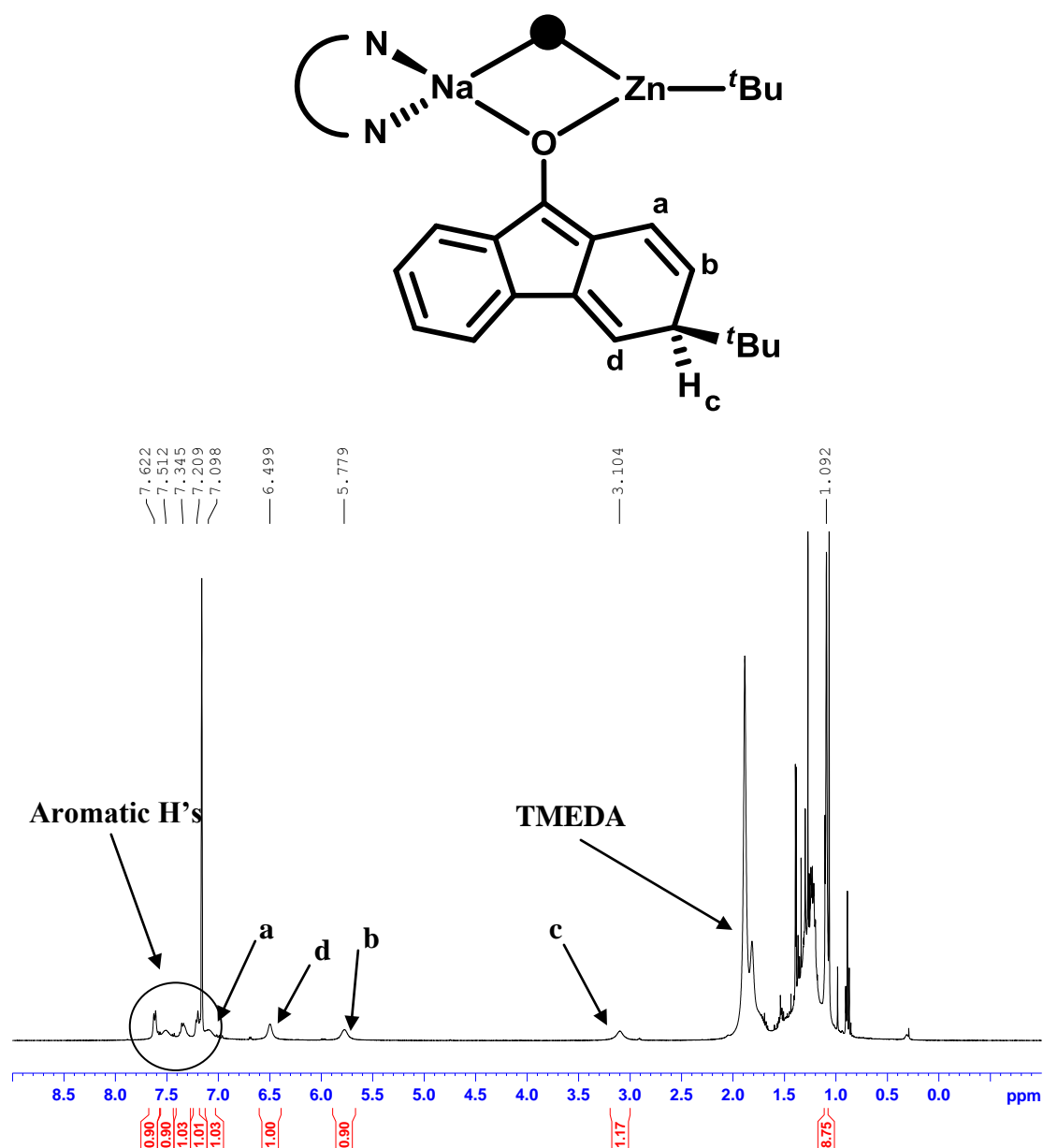
Fig. 3.7: ^{1}H NMR spectrum (in C$_6$D$_6$) of compound **3b**.

Following disruption of aromaticity after nucleophilic addition, the number of signals attributed to aromatic protons is diminished, giving rise to a number of vinylic and allylic H atoms associated with the newly substituted ring. A broad singlet appears at 3.10 ppm corresponding to the proton attached to the carbon which is also bound to the newly attached ^{t}Bu group. This ^{t}Bu group appears at 1.09 ppm as broad singlet. The remaining hydrogen atoms attributed to the dearomatized ring fall at 5.78 ppm (**b**), 6.50ppm (**d**) and 7.10 (**a**), each appearing as broad singlets. The TMEDA signals appear at 1.89 and 1.82 ppm, upfield of values obtained for some related structures.

This sample was then quenched with D_2O, trapping the deuterated enol species. This time, the peaks in the aromatic region have sharpened, elucidating their previously indistinct nature. Two doublets, corresponding to the proton peri- to the oxygen, and the proton three positions from this on the same ring are observed. Completing the aromatic region are two distinct triplets, indicative of the remaining aromatic protons, adjacent to one another.
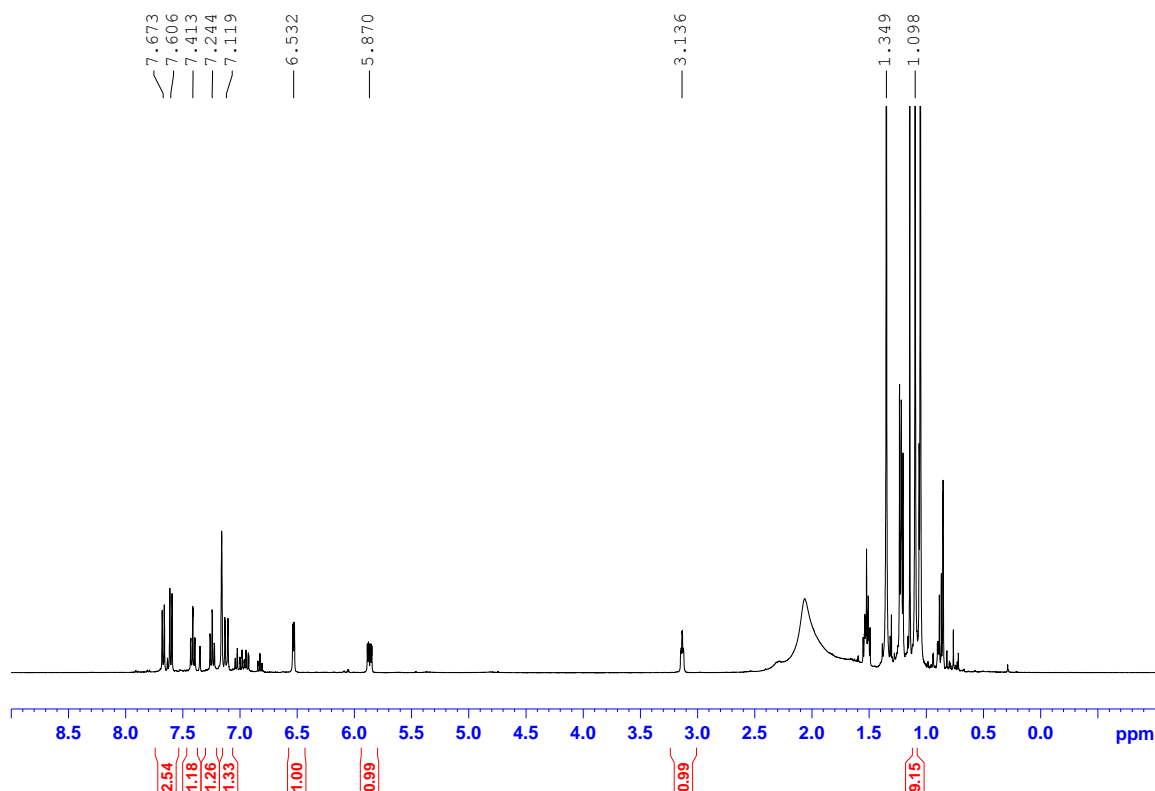
Fig. 3.8: Complex **3b** quenched with D_2O after 10 minutes (in C_6D_6).

The purpose of this quench, other than to establish the existence of the enolate species in solution as a certainty, was revealed after the sample was left exposed to air for 3 days. Owing to the thermodynamic instability of the enolate species, oxidation readily occurs in the presence of atmospheric oxygen, resulting in DH elimination with concomitant generation of the *tert*-butylated fluorenone species (**Scheme 3.2**).
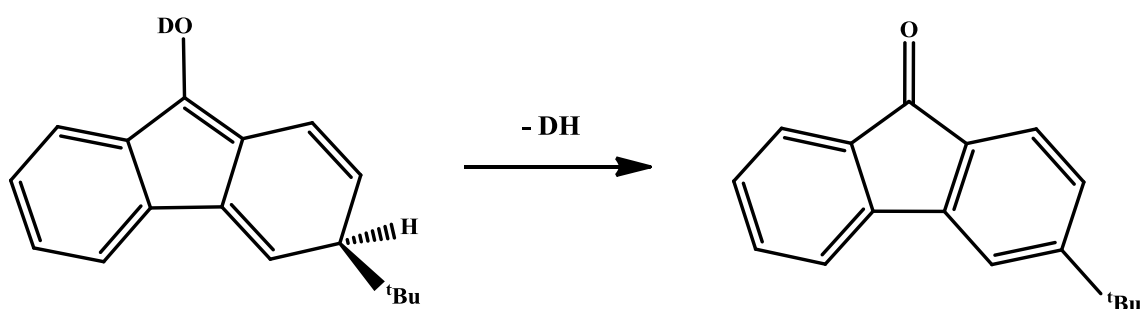
Scheme 3.2: H_2 elimination and enolate oxidation.

Examination of the ^{1}H NMR spectrum taken three days later reveals the existence of this proposed oxidation species. The first notable difference between these spectra, is the disappearance of protons attached to the functionalised ring, previously dearomatized (3.14, 5.87, 6.53 and 7.12 ppm), and subsequent increase in aromatic signals, integrating to a total of seven protons, the number expected for the newly formed ketonic species.
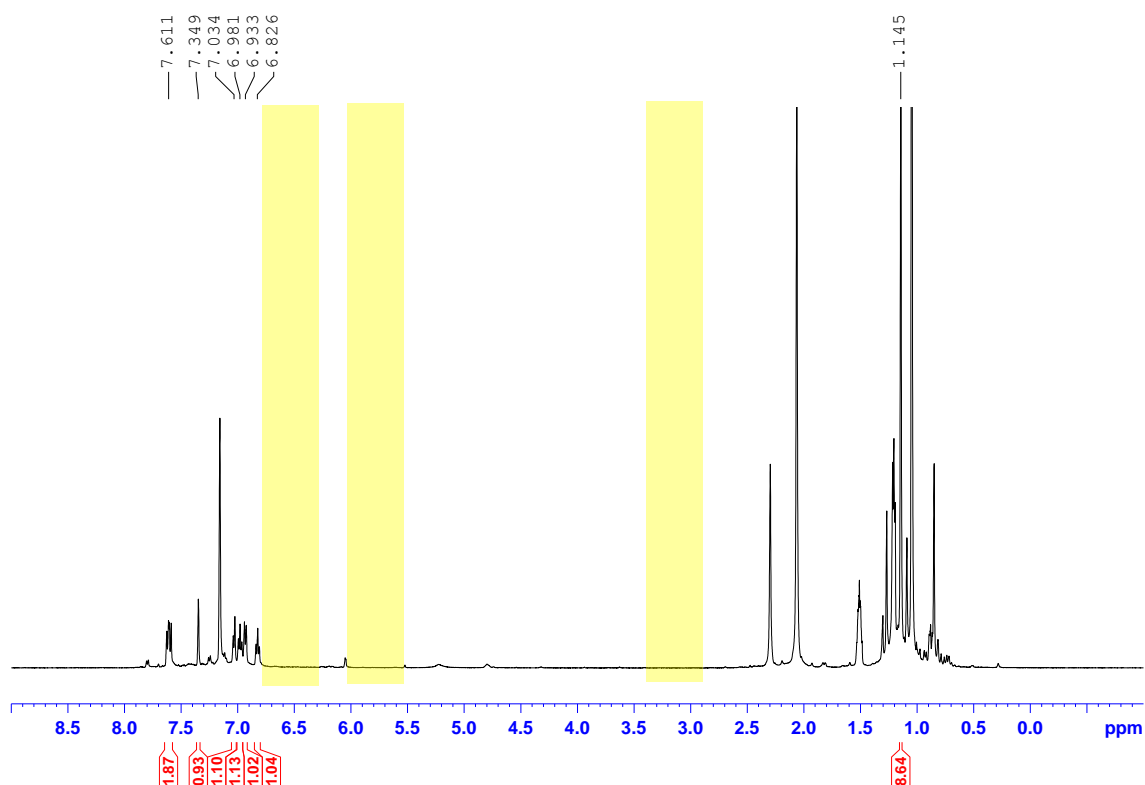
Fig. 3.9: Complex **3b** quenched with D_2O after 3 days (in C_6D_6) (Regions in yellow denote absence of signals attributed to deromatised product).

The appearance of a singlet at 7.35ppm is indicative of the proton located between the [t]Bu group and C-C bond bridging both rings, now no longer coupled to any other H

atoms. Overlapping doublets at an average of 7.61 ppm correspond to the protons again peri to the carbonyl group on the unfunctionalised ring, and the proton 3 carbon atoms away. Triplets at 6.98 and 6.83 ppm represent the two remaining protons of this ring, adjacent to one another. The remaining doublets belong to the two remaining protons of the *tert*-butylated ring, neighbouring one another. Evidence in support of ketone formation is found in comparison of the ^{13}C NMR spectrum of quenched both species. In the spectrum of the initially formed enolate species, no peak above 160 ppm is observed. Comparing this with the carbon spectrum taken three days later, and we see a clear peak at 192 ppm, a significantly downfield shift, indicating with some certainty the presence of a carbonyl carbon. Definitive formation of this *tert*-butylated ketone at the 6- position, represents the first direct alkylation of its kind on the fluorenone molecule, a result the scope of which it is our desire to extend.

3.5 Electrophilic quenching studies of zincate 2a with fluorenone

It is perhaps unsurprising that isolated crystalline material of **3b,** when reacted with D$_2$O, gives exclusively the 1, 6- deuterated enolate adduct, followed by ketone formation. What is less straightforward is the complete picture i.e. what products would be achieved on direct addition of water to the reaction *in situ*, without attempting any crystallisation first. This seemed very important, as in innumerable previous publications, it is shown that the compound crystallised rarely represents 100% of all those present in the solution, sometimes even only a minor component, or simply the least soluble species in the pot.

One such example, eminently pertinent to this particular discussion, is that of the same sodium zincate **2a** towards the related ketone benzoylferrocene.[120] The inherent difference of this substrate compared with those previously described, is the availability of acidic C-H positions on the ferrocene ring, in turn also in close proximity to the polar C=O anchor connecting both rings. It was discovered that upon reaction and crystallisation, the product obtained was that of both 1, 2- nucleophilic addition and simultaneous deprotonation of the ferrocene ring. This remarkable example shows double activation of the sodium zincate ^{t}Bu arms, with each exhibiting different modes of reactivity (**Figure 3.10**). The downside of this reaction was the modest yield of only 12% crystalline material. ^{1}H NMR spectroscopic studies of the solution revealed only a small number of resonances associated with the characterised species. Instead, the

predominant product appeared to be attributed to a series of signals between 3 and 7 ppm. When further studies in order to trap the metallated intermediate with I_2 were conducted, the true nature of product distribution was uncovered. The expected iodinated tertiary alcohol was isolated from the crude mixture along with the 1, 6- addition product, similar to those mentioned in the previous examples, in yields of 29 and 24% respectively. Further studies finally proved the 1, 6- addition product to be the dominant species present in the reaction.
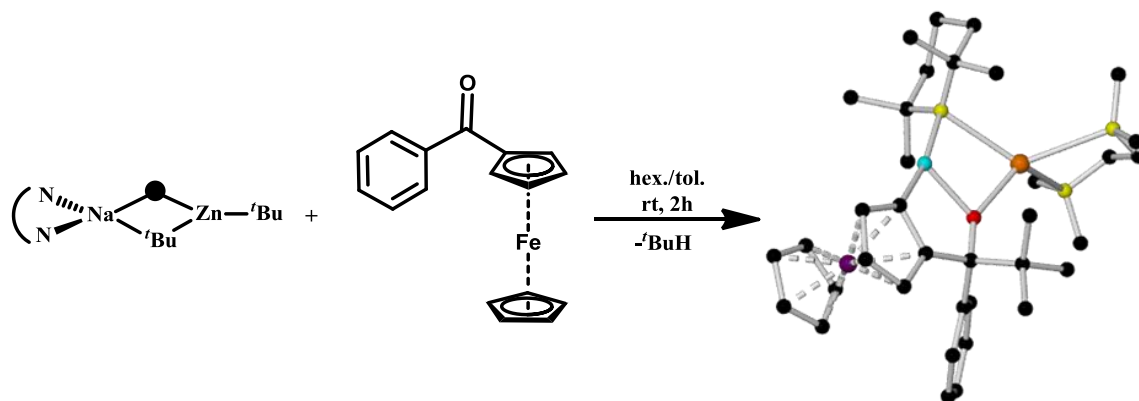
Fig. 3.10: Reaction of sodium zincate **2a** with benzoylferrocene.

These studies nicely parallel our own in terms of utilising **2a** as an alkylating agent towards fluorenone. The reaction was performed as before, except this time after reacting for one hour, an aqueous solution of NH_4Cl was added. After work up, the crude oily solid produced was analysed by ^{1}H NMR spectroscopy (**Figure 3.11**).
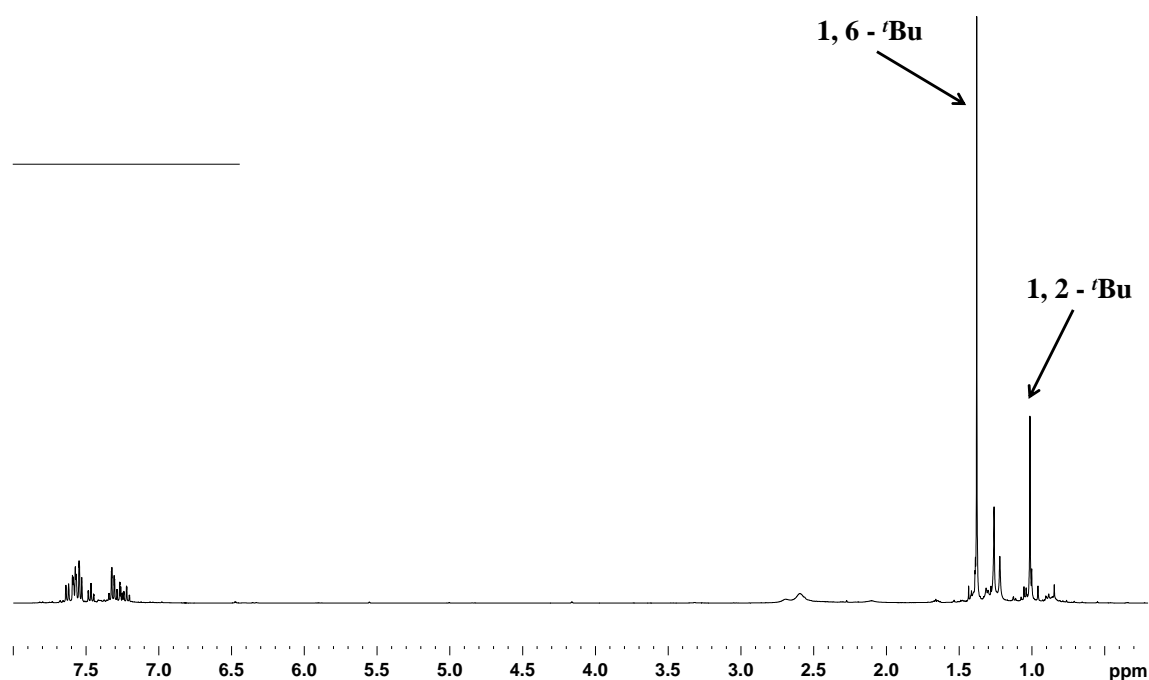
Fig. 3.11: ^{1}H NMR spectrum of crude reaction mixture.

The spectrum showed an overlap of signals, pertaining to two major species, with apparent total consumption of starting material. To elucidate the identity of both species, the crude mixture was separated via a silica gel column, with only hexane used as the eluent; so soluble were these compounds, that even the slightest increase in solvent polarity (>99:1 hexane: ethyl acetate), caused significant co-elution in a very short period of time. They were identified as the both the major 1, 6- (59 %, isolated product) and minor 1, 2- (17 %, isolated product) with no evidence of the reduction product fluoren-9-ol. The ^{t}Bu shifts of both the ring substituted ketone, and tertiary alcohol appear at 1.38 and 1.02 ppm respectively. The OH signal of the alcohol appears at 1.98 ppm.
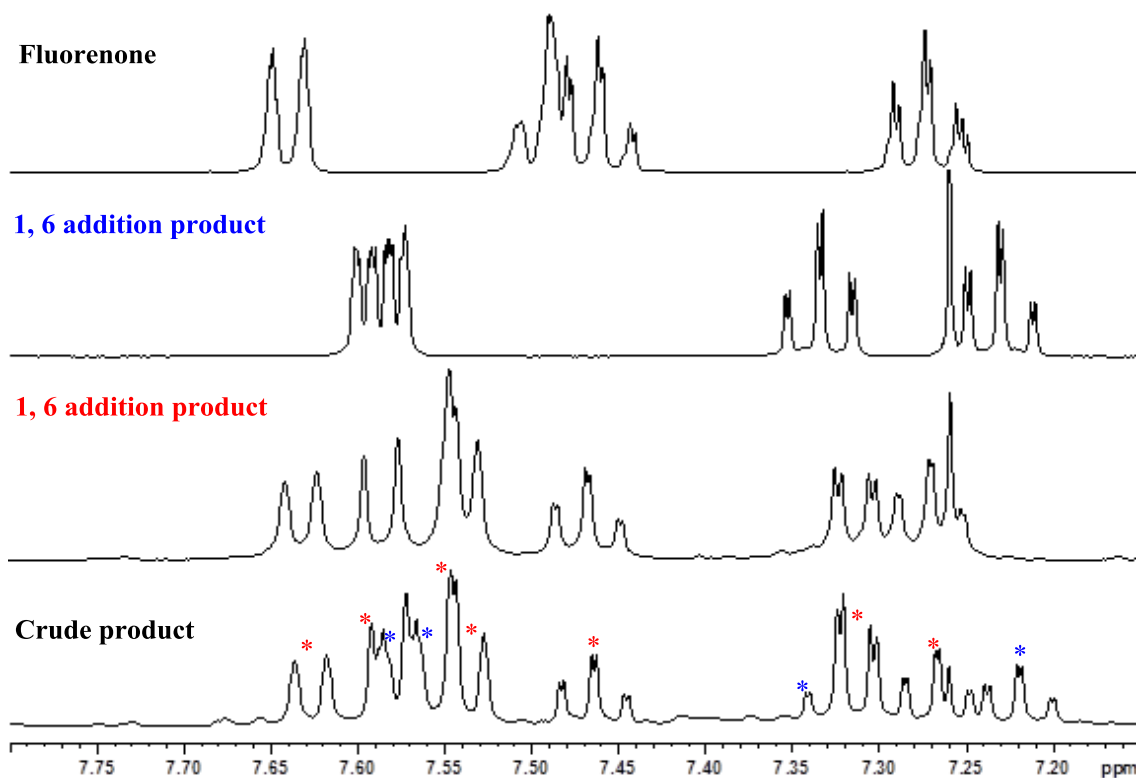
Fig. 3.12: Stacked plot of crude mixture (bottom), 1, 6- addition product (second, red asterisk), 1, 2- addition product (third, blue asterisk), fluorenone (top).

Based on the work previously reported by Holm and Crossland,[121] Olah [122] etc., they discovered that simple addition of water and air oxidation to reform the ketone after reaction of benzophenone with ^{t}BuLi resulted in diminished yields of the desired product, with a competitive decomposition pathway possible, whereby butane is expelled from the enolate species preferentially over H_2 (**Scheme 3.3**).
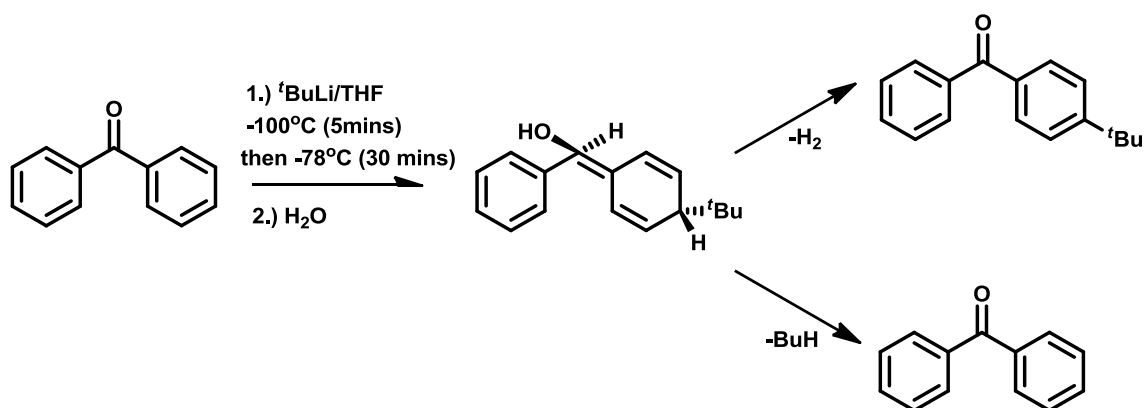
Scheme 3.3: Different oxidation pathways of *tert*-butylated benzophenone.

They resolved this issue by first oxidising the lithium enolate species, forming the *tert*-butylated benzophenone, followed by aqueous workup. This they achieved using the powerful oxidising agent thionyl chloride (SOCl$_2$). In order to see the effect this would have on our own systems, we reacted **2a** with fluorenone under identical conditions, except this time first treated the solution with excess SOCl$_2$ for three hours prior to aqueous workup. The result was an increased yield of 3-*tert*-butyl-9*H*-fluoren-9-one, with subsequent decrease of 1, 2- addition observed.
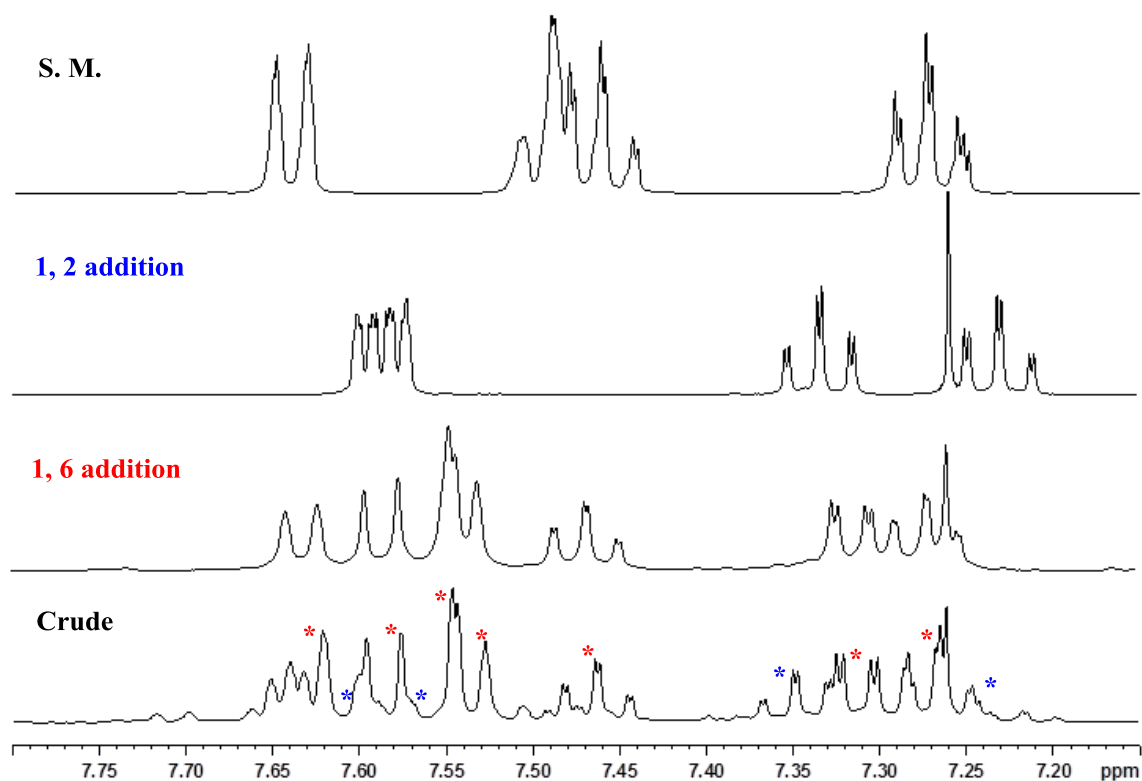
Fig. 3.13: Crude reaction mixture of fluorenone + **3b** (CDCl$_3$) with SOCl$_2$ oxidation after aqueous workup.

3.6   Reaction of [(TMEDA)·Na(μ-HMDS)(μ-*^{t}*Bu)Zn(*^{t}*Bu)] with fluorenone

In order to ascertain further the generality of these bimetallic zincates as agents of addition, we substituted the bulky TMP(H) ligand to the related, yet far less sterically demanding utility amine HMDS(H). Solid NaHMDS (1 mmol, 0.188g) was suspended in 10 ml hexane, and to this added equimolar equivalents of ^{t}Bu$_2$Zn and TMEDA, forming a clear, pale yellow solution. After a few minutes, fluorenone was added, turning this solution deep red almost immediately. Subsequent overnight cooling at -28ºC afforded a crop of yellow crystals, of suitable quality for X-ray analysis. Gratifyingly, we discovered that alkylation had again been achieved in the 6 position

(relative to the O atom), with replacement of a single ^{t}Bu ligand by a newly formed enolate anion.

3.7 Crystallographic studies of [(TMEDA)·Na{μ-OC(Ph)(4-^{t}Bu-C$_6$H$_4$)}(μ-HMDS)Zn(^{t}Bu)] 3c
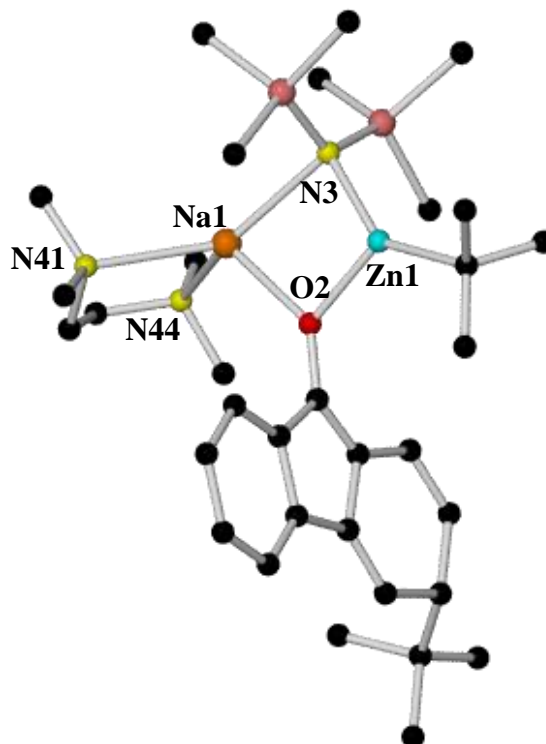
Fig. 3.14: Molecular structure of **3c**. Key bond distances (Å) and angles (°): Na1-O2 2.227(2), Na1-N3 2.361(12), Na1-N41 2.437(3), Na1-N44 2.510(3), Zn1-C1 1.980(4), Zn1-O2 2.016(2), Zn1-N3 2.038(8), 1.323(4), O2-Na1-N3 81.1(2), O2-Na1-N41 110.53(11), N3-Na1-N41 139.5(2), O2-Na1-N44 120.49(10), N3-Na1-N44 132.52(15), N41-Na1-N44 141.4(3), C1-Zn1-O2 115.87(14), C1-Zn1-N3 149.1(4), O2-Zn1-N3 94.8(3), C21-O2-Zn1 128.66(19), Zn1-O2-Na1 94.28(9).

This structure retains many similar features of the related complex **3b**, including the four membered Na-N-Zn-O ring. The Na is still, as expected, four coordinate, bound datively to and pinioned between both N atoms of the TMEDA ligand. There is no real demonstrable difference in the bond distances (Å) within this central ring as a consequence of diminished bulk in the bridging amine [(Na1-O2 2.227(2), Na1-N3 2.361(12), Zn1-O2 2.016(2) and Zn1-N3 2.038(8) Å] in **3c** *c.f.* [(Na1-O2 2.242(2), Na1-N3 2.442(12), Zn1-O2 2.018(2) and Zn1-N3 1.951(8) Å] in **3b**. As before, both ^{t}Bu ligands point towards opposing faces of the molecule, minimising any steric interference. The difference this time with the bridging amine having greater freedom of

movement, is that the methyl groups turn away from the metal centres, and as such exhibit far longer carbon-metal distances than that of the corresponding TMP complex. The shortest C_{HMDS}-Na and C_{HMDS}-Zn distances are 3.566 Å and 3.172 Å respectively, whereas the more sterically constrained environment engendered by the TMP ligands sees these related C_{TMP}-Na and C_{TMP}-Zn distances shorten to 3.342 Å and 2.831 Å respectively. The Na atom is again in a distorted tetrahedral geometry, with the most severe deviation from true tetrahedral observed in the N41-Na1-N44 angle [141.4 (3) °, Δ= 34.4°].

3.8 Electrophilic quenching studies of [(TMEDA)·Na(µ-HMDS)(µ-^{t}Bu)Zn(^{t}Bu)]with fluorenone

We then quenched this reactive intermediate with water in order to ascertain the ratio of different products in solution, showing a direct comparison to the analogous reaction with **2a**. After workup, the crude mixture was dried *in vacuo* and analysed via ^{1}H NMR spectroscopy prior to separation by silica column chromatography.
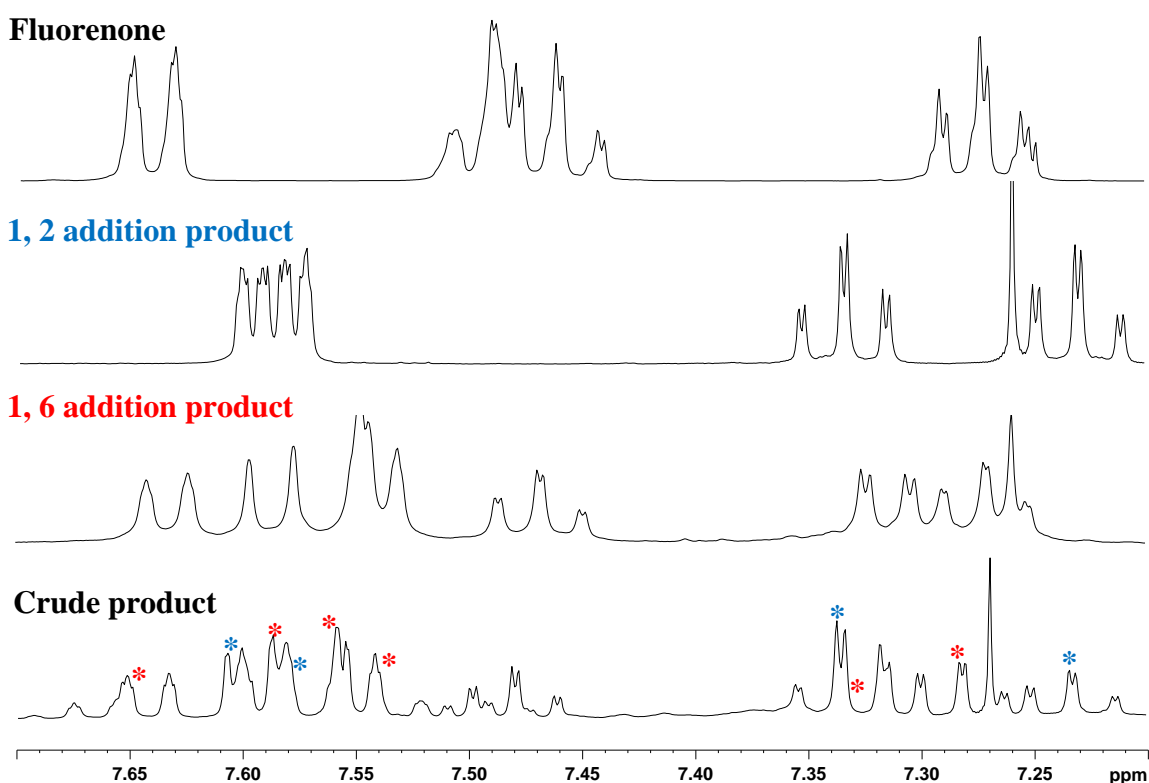
Fig. 3.15: ^{1}H NMR spectrum of crude reaction mixture of Fluorenone + [(TMEDA)·Na(HMDS)Zn(^{t}Bu)$_2$] after aqueous workup.

It was found that both 1,6 and 1, 2 addition products could also be achieved by switching the bridging amine to HMDS, with with respective isolated yields of 57 and 24 %.

3.9 Preparation of [(TMEDA)·Na{μ-OC(Ph)(4-^{t}Bu-C$_5$NH$_4$)}(μ-TMP)Zn(^{t}Bu)] 3d

Next, we turned our attention to the related heterocyclic ketone 2-benzoylpyridine (**Figure 3.16**), a molecule of pharmaceutical relevance, derivatives of which have proven to possess antibacterial and antifungal properties,[123] as well as high cytotoxicity towards leukaemia cells.[124] As is the case with fluorenone, synthesis of functionalised benzoyl pyridine species is no trivial operation.
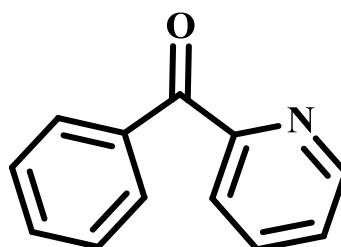
Fig. 3.16: ChemDraw representation of 2-benzoylpyridine

This species was reacted with the synergic base **2a** in hexane at room temperature for approximately 30 minutes. Subsequent cooling for two days in a freezer operating at -27°C yielded a small crop of yellow crystals. Resolution of the crystal structure showed once again a 1, 6 – addition had been achieved, with a ^{t}Bu arm of the sodium zincate adding selectively at the C-3 position of the pyridyl ring. What makes this even more unusual than the previous example, or even the benzophenone example, is that in this molecule there is a site which is greatly favourable in terms of nucleophilic addition. The position α to the N heteroatom is more electropositive than any other on either ring, so if this addition were subject to normal electronic dictates, addition should surely occur here but does not in this case. Normal rules of nucleophilicity are circumvented and again this unusual alkylation takes place (**Figure 3.17**). Addition at the C-3 position is generally only accomplished when this carbon carries a good leaving group. In our system, we can dupe the ligand into conducting a C-3 pyridyl addition since we generate an enolate anion—that is a canonical form where the negative charge still resides on an electronegative atom, this time an O atom.

71

3.10   Crystallographic studies of 3d
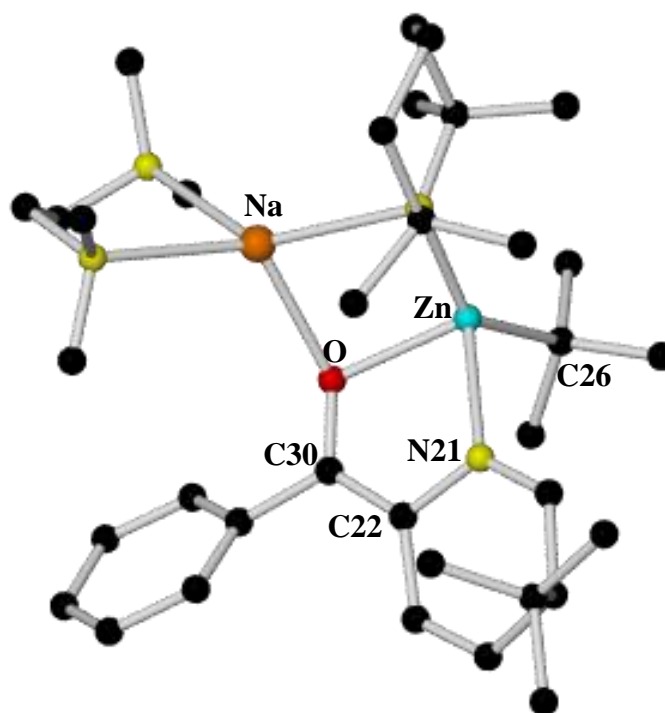
Figure 3.17: Molecular structure of **3d** (H atoms are omitted for clarity).

The familiar four membered ring made up of four disparate atoms (Na-N-Zn-O) is observed, with the Na and Zn atoms doubly bridged, first by the N atom of the TMP, and secondly by the O atom of the newly generated enolate species. The Na is ligated by the TMEDA and the Zn bound to its remaining ^{t}Bu arm. What marks this structure as different and distinct from the previous examples is that this time is that the Zn does not exist in a trigonal arrangement, but rather, due to its close proximity to the N atom of the pyridine ring (2.195Å), forms a dative bond with it, thus its new configuration can be described as distorted tetrahedral. This structure can be considered as possessing three rings attached to one another of increasing size i.e., four membered (Na-N-Zn-O), five membered (Zn-O-C-C-N) and six membered (C_5-N). With the influence of the N atom bound to the zinc, each of the M-O bonds within the four membered ring are elongated compared to the fluorenone example **3b**, with the Na-O distance moving to 2.259(13) Å (cf. 2.242 Å), the Zn-O distance moving to 2.104 Å (cf. 2.018 Å). The Na-Zn distance is relatively unchanged, accounted for by slight distension of bond lengths between the metals and the N atom of the TMP ligand, with subsequent Na-N-Zn angle

contraction to 88.05(6) ^{o} (*cf.* 90.19^o). In keeping with the previous two examples of this 1,6-carbonyl addition, loss of aromaticity in the six-membered pyridyl ring is evident due to alternating short and long bonds (and in this case also C–N bonds).

	Bond lengths (Å)		Bond angles (°)
Na-O	2.259(13)	Na-O-Zn	91.08(5)
Na-N4	2.448(16)	Na-N4-Zn	88.05(6)
Na-Zn	3.116(7)	N4-Zn-O	96.27(5)
Zn-C1	2.043(17)	N4-Na-O	81.20(5)
Zn-O	2.104(12)	O-C30-C22	122.71(16)
Zn-N4	2.103(14)	C30-C22-N21	116.05(15)
Zn-N21	2.195(13)	C22-N21-Zn	108.63(11)
C30-O	1.304(19)	N21-Zn-O	78.17(5)
C30-C22	1.382(2)	Zn-O-C30	112.24(10)
C22-N21	1.407(2)	N21-Zn-C1	99.26(6)
C26-N21	1.286(2)	C31-C30-O	115.44(15)
C20-C25	1.567(2)	C30-O-Na	136.55(11)

Table 3.2: Selected distances and angles within compound **3d**.

Again, the lack of a "bridge" between both rings means that they are again puckered, not held fixed as in the previous example. The ring closest to the Na atom (the phenyl ring) is orientated upwards towards it, maximising any potential π interactions. This effect is most keenly observed when we consider the relative distances between the Na atoms and the C atom adjacent to the carbonyl C on each of these rings. In the fluorenone example, where the phenyl rings are held fixed, the Na-C distance is 4.167 Å, whereas in this 2-benzoylpyridine example, the distance is shortened to 3.946 Å, maximising any possible interactions.

3.11   NMR spectroscopic studies of 3d

The next necessary step was to monitor the behaviour of this species in solution. This was achieved by NMR spectroscopy, and found that it too retained its structure in C_6D_6 (**Figure 3.18**).
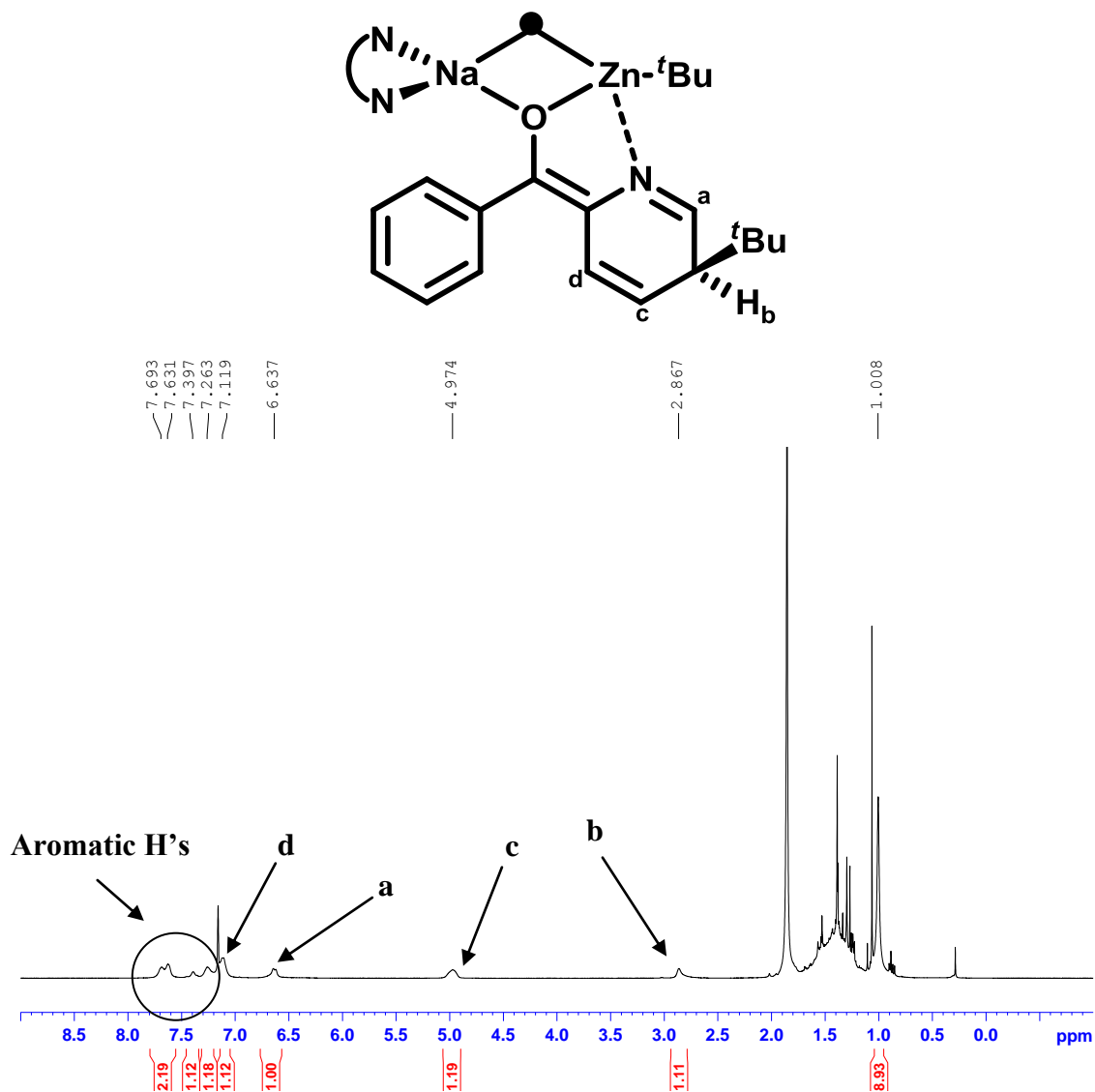
Fig. 3.18: ^{1}H NMR spectrum (in C_6D_6 solution) of compound **3d**.

A broad singlet appears at 2.87 ppm, corresponding to the proton residing on the carbon bearing the ^{t}Bu group of the addition. The methyl protons of this ^{t}Bu are likewise represented by a singlet at 1.01 ppm, integrating to the expected value of 9. As before, alkylation on the pyridine ring has brought about dearomatization, accounting for increased number and upfield shift of the now non-aromatic H-atoms. Of these, the

proton appearing furthest downfield, owing to the δ^+ character of the position α to the heteroatom, is the proton associated with this position, appearing as a singlet at 7.40 ppm. The remaining two protons of the "ex-pyridine" ring appear as singlets at 6.64 (**a**) and 4.97 (**b**) ppm respectively. Owing to overlap and broadness of the aromatic signals in this spectrum, the integration does not correspond exactly, with the benzene signal masking one of the H atoms. Two virtually coincident signals appear 7.69 and 7.63 ppm, corresponding to the positions 2 and 4 of the phenyl ring ("*meta*" signals). The two "*ortho*" protons of this ring appear at 7.12 ppm, with one signal masked by the benzene. The final "*para*" H atom appears at 7.26 ppm, completing the spectrum.

As before, quenching of this enolate species was achieved by using deuterium oxide, and the spectrum recorded after 10 minutes (**Figure 3.19**).
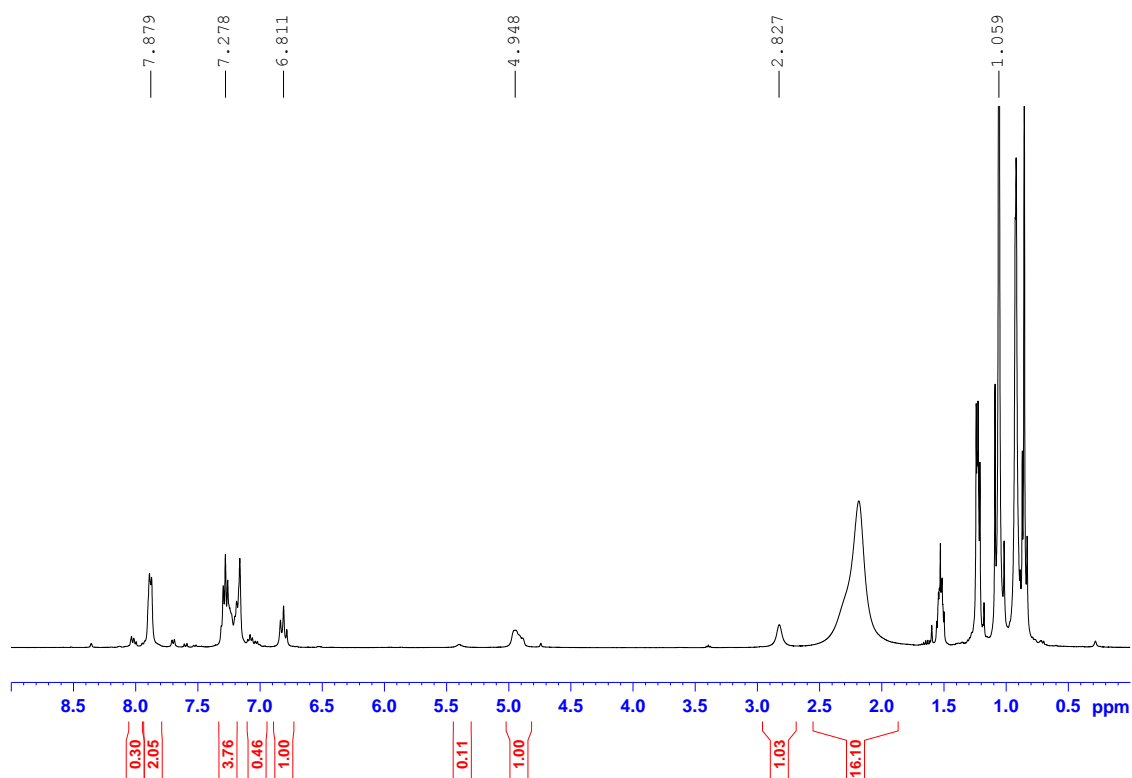
Fig. 3.19: 2-benzoylpyridine complex **3d** quenched by D_2O after 10 minutes (in C_6D_6).

Quenching this time with D_2O has done little to resolve poor peak shape, and thus the signals remain relatively broad throughout the spectrum. The coincident signals furthest downfield have shifted even more so to a value of 7.88 ppm. Three of the signals attributed to the dearomatized ring remain in similar positions (**a, b** and **c** from the key),

whilst the remaining signal has shifted downfield and joins three overlapping signals at approximately 7.28 ppm, corresponding to the remaining aromatic protons.

Poor peak resolution aside, it remained our ultimate objective to ensure oxidation to the more thermodynamically favourable ketone should occur when the sample was exposed to air for three days. This exposure was carried out and the spectrum recorded accordingly (**Figure 3.20**).
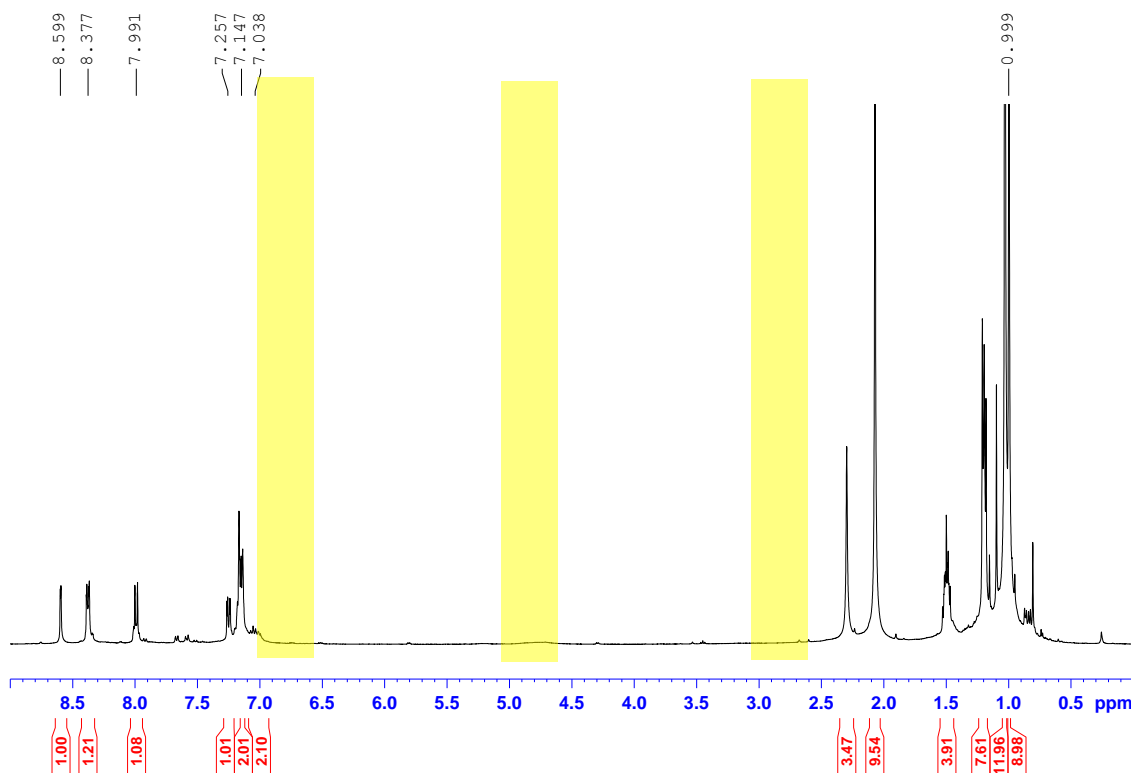
Figure 3.20: 2-benzoylpyridine complex **3d** quenched by D_2O after 3 days (Regions in yellow denote absence of signals attributed to a dearomatised product).

As before, disappearance of the aliphatic signals is observed even at a glance, with subsequent increase in aromatic resonances. Due to the increased electron-withdrawing power of the carbonyl group compared to the C-O carbon of the enolate, all signals have experienced a downfield shift. The proton residing on the C atom α to the N of the pyridine ring appears furthest downfield as a singlet at 8.60 ppm. The next two protons signals correspond to the protons of the phenyl ring "*ortho*" to the carbonyl substituent, at values of 8.38 and 7.99 ppm. The remaining signals appear in convoluted regions either side of the benzene signal. Definitive formation of the desired ketonic species evidenced by comparison, as before, of ^{13}C spectra, recorded 10 minutes after D_2O

quenching, then again 3 days later. Appearance where there was none previously of a signal at 192.7 ppm, with simultaneous disappearance of the signal at 166.36 ppm, corresponding to the enol carbon, indicates with some degree of certainty that the ketone is formed.

3.12 Electrophilic quenching studies of zincate 2a with 2-benzoylpyridine

The same strategy was then applied as before in the fluorenone example, seeking to elucidate both the identity and quantity of all species in solution. To achieve this water alone was added to the reaction media in one instance, and in the second reacted the metallo-intermediates with the strongly oxidising reagent $SOCl_2$ prior to aqueous workup. In the first example, there was evidence of only negligible quantities of starting material and thus full conversion of the pyridyl ketone. As observed in the previous example, two products are exclusively formed, namely the 1, 2- and the 1, 6- addition products, the latter of which was trapped as an enolate in compound **3d**. Oddly enough, when only water was used directly, with no prior oxidation, we recovered the tertiary alcohol as the major product (48%), albeit by a small margin, compared with the yield of the ring tert-butylated product (37%). Also, we don not observe any regenerated 2-benzoylpyridine, akin to the work of Olah.
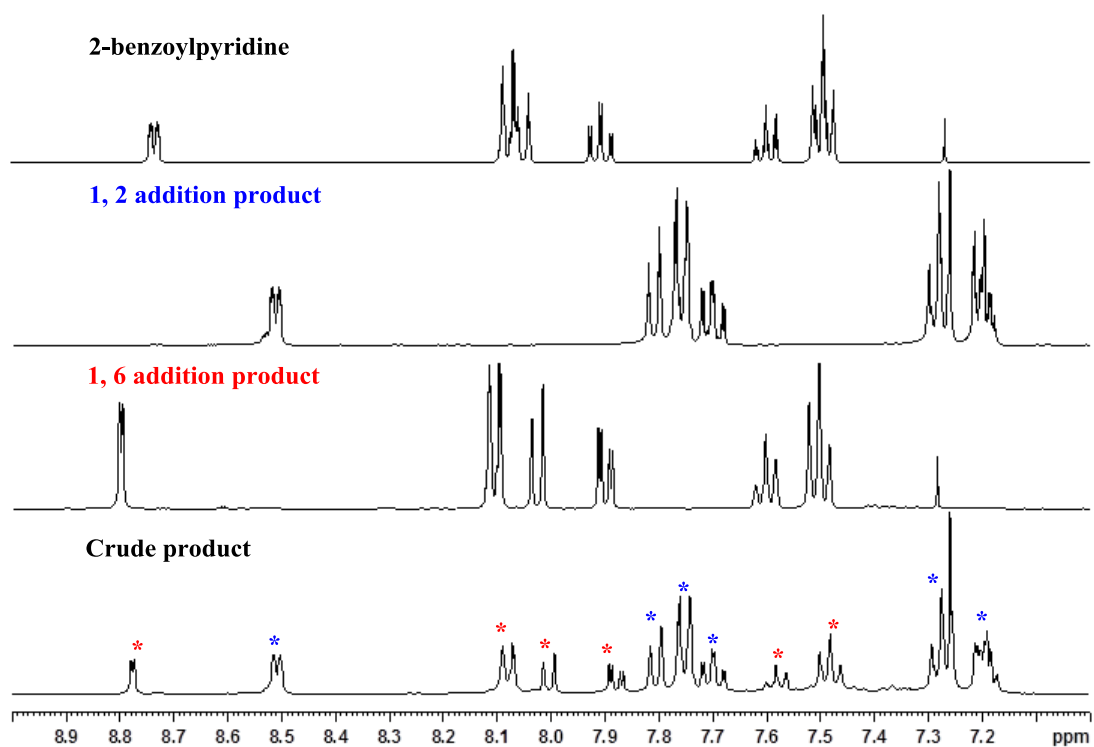
Fig. 3.21: Crude ^1H NMR spectrum of **2a** with 2-benzoylpyridine + NH_4Cl(aq.).

In the case of the desired 1, 6 addition product, we observe 6 distinct aromatic signals, the most downfield of these corresponding to the single H atom between the N and the newly formed C-C bond. This singlet exhibits hyperfine ^4J coupling (coupling constant = 2.18 Hz) to the H atom in the 4-position of the pyridine ring. The remaining two doublets (positions 4 and 5) are observed as resonances at 7.90 ppm and 8.03 ppm respectively. The remaining signals correspond to the unsubstituted phenyl ring. The important ^tBu signal, as it resides on the pyridine ring, exhibits a shift of 1.43 ppm, significantly upfield downfield in comparison to the ^tBu signal of the tertiary alcohol (1.11 ppm). What was surprising in this result was recovery of a majority 1, 2 addition product when experimentally, a yield of greater than 50% was obtained for the 1, 6-addition product as a crystalline material. This situation was significantly augmented when the reaction mixture was first subjected to $SOCl_2$, prior to aqueous workup. Analysis of the crude mixture revealed no appreciable quantity of starting material, but instead a large increase in recovered *tert*-butylated ketone (69%) compared to tertiary alcohol (18%) (**Figure 3.22**).
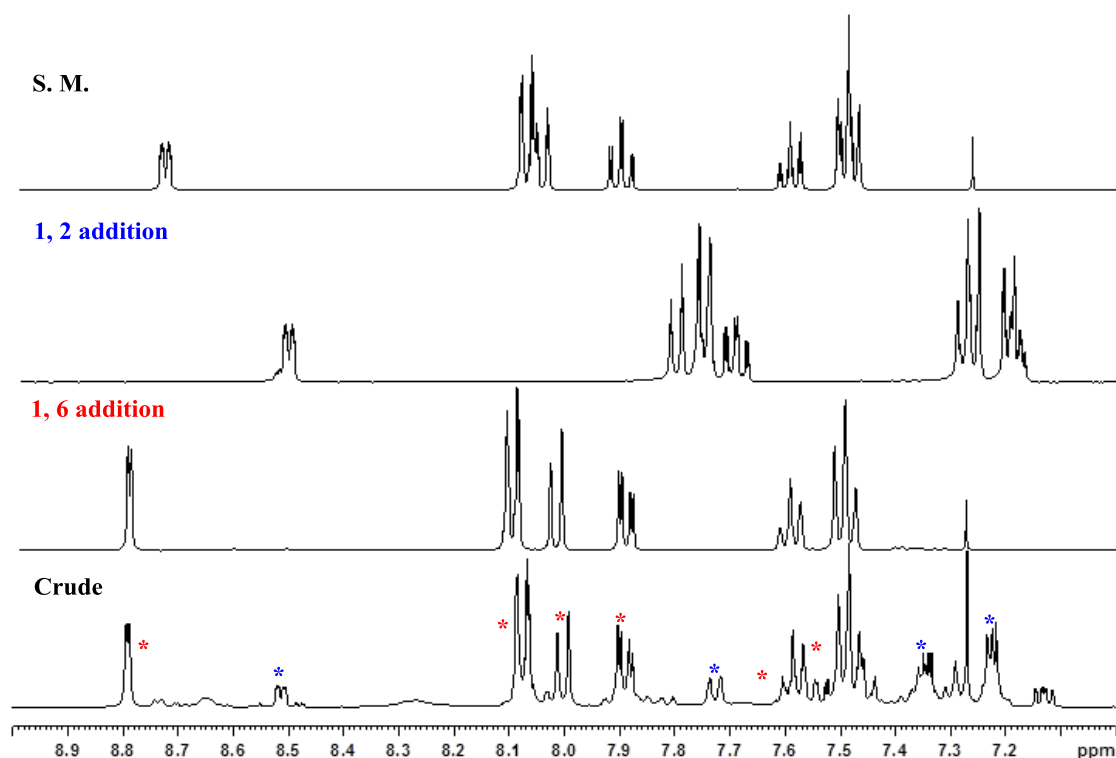
Fig. 3.22: Crude ^{1}H NMR of **2a** with 2-Benzoylpyridine followed by $SOCl_2$ oxidation and aqueous workup.

The disparity between the amount of each product is perhaps most easily observed when looking at the ^{t}Bu signals present in the crude mixture (**Figure 3.23**). A more concentrated crude sample has resulted in an overall downfield shift, but the ^{t}Bu signal attributed to the 1, 6 addition product is visibly far more intense than that of the tertiary alcohol, complimenting nicely the situation observed both in the aromatic region of the stacked spectra and in the final yields of recovered product.

1, 2- addition

1, 6- addition
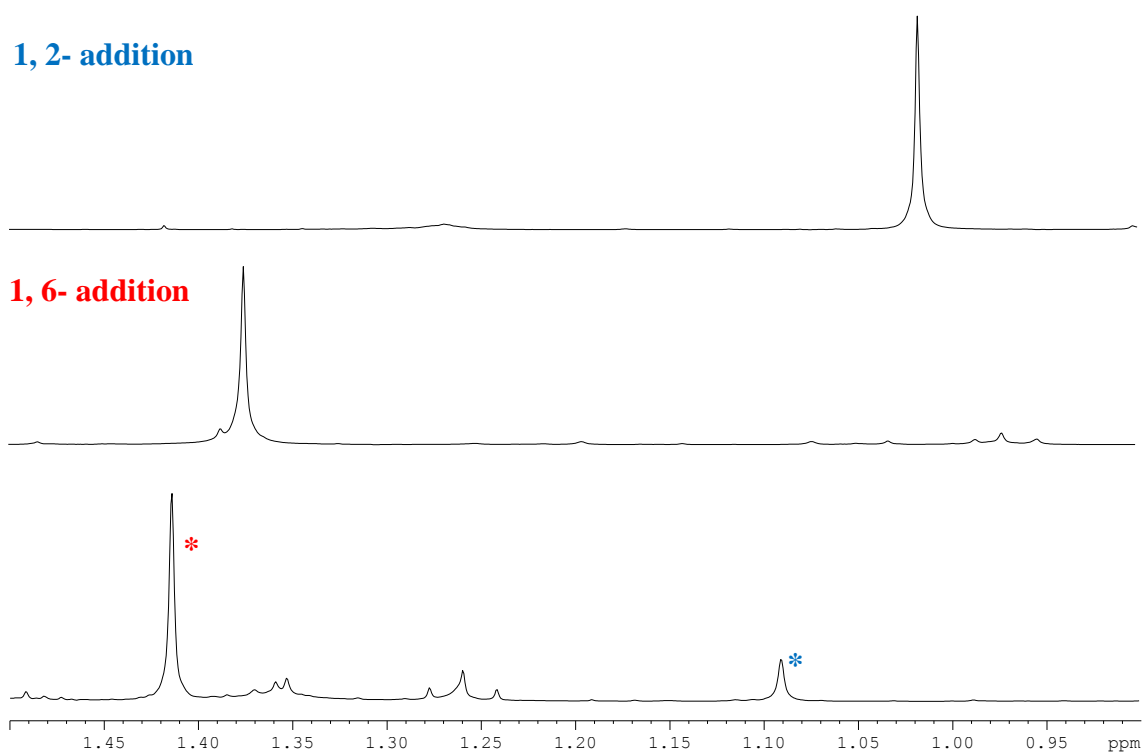
Fig. 3.23: Close up of the aliphatic region of **2a** with fluorenone followed by SOCl$_2$ oxidation and aqueous workup.

In an attempt to rationalise these findings, it was proposed that on quenching with water alone, with no prior oxidation by SOCl$_2$, a highly reactive enolate species still exists. With benzophenone, Olah proposed a competitive pathway whereby either H$_2$ or butane could be expelled preferentially, but since we observe no regenerated 2-benzoylpyridine, we tentatively describe a 1, 5- sigmatropic shift of the ^{t}Bu group from the ring to the C-O position of the enolate (**Scheme 3.4**), although a radical mechanism cannot be ruled out. 1, 5- alkyl migrations, though unusual, have precedent in a number of organic transformations.[125]
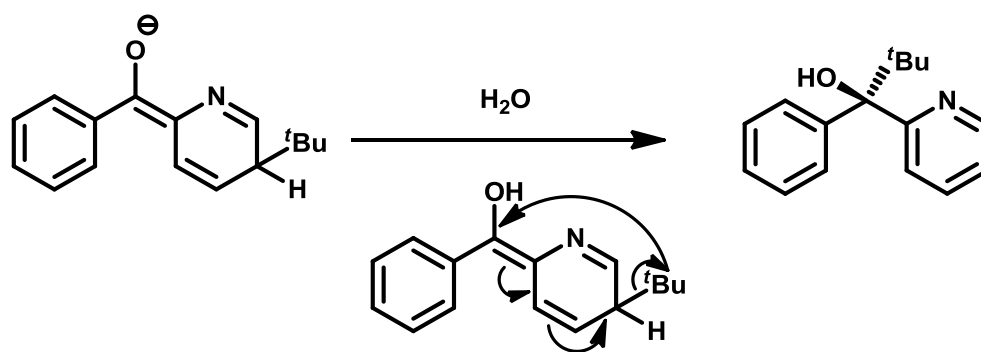
Scheme 3.4: Proposed generation of tertiary alcohol from quenching of in situ reaction of **2a** with 2-benzoylpyridine using water only.

3.13 Reaction of [(TMEDA)·Na(μ-HMDS)(μ-^{t}Bu)Zn(^{t}Bu)] with 2-benzoylpyridine

In an attempt to replicate the results achieved in exchanging the bridging TMP ligand for the less sterically hindered HMDS in the fluorenone example, an attempt was made again to see the effect of the amine in these addition reactions, this time applied to 2-benzoylpyridine. When the sodium zincate [(TMEDA)·Na(μ-HMDS)(μ-^{t}Bu)Zn(^{t}Bu)] was formed in hexane as before by combination of equimolar quantities of NaHMDS, ^{t}Bu$_2$Zn and TMEDA, we then reacted it at room temperature with a single molar equivalent of 2-benzoylpyridine, turning the colourless solution dark green instantaneously. Subsequent overnight cooling to -27°C gave a crop of yellow crystals, suitable for X-ray analysis. It was discovered, incredibly, two products of different selectivity were co-crystallised together in a single cell, both the 1, 2- and 1, 6- addition products.

3.14   Crystallographic studies of 3e
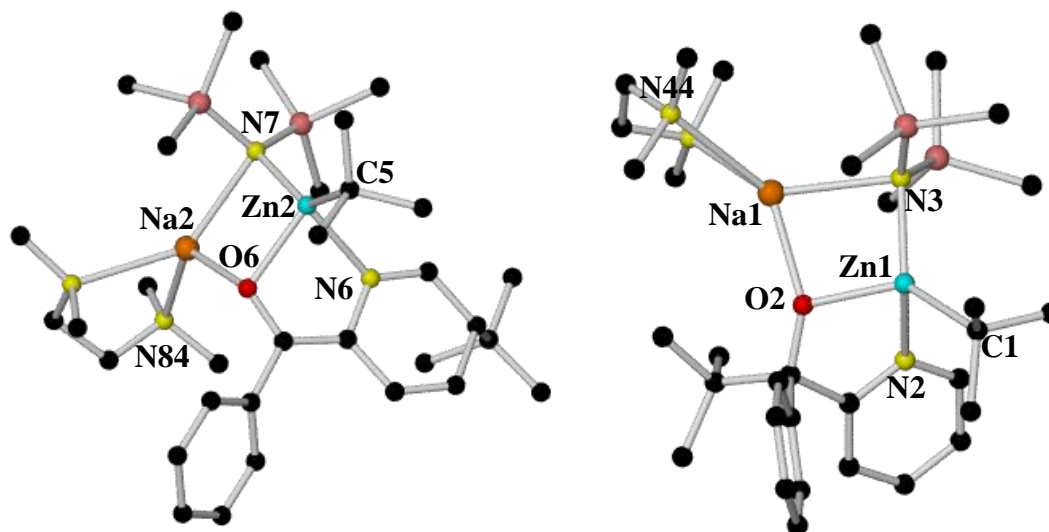
Fig. 3.24: Structure of both 1, 6 (left) and 1, 2 (right) adducts (**3e**) from the reaction of

[(TMEDA)·Na(μ-HMDS)(μ-^{t}Bu)Zn(^{t}Bu)] with 2-Benzoylpyridine.

This remarkable capture of the alkylating zincate reacting in two different modes of activity, gives rise to two consequently different structures. Concentrating first on the 1, 6- addition product, we can see again that the Zn atom is bound datively through the lone pair of the N heteroatom of the pyridine ring, resulting in the same 4-5-6 fused ring system observed in **3d**. The four-coordinate sodium atom is again in a severely distorted tetrahedral environment, with the sum of its six surrounding angles totalling 658° (c.f. 654° in true tetrahedral), the greatest deviation present in the N7-Na2-N84 angle (Δ= -29.8°). With the additional dative bond now making up part of the Zn atom's coordination sphere, it too finds itself in a very similar type of geometry, as opposed to its essentially trigonal planar nature in both the fluorenone and benzophenone instances. The sum of the angles around the Zn total 641.72° [N7-Zn2-C5 135.97(9), N7-Zn2-O6 97.94(7), C5-Zn2-O6 112.99(9), N7-Zn2-N6 114.13(7), C5-Zn2-N6 102.84(9), O6-Zn2-N6 77.85(6)], an even more pronounced deviation than that present in the sodium case. The Zn is bound to three different atom types, which nonetheless exhibit very similar distances [Zn2-N7 2.02 (19), Zn2-C5 2.03(3), Zn-O6 2.09(15) Å], the only exception being the slightly longer Zn-N$_{py}$ distance of 2.18(18) Å, the N atom not formally charged as is the case with the others. As expected, both ^{t}Bu groups, being in such close proximity, orientate themselves in opposing directions, minimising any steric repulsion.

	Bond length (Å)			Bond angle (°)
Na2-O6	2.26(18)	O6-Na2-N81		118.28(8)
Na2-N81	2.46(2)	O6-Na2-N7		81.66(6)
Na2-N7	2.48(2)	N81-Na2-N7		135.96(7)
Na2-N84	2.50(2)	O6-Na2-N84		108.04(7)
Zn2-N7	2.02(19)	N81-Na2-N84		75.57(7)
Zn2-C5	2.03(3)	N7-Na2-N84		138.80(7)
Zn2-O6	2.09(15)	N7-Zn2-C5		135.97(9)
Zn2-N6	2.18(18)	N7-Zn2-O6		97.94(7)
C6-O6	1.31(3)	C5-Zn2-O6		112.99(9)
C6-C612	1.38(3)	N7-Zn2-N6		114.13(7)
N6-C612	1.414(3)	C5-Zn2-N6		102.84(9)
		O6-Zn2-N6		77.85(6)

Table 3.3: Selected bond lengths and angles of 1, 6- adduct.

Turning to the 1, 2- adduct, it can be clearly seen that greater steric congestion around the bridging C-O bond has led to some significant structural differences, mostly in the orientation of the ring systems. The C-C distance from the C_O-C_{ring}, being a single bond, is inevitably elongated, at a distance of 1.553(3) Å, when compared to the formally C=C double bond present in the 1, 6 enolate complex [1.376(3) Å]. The C-O bond distances also vary considerably, with the high degree of delocalisation present in the ring-alkylated product resulting in a contracted C-O distance of 1.306(3) Å (*c.f.* 1.389(3) Å in 1, 2 adduct). With the addition of the ^{t}Bu group occurring now across the carbonyl group, the C2 carbon is now sp^3, resulting in both the phenyl ring and the TMEDA ligand being pushed away to escape the bulk of the projecting ^{t}Bu ligand, and consequently near perfect tetrahedral geometry. This change from sp^2 to sp^3 carbon centres results in a dramatic difference in bond angles of the C_{ipso}-C_O-C_{ipso}, *i.e.,* the angle of the bridge between the rings of the benzoyl pyridine unit. In the 1, 6- adduct, this angle is more obtuse, at a value of 123.1°, a consequence of both the sp^2 centre, and the greater freedom afforded by the lack of protruding ^{t}Bu group on the bridging carbon atom (*c.f.* 109.6° in the 1, 2- adduct). A further consequence of this diminished steric congestion, is that the pi-face of the phenyl ring turns upwards, finding itself in closer

proximity to the Na atom [Na-C$_{ipso}$ distance 4.01 Å *cf.* 4.52 Å in the 1, 2 adduct being the closest contacts]. The rings twist in contrasting fashions for both products: in the 1, 6- adduct, the pyridine ring tends more towards the zinc atom, and the phenyl ring more towards the sodium atom. In the 1, 2- adduct, the rings almost fold together towards one side of the molecule, namely the less sterically hindered zinc portion.

	Bond length (Å)		Bond angle (°)
Na1-O2	2.24(18)	O2-Na1-N41	130.12(7)
Na1-N41	2.72(2)	O2-Na1-N3	80.12(7)
Na1-N3	2.49(2)	N41-Na1-N3	126.39(8)
Na1-N44	2.57(2)	O2-Na1-N44	131.34(8)
Zn1-N3	2.07(19)	N41-Na1-N44	69.76(8)
Zn1-C1	2.05(3)	N3-Na1-N44	127.59(8)
Zn1-O2	2.00(15)	N3-Zn1-C1	126.02(9)
Zn1-N2	2.21(2)	N3-Zn1-O2	97.11(7)
C2-O2	1.39(3)	C1-Zn1-O2	112.99(9)
C2-C212	1.56(3)	N3-Zn1-N2	117.51(7)
N2-C212	1.34(3)	C1-Zn1-N2	98.87(9)
		O2-Zn1-N2	74.90(7)

Table 3.4: Selected bond lengths and angles of 1, 2- adduct.

3.15   Electrophilic quenching studies of [(TMEDA)·Na(μ-HMDS)(μ-^{t}Bu)Zn(^{t}Bu)] with 2-benzoylpyridine

In attempting to investigate the true ratio of products present in solution, water was added to the reaction of **3c** with 2-benzoylpyridine, and analysed the crude mixture after aqueous workup. It was found this time that the 1, 2 addition product was the predominant species, depsite crystallization of both adducts in a single unit (**Figure 3.24**). Utilizing in this instance hexamethylbenzene as an internal standard instead of recovery by silica column, the yields of 1, 6- and 1, 2- addition products were calculated to be 16% and 61% respectively, with only negligible amounts of other products evident. This is surprising, as the expected ratio would be 50:50, yet here we see a ratio

of 21:79 (1, 6: 1 2). This could be due to a similar alkyl migration rearrangement which was proposed in **Scheme 3.4**.
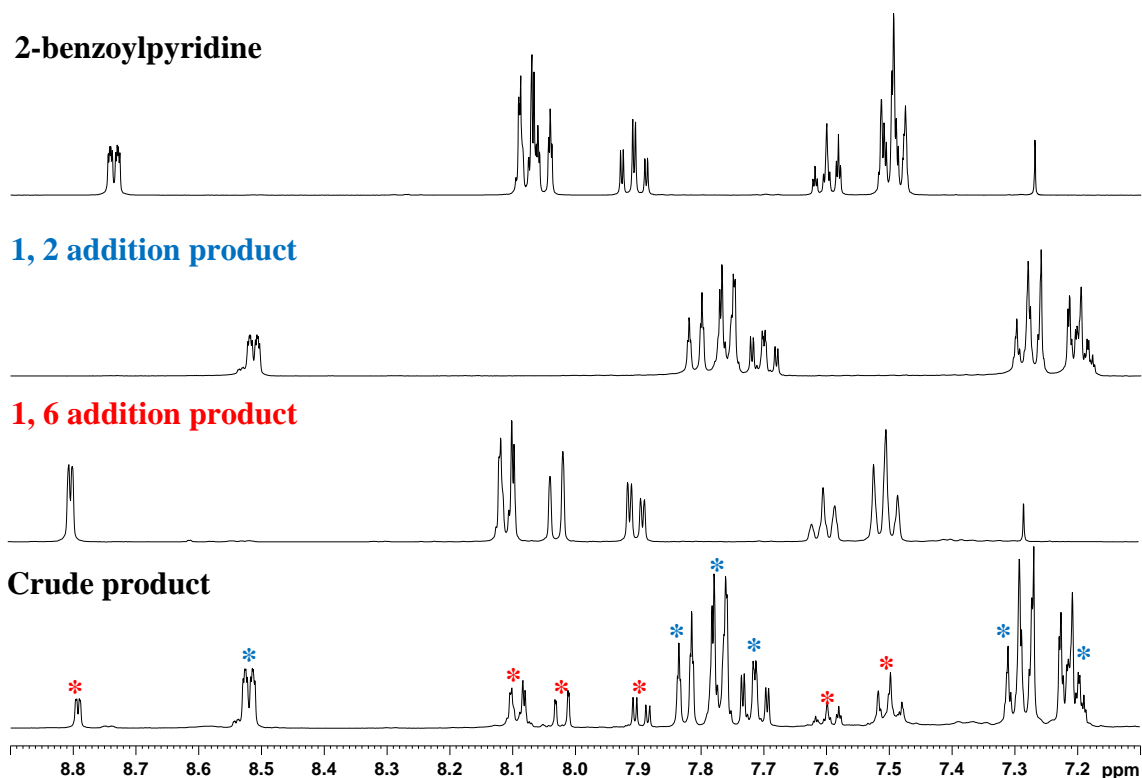
Fig. 3.25: Stacked plot of aromatic region of **3c** + 2-benzoylpyridine after aqueous workup.

3.16 Reaction of [(PMDETA)·Na(μ-TMP)(μ-Et)Zn(Et)] with fluorenone

Having explored in depth the reactions of both **2a** and [(TMEDA)·Na(μ-HMDS)(μ-^{t}Bu)Zn(^{t}Bu)] with fluorenone, both in solution and by NMR, an attempt was made to see if the same anomalous substitution pattern exhibited by the ^{t}Bu ligand could be observed with another alkyl group. To this end, the related sodium amido-zincate [(PMDETA)·Na(μ-TMP)(μ-Et)Zn(Et)] was prepared via the same methodology as **2a**, except this time using commercially available diethylzinc solution (1M in hexanes) in place of sublimated ^{t}Bu$_2$Zn solid which was purified by sublimation. When reacted with fluorenone in hexane, the colourless solution turned a deep, almost navy blue colour, which after a period of several days yielded a small amount of crystalline material. To our surprise, the species obtained was not the desired ring substituted bimetallic species.
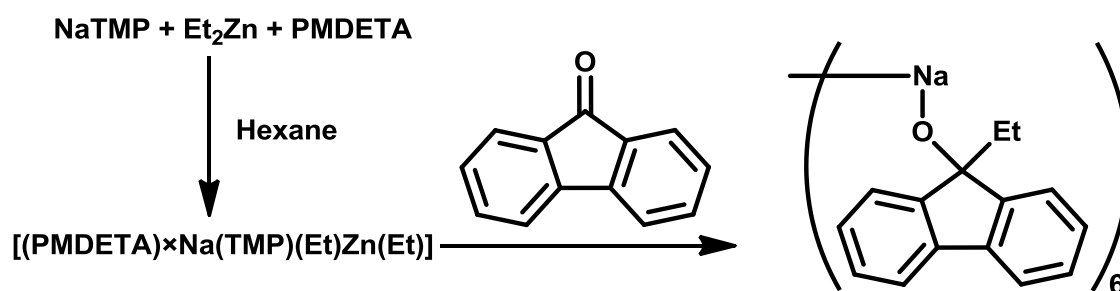
Fig. 3.26: Reaction of [(PMDETA)·Na(μ-TMP)(μ-Et)Zn(Et)] with fluorenone.

3.16.1 Crystallographic studies of [(Na-9-Et-9*H*-Fluoren-9-olate)$_6$]

Instead what we obtained was an unusual hexameric, sodium-only species, exhibiting an attractive barrel-like motif. In each fluorenone molecule, an ethyl group has added across the carbonyl group in the traditional 1, 2- fashion, with each newly formed oxygen anion bound to three surrounding sodium atoms, and likewise each sodium bound to three oxygen atoms. The structure is comprised of two six membered (Na-O)$_3$ rings, the interannular distance of each 2.324(15) Å (Na1-O1). When compared to the Na-O distances within the same ring [(2.216(15) and 2.276(16) Å], we can see only a very slight bond elongation. These Na-O distances are consistent with the literature related hexamer [Na$_6$(Ph$_2$CHO)$_6$],[126] with corresponding values of Na1-O1 2.304(2) Å, Na1-O2 2.292(2) Å and Na1-O3 2.209(2) Å. As each Na atom is, unusually, three coordinate, a trigonal planar environment may be supposed as the most likely geometry. If however we envisage the three O atoms as the plane vertices, the Na atom is raised considerably, at a value of 0.98 Å, adopting an apical position, almost mimicking a pseudo-pyramidal geometry. Placed at the edges of an almost perfect hexagon, the angles around the sodium atom are quite extreme, almost forming a T-shape, with the Na in the centre [O2-Na1-O3 122.93(6)°, O2-Na1-O1 94.62(6)°, O3-Na1-O1 91.49(5)°].
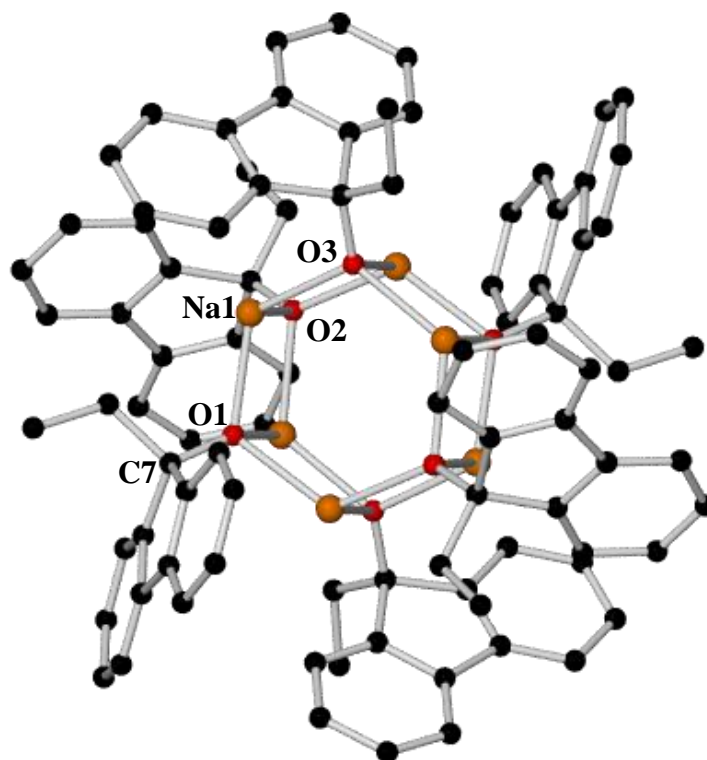
Fig. 3.27: Structure of **3f**. Key bond distances (Å) and angles (°): Na1-O2 2.216(15), Na1-O3 2.276(16), Na1-O1 2.324(15), O1-C7 1.393(2), O2-Na1-O3 122.93(6), O2-Na1-O1 94.62(6), O3-Na1-O1 91.49(5), O2-Na1-C41 121.00(6), O3-Na1-C41 52.68(5), O1-Na1-C41 138.56(6), O2-Na1-C47 135.87(6), O3-Na1-C47 26.10(5).

Each oxygen atom is distorted tetrahedral, with the largest deviation form true tetrahedral present in the Na1-O3-Na1 angle [84.22(5)°, Δ from perfect tetrahedral = 24.78°]. Each sodium atom, though formally three coordinate, enjoys substantial π-interactions through four carbon atoms, two on each different fluorenone molecule, both orientated in such a way as to afford the greatest number of stabilising contacts. It is easier to envisage this coordination chemistry when focusing on a sodium atom in isolation, replete with both stabilising fluorenone moieties (**Figure 3.28**). The Na1-C47 (C_{ipso}) distance is 2.984(2) Å, and the distance to the adjacent Na-C41 distance 3.005(2) Å, both well within the range of cation-π interactions deemed to be significant.[127] Turning to the second fluorenone molecule, the distances are comparable at 3.111(2) Å for the Na-C8 distance, and 2.991 Å from sodium to the C9 position.
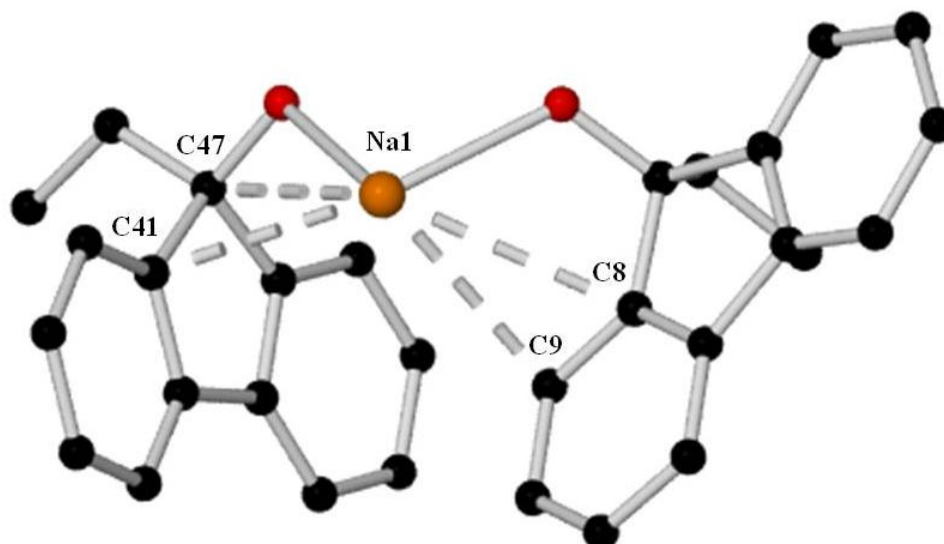
Fig. 3.28: Close up of a single sodium atom surrounded by two fluorenone molecules

It is interesting to note that this large aggregate forms in the absence of any donor, and lack of any zinc atoms (present in the initial reaction mixture), suggests that this is a product of disproportionation.

3.16.2 NMR spectroscopic studies of [(Na-9-Et-9*H*-Fluoren-9-olate)$_6$]

The ^{1}H NMR spectrum of this complex in C_6D_6 revealed a high degree of hindered rotation, evidenced by the extremely broad resonances associated with all relevant peaks. Three resonances are observed in the aromatic region, which can be tentatively assigned to the *ortho*, *meta* and *para* protons of each ring with respect to the C-O bridging unit. The furthest downfield resonance can be ascribed to the *ortho* protons of each ring, appearing as a broad hump at 7.53 ppm, integrating to two H atoms. The *meta* signals are all observed as identical, falling underneath the C_6D_6 solvent signal at an approximate value of 7.15 ppm. These signals can be assigned as *meta* due to their apparent coupling in the COSY spectrum to both the *ortho* and *para* signals. Further evidence of all four *meta* positions being spectroscopically equivalent is obtained by analysing the HSQC spectrum, which shows only a single signal attributed to these positions. The final aromatic signal within the ^{1}H NMR spectrum falls at 6.91 ppm, indicative of the fluorenone *para* position. In the aliphatic region, again two broad resonances are observed for the ethyl groups within this complex, representing the C*H$_2$*CH$_3$ (1.09 ppm) and the CH$_2$C*H$_3$* (0.26 ppm) positions. Interestingly, there appears to be a large quantity of residual free PMDETA, which although not present in the final

crystalline product, was utilised in the original reaction. It is perhaps unsurprising due to the high boiling point of this ligand (198 °C), that we were unable to remove it entirely from the surface of the crystalline material by washing and vacuum alone. These signals appear between 2 and 2.6 ppm [(t, CH_2, 2.5 ppm), (t, CH_2, 2.4 ppm), (s, CH_3 central, 2.2 ppm) and (s, CH_3 terminal, 2.1 ppm)].
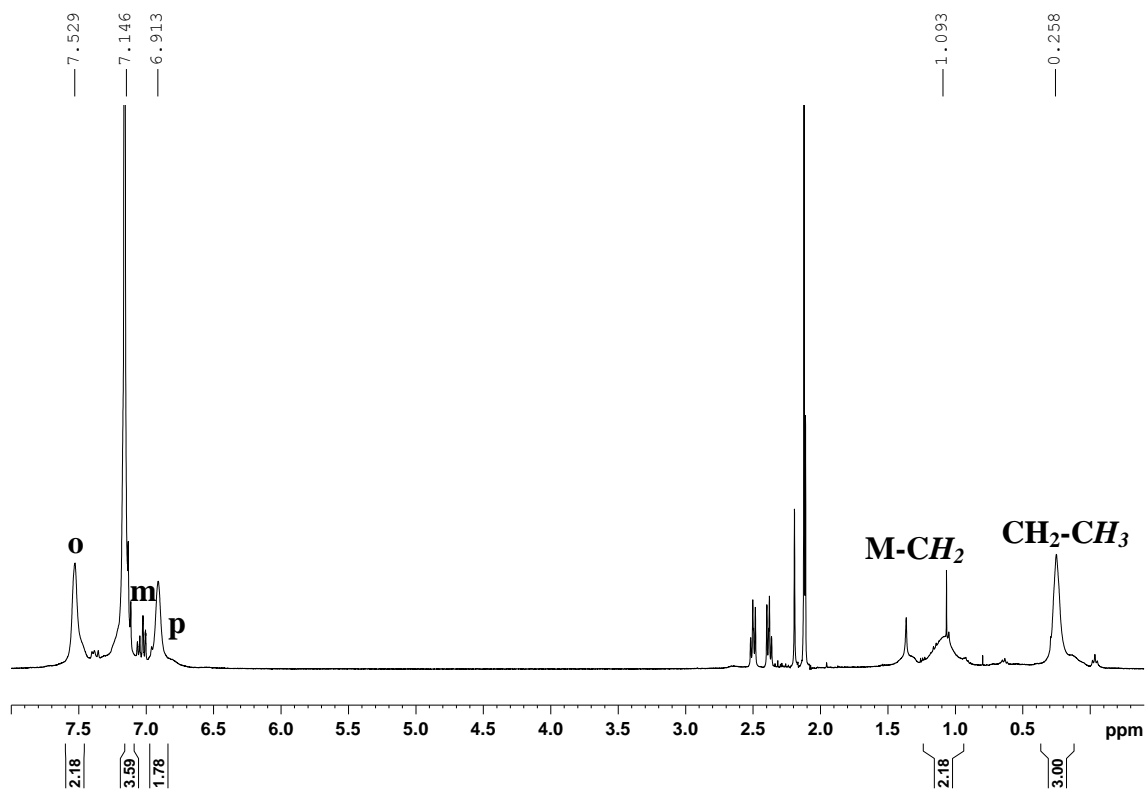
Fig. 3.29: ^{1}H NMR spectrum of **3f** in C$_6$D$_6$.

The ^{13}C NMR spectrum mirrors the ^{1}H NMR data above, with three predominant signals in the aromatic region, representing the *ortho* (120.5 ppm), *meta* (128.8 ppm) and *para* (121.4 ppm) H atoms. Interestingly, we can also observe the quarternary C-O signal at a value of 140.0 ppm. As in the ^{1}H NMR spectrum, the *meta* signals also fall underneath the solvent peaks, and can only be observed with genuine clarity in the corresponding HSQC spectrum. In the aliphatic region, we again observe two signals attributed to the ethyl group, at values of 37.0 (CH_2) and 9.3 (CH_3) ppm.

In summary, we have have investigated in depth the ability of the zincate [(TMEDA)·Na(μ-TMP)(μ-[t]Bu)Zn([t]Bu)] to add a single [t]Bu group selectively at the 6 position (with respect to the carbonyl O atom) of both fluorenone and 2-benzoylpyridine. We have also shown how stable crystalline samples of each product

can be isolated, generating the ring tert-butylated product by reaction with D_2O and aerobic oxidation. We can also quench the *in situ* mixtures with H_2O, achieving separation of both, 1, 2- and 1, 6- addition products by silica column. We are also able to achive enhancement of the yield of 1, 6- addition product by oxidation of the metallo intermediate with $SOCl_2$ prior to aqueous workup. By changing the parent amine of the starting zincate to HMDS, we are able to effect the same anomalous substitutions, generating the tertiary alcohol and ^tBu ketone via an identical aqueous workup procedure. In changing the zincate to [(TMEDA)·Na(μ-TMP)(μ-Et)Zn(Et)] by using the less bulky $ZnEt_2$, when we react this with fluorenone, carbonyl addition by the ethyl group occurs, forming an unusual monometallic hexameric unit (Na-9-Et-9*H*-Fluoren-9-olate)$_6$, characterized in both solid and solution state. These alkylation reactions have set a promising precedent for potential substitutions of this type utilizing different alkyl or even aryl groups, with a variety of different organic substrates, providing a new and exciting route for functionalizing molecules in positions unachievable by any conventional means.

4. <u>Selected other results with potential to lead to further PhD projects</u>

4.1 Introduction to carboranes

First synthesised and simultaneously reported by groups of both the Olin Corporation and the Reaction Motors Division of Thiokol Chemical Company in 1963,[128] carborane compounds can best be described as clusters, or more specifically polyhedra containing both boron and carbon atoms. Of particular pertinence to this work are the icosahedral *closo* carboranes ($C_2B_{10}H_{12}$),[129] so called due to their completeness, existing as polyhedra which have no vertices absent. Subsequent removal of vertices would have them described as *nido-*(missing one), *arachno-*(missing two), *hypho-*etc (**Figure 4.1**).
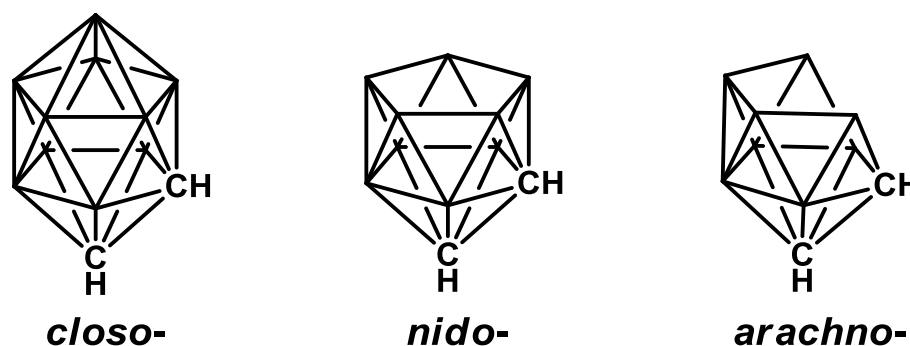
Fig.4.1: Representative *closo-*, *nido-* and *arachno-* carboranes.

These initial syntheses involved reaction of decaborane ($B_{10}H_{14}$) with acetonitrile to isolate the $(B_{10}H_{12})^{2-}$ intermediate which upon further reaction with ethyne generated the closo carborane $C_2B_{10}H_{12}$.[128a] They found however in practise that reaction of decaborane with ethyne in the presence of acetonitrile in benzene negated the need to first isolate the anion and instead generated the carborane directly (**Scheme 4.1**).

$$B_{10}H_{14} \ + \ 2CH_3CN \ \longrightarrow \ B_{10}H_{12}(CH_3CN)_2 + H_2 \qquad (1)$$
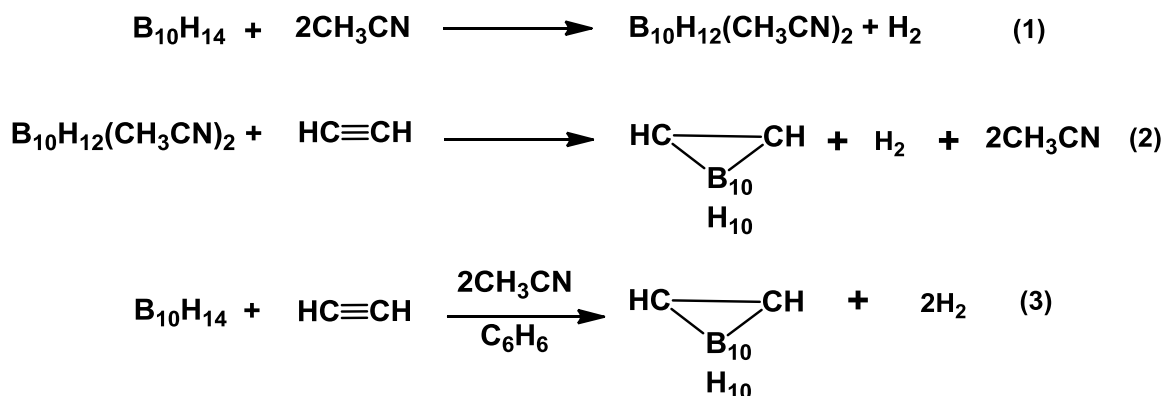
Scheme 4.1: Original *closo*-carborane synthesis.

These *closo* carboranes have sparked great synthetic interest due to their great stability, and shown themselves useful in a wide range of applications, from Neutron Capture Therapy[130] to heat resistant polymers.[131] The carborane acid $H(CHB_{11}H_5Cl_6)$ is the strongest known isolable Brønsted Acid, and the only acid, or "superacid" known to protonate fullerene (C_{60}) without decomposing it.[132] Such is the interest in carborane complexes that since their original synthesis right up to present day, they can be seen regularly in many high ranking journals and publications. An example by Xie *et al* shows how lithiation of *o*-carborane and subsequent formation of highly reactive carboryne, can then facilitate its insertion into a number of aromatic rings, generating a class of previously unknown compounds i.e., cyclooctatetraenocarboranes[133] (**Figure 4.2**):
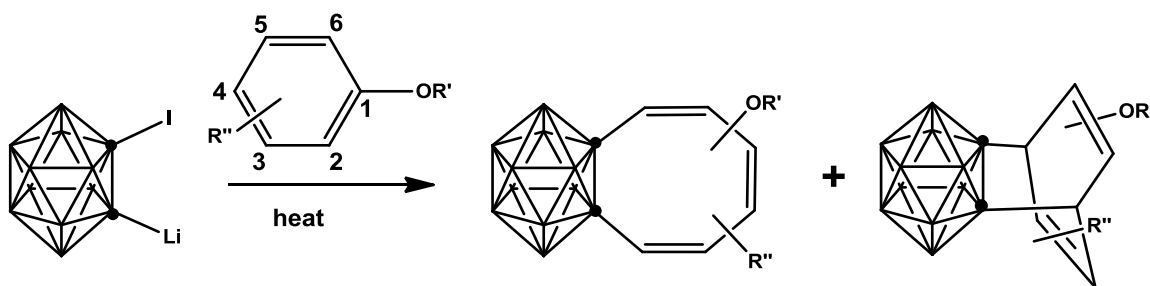
Fig. 4.2: Carboryne insertion into functionalised arenes. The vertices denoted by • are C atoms and the others are B-H.

A report by the same group a year previously showed how dilithiated *ortho*-carborane could be used further in metathesis reactions with a variety of zirconium chlorides to produce the corresponding zirconocene-carboryne complex[134] (**Scheme 4.2**).
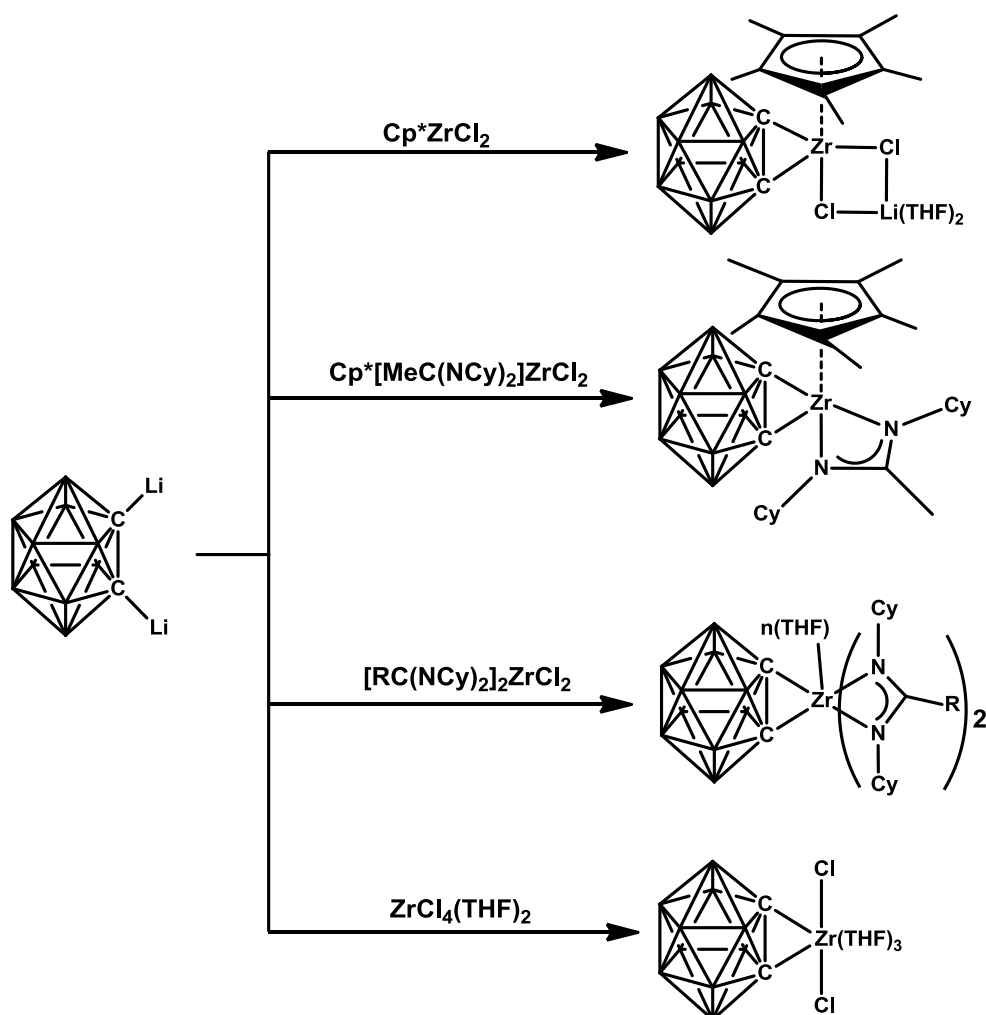
Scheme 4.2: Zirconocene-carboryne formation.

A wealth of publications exists concerning carboranes, proving their worth both in application and in structural diversity. These carboranes exist in three different isomers, known simply as *ortho*-(1, 2), *meta*-(1, 7) and *para*-(1, 12).[135] The *ortho* carborane is the isomer formed in the initial synthesis, which is converted on heating at 420°C to the more thermodynamically stable *meta*- isomer, and then to the *para*- at temperatures exceeding 900°C (**Figure 4.3**).
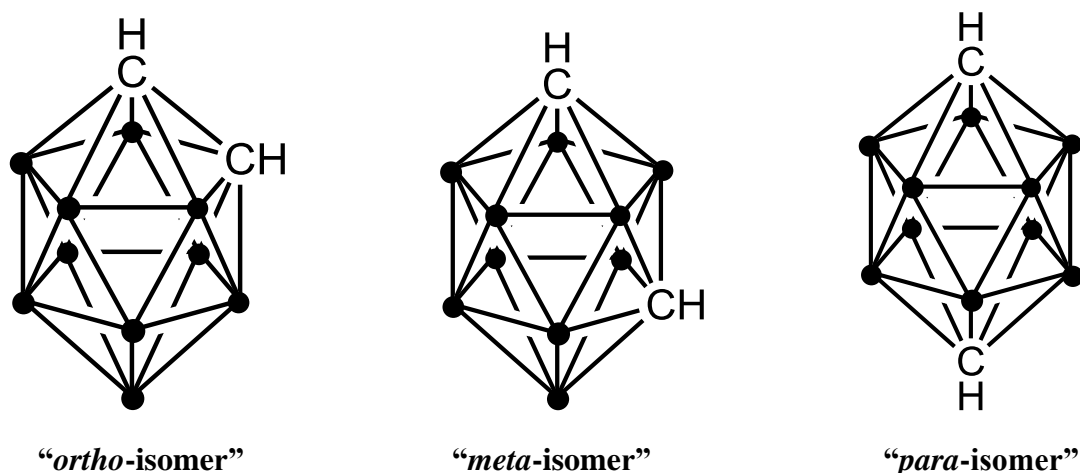
Fig. 4.3: Closo carborane isomers (B-H atom labels omitted for clarity).

It seemed natural then to extend the already unique chemistry inherent in these carboranes to our own systems and see if reactions with our bimetallic bases could effect deprotonations in unusual positions (e.g., circumventing the effects of the relatively highly acidic protons bonded to the carbon atoms of the carboranes), or whether unique structures could be achieved otherwise impossible with reagents presently employed by other groups.

In 1987, Wade *et al* generated an unusual magnesiated carborane structure, comprising a central magnesium atom in a distorted tetrahedral environment, bonded to two methylcarborane units and two dioxane ligands.[136] Initially, they hoped to generate, via prior formation of the Grignard RMgBr [where R= (2-Me-1, 2-C$_2$B$_2$H$_{10}$)] the dialkyl magnesium structure R$_2$Mg. This they obtained as the dioxane adduct through a series of reactions (**Scheme 4.3**), culminating in a dioxane induced disproportionation, akin to that described previously by the Schlenk equilibrium. The MgR$_2$.dioxane adduct was removed from the MgBr$_2$.dioxane mixture resulting from the disproportionation, by evaporation and subsequent extraction from hot toluene. This result represented the first structural characterisation of a group 2 metal covalently bonded to a carbon atom in the *exo* position of a carborane molecule.

$$RLi \xrightarrow[\text{(ii) - LiBr}]{\text{(i) Br}_2\text{/Et}_2\text{O}} RBr \xrightarrow{\text{Mg/ Et}_2\text{O}} RMgBr \xrightarrow[\text{(ii) - MgBr}_2\text{.2 dioxane}]{\text{(i) 1, 4- dioxane}} MgR_2$$

Scheme 4.3: Formation of MgR$_2$.2dioxane adduct.
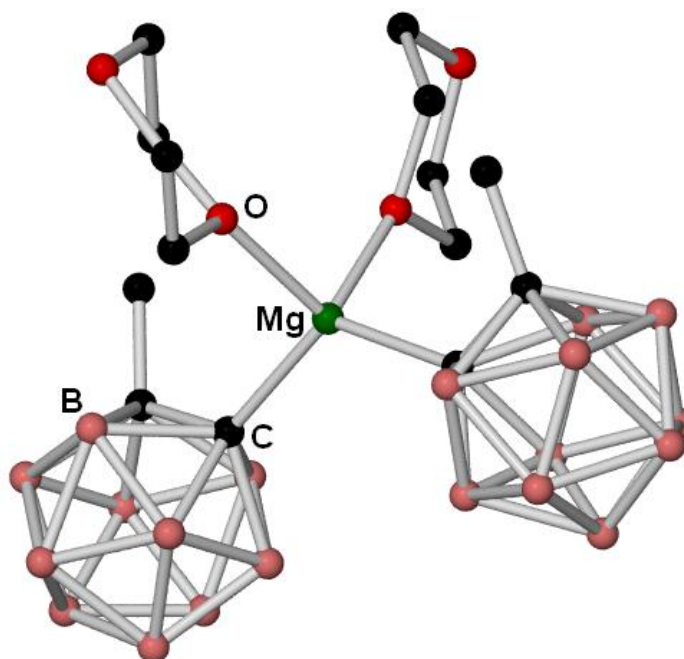
Fig. 4.4: Molecular structure of MgR$_2$.2dioxane adduct.

4.1.1 Reaction of [TMEDA.Na(μ-^{n}Bu)(μ-TMP)Mg(TMP)] with the *ortho-*carborane

In order to ascertain the reactivity of the *ortho*-carborane isomer with our own synergic magnesiate bases, the monoalkyl bis-amido complex [TMEDA.Na(μ-^{n}Bu)(μ-TMP)Mg(TMP)] **4a** was first generated by reaction of BuNa (1 mmol) with ^{n}Bu$_2$Mg (1mmol), to which was added TMP(H) (2 mmol) and TMEDA(1 mmol). Addition of three molar equivalents of the *ortho*-carborane turned the previously straw coloured solution to a milky white suspension, which owing to its insolubility in non-polar hexane, was re-dissolved in 10 ml THF. Subsequent cooling to -27°C in the freezer brought about deposition of colourless crystals which upon analysis by X-ray crystallography gave a highly disordered solvent separated structure. The anionic portion of the molecule shows a central magnesium atom in a distorted tetrahedral arrangement, bonded to a single carbon atom of three carborane molecules. Its coordination sphere is satisfied finally by a single THF molecule. This unusual anion

has its charge balanced by the comparatively common cation, comprising a sodium atom sequestered by six THF molecules.
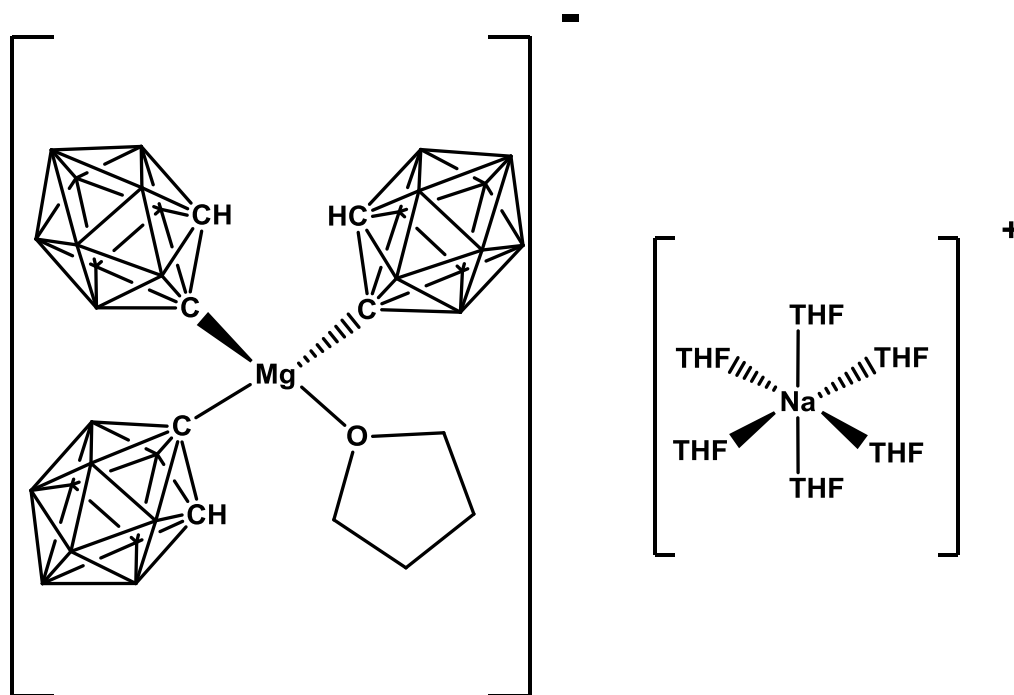
Fig. 4.5: Solvent separated carborane structure **4b**.

Further discussion of bond lengths and angles is, unfortunately, not possible owing to the highly disordered nature of the crystal data.

4.1.2 Reaction of [(THF)·Li(μ-^{t}Bu)(μ-TMP)Zn(^{t}Bu)] with the *meta*-carborane

Following several unsuccessful attempts to produce an analogous zinc containing structure by combination of the *ortho*-carborane with the synergic base **2a**, a donor free lithium zincate was generated by combining a single molar equivalent of both ^{n}BuLi and ^{t}Bu$_2$Zn with two equivalents of TMP(H). To this mixture a single equivalent of the *meta-* isomer was added, producing a similar creamy white suspension to that observed previously, which upon removal of hexane and subsequent dissolution in THF produced, on cooling, crystals of sufficient quality to be analysed via X-ray diffraction.

Although a structure could be generated, the highly disordered nature of the crystal makes assignment of certain features within the molecule the subject of some, albeit educated, guesswork. To the best of our knowledge however, the molecule presents

95

itself as a solvent separated species, with the anionic fragment comprising a core 12-membered ring. Each carborane moiety is doubly deprotonated at their acidic C-H positions, and bridged to another similarly deprotonated carborane fragment by a Zn atom, bonded to a single butyl group of indeterminate configuration (i.e., ^{n}Bu or ^{t}Bu). Three of these zincated carborane units join up to form the anion. The cationic portion is again one which features commonly in many of these mixed metal systems, a single lithium atom surrounded by six THF molecules.
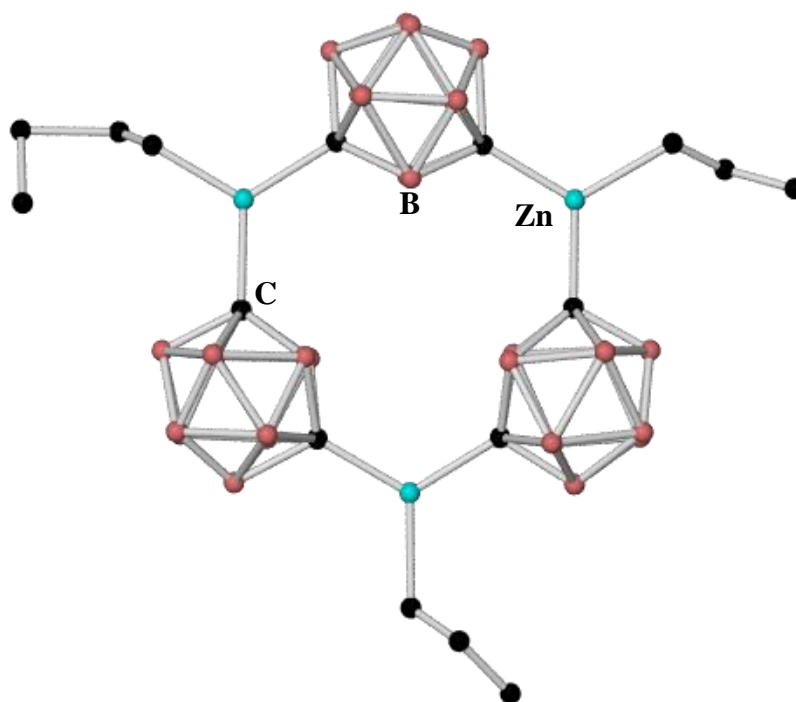
Fig. 4.6: Molecular structure of anionic fragment **4c** (disordered)**.**

A related example to that described above was synthesised by Hawthorne *et al*,[137] whereby his group took the dilithiated *ortho*-carborane, then reacted it with stoichiometric $Hg(OAc)_2$ in a metathesis reaction, producing a neutral mercuric trimer (**Figure 4.7**). This represents the closest structural mimic we could find, though being neutral the Hg atoms bear no surplus R group, an obvious difference between both motifs.

As previously mentioned, the highly disordered nature of the doubly zincated *meta*-carborane crystal structure makes further discussion of bond lengths, angles etc., unfortunately, impossible.
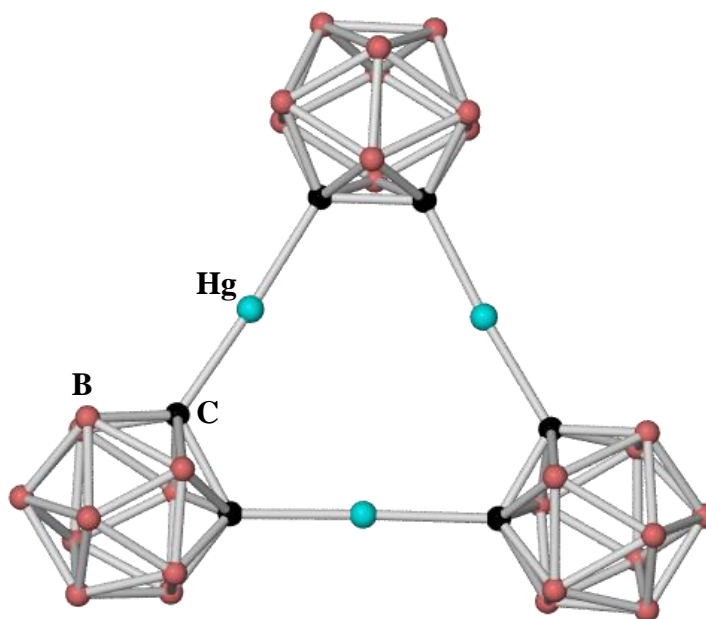
Fig. 4.7: X-ray structure of [9]mercuracarborand-3 [cyclo-$(C_2B_{10}H_{10}Hg)_3$

4.2 Grignard and organolithium reagents in single electron transfer reactions

In has been previously asserted by numerous publications that reactions of traditional Grignard reagents (RMgX) with ketones proceeds through a single electron transfer (SET) mechanism,[121] the nature of the addition related to the stability of the alkyl radical (R·). Direct evidence of this was provided by Mosher in 1969,[138] whereby he reacted the Grignard reagent neopentyl magnenesium chloride [$(CH_3)_3CCH_2MgCl$] with benzophenone. They chose these particular reagents due to the inability of benzophenone to readily enolise, the impossibility of ketone reduction due to the lack of β-hydrogens present in the neopentyl group, and the steric constraints of the alkyl group being sufficient to ensure reasonable reaction rates. Unexpectedly, SET transfer had occurred, resulting in the coupling of two benzophenone units together, giving neopentane and benzpinacol on hydrolysis.
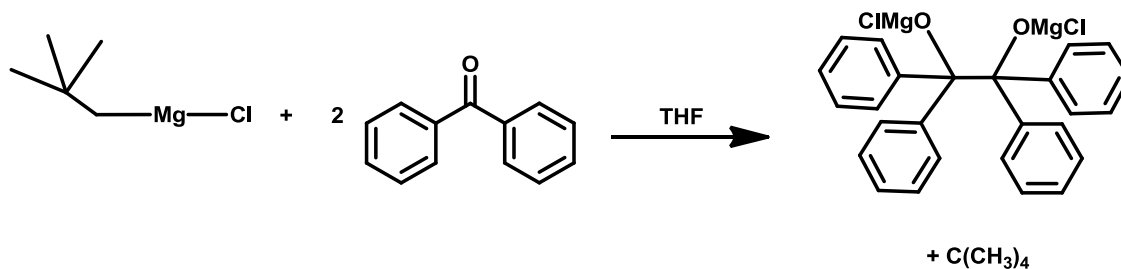
Scheme 4.4: Reaction of benzophenone with neopentyl magnesium chloride.

Indeed, in the study mentioned earlier by Olah, he suggests the reaction of ^{t}BuLi with benzophenone most like proceeds by SET (**Scheme 4.5**).[139]
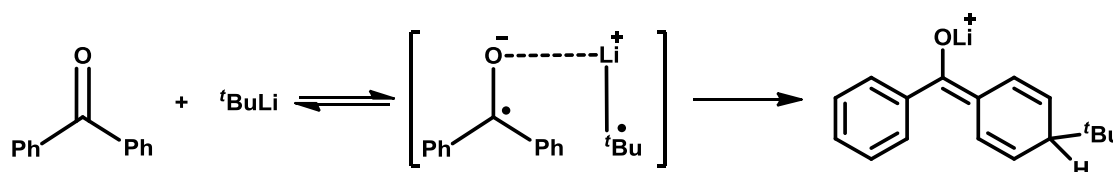
Scheme 4.5: Ring substitution of benzophenone by ^{t}BuLi *via* proposed SET mechanism.

4.2.1 Single electron transfer reactivity of the sodium zincate 2a

To ascertain whether **2a** can function as a SET reagent, parallel to our own studies, other group members first studied its reaction with the stable nitroxy radical 2,2,6,6-tetramethylpiperidinyloxy (TEMPO). Popular in radical chemistry,[140] TEMPO has recently been employed as an oxidant in the transition metal-free coupling of *ortho*-substituted aryls with alkynyl ''turbo-Grignard'' reagents.[141] In a 1 : 1 stoichiometric reaction (**Scheme 4.5**) between **2a** and TEMPO in hexane medium, [(TMEDA)·Na(μ-TMP)(μ-TEMPO)Zn(^{t}Bu)] **4d** was isolated (yield, 34%). A key feature of this reaction is the conversion of a TEMPO radical to a TEMPO⁻ anion (with concomitant conversion of a ^{t}Bu⁻ anion to a ^{t}Bu· radical). It is envisaged that the tertiary alkyl radicals combine to give isobutane and isobutene. Indeed by DFT calculations, it was estimated that the conversion of **2a** and TEMPO to **4d** and hydrocarbon co-products is exothermic by 40.27 kcal mol^{-1}.

Fig. 4.8: Crystal structure of [(TMEDA)·Na(μ-TMP)(μ-TEMPO)Zn(^{t}Bu)] **4d**.

The molecular structure of **4d** (**Fig. 4.8**) revealed a contacted ion pair, bimetallic motif with a tetracoordinate Na centre [range of angles around Na1, 73.19(4)–136.10(5)°] and a distorted trigonal planar Zn centre. The connectivity framework of **4d** is retained except that a *tert*-butyl bridge is replaced by a TEMPO ligand. By comparing the N–O bond length [2.2492(12) Å] in **4d** with that in related TEMPO-containing complexes,[142] it is clear that the ligand here is anionic as it must be from valency considerations.

Scheme 4.6: Sodium amido-zincate **2a** reacted with one equivalent of TEMPO.

In an effort to trap the ^{t}Bu radical released in the reaction (to give TEMPO-^{t}Bu),[143] two molar equivalents of TEMPO were added to the zincate **2a** (**Scheme 4.7**). Surprisingly, this reaction did not yield **4d**, instead [(TMEDA)·Na(μ-TEMPO)$_2$Zn(^{t}Bu)] **4e** was isolated as colourless crystals (31% yield). It is unlikely that **4e** forms due to a

disproportionation reaction as the complex was never detected when only one molar equivalent of TEMPO is used; therefore to produce **4e**, it seems that **2a** has acted as a dual SET reagent whereby both a ^{t}Bu radical and perhaps counterintuitively a TMP radical have been generated *in situ*, emphasising the strong carbophilicity of zinc. Again this structure retains the majority of the structural integrity of **2a**. The s-block coordination chemistry of TEMPO has been studied recently and the key structural parameters of **4d** and **4e** (including N–O and Na–O bond distances) are essentially identical to those in the earlier reported structures including NaTEMPO.[142]
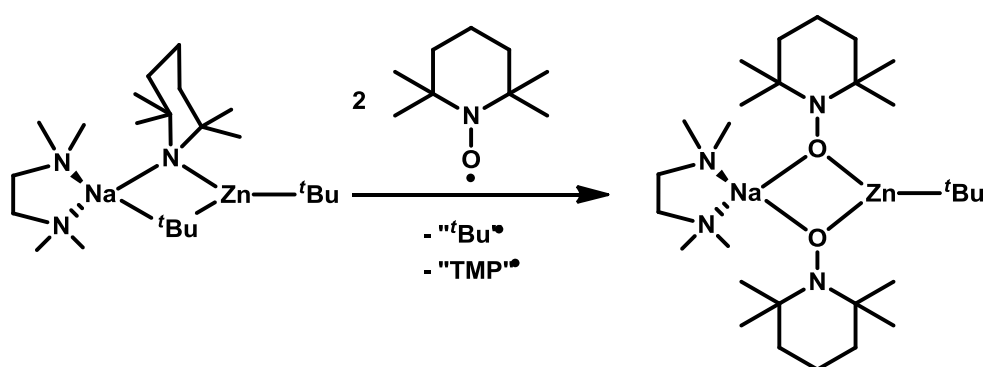
Scheme 4.7: Synthesis of bis-TEMPO zincate **4e**.

4.2.2   2a acting as a SET reagent towards chalcone

After realising that **2a** could function as a SET reagent, it was decided to probe its chemistry further with the pharmaceutically-important aromatic α,β-unsaturated ketone, chalcone (1, 3-diphenyl-2-propen-1-one). Among their numerous therapeutic properties, substituted chalcones are known as antihyperglycemic agents,[144] and have shown themselves effective in the prevention of ageing and various cancers.[145] Chalcones are highly conjugated molecules, with complete delocalisation of each benzene ring's π-electron system. Their enone functionalities also imbue these species with fairly low redox potentials, thus allowing them to participate in electron transfer reactions with relative ease.[146] The reaction of **2a** with chalcone was intriguing due to the diverse range of possible reaction types/regiochemistries which could occur. To elaborate, we envisaged that it was possible for chalcone to undergo 1,2-, 1,4-, 1,6- (or even 1,8-) addition, deprotonation or SET (due to the extensive conjugation within the molecule) (**Figure 4.9**).
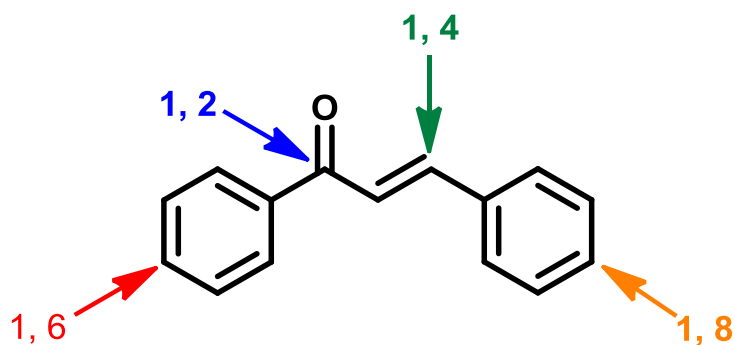
Fig. 4.9: Positions of possible addition to chalcone.

On treating **2a** with an equimolar quantity of chalcone (**Scheme 4.8**), the isolated crystalline product revealed that no ^{t}Bu addition had occurred and that [(TMEDA)·{Na(µ-TMP)Zn(^{t}Bu)}$_2$(µ-OCPhCH=CHPhCHPhCH=CPh-µ-O)] **4f** was isolated as the sole product (**Figure 4.11**). The formation of **4f** can be rationalised in terms of a SET reaction. One canonical form of chalcone (**Figure 4.10**) can be compared to that of TEMPO – it has an oxy radical centre (as well as a benzyl radical centre).
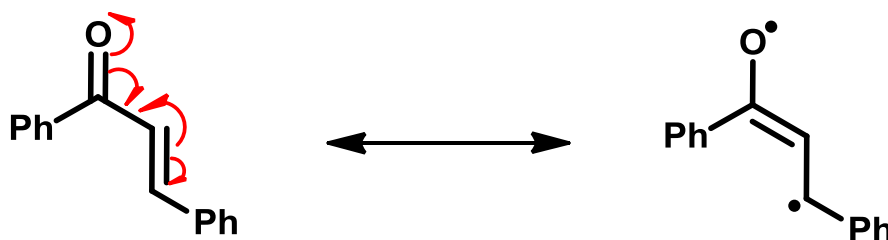
Fig. 4.10: Generation of a diradical canonical form of chalcone.

4.2.3 Crystallographic studies of [(TMEDA)·{Na(µ-TMP)Zn(^{t}Bu)}$_2$(µ-OCPhCH=CHPhCHPhCH=CPh-µ-O)] 4f

When **2a** is treated with chalcone it is proposed that a dinuclear sodium zincate containing the familiar Na-N$_{TMP}$-Zn-O ring is formed which spontaneously dimerises due to the presence of the benzyl radical to form the bimetallic *tetra*nuclear species **4f**. The mean sum of these internal angles of each ring totals 358.95°. The zinc atom resides in a trigonal planar environment, bound to a remaining unreacted ^{t}Bu arm, displaying a short Zn-C distance of 2.011(5) Å. On moving form an enone C=O to an enol C-O bond, this C-O distance moves from 1.204(6) Å in chalcone[147] to a longer distance of 1.339(5) Å. The C7-C8 double bond distance from the unreacted chalcone molecule moves from 1.319(6) Å, to an elongated distance of 1.493(6) in the newly

formed single bond of the zincate species. Concommitant formation of a new enolate C-C double bond occurs, with resultant shortening to a value of 1.332(6) Å from 1.478(6) Å of the C8-C9 carbon atoms. The Na atom exists in a severely distorted tetrahedral geometry, with the sum of its surrounding angles 676.03° (O1–Na1–N1 104.70(14), O1–Na1–N2 153.70(16), O1–Na1–N3 77.72(13), N1–Na1–N2 73.12(15), N1–Na1–N3 148.55(17), N2–Na1–N3 118.24(15)). The greatest deviation from true tetrahedral occurs (Δ 44.7°) in the O1-Na1-N2 angle. The torsion angle between the atoms C(8)-C(7)-C(59)-C(58) is 53.4(6)°, and the torsion angle on the opposing face of the alkene (*i.e.,* between the two phenyl rings), between the atoms C(1)-C(7)-C(59)-C(60) is -54.0(6)°.
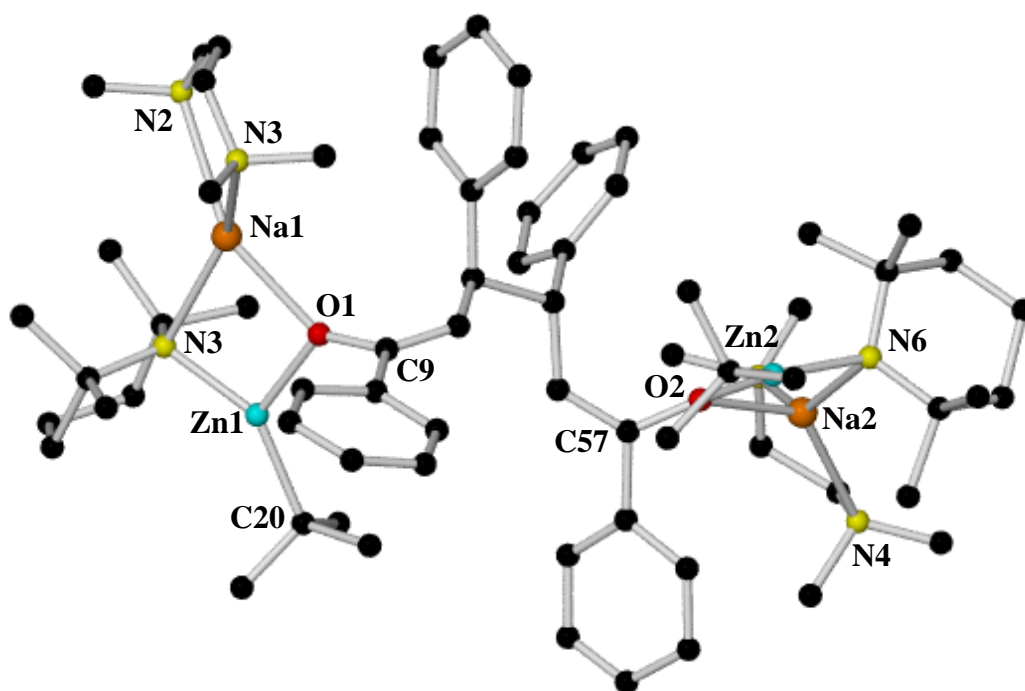
Fig. 4.11: Molecular structure of **4f**. Only one diastereomer (1Z, 3S, 4S, 5Z) is shown. This co-crystallises only with its enantiomer to give an overall racemic crystal. Key bond distances (A˚) and angles (1): Na1–O1, 2.264(3); Na1–N1, 2.530(5); Na1–N2, 2.582(4); Na1–N3, 2.494(5); Na2–O2, 2.259(4); Na2–N4, 2.421(5); Na2–N5, 2.620(6);Na2–N6, 2.433(5); Zn1–O1, 1.995(3); Zn1–N3, 1.983(4); Zn1–C20, 2.011(5); Zn2–O2, 2.004(4); Zn2–N6, 1.951(4); Zn2–C70, 1.987(6); C9–O1, 1.339(5); C57–O2, 1.331(6); O1–Na1–N1, 104.70(14); O1–Na1–N2, 153.70(16); O1–Na1–N3, 77.72(13); N1–Na1–N2, 73.12(15); N1–Na1–N3, 148.55(17); N2–Na1–N3, 118.24(15); O2–Na2–N4, 109.75(17); O2–Na2–N5, 137.5(2); O2–Na2–N6, 78.67(15); N4–Na2–N5, 73.27(17); N4–Na2–N6, 141.4(2); N5–Na2–N6, 126.49(18); O1–Zn1–N3, 97.48(15);

O1–Zn1–C20, 120.58(18); N3–Zn1–C20, 141.7(2); O2–Zn2–N6, 97.67(17); O2–Zn2–C70, 119.1(2); N6–Zn2–C70, 143.1(2).
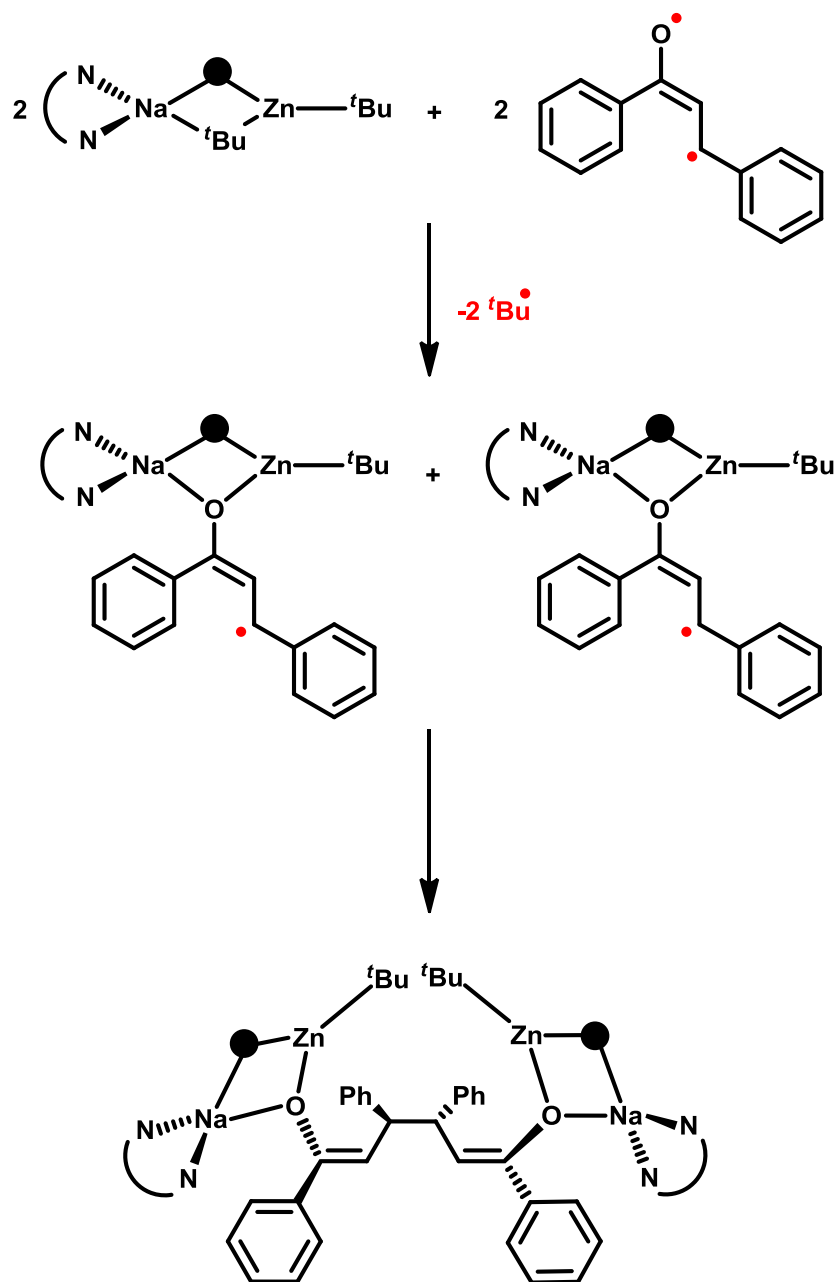
Scheme 4.8: Initial SET by the sodium zincate, followed by coupling of two end-capped chalcone units.

To the best of our knowledge there has been no firm structural evidence of the intermediates of SET reactions involving chalcone. Some examples of this transformation do exist. For instance when chalcone is treated with an excess of anthracene hydride, the major product (82%) is the reduced saturated ketone PhCH$_2$CH$_2$COPh whilst a minor product (17%) was the 1,6-diketone, 1,3,4,6-tetraphenylhexane-1,6-dione.[148] This unusual zincate-induced chalcone-coupling

product therefore represents the first crystallographically characterized species of this type, setting great precedent for other potential SET coupling reactions.

4.2.4   NMR spectroscopic studies of 4f

NMR spectroscopic studies of d_8-THF solutions of **4d, 4e** and **4f** revealed that the TMEDA donor ligand is displaced by the ethereal solvent, but otherwise the solid state structures appear to be retained in solution. For the chalcone example, four distinct signal sets are observable in the aromatic region, telling of an unusual scenario where all four phenyl rings exhibit accidentally spectroscopically equivalent *meta* and *para* signals, yet two different *ortho* environments. These two *ortho* doublets fall furthest downfield, at values of 7.74 and 7.33 ppm respectively, each integrating to 4 H atoms. An impurity giving rise to a number of overlapping signals underneath the *para* resonance, increases the integration value associated with this signal. The remaining *meta* and *para* signals fall as multiplets at values of 7.13 and 6.99 ppm respectively. The allylic and benzylic C-*H* resonances are markedly different, appearing at 4.96 and 3.82 ppm. Since d_8-THF is utilised as the bulk solvent, the TMEDA ligand has been displaced, thus appearing free at 2.30 ppm (CH_2CH_2) and 2.15 ppm (CH_3). The TMP signal appears in the usual three environments [γ-CH_2 1.63 ppm, β-CH_2 1.29 ppm and α-CH_3 1.06 ppm], the final remaining resonance of the spectrum attributed to the still intact ^{t}Bu carbanion, at a value of 0.94 ppm (**Figure 4.12**).

The ^{13}C spectrum mirrors the ^{1}H spectrum, with four distinct aromatic signals, not three as might be supposed. The two *ortho* signals appear at 130.9 and 126.1 ppm, with the remaining *meta* and *para* resonances at values of 127.7 and 125.4 ppm respectively. There is an even more pronounced difference in allylic and benzylic signals here, their respective resonances appearing at 91.4 and 53.9 ppm. Note that the allylic C-H resonance is very small within the ^{13}C spectrum but is clearly evident in the corresponding HSQC spectrum. The free TMEDA signals fall at 58.9 ppm (CH_2) and 46.2 ppm (CH_3), followed by the more upfield TMP resonances (α-CH_3 32.3 ppm, β-CH_2 30.6 ppm and γ-CH_2 19.3 ppm). The final resonance within this spectrum is that of the ^{t}Bu carbanion, appearing upfield at 29.0 ppm.
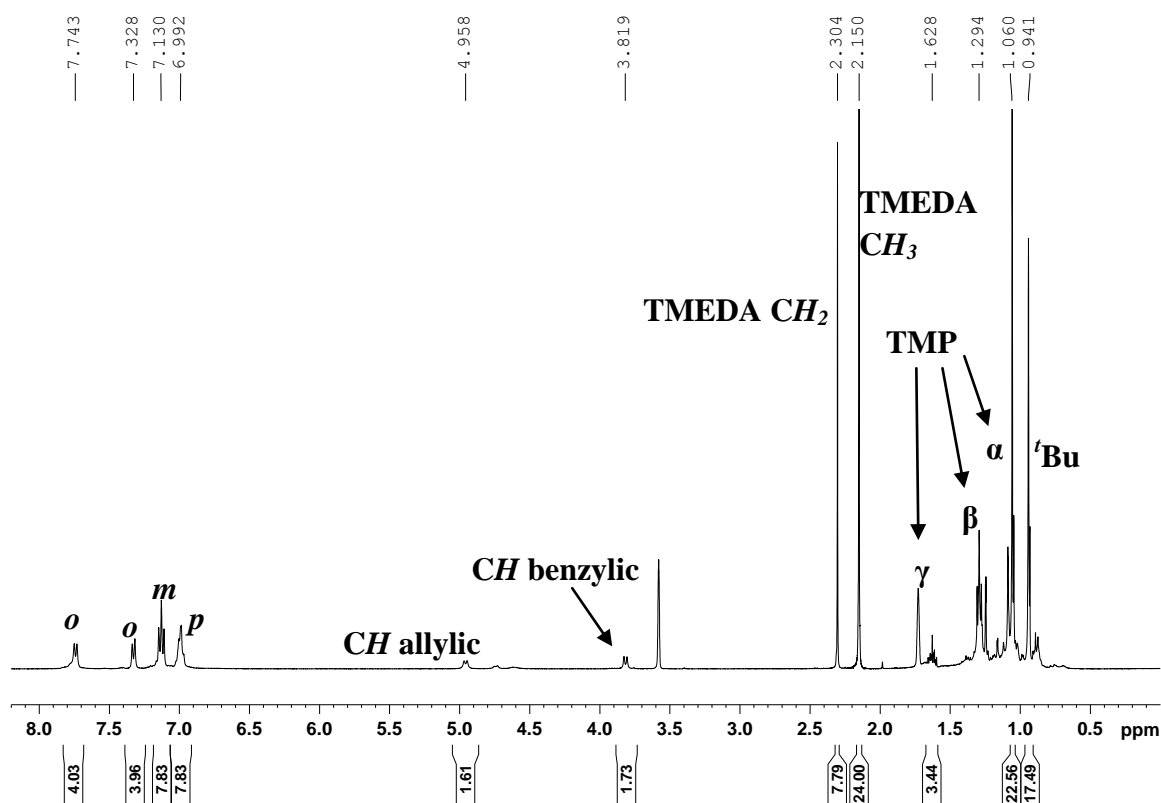
Fig. 4.12: ^{1}H NMR spectrum (400.13 MHz, 300 K, d$_8$-THF) of **4f.**
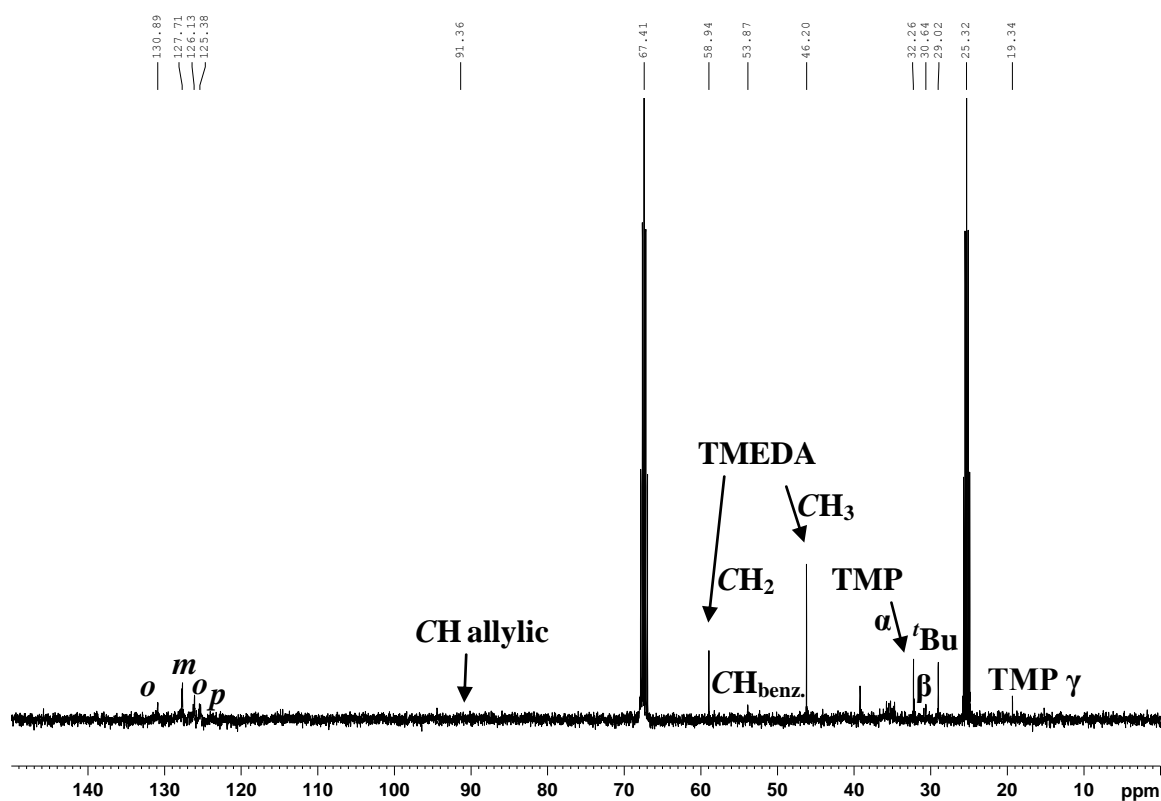
Fig. 4.13: ^{13}C NMR spectrum (100.62 MHz, 300 K, d$_8$-THF) of **4f.**

4.2.5 Reactivity of 2a towards di-tert-butyl nitroxide (DTBN)

With the results of both the chalcone and TEMPO reactions with the sodium zincate providing compelling evidence of its acting as an agent of SET, a further example to bolster its profile in this area was investigated. To this end, another stable nitroxyl radical was selected, very closely related to TEMPO, namely di-*tert*-butyl nitroxide. This room temperature stable radical species has shown itself an efficient quenching entity in photoaddition reactions,[149] and as a sensitizer of cells to the effects of X-ray radiation.[150] Under the same conditions as the previous reactions, equimolar equivalents of **2a** and di-*tert*-butyl nitroxide (DTBN) were reacted together in hexane, producing a bright red solution almost instantaneously. After resting on the bench overnight, a crop of large colourless block crystals was obtained, of sufficient quality for X-ray. Upon analysis they were found to be the bis-nitroxyl containing sodium zincate [(TMEDA)·Na(μ-DTBN)$_2$Zn(^{t}Bu)] **4g**. Unlike the previous example with TEMPO as the radical species, utilising only a single equivalent of DTBN here results in dual radical activation of the parent zincate i.e. both bridging TMP· and ^{t}Bu· radicals are expelled and replaced with two newly created bridging di-*tert*-butyl nitroxyl anions. This is perhaps a disproportionation product, as previously only two equivalents of the radical brought about this dual reactivity, whereas a single equivalent resulted only in SET by the bridging ^{t}Bu ligand. Attempts to produce a compound containing only a single DTBN unit were unfortunately unsuccessful.
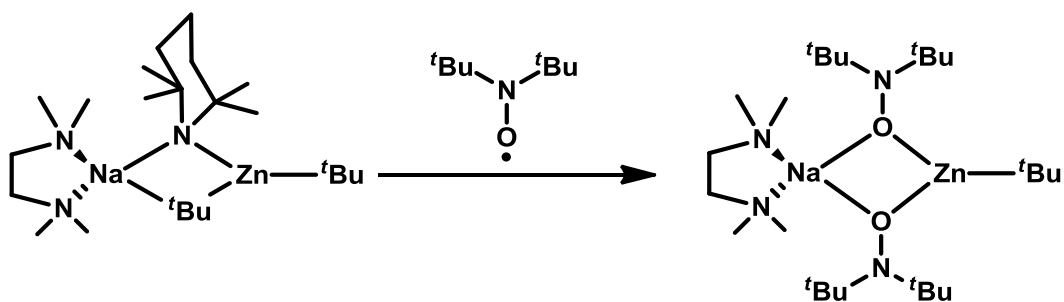
Scheme 4.9: Reaction of 1:1 **2a** with DTBN.

4.2.6 Crystallographic studies of [(TMEDA).Na(μ-DTBN)$_2$Zn(^{t}Bu)] 4g

At the centre of the structure is a four membered Na-O-Zn-O ring, with the sum of the internal angles totalling 355.87°. This four membered ring is slightly puckered, with an O1*-Na1-O1-Zn1 torsion angle of -16.17(6)°. After reaction, the zinc atom is still bound to a single carbon atom of the remaining terminal ^{t}Bu group, a short strong

contact of 1.992(2) Å. The anionic nature of the nitroxyl ligand is evidenced definitively by the N-O bond distance of 1.448(14) Å, identical to that of the related Na TEMPO complex [1.448(15) Å]. The sodium atom exhibits a four coordinate distorted tetrahedral geometry, with the greatest deviation from true tetrahedral the N1-Na1-N2 angle (Δ-33.89°).
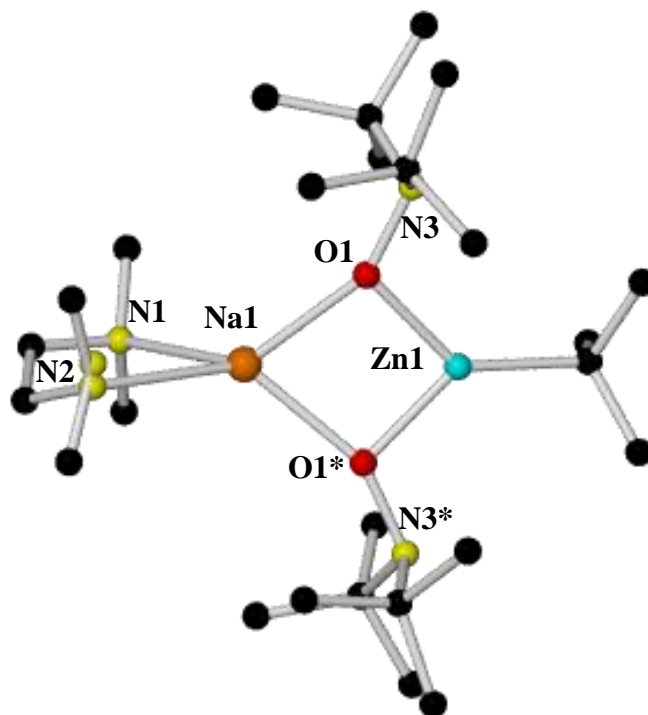
Fig. 4.14: Molecular structure of **4g**. Key bond distances (Å) and angles (°): Zn1-O1 1.938(10), Zn1-C5 1.992(2), Na1-O1 2.219(11), Na1-N1 2.453(2), Na1-N2 2.598(2), O1-N3 1.448(14), Na1-O1-Zn1 95.04(4), O1-Zn1-O1* 89.72(6), O1-Zn1-C5 134.91(3), O1-Na1-O1* 76.07(5), O1-Na1-N2 127.29(4), N1-Na1-N2 74.11(2), O1-Na1-N1 133.64(19). Symmetry operation to generate equivalent atoms marked with an asterisk: x, -y-0.5, z.

4.2.7 NMR spectroscopic studies of 4g

In solution the structure appears to be retained, though with displacement of the TMEDA ligand by the deuterated THF solvent. We were forced to move to d_8-THF from C_6D_6 owing to the unfortunate broadness and lack of peak distinction present in the latter. In d_8-THF, a relatively simple ^{1}H NMR spectrum is observed. The now free TMEDA signal moves downfield and sharpens into two distinct resonances. The ^{t}Bu signals of the nitroxyl ligand appear as a single resonance at 1.19 ppm, and the ^{t}Bu resonance, bound to the zinc, slightly upfield at 1.14 ppm, completing the spectrum. It is

interesting to note this extra evidence of the anionic nature of the nitroxyl ligand within the zincate **4g**, as previously the paramagnetism inherent in the free radical species would have made accurate study by ^{1}H NMR spectroscopy impossible.
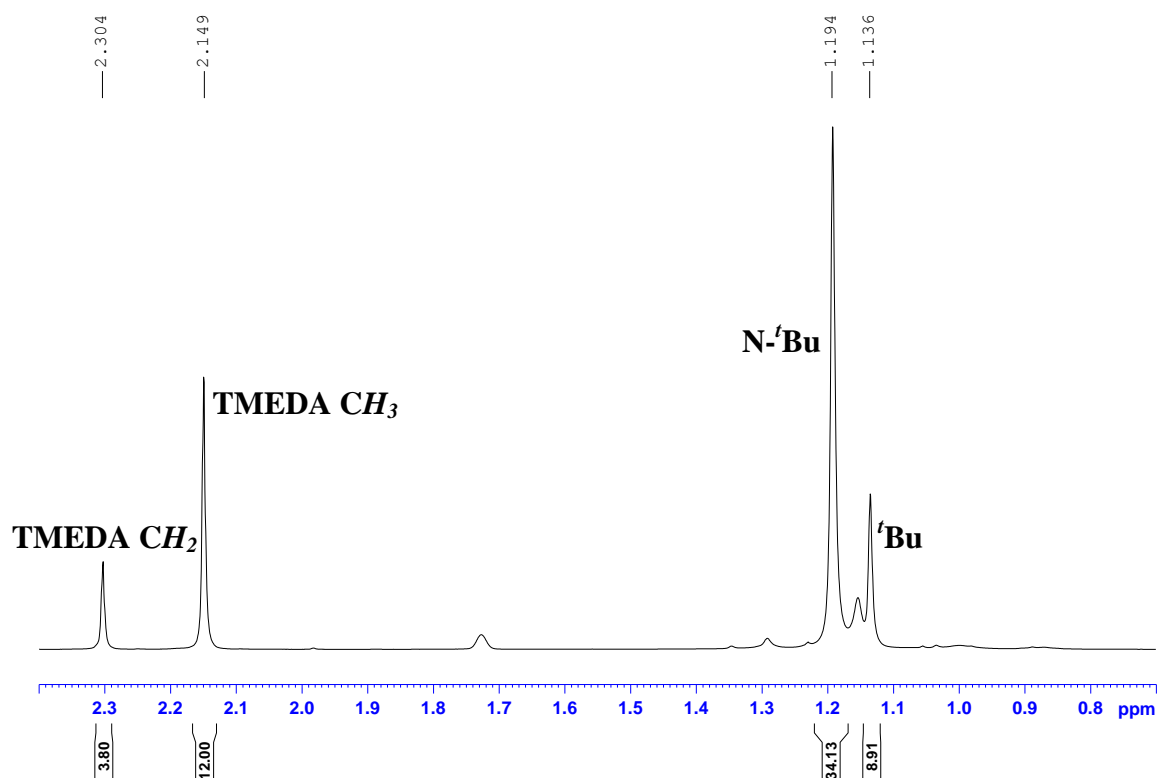
Fig. 4.15: ^{1}H NMR spectrum of **4g** (400.13 MHz, 300 K) in d_8-THF solution.

4.3 Synthsesis of a potassium magnesiate exhibiting unusual bonding modes

In recent years the solid- and solution-state structures of several alkali metal amido magnesiate complexes have been reported, and knowledge of these has led towards greater understanding of the complex reaction mechanisms involved in a seemingly simple deprotonation. Such structural studies include significant work on lithium[78, 151] and sodium reagents.[152] However, and of particular interest to this work, the X-ray structures of only three simple amido magnesiates containing the heavier alkali metal potassium have thus far been elucidated.[152a, 153] In addition, these potassium reagents have been utilized in metallation protocols and the subsequent heterobimetallic organometallics have been isolated and structurally characterized prior to electrophilic quenching.[82, 154] The simple complexes have tended to adopt similar structural motifs to their lithium and sodium counterparts (**Figure 4.16**). In a quest to expand this

underdeveloped area, we have achieved the solid- and solution-state (in C_6D_6 solution) characterization of the tris(diphenylamide) potassium magnesiate, [(PMDETA)·K(μ-NPh$_2$)Mg(THF)(NPh$_2$)$_2$] **4h** which contains several unusual bonding features.
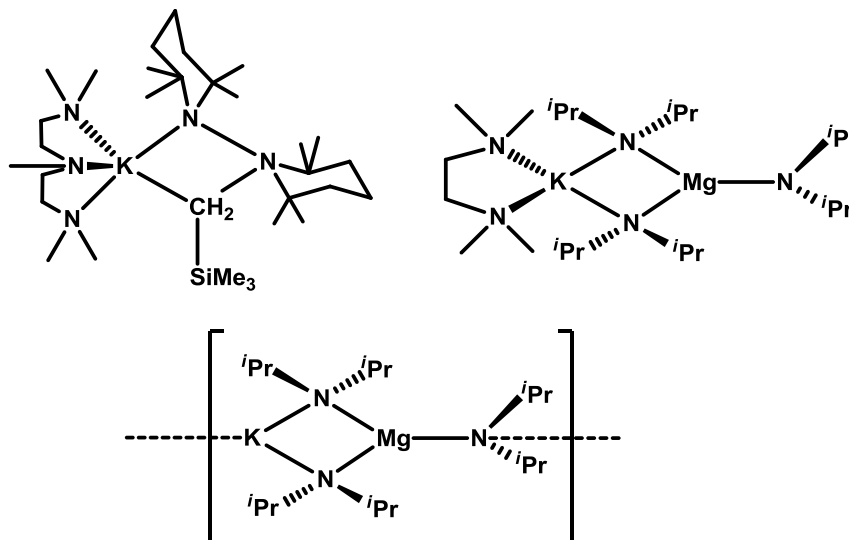
Fig. 4.16: Previous structurally elucidated potassium amido-magnesiate complexes.

4.3.1   Preparation of [(PMDETA)·K(μ-NPh$_2$)Mg(THF)(NPh$_2$)$_2$] 4h

The synthesis of **4h** was achieved by fully aminating the distinct metals. This was achieved by combining an equimolar mixture of benzylpotassium and di-*n*-butylmagnesium with three molar equivalents of diphenylamine (**Scheme 4.10**) hence, bringing the metals together into a single complex. For the reaction to proceed, to achieve homogeneity and to aid crystallization, it was performed by heating gently a medium consisting of a mixture of hexane (10 ml), THF (6 ml) and one molar equivalent of the triamine PMDETA (0.42 ml). The Schlenk tube was allowed to cool in a Dewar flask filled with hot water and colorless crystals of **4h** (in an unoptimized yield of 42%) deposited from the solution.

$^{n}Bu_2Mg + PhCH_2K + 3 Ph_2NH \xrightarrow[\substack{PMDETA \\ - 2\,^{n}BuH \\ - PhCH_3}]{hexane/THF}$
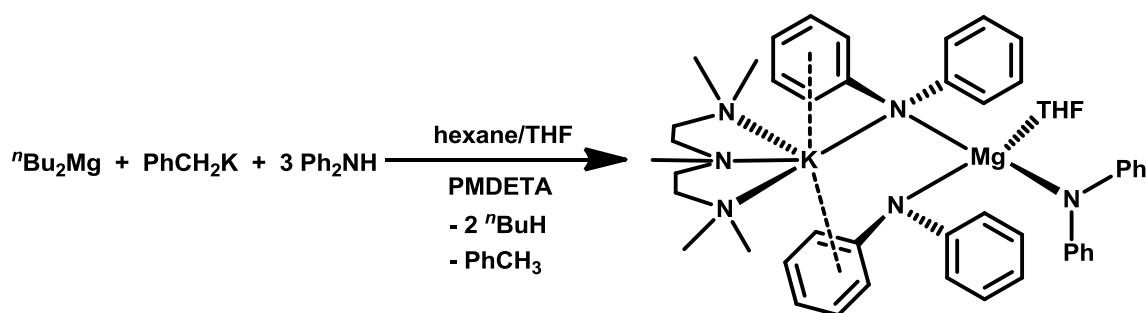
Scheme 4.10: Synthesis of **4h** by reaction of $^{n}Bu_2Mg$, $PhCH_2K$ and Ph_2NH in a 1:1:3 ratio.

4.3.2 Crystallographic studies of 4h

X-ray crystallographic studies reveal that **4h** crystallizes in the monoclinic system with space group $P2_{1/n}$. The molecular structure of **4h** reveals a monomeric, dinuclear potassium magnesiate motif in a contacted ion pair arrangement. Dealing with each metal in turn, the magnesium center is tetracoordinate (binding to three N_{amide} and one O_{THF} atom) adopting a distorted tetrahedral arrangement [range of bond angles around Mg1, 94.42(4)–122.58(5)°]. Distortion from a perfect tetrahedron is most pronounced at the N1–Mg1–O1 (closed) and N1-Mg1-N2 (opened) fragments. In the other crystallographically-characterized potassium amido magnesiates the magnesium centers adopt three-coordinate, trigonal planar geometries.[152a, 153] In **4h** we presumably see coordination expansion due to the relatively low steric demand and planar rotational flexibility of the diphenylamide ligand in comparison to that of the TMP and di-isopropylamide ligands previously used. Despite the tetracoordination of the Mg center, the Mg–N bond distances in **4h** are similar to those observed in the previous magnesiates.

Turning to the potassium atom, it has rather complex coordination chemistry due to the presence of phenyl groups on the amido ligand. It bonds to a crystallographically disordered PMDETA ligand in the normal tridentate N3-fashion but to only one amido-N atom [K1–N3 distance, 3.0784(11) Å]. The K–N_{amide} in **4h** distance is significantly longer (0.12–0.22 Å) than that observed in the previous magnesiates, which is surprising considering that diphenylamide exhibits the smallest steric demand. Note that the dative K–N interactions are 0.1–0.2 Å shorter than the K–N_{amido} interaction, as if the alkali metal is moving towards a solvent separated scenario. Reflecting the soft nature

of the heavy alkali metal, the remainder of the potassium centre's coordination sphere comprises a series of π-K$\cdots$C$_{aryl}$ interactions. The strongest of these adopt an η^6-bonding mode to a phenyl ring residing on N2 (C29, C30, C31, C32, C33 and C34; K$\cdots$centroid distance, 3.031 Å). The second phenyl ring on N2 does not contribute to the stabilization of the K atom. One of the phenyl rings on N1 weakly contributes to the cumulative stabilization of the K center (η^2-contributions from C23–C28 bond, 3.183 Å); whilst the second ring has a relatively negligible interaction with the metal (η^2-contribution from C17–C22 bond, 3.400 Å). Turning to the constituent monomeric parts of **4h**, the molecular structures of several potassium homometallic diphenylamide solvates including a monomeric solvent-separated18-crown-6 species,[155] a dimeric tris(THF)-solvate,[156] and polymeric dioxane[102] and TMEDA solvates[157] are known. In these neutral complexes (as opposed to an anionically-charged ate species) the prevalence of K$\cdots$C interactions appears not to be as great as that found in **4h**. The synthesis of magnesium bis(diphenylamide) was first reported in 1964 by Issleib and Deylig,[158] with the first structural information coming to light a decade later by Fröhlich.[159] Recently, the chemistry of a four-coordinate, monomeric THF adduct of magnesium bis(diphenylamide) (THF)$_2$Mg(NPh$_2$)$_2$ has been studied by Westerhausen and co-workers.[160] The mean Mg–N bond in **4h** (2.051 Å) is only slightly longer than that in Westerhausen's monomer (2.012 Å), despite the fact that three amido anions surround the metal in **4h**.
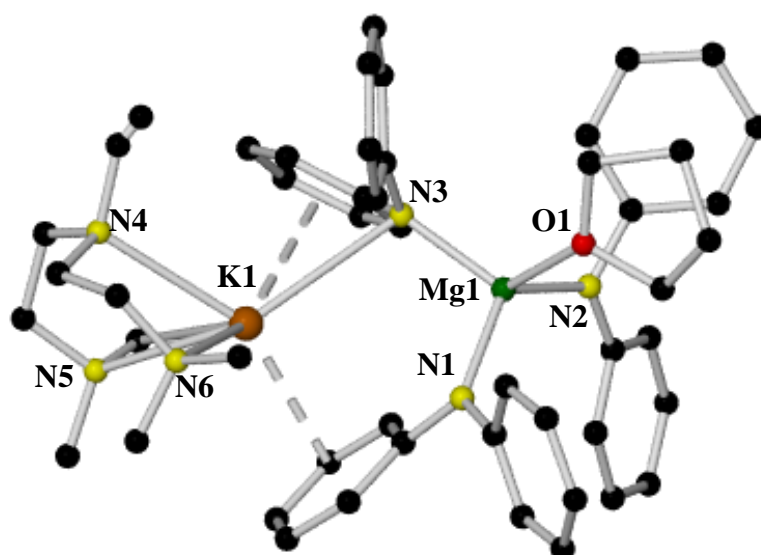
Fig. 4.17: Molecular structure of **4h**. Hydrogen atoms, the weak K1–C17/C22 centroid interaction and disorder component involving the PMDETA ligand have been omitted for clarity. Key bond distances (Å) and angles (°): Mg1–N1, 2.0434(11); Mg1–N2, 2.0472(11); Mg1–N3, 2.0610(10); Mg1–O1, 2.0434(10); K1–N3, 3.0784(11); K1–N4,

2.8690(13); K1–N5, 2.830(3); K1–N6, 2.971(3); 3.2440(13); K1–C23, 3.2441 (14); K1–C28, 3.2770(14); K1–C29, 3.1697(13); K1–C30, 3.0784(11); K1–C31, 3.3011(17); K1-C32, 3.5030(14); K1-C33, 3.5203(14); K1–C34, 3.3605(15); N1–Mg1–N2, 122.58(5); N1–Mg1–N3, 112.92(4); N1–Mg1–O1,94.42(4); N2–Mg1–N3, 108.06(4); N2–Mg1–O1, 103.16(4); N3–Mg1–O1, 114.76(5);N3–K1–N4, 124.04(3); N3–K1–N5, 114.07(7); N3–K1–N6, 137.04(7); N4–K1–N5,68.16(6); N4–K1–N6, 95.68(8); N5–K1–N6, 62.79(9).

4.3.3 NMR spectroscopic studies of 4h

The solubility of **4h** in C_6D_6 allowed the complex to be characterized by ^1H and ^{13}C NMR spectroscopy. Despite **4h** being isolated *in vacuo*, its ^1H NMR spectrum indicated that the Mg-bound THF was not lost on isolation. As the quantity of THF in solution is consistent with that in the solid-state it is unlikely that the ether disengages from the magnesium atom in solution. The two THF resonances appear broad and the upfield resonance (attributed to OCH_2CH_2) has shifted dramatically further upfield in the ^1H NMR spectrum from its usual position in unbound THF (from 1.74 to 0.90 ppm). The broadness of these resonances is indicative of the molecule undergoing dynamic processes in solution (*i.e.*, probably enduring NMR-time scale conformational changes whilst attached to the metal). The ^{13}C NMR spectrum also shows two broad THF resonances whose chemical shifts (69.1 and 25.1 ppm) are much less discriminatory with respect to uncoordinated THF (67.4 and 25.5 ppm). The remainder of the resonances in the ^1H NMR spectrum appear to show that the potassium magnesiate does not stay intact in arene solution as only three resonances (at *ortho*-7.52, *meta*-7.13 and *para*-6.60 ppm) are observed. This indicates – differently from the crystal structure – that all three of the diphenylamide ligands in **4h** are chemically and spectroscopically identical in C_6D_6 solution under the conditions studied, with the likelihood that a solvent-separated species [*e.g.*, $\{K(C_6D_6)_x\}^+\{(THF)Mg(NPh_2)_3\}^-$] exists to optimize the number of π–K$^\cdot$ $^\cdot$C contacts involving the small π-rich C_6D_6 molecules, satisfying potassium's well-established carbophilicity.[103d, 161] This phenomenon is in concordance with the surprisingly long K–N$_{amide}$ bond distance in the solid state structure of **4h**, which exists as weakly bonded contacted ion pair.
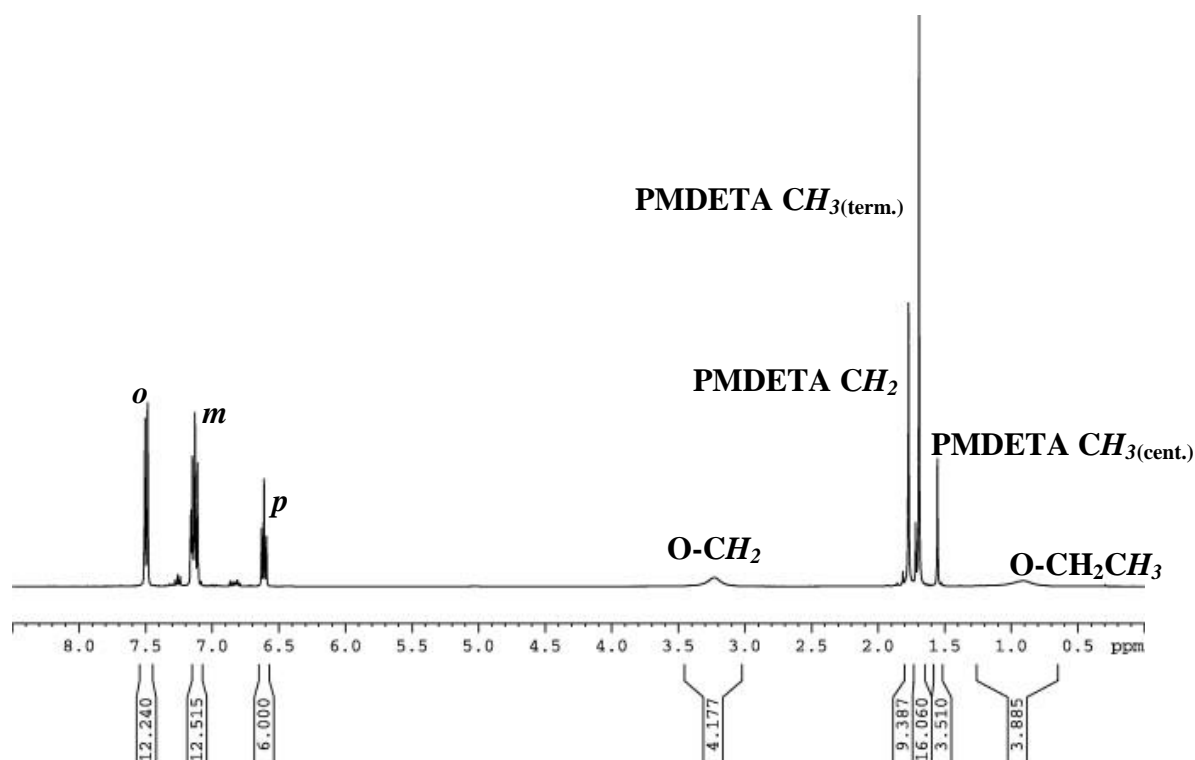
Fig. 4.18: ^{1}H NMR spectrum (400.13 MHz, 293K) of a C$_6$D$_6$ solution of **4h.**

4.4 Synthesis of the bis-phenyl analogue of [(TMEDA)Na·(μ-TMP)(μ-^{t}Bu)Zn(^{t}Bu)] for use in new alkylation reactions

It has been previously discussed how the bis-alkyl amido zincate **2a** has been utilised in effecting anomalous 1, 6- addition of its ^{t}Bu group towards the related ketones benzophenone, fluorenone and 2-benzoylpyridine. In addition to this, we have shown how changing the ^{t}Bu to the less sterically hindered Et group dramatically effects the outcome of the reaction. As a direct continuation of this work, we wished to generate a reagent with the potential of effecting addition of an arguably more exciting phenyl group, so opted in this instance for the biaryl zinc reagent diphenylzinc.

Adding equimolar quantities of NaTMP and Ph$_2$Zn in hexane, followed by addition of TMEDA provided a colourless solution. Overnight cooling at -28°C gave a small deposit of crystalline material, which on analysis, was found to be the monomeric unit [(TMEDA)Na·(μ-TMP)(μ-Ph)Zn(Ph)] **4i**. Direct co-complexation had occurred as expected, with the sodium chelated by the TMEDA ligand, bridged to the Zn centre through the N atom of the TMP, and also through a single phenyl group, which binds η^2

113

to the sodium. The Na-C contacts to this group are 2.75 Å (Na-C$_{ipso}$) and 2.86 Å (Na-$_{ortho}$) respectively, the C$_{ipso}$ referring to the carbon atom of the phenyl ring bound to both the Na and Zn centres, forming the centre of the bridge and a single vertice of the Na-N-Zn-C four membered ring at the heart of the molecule. The bonds within this ring are markedly different, evident in the far shorter Zn-C$_{ipso}$ distance exhibited [2.027(5) Å)]. Though the M-N$_{TMP}$ do not vary to such a degree, the Zn-N distance is, unsurprisingly, shorter [2.008(4) Å cf. 2.420(5) Å in Na-N distance]. The zinc centre is trigonal planar, with relatively little deviation in each angle from the true trigonal planar value of 120° [N13-Zn1-C121 127.77(18), N13-Zn1-C111 111.44(18) and C121-Zn1-C111 119.61(19)^{o}]. The pentacoordinated sodium centre experiences a large range of angles, from the highly acute C116-Na1-C111 angle of 28.69(13)^{o} to the obtuse N13-Na1-N141 angle of 133.84(15)^{o}.
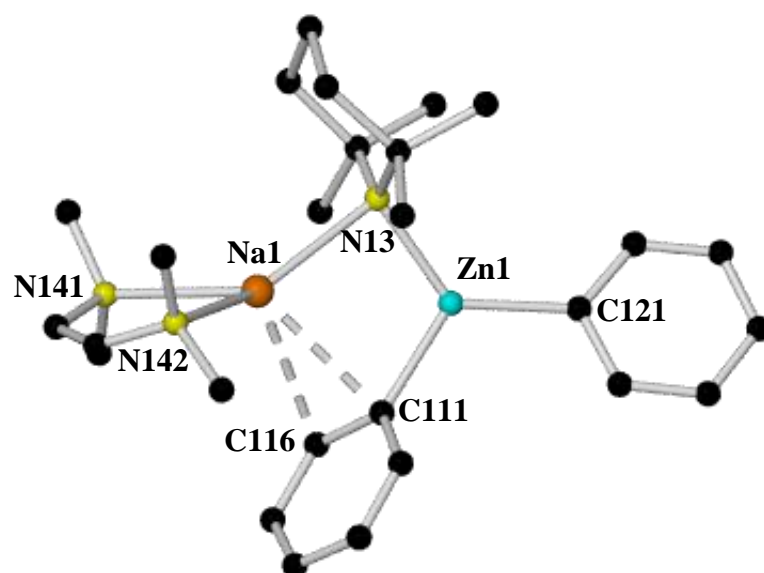
Fig. 4.19: Molecular structure of [(TMEDA)·Na(μ-TMP)(μ-Ph)Zn(Ph)] **4i**. Key bond distances (Å) and angles (°): Zn1-C121 2.007(5), Zn1-N13 2.008(4), Zn1-C111 2.027(5), Na1-N13 2.420(5), Na1-N141 2.488(4), Na1-N142 2.469(5), Na1-C111 2.753(5), Na1-C116 2.850(5), N13-Zn1-C121 127.77(18), N13-Zn1-C111 111.44(18), C121-Zn1-C111 119.61(19), N13-Na1-N142 133.52(17), N13-Na1-N141 133.84(15), N142-Na1-N141 75.12(16), N13-Na1-C111 79.96(15), N142-Na1-C111 111.99(17), N141-Na1-C111 128.05(16), N13-Na1-C116 99.12(15), N142-Na1-C116 111.89(16), N141-Na1-C116 99.56(15), C111-Na1-C116 28.69(13).

4.4.1   NMR spectroscopic studies of 4i

The ^{1}H NMR spectrum of this species is fairly simple and matches nicely the structure elucidated previously, indicating that it is mostly retained in solution. Focusing initially on the aromatic region of the spectrum, we see three distinct sets of signals, with well defined *ortho* (4H, d, 8.03 ppm), *meta* (4H, t, 7.36 ppm) and para (2H, m, 7.24 ppm) resonances. The fact that only three signals are observed means that in C_6D_6 solution, each phenyl ring is seen as spectroscopically equivalent, different to the solid state structure, as in this one phenyl ring makes significant Na-π contacts. The aliphatic region is slightly more convoluted, with the TMEDA appearing at two sharp and distinct resonances in the usual 12:4 ratio (at values of 1.5 and 1.43 ppm representing the methyl and ethyl H atoms respectively), whereas the TMP signal is observed as two signals; the methyl and β-CH_2 signals appear as a single broad hump (1.36 ppm), presumably due to dynamic exchange in solution, the remaining γ-CH$_2$ signal downfield at a value of 1.93 ppm.
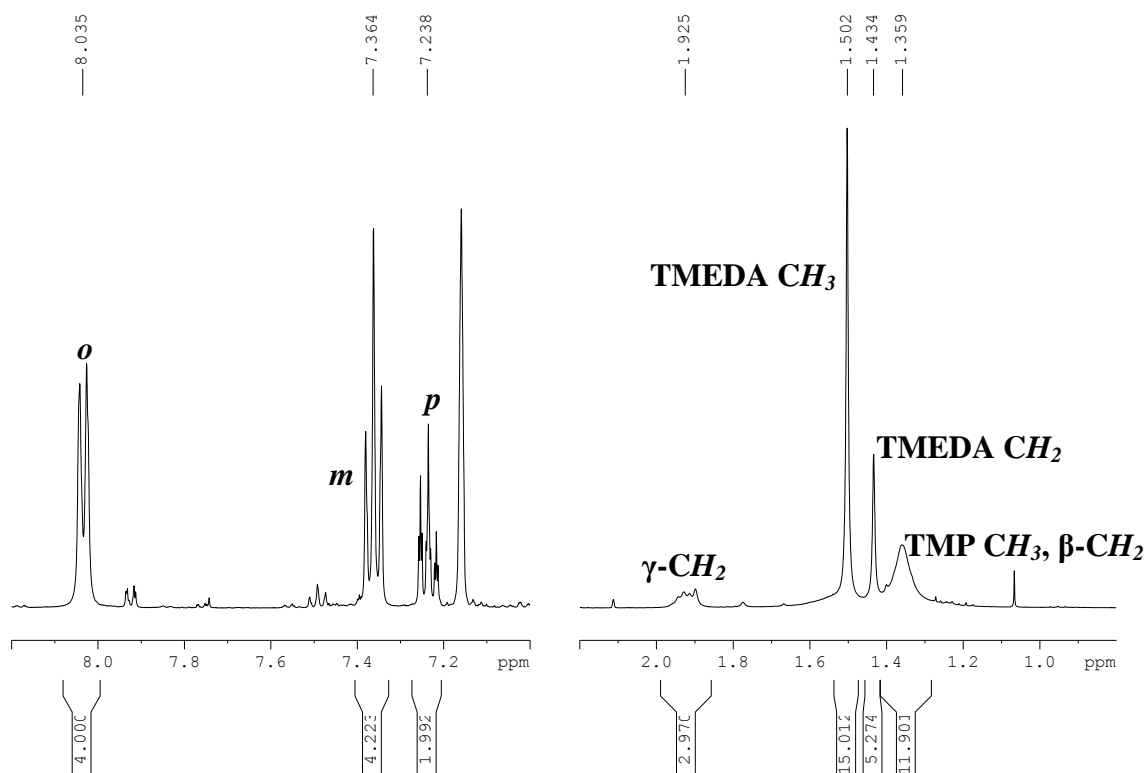
Fig. 4.20: ^{1}H NMR spectrum of **4i** in C_6D_6 solution.

Again, the ^{13}C NMR spectrum exhibits three distinct aromatic resonances, corresponding to the *ortho*, *meta* and *para* positions, at values of 139.5, 127.5 and 125.6 ppm respectively. In the aliphatic region, two signals are observed for the TMEDA

ligand, the methyl groups all equivalent at a value of 45.6 ppm, and the remaining CH_2 resonances at 56.7 ppm. The TMP exhibits a broad resonance at 35.4 ppm, indicative of the four methyl groups, its broadness a direct mimic of that observed in the ^1H NMR spectrum. The β and γ CH_2 signals are by contrast sharp, appearing at 40.8 and 20.3 ppm respectively (**Figure 4.21**).
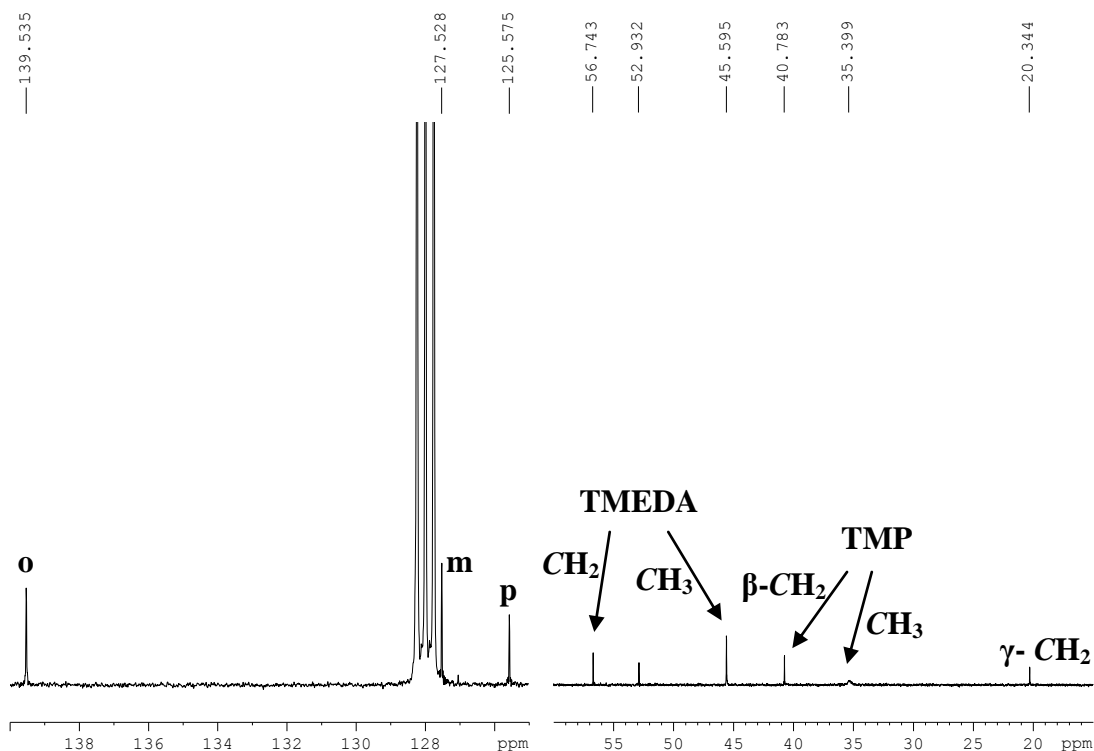
Fig. 4.21: ^{13}C NMR spectrum of **4i** in C_6D_6 solution.

Owing to the low steric demand of the phenyl groups bound to the zinc, species **4i** is unlikely to act as an effective Brønsted base, however, the hope is that future projects can show that perhaps this species can facilitate addition of a phenyl group in a manner consistent with the alkylation reactions discussed earlier, C-C bond formations of this type without the need for a transition-metal catalyst being of great importance in synthetic chemistry.

In summary, unstudied thus far in the field of bimetallic chemistry, reactions of both *ortho-* and *meta-* isomers of the closo carborane molecule were carried out. It was discovered that the reaction of [(TMEDA)·Na(μ-^{n}Bu)(μ-TMP)Mg(TMP)] with the *ortho-* isomer resulted in a solvent separated structure on dissolution by THF, commonly encountered when utilising this polar solvent. The cation was a familiar Na$^+$, sequestered by six THF molecules, whereas the more interesting anionic portion consisted of a Mg centre surrounded by three monodeprotonated carborane anions and a

single THF molecule [{(THF)$_6$·Na}$^+${(THF)·Mg(o-carborane)$_3$}$^-$]. This structure was unfortunately of insufficient quality to infer even definitive connectivity, the main drawback of the carborane substrates being their apparent inability to give high quality crystalline material. Turning to the related lithium zincate [(THF)·Li(μ-^{t}Bu)(μ-TMP)Zn(^{t}Bu)], which was reacted with the *meta-* isomer, followed by dissolution with THF. Again a solvent separated species of poor quality was observed, consisiting of three cationic [(THF)$_6$·Li$^+$] moieties, the anionic portion consisting of a cyclic structure, with three dideprotonated carborane units, and each Zn centre bearing a third anion, a single ^{t}Bu group. As with the previous structure, poor quality has precluded any useful insight into key structural features. Although these structures regrettably did not diffract well, they serve to highlight the unusual modes of reactivity which carboranes can undergo in the presence of our complex metallators, and in future a more in-depth study would undoubtedly reveal both novel structural motifs and even unusual reactivity types such as potential polymetallation, with carboranes presenting themselves as an untapped vein in the field of metallation chemistry.

A third reactivity type which the zincate [(TMEDA)·Na(μ-TMP)(μ-^{t}Bu)Zn(^{t}Bu)] can exhibit is detailed, namely its ability to act as a single electron transfer reagent. It was shown by a previous group member that when reacted with a single molar equivalent of TEMPO, a ^{t}Bu· radical is liberated, reacting with another radical to form isobutene and isobutene, whilst simultaneously generating the TEMPO anion, which is trapped within the zincate, the structural integrity of which is obtained. The reaction of two molar equivalents of TEMPO results in twofold activation of the zincate, producing both TMP· and ^{t}Bu· radicals and subsequent replacement of these with two TEMPO anions within the bimetallic motif. This zincate with then reacted with the highly conjugated organic molecule chalcone, originally as part of the addition project, owing to the numerous different positions of reactivity within it. Surprisingly, SET had again occurred, resulting in homocoupling of two chalcone fragments, made stable and isolable by the stable zincate moieties capping each end ([(TMEDA)·{Na(μ-TMP)Zn(^{t}Bu)}$_2$(μ-OCPhCH=CHPhCHPhCH=CPh-μ-O)]). Isolation of a molecule of this type was unprecedented, representing a synthetically useful example of the zincate acting as an agent of SET, providing a solid foundation for further reactions of this type. Since these reactions can be carried out in non-polar solvents at room temperature, they could represent another new method of transition-metal free C-C coupling.

5. Investigating precursors of sodium and potassium magnesiates in inverse crown chemistry and their application in new and novel reactivities

5.1 Introduction

Magnesiation, as previously alluded to, is the process whereby a comparatively inert C-H bond is converted to a C-Mg bond by a process of deprotonation. Traditional dialkylmagnesiums and Grignard reagents have proven themselves weak Brønsted bases, and have historically played second fiddle to their more aggressive (and consequently more useful metallators) Group 1 counterparts. In moving to the magnesium bis-amides, an example of their synthetic utility had been documented by Kerr *et al*. In this study, the chiral magnesium bis-amide $[(Ph)N(Me)]_2Mg$ has been used in asymmetric deprotonation of prochiral ketones at elevated temperatures.[162] The amine most commonly utilised in these deprotonations is the bulky TMP unit, used to great effect in our own chemistry, appearing in many alkali-metal magnesium alkyl-TMP mixtures, able to deprotonate a number of weakly acidic substrates at room temperature.[163] A vast body of work conducted by Knochel has also shown the breadth and scope of magnesiation possible by his Turbo-Hauser TMPMgCl.LiCl combinations (Hauser base is an amidomagnesium halide R_2NMgX), performing Mg-H exchange on functionalized anilines, pyridines,[164] alkenes and cycloalkenes,[165] to name but a small number.

Focusing primarily on our previous research carried out at Strathclyde, it was found that more interesting chemistry could be achieved, in both structural novelty and synthetic utility, when using alkali-metal amido magnesiates in the absence of donor solvents *e.g.* THF, TMEDA. Elaborating on the example mentioned in the introduction, when BuNa, $^nBu_2Mg$ and HMDS(H) were combined in a 1:1:3 ratio, an attempt was made to achieve an elusive sodium analogue of the difficult to prepare, tris amido lithium magnesiate LiMgHMDS$_3$. Hampered by the same issues present in the synthesis of the lithium congener they isolated (in the same guise both a blessing and a burden) the familiar oxo-inverse crown species $[\{Me_3Si)_2N]_4Na_2Mg_2(O_2)\}_\infty]$. Whilst unquestionably novel, the same issues of advantitious oxygen made isolation of the more structurally understated tris-amido species impossible. Consequently, any information concerning the active species in this O^{2-} anion capture reaction was to remain elusive for more than

a decade, with the postulated tris-amido species the main contender, for want of further evidence.

It is not difficult to see why this position was easily maintained, considering the emergence of a number of representative tris-amido magnesiate species structurally characterised over the coming years. In 2003, the related entities [(TMEDA)·NaMg(^{i}Pr$_2$N)$_3$] and [(TMEDA)·KMg(^{i}Pr$_2$N)$_3$] were structurally identified,[154c] essentially TMEDA solvated monomers and direct diisopropylamine-containing analogues of the original HMDS species (**Scheme 5.1**).
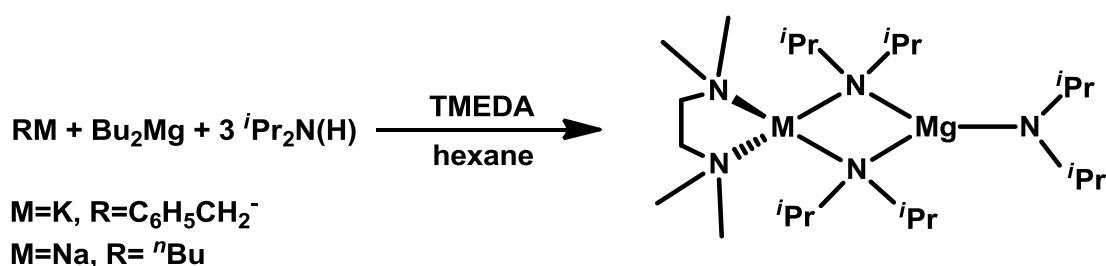
Scheme 5.1: Formation of tris-amido magnesiates containing sodium and potassium.

It was also found that the original tris-amido lithium magnesiate "LiMg(HMDS)$_3$" could be isolated in more stable donor complexes, solvated by both pyridine and THF respectively,[159] without formation of the ubiquitous inverse crown ether generated in the donor-free systems. Regardless of these findings, solid state characterization of the corresponding sodium complex "NaMg(HMDS)$_3$" was to prove impossible. So it was a decade hence within this project, on a reaction unrelated to the original magnesiate research, we gleaned by chance an insight into the precursor of the sodium oxo-inverse crown.

5.2   Preparation of [Na(μ-HMDS)$_2$Mg(^{n}Bu)]$_\infty$ 5a

We were attempting the dimetallation of three isomers of dicarbododecaborane (*ortho*, *meta* and *para* carborane), a substrate of significant focus earlier within this thesis. To achieve this, we employed the originally prescribed inverse crown mixture, namely the reaction of ^{n}BuNa, ^{n}Bu$_2$Mg and three equivalents of HMDS(H) in hexane solution. Addition of the *meta* isomer accompanied by heating of the reaction to reflux, gave a colourless solution, with slow overnight cooling yielding a crystalline material. X-ray analysis of the colourless crystals collected revealed a structure bereft of the carborane incorporation we had anticipated. The actual structure was a linear polymer, comprising a Na atom, bridged by two HMDS anions to a Mg centre, each of these four-membered

Na-N-Mg-N units propagating through a single carbon atom of an *n*-butyl group. We had unwittingly discovered the potential "parent base" of sodium inverse crown chemistry; not the tris-amido entity previously envisaged, but a bis-amido alkyl magnesiate, of composition $[Na(\mu\text{-HMDS})_2Mg(^{n}Bu)]_\infty$ **5a.**

5.2.1 Crystallographic studies of 5a

Within this polymer the sodium atom is distorted trigonal planar, almost equidistant to both N atoms of the bridging HMDS units, forming short contacts of 2.486(18) and 2.451(19) Å respectively. This degree of distortion is most likely a consequence of the tight acute N1-Na1-N2 bite angle of 84.16(6), the other obtuse angles [N1-Na1-C13 142.0(7), N2-Na1-C13 133.57(7)°] bringing the total of the angles surrounding sodium to 359.73°. The angle of the Na1-C13-Mg1* bridge between the four-membered rings deviates only slightly form linearity, at a value 164.94(12)°. The magnesium atom is likewise distorted trigonal planar, exhibiting short, strong contacts to both bridging N atoms and the carbon atom of the butyl group, which could also be considered bridging [Mg1-N1 2.077(18), Mg1-N2 2.063(17), Mg1-C13 2.155(2) Å]. The angles around the Mg centre are far more relaxed, most notably the N1-Mg1-N2 bond angle [106.13(7)°], the easing of this strain commensurate in the N1-Mg-C13 and N2-Mg1-C13 angles [124.32(9) and 129.48(9)°] respectively. Each sodium atom also experiences significant electrostatic interactions to a single methyl group from both HMDS units (mean distance of 2.913 Å).
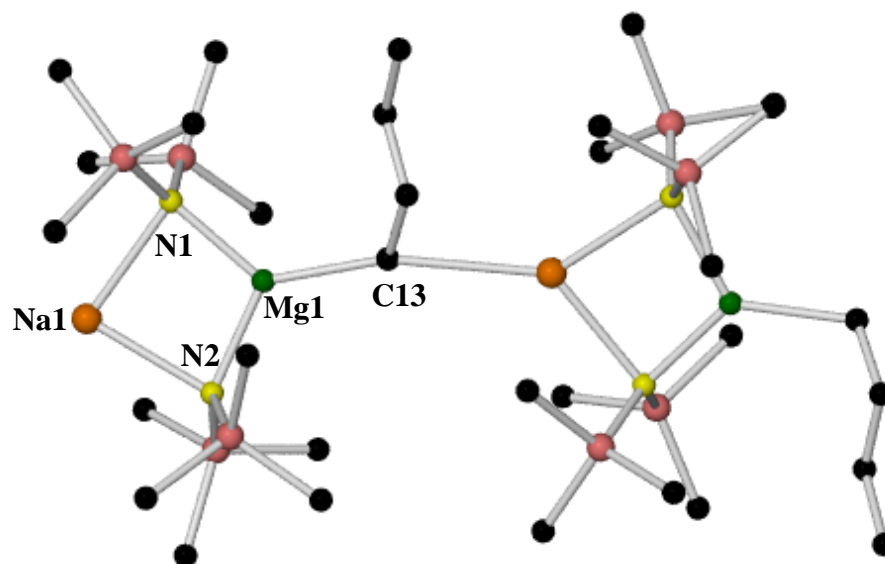
Fig. 5.1: Molecular structure of [Na(HMDS)$_2$Mg(^{n}Bu)]$_\infty$ **5a**, showing two repeating units. Key bond distances (Å) and angles (°): Mg1-N2 2.063(17), Mg1-N1 2.077(18), Mg1-C13 2.155(2), Na1-N1 2.486(18), Na1-N2 2.451(19), Na1-C13 2.781(2), N2-Mg1-N1 106.13(7), N2-Mg1-C13 129.48(9), N1-Mg1-C13 124.32(9), Mg1-N2-Na1 85.38(6), Na1-C13-Mg1 115.17(6), Mg1-N1-Na1 84.19(6).

5.2.2 NMR spectroscopic studies of 5a

As **5a** is soluble in C$_6$D$_6$ it is assumed that upon dissolution, the polymer will break up into smaller oligomers. In keeping with previous examples, it is likely that these exist as binuclear monomers, where the Na atom is stabilised by interactions with the arene solvent. In C$_6$D$_6$ there appeared to be no evidence of other likely species existing in equilibrium namely NaHMDS (s, SiCH_3, 0.12 ppm), Mg(HMDS)$_2$ [0.45 (SiCH_3), 0.37 (SiCH_3), 0.16 (SiCH_3) ppm], and only minute evidence of resonances pertaining to the species [^{n}BuMg(HMDS)]$_2$ [(t, 0.05, Mg-CH_2), (s, 0.28, SiCH_3), (t, 1.17, n-Bu CH_3), (m, 1.66, CH_2-CH$_3$) and (m, 1.87, CH_2-CH$_2$)]] and no evidence of the broad resonances associated with free ^{n}Bu$_2$Mg. The ^{n}Bu group in **5a** exhibits four distinct resonances, the most upfield of which belongs to CH$_2$ group attached to the metal (virtual t, 2H, 0.08 ppm). The remaining resonances of the ^{n}Bu group fall downfield in the order -CH$_2$-CH_3 (t, 3H, 1.26 ppm), CH_2-CH$_3$ (m, 2H, 1.79 ppm) and CH_2-CH$_2$ (m, 2H, 2.05 ppm). The final signal appears as a broad singlet at a value of 0.21 ppm, indicative of the methyl groups residing on the bridging HMDS units (**Figure 5.2**).

Fig. 5.2: ^{1}H NMR spectrum of **5a** in C_6D_6.

The ^{13}C NMR spectrum (**Figure 5.3**) similarly shows five key resonances, representing the four distinct carbon atoms of the *n*-butyl group, and a single HMDS methyl resonance, showing that each methyl group in solution is seen as spectroscopically equivalent [HMDS-CH_3 (6.09 ppm), Bu-CH_3 (12.14 ppm), M-CH_2 (14.58 ppm), CH_2CH_2 (32.16 ppm), CH_3CH_2 (33.15 ppm)].
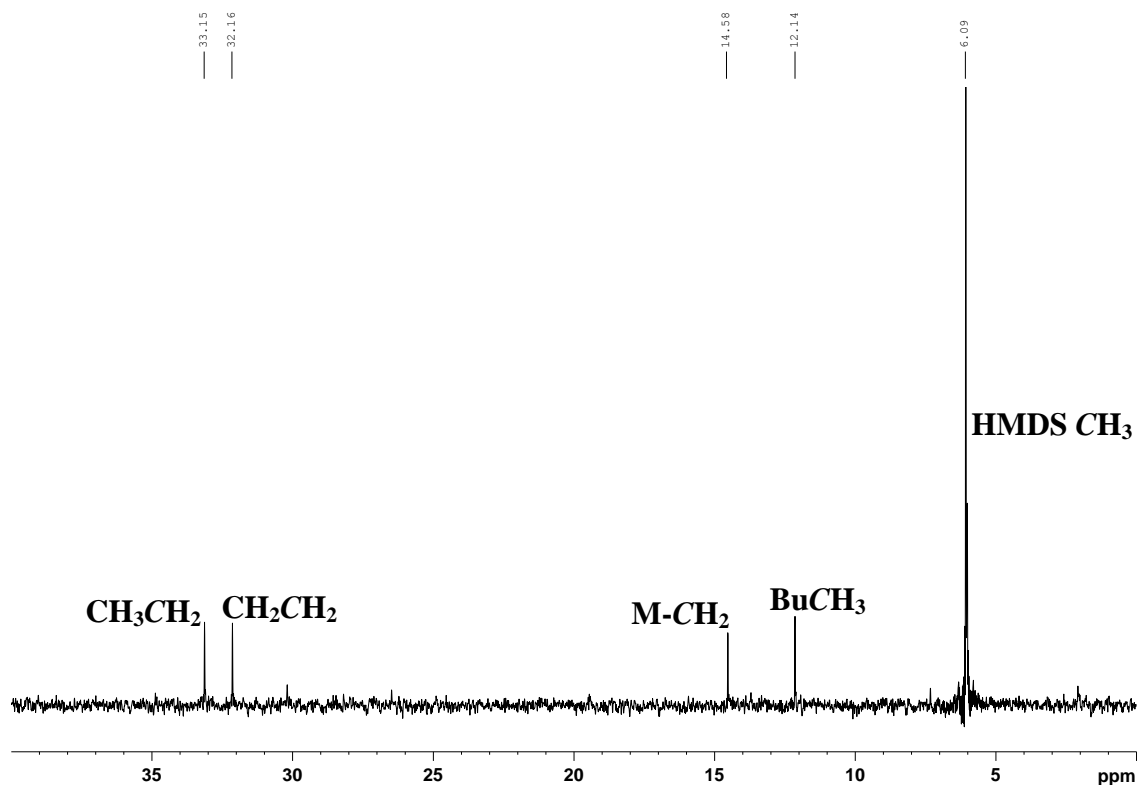
Fig. 5.3: ^{13}C NMR spectrum of **5a** in C_6D_6.

Discovery of this polymeric species gave for the first time insight into the potential precursor to these inverse crown complexes. Since only two equivalents of amine are consumed in this reaction, regardless of it being used in excess, rational synthesis of this compound was attempted. To achieve this, one equivalent of HMDS(H) was reacted with one equivalent of $^{n}Bu_2Mg$ in a Schlenk tube, and to this added solid NaHMDS. Subsequent cooling of this solution gave a large amount of crystalline material, confirmed by both ^1H NMR spectroscopy and X-ray crystallography as the same polymeric species **5a**.

5.3 Introduction into Na/Mg inverse crown chemistry

Turning from this species, it seemed prudent to investigate whether or not precursors to the reactions involving twofold deprotonation of benzene could be similarly elucidated, or any other relevant insight gleaned. In 1999, it was found by Mulvey *et al* that a mixture of equimolar amounts of BuNa and $^{n}Bu_2Mg$, followed by three equivalents of TMP(H) could bring about twofold deprotonation of both toluene and benzene,[85] incorporating these doubly deprotonated species into the guest-host environments noted in the previously prepared inverse crown ether complexes.

BuNa + ^{n}Bu$_2$Mg + 3TMP(H)

$\downarrow$ - 2 BuH

"NaMg(Bu)(TMP)$_2$"

$\bullet$ =

Excess

R
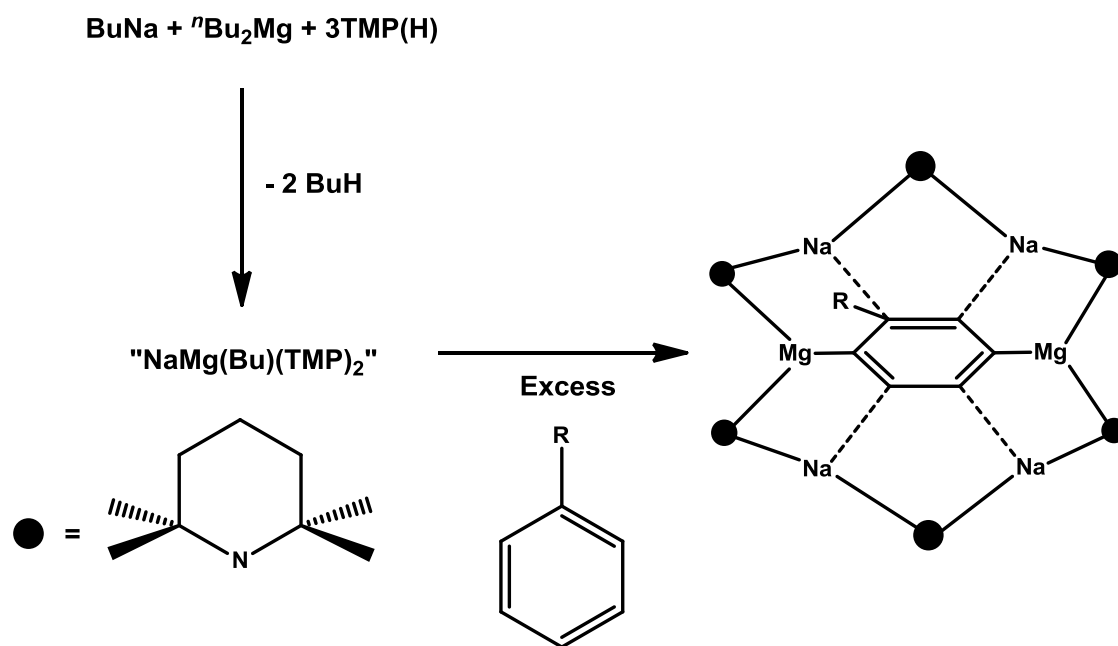
Scheme 5.2: Na/Mg Inverse crown formation.

In this fashion, benzene is selectively metallated in the 1, 4 positions, and toluene selectively metallated in positions 2 and 5 *i.e.*, *ortho* and *meta* deprotonation. What is most interesting about the latter doubly deprotonated species, is that the effects of thermodynamic acidity have been overcome; the base deprotonates at positions several pKa units higher than the methyl substituent. Conventional deprotonating reagents e.g. (TMEDA)·^{n}BuLi[166] and ^{n}BuNa[167] deprotonate almost exclusively at this position (lateral metallation) due to formation of the resonance stabilised benzyl anion (PhCH$_2{}^{-}$), but in this instance these effects are circumvented. When geometry-optimised *ab inito* MO calculations were carried out on the ten possible isomers which could arise from toluene di-deprotonation, it was found that the experimentally observed species was 14.0 kcal mol^{-1} less stable than the most stable by calculation (methyl-*para* or methyl-*meta*). This energy deficit is overcome by the numerous strong π interactions (in combination with σ), which lateral metallation alone is incapable of achieving. What is most remarkable is when we consider the effects of both monometallic components *i.e.*, BuNa and ^{n}Bu$_2$Mg individually. Neither of these component parts is capable of even singly deprotonating toluene on the ring, with BuNa attacking the methyl group exclusively, and ^{n}Bu$_2$Mg unable to react with toluene whatsoever.

The identity of the active base present in this reaction was never fully realised, though intriguingly it was discovered that by addition of TMEDA to the putative magnesiate species "NaMg(TMP)$_3$", a surprising monomeric species was isolated. Irrespective of an additional molar equivalent of amine in the starting mixture, the complex isolated time and again was the alkyl bisamido intermediate "NaMg(Bu)(TMP)$_2$", trapped by the chelating ligand TMEDA: [(TMEDA)·Na(μ-^{n}Bu)(μ-TMP)Mg(TMP)][168] **4a** (**Figure 5.4**).
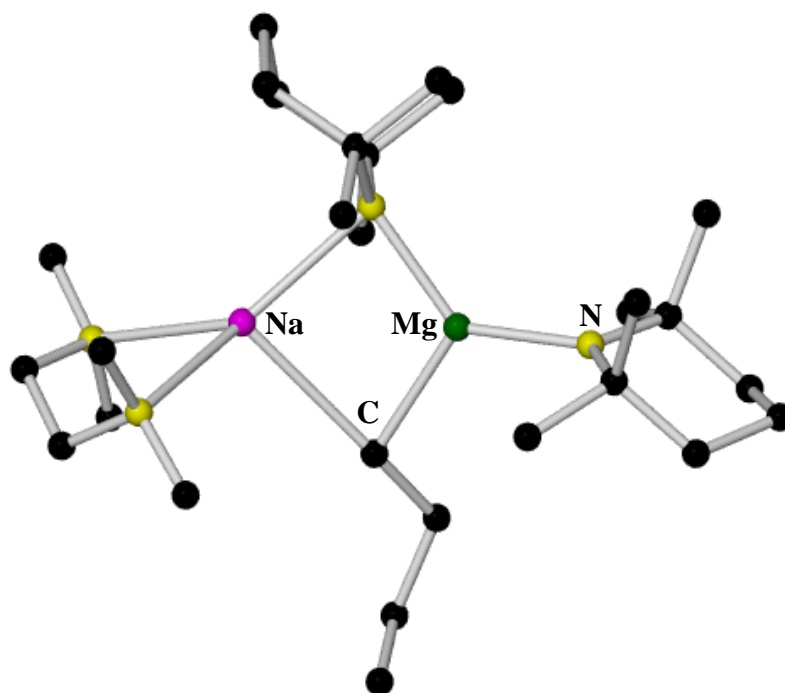
Fig. 5.4: Molecular Structure of [(TMEDA).Na(μ-^{n}Bu)(μ-TMP)Mg(TMP)] **4a**.

Reaction of this active species with a stoichiometric amount of the arene previously used as a bulk solvent (benzene and toluene) furnished, in the case of benzene, a monometallated species where a butyl arm is essentially replaced by a phenyl ring, further stabilising the sodium through π interactions. Reaction with toluene under reflux again yields a selectively deprotonated toluene species at the *meta* position. This selective *meta* deprotonation is a result which cannot be achieved through any known homometallic base. Like the benzene example, the magnesium is bound in a σ fashion to the *meta* carbon, lying almost coplanar with the ring, whilst the sodium by comparison engages the ring through π interactions. This feature of complimentary σ and π bonding is common in these mixed-metal systems. In this instance the *meta* isomer was calculated by DFT to be the most stable, primarily because of these stabilising Na − arene interactions. Formation of the benzylic anion which would be

expected with almost all monometallic reagents does not occur here therefore because such stabilising interactions could not exist, since the sodium would lie almost coplanar with the ring.
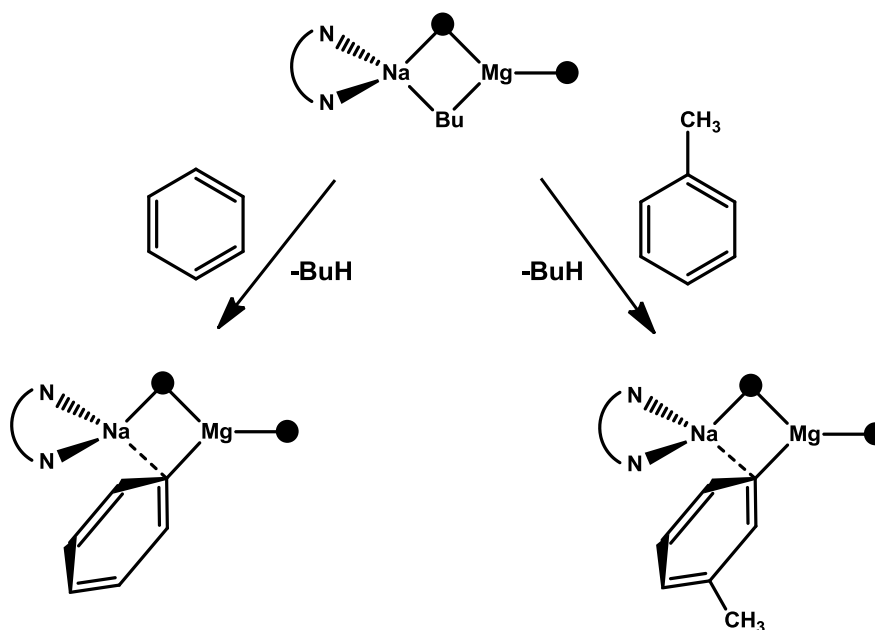
Scheme 5.3: Synergic deprotonation of benzene and toluene.

In the years following these initial mono and di-metallation reactions, both with and without donor solvent present, the additional bulk imparted by the TMP anion has made isolation of any neutral species containing a magnesium centre surrounded by three TMP units impossible. The only notable exception is in the solvent separated species $[\{(\text{PMDETA})_2\cdot\text{Na}\}^+\{\text{Mg}(\text{TMP})_3\}^-]^{[160]}$, where addition of two molar equivalents of the tridentate ligand PMDETA were added to the 1:1:3 mixture. The Mg atom, existing "apart" from its cationic neighbour, is unburdened by the extra steric strain involved in a contact ion-pair relationship, and can thus accommodate the extra TMP anion. This difference is fundamental, as the solvent-separated nature of the complex renders communication between the alkali metal and magnesium centre mute, negating its effectiveness in performing metallations of the type mentioned above. These examples served to form the basis of an idea, when coupled with the isolation of the related **5a**, the idea being that the species reckoned to carry out the di-metallation of benzene and toluene could not be the tris-amido "NaMg(TMP)$_3$" originally postulated.

5.4 Rational synthesis of the dimetallated inverse crown [Na$_4$Mg$_2$(TMP)$_6$(C$_6$H$_4$)] 5c

To achieve this, an attempt was made to isolate the base in the absence of any substrate, then to see if the di-metallation reactions could be performed using our "rational" method. In a first Schlenk tube, NaTMP was generated by reaction of BuNa with TMP(H), and in a second BuMgTMP generated by reaction of Bu$_2$Mg with a single equivalent of TMP(H). When the BuMgTMP solution was added to the NaTMP suspension, a yellowish solution was achieved almost immediately, suggesting that co-complexation of the starting materials had occurred. This synthesis, carried out in both cyclohexane and methyl-cyclohexane (due to its low melting and high boiling points), afforded in many instances crystalline material, which was never unfortunately of suitable quality even to infer connectivity within the structure. However, within our laboratory group, another member was able to achieve the elusive compound by changing to pentane solution. Gratifyingly, a linear polymeric species was obtained of the desired composition "NaMg(TMP)$_2$Bu" **5b** (**Figure 5.4**).
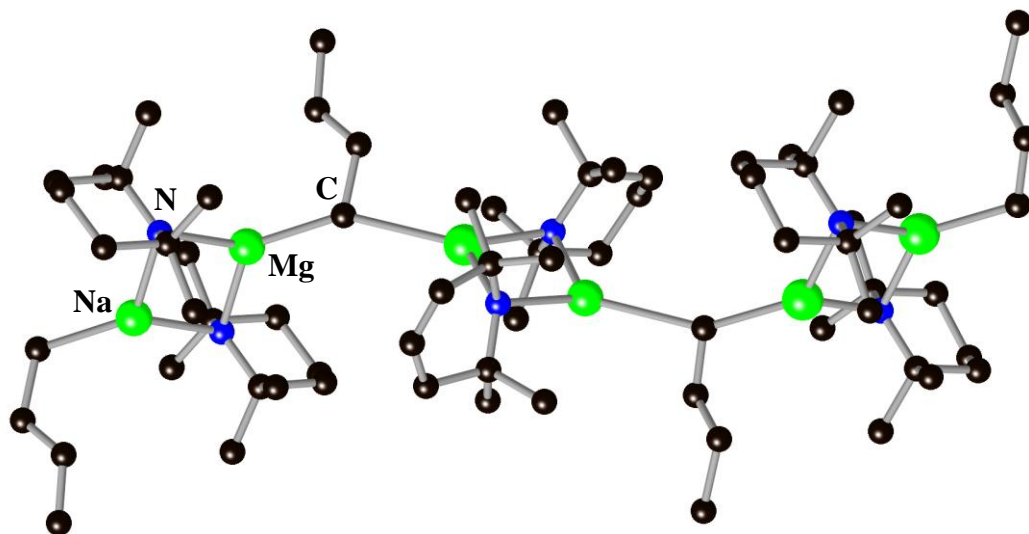
Fig. 5.4: Molecular structure of the polymeric sodium magnesiate **5b**.

Structurally, this species resembles closely the related **5a**, its key structural features the four membered Na-N-Mg-N rings containing two bridging TMP anions, with the polymer propagating through a single carbon atom of each *n*-butyl group, which could be described as bridging. Each of these *n*-butyl groups points alternately up and down from one repeating unit to the next. In the original paper from 1999,[85] the reaction called for a both a vast excess of the arene solvent to be deprotonated, and an extra equivalent of TMP(H), two matters which we hoped ourselves able to improve upon.

The sodium magnesiate **5b** was formed *in situ* (in methyl-cyclohexane) by the previously described method, and instead of employing the arene in vast excess, only two equivalents were added, the solution left to stir at room temperature for one hour. Overnight cooling produced the di-metallated benzene inverse crown in a crystalline yield of 63%.
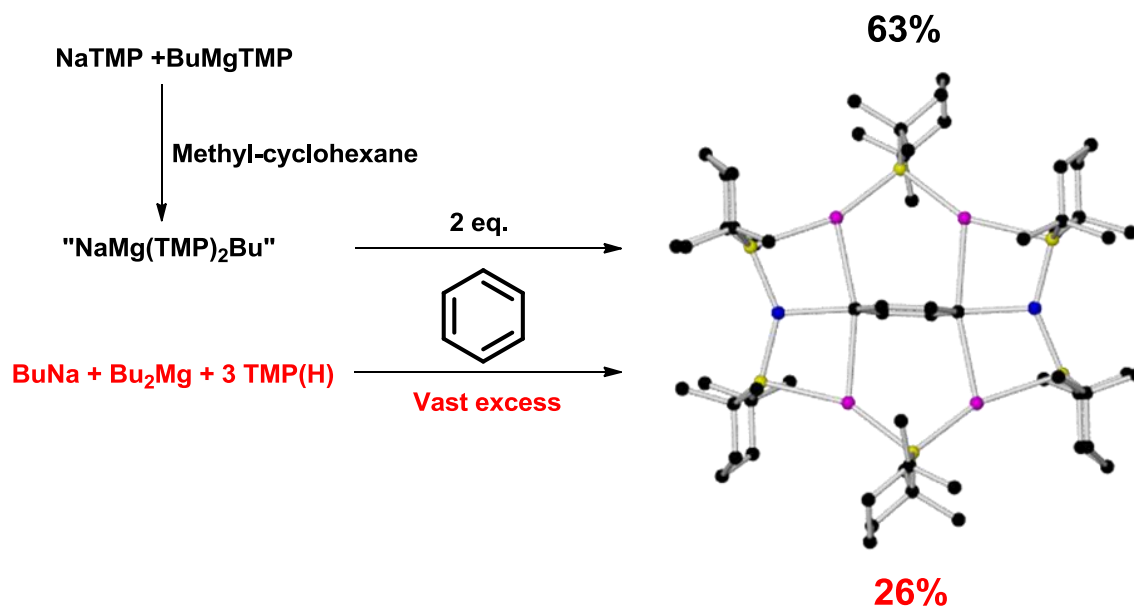
Fig. 5.5: Formation of dimetallated benzene species **5c** by the improved method (Top: **Black**) and by the original method (Bottom: **Red**).

5.4.1 NMR analysis of [Na$_4$Mg$_2$(TMP)$_6$(C$_6$H$_4$)] 5c

In lieu of spectroscopic data for this complex within the original publication, it was decided to characterise it further by ^{1}H NMR spectroscopy. In the original document it was remarked that the stubbornly insoluble complexes required a vast excess of arene to aid solubility and hence to provide X-ray quality crystals. We found surprisingly that when utilising methyl-cyclohexane as our solvent and only two equivalents of TMP(H), a solution was maintained throughout, but after precipitation of the inverse crown complex, redissolving the material proved difficult. With the aid of heating and sonication however, dissolution of sufficient quantity of the crystalline inverse crown material in deuterated cyclohexane solution (C$_6$D$_{12}$) provided a suitable ^{1}H NMR spectrum (**Figure 5.6**).

Fig. 5.6: ^{1}H NMR spectrum of [Na$_4$Mg$_2$(TMP)$_6$(C$_6$H$_4$)] **5c** in C$_6$D$_{12}$ solution (close up of aliphatic region).

What was observed, unusually, is the appearance of three distinct sets of methyl groups, the most upfield of which (0.86 ppm) we attribute to the TMP anion bridging between the two most electropositive Na centres. In assigning the remaining signals, it was noted within the structure, in each TMP ligand, two methyl groups point in toward the centre of the structure and two away, so the signals at 1.34 and 1.46 ppm can be tentatively assigned as belonging to these two different chemical environments. The isolation of both the polymeric species **5b** then its subsequent reaction with near-stoichiometric benzene has led to the conclusion that bis-amido alkyl magnesiates and not tris-amido magnesiates are in fact the active species in performing these dimetallation reactions and generating the unique macrocyclic frameworks present in sodium inverse crown complexes.

5.5   Formation of BuO$^-$ inverse crown by adventitious oxygen

As an interesting aside in our research into sodium magnesiates, an attempt was made to isolate the precursor to the tetrametallated ferrocene inverse crown complex discussed in detail within the main introduction. In this reaction, three equivalents of parent amine [^{i}Pr$_2$N(H)] were combined with a single equivalent of both BuNa and Bu$_2$Mg to form the active base.[83] Attempting a rational synthesis of what was believed to be the

potential active species in these reactions, BuMgDA solution was added to a NaDA suspension. Unfortunately, only an intractable mixture was ever achieved when we used a fresh sample of commercial Bu_2Mg, with no crystalline material ever forthcoming, despite the variety of solvents and concentrations utilised. If however a bottle of Bu_2Mg was used which had been opened (and albeit resealed) for some time, on several occasions a product which had already been published was observed.[169] This product was the BuO^- containing inverse crown, akin to the oxo-inverse crown $[\{Me_3Si)_2N]_4Na_2Mg_2(O_2)\}_\infty]$, except in this instance diisopropylamine units providing the polyamide framework. We tentatively suggest that formation of this unwanted product is a consequence of unwanted oxygen insertion into a single Mg-C bond in the old Bu_2Mg sample, forming perhaps the putative species "BuOMgBu". The remaining Mg-C bond is likely still of sufficient activity to deprotonate the DA(H) added, forming "DAMgOBu", which on addition to the NaDA mixture in *n*-hexane, co-complexes to form the inverse crown (**Figure 5.7**).
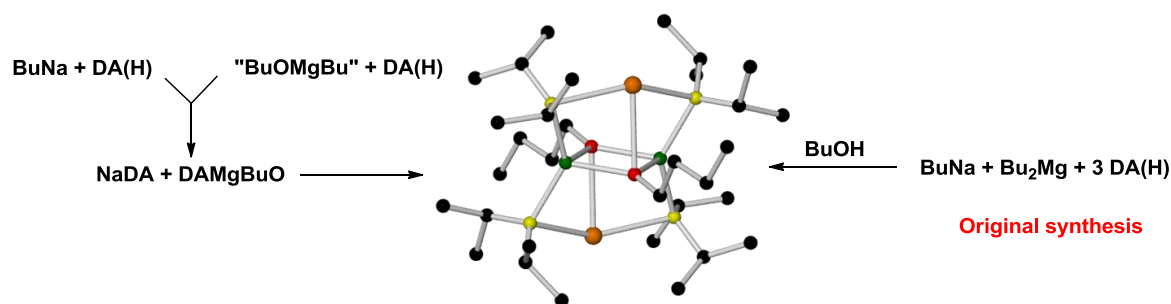
Fig. 5.7: Comparison of BuO inverse crown syntheses [(new synthesis – left) and (known synthesis[169] – right).

The repeated crystallisation of this BuO^- inverse crown species, evidenced by both X-ray crystallography (**Figure 5.7**) and ^1H NMR spectroscopy (**Figure 5.8**), although mentioned here almost anecdotally, serves two important purposes. First it shows that this sodium-magnesiate system containing diisopropylamine is an effective model for BuO^- capture, and secondly, that utmost care must be taken in handling and storage of pyrophoric starting materials, both in terms of safety and avoidance of unwanted final products.
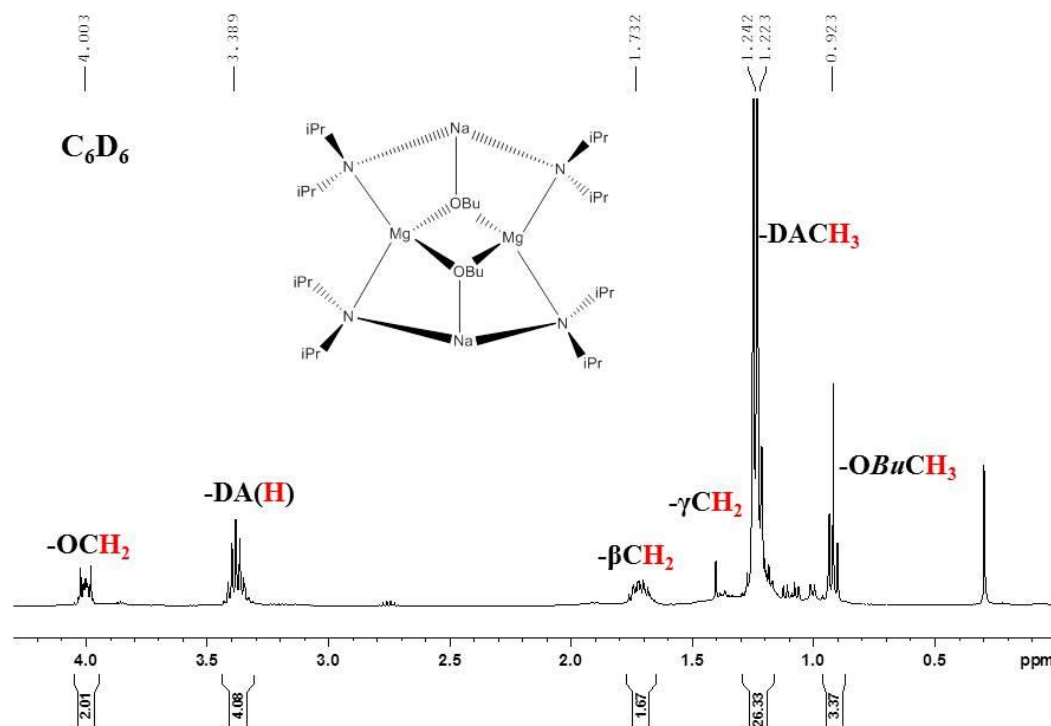
Fig. 5.8: ^{1}H NMR spectrum of butoxide encapsulated inverse crown complex in C_6D_6.

5.6   Introduction to potassium magnesiate oxo inverse crown chemistry

In the case of our own research groups, the term alkali-metal mediated magnesiation (AMM*Mg*) has focused in the past primarily on lithium and sodium magnesiate species. Compared to the quantity of literature focusing on these combinations, there is a definite paucity of attention paid to magnesiate species containing the heavier utility metal potassium. The first potassium magnesiate structurally characterised (fourteen years ago) was the inverse crown ether (ICE) complex $[\{Me_3Si)_2N]_4K_2Mg_2(O_2)\}_\infty]$,[82] made by combining ^{n}BuK, $^{n,\,s}$Bu$_2$Mg and HMDS(H) in a 1:1:3 ratio. Unlike in the previous sodium and lithium ICE complexes, the potassium structure is not discrete, but instead exists as a polymer of ICE units, perhaps unsurprising due to the larger atomic radius of K. As previously reported in both the lithium and sodium cases, the source of this oxygen could not be proven definitively, but generation time and again of this species lends credence to the ability of the intermediate potassium magnesiate species to act as an oxygen scavenger. The nature and composition of the initial mixed-metal species, as with its sodium counterpart, was to remain a mystery for more than a decade. The originally described mixture called for three equivalents of amine HMDS(H), in comination with ^{n}BuK and ^{n,s}Bu$_2$Mg, forming the putative tris-amido potassium

magnesiate species "KMg(HMDS)$_3$", this formula proposed on the assumption that each equivalent of amine was deprotonated by the butyl groups of the initial alkyl-metal reagents. As a consequence of the illuminating evidence garnered in the sodium inverse crown systems, it was postulated whether the active species in these reactions was indeed this tris-amido species, or in fact the bis-amido potassium magesiate [KMg(HMDS)$_2$Bu]$_\infty$.

5.7   Preparation of [KMg(HMDS)$_2$Bu]$_\infty$ 5d

In order to approach formation of this species rationally, BuMgHMDS was formed in an argon-filled Schlenk tube by combination of ^{n}Bu$_2$Mg and one equivalent of HMDS(H), followed by addition of KHMDS (via solid addition tube), in hexane solution. This time, unlike the sodium example, a white precipitate was formed which proved insoluble even on vigorous heating. Addition of a small amount of toluene gave immediate dissolution, and the colourless solution achieved was duly placed in a freezer at -27°C. On inspection the following day, a modest quantity of colourless crystalline material was recovered, which on X-ray analysis, was not a structural mimic of the previously discussed sodium magnesiate **5a**. What had in fact been crystallised was the previously published, formally solvent separated species [{K(toluene)$_2$}$^+${Mg(HMDS)$_3$}$^-$],[31b] a possible outcome overlooked prior to the addition of the toluene.
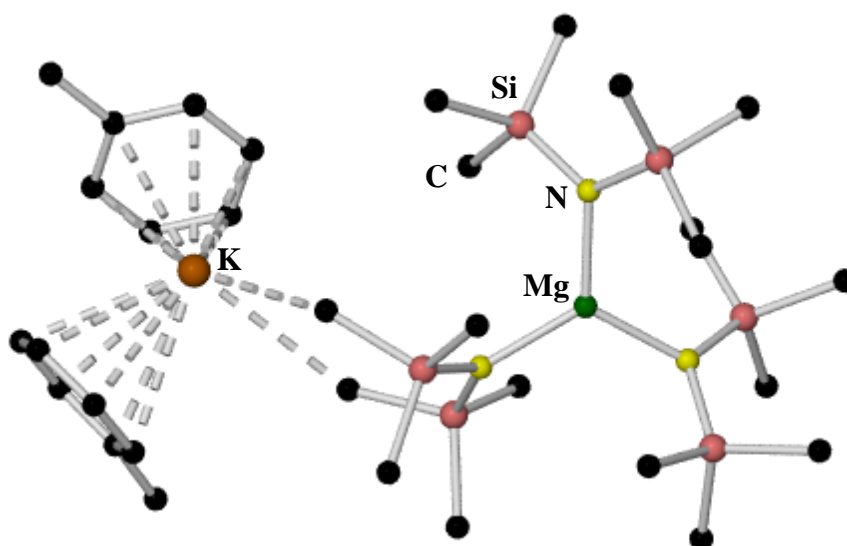
Fig. 5.9: Molecular structure of [{K(toluene)$_2$}$^+${Mg(HMDS)$_3$}$^-$].

This result prompted consideration of several factors, namely: which solvent could be added which would aid solubility, yet neither react with the magnesiate species nor

affect its structure to any real extent *i.e.* how could we achieve a solvent-free potassium magnesiate structure. Knowing that further hexane addition could not dissolve the complex and that toluene gave us an "alkyl-free" solvent separated polymer (a suspected disproportionation product), it was decided that the relatively non-polar aryl solvent mesitylene should be used. This decision may seem counterintuitive, since mesitylene is a stronger donor than toluene,[170] but it was reasoned the extra steric contributions of the three methyl groups could discourage direct complexation of the arene to the potassium in the solid state. By employing the same methodology as before, the same white suspension in hexane was achieved, followed by addition of 2 ml mesitylene, resulting in an immediate clear solution. Cooling to -28°C resulted in a larger amount of crystalline material, also suitable for X-ray analysis. Structural elucidation revealed that the desired potassium analogue of the previous sodium example was achieved.
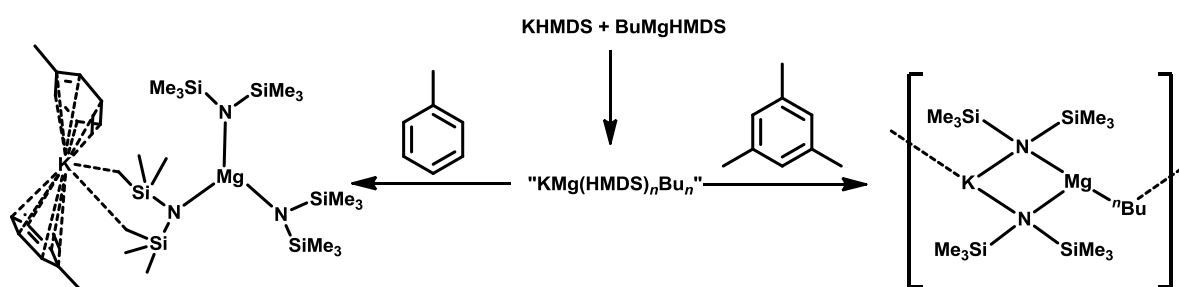
Scheme 5.4: Difference in structure achieved by addition of toluene vs. mesitylene.

The donor-free potassium magnesiate species was again both linear and polymeric in nature, with four membered K-N-Mg-N rings bridged through a single carbon atom of an *n*-Bu group. Each K and Mg atom is bridged by two HMDS units within each ring, and the *n*-Bu groups pointing alternatively up and down.
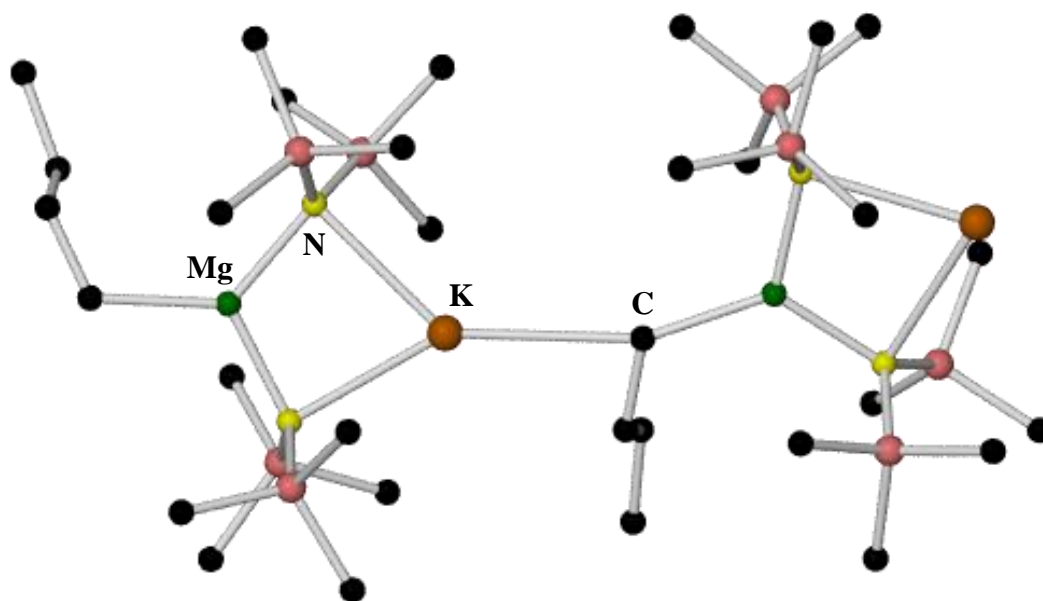
Fig. 5.10: Molecular structure of [KMg(HMDS)$_2$Bu]$_\infty$ **5d.**

Unfortunately, the structure was disordered to such a degree that further discussion on the particulars of bond angles and distances is impossible, but only the atom connectivity can be inferred with some degree of certainty.

5.7.1 NMR analysis of 5d

The crystalline material was dissolved in C$_6$D$_6$ and analysed by both ^{1}H and ^{13}C NMR, which suggested to us that the structure is maintained in solution. Furthest upfield is the triplet at   -0.35 ppm associated with the CH$_2$-M resonance, followed by two separate singlets, suggesting spectroscopically inequivalent HMDS methyl signals, at values of 0.26 and 0.48 ppm respectively. The remaining three resonances belong to the remaining H atoms of the *n*-Bu group, appearing as a triplet at 1.26 (3H, Bu-C*H$_3$*), and two multiplets at 1.76 and 2.02 ppm, both indicative of the butyl C*H$_2$* H atoms (**Figure 5.11**).

Fig. 5.11: ^{1}H NMR spectrum of **5d** in C_6D_6 solution.

The ^{13}C NMR spectrum nicely corroborates that of the ^{1}H NMR spectrum above, showing six distinct sets of signals. Furthest upfield are the two spectroscopically inequivalent HMDS signals, at values of 6.2 and 7.2 ppm respectively, with the remaining ^{n}Bu signals completing the spectrum [(CH_2-M, 14.2 ppm), (CH_3-nBu, 14.4 ppm), (CH_2-nBu, 32.0 ppm), (CH_2-nBu, 32.9 ppm)].

5.8 Previous preparation of hexapotassium macrocycle [KMg(TMP)$_2$(C$_6$H$_5$)]$_6$ 5e

Whilst O^{2-} encapsulation within these mixed-metal HMDS systems was indeed novel and could be performed by a series of increasingly heavy alkali metal partners, like in the case of Na, potassium magnesiate chemistry had yet to reveal its most impressive specimen. In 2000,[154a] a mixture of unrefined ^{n}BuK, Bu$_2$Mg and TMP(H) were added together in a 1:1:3 ratio, followed by a huge excess of either benzene or toluene, forming a solution which was heated then cooled slowly. Structural elucidation revealed a structure very different to the analogous sodium reaction, which contained at its heart a single benzene di-anion. By making what superficially appears a relatively minor change in moving to the heavier potassium metal, significant expansion of the macrocyclic framework was observed, to an unprecedented 24-membered [(KNMgN)$_6$]$^+$ ring system, capturing this time six *mono*-deprotonated arene units (**Figure 5.12**).

135
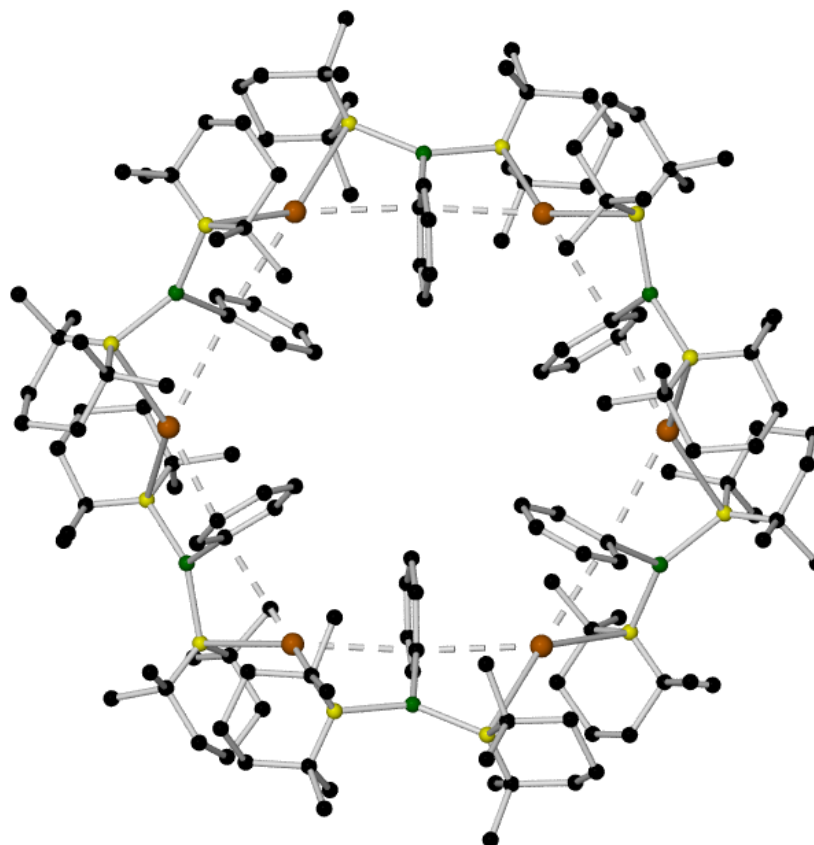
Fig. 5.12: Structure of [KMg(TMP)$_2$(C$_6$H$_5$)]$_6$ **5e**.

As is common in these mixed-metal systems, the unusual *meta*-selectivity in the toluene example is a consequence of strong Mg-C σ bonds and significant K-π engagements, these metals together performing a deprotonation the cumulative energy of which is greater than the CH$_3$ metallation more energetically favoured by traditional monometallic reagents.

When moving to the heavier alkali metal potassium, a change in both reactivity and structure is observed. One would believe a potassium base to be inherently more aggressive and more reactive, yet it performs only a single deprotonation compared to the di-deprotonation effected by the analogous sodium containing mixture. The 2000 paper remarks on the inability to isolate the intermediates performing this potassium mediated magnesiation, prompting an attempt their elucidation within this project, and explanation how any potential structural differences of these species could account for the difference in reactivity observed.

5.9 Preparation of [KMg(TMP)$_2$^{n}Bu]$_\infty$ 5f

What was to be pivotal in the entire subsequent undertaking was the choice of solvent, a basic yet crucial element, considering an attempt was being made to generate essentially "solvent-free" structures. It was discovered that formation of the desired species "KMg(TMP)$_2$Bu" in hexane led to an insoluble product, dissolution of which could be achieved neither by heating nor sonication. Surprisingly however, when utilising cyclohexane, or methyl-cyclohexane (higher boiling point), it was observed that on addition of the BuMgTMP solution to the KTMP suspension, a clear orange/red solution was obtained almost instantly. To this end, in a preliminary study to pin down the identity of this active species, a solution of BuMgTMP in cyclohexane (made by reaction of ^{n}Bu$_2$Mg with one equivalent of TMP(H)) was added via cannula to a suspension of KTMP, also in cyclohexane, resulting in an immediate solution. An aliquot of this solution was transferred to a Young's NMR tube, dried *in vacuo*, redissolved in C$_6$D$_{12}$, followed by cooling for three days at 3°C, yielding a small amount of crystalline material. Upon X-ray analysis, it was indeed found to be a bis-amido potassium magnesiate of composition [KMg(TMP)$_2$Bu]$_n$. But crucially for us, it was a species featuring several distinct structural differences when compared with the related sodium examples, or for that matter, even the related [KMg(HMDS)$_2$Bu]$_\infty$ polymer.

5.9.1   Crystallographic studies of 5f
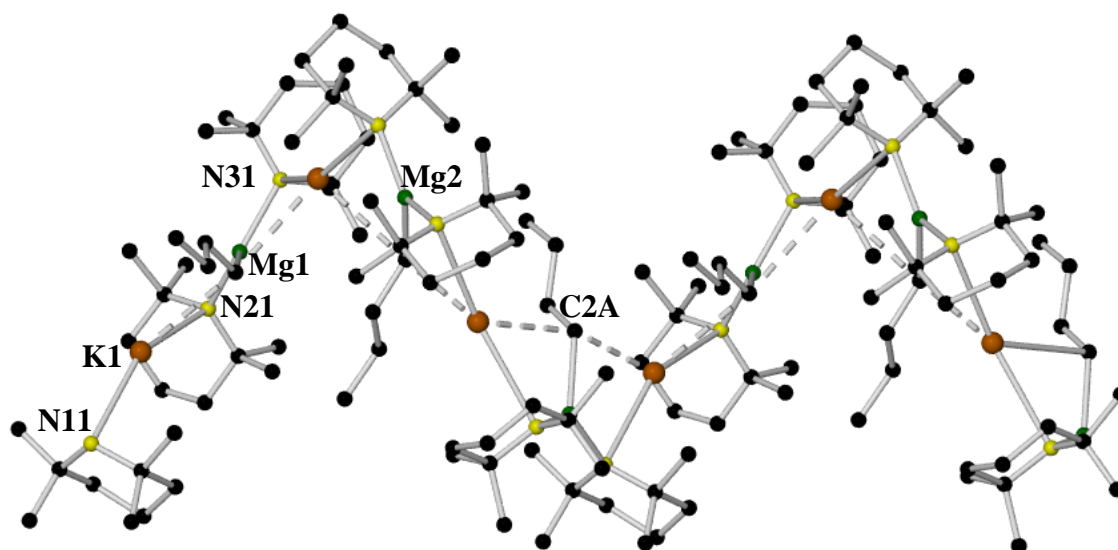
Fig. 5.13: Structure of [KMg(TMP)$_2$Bu]$_\infty$ **5f**. Key bond distances (Å) and angles (°): K1-N21 2.951(5), K1-N11 3.011(5), K1-C1A 3.331(6), K1-C2A 3.126(6), Mg2-N21 2.084(5), Mg2-N31 2.038(5), Mg2-C2A 2.175(6), N11-K1-N21 150.57(14), N21-K1-C2A 71.01(14), N11-K1-C1A 68.00(13), N11-K1-C2A 137.93(15), C1A-K1-C2A 90.45(15), N21-K1-C1A 127.35(14), N21-Mg2-N31 133.4(2), N31-Mg2-C2A 114.3(2), N21-Mg2-C2A 112.1(2).

Instead of the more commonplace linear polymers previously characterised, this unusual potassium magnesiate describes a helix, doubtless a consequence of both the increased size of the potassium atom and the steric bulk inherent in the TMP anion. In understanding the core of the structure, it is prudent to view it without the extra complication of the TMP and ^{n}Bu groups, stripped back most simply to its central thread (**Figure 5.14**).
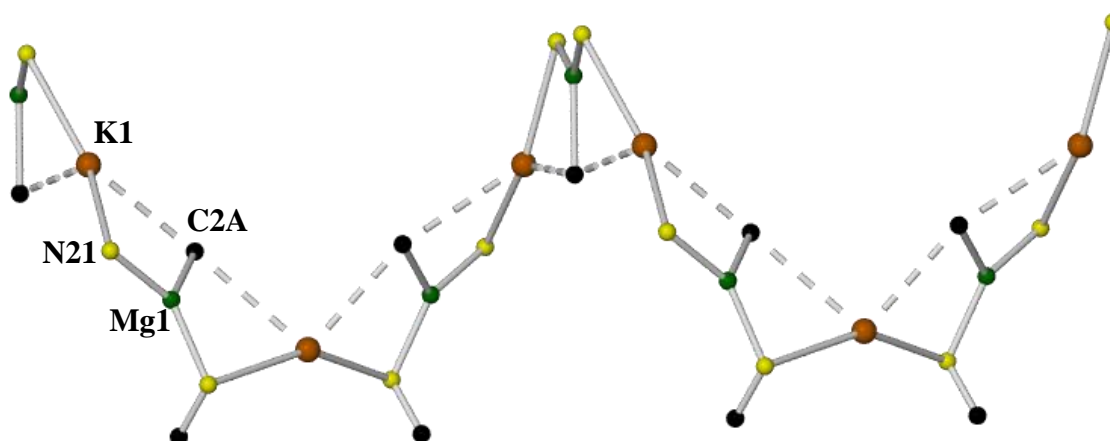
Fig. 5.14: Structure of **5f** showing only the metallic components, connecting N and C atoms of the TMP and *n*-butyl ligands.

It can be considered as a series of four-membered heteronuclear rings (K-N-Mg-C), fused together along the Mg-C face to another ring of identical composition. Each potassium atom within the ring occupies the vertex of both the first and the next set of doubly-fused tetranuclear ring systems. This polymer differs from a more traditional zig-zag structure as it moves down and up through a series of five K-C contacts, plateaus essentially horizontally through three K-C contacts, then propagates in this same fashion indefinitely, the K atom in each instance the inflection point (or turning point), initiating an immediate change in direction of the polymer. The Mg atom forms short, strong bonds to the N atoms of both bridging TMP units [Mg2-N21 2.102(4) Å, Mg2-N31 2.045(4) Å], and the C atom of the ^{n}Bu anion [2.169(5) Å], placing the Mg centre in a highly reactive distorted trigonal planar environment [N21-Mg2-N31 134.44(17)°, N21-Mg2-C2A 113.45(18)° and N31-Mg2-C2A 111.97(17)°]. Being the point on which the entire polymer turns, providing its helix shape, the angles around the K atom are understandably severe, its trigonal-pyramidal geometry greatly distorted. The three-coordinate base of the pyramid consists of one extremely acute [N41-K2-C3A 71.13(10)°, Δ from perfect trigonal pyramidal geometry = - 48.87°], and two commensurately obtuse angles [{N31-K2-N41 149.85(10)°, Δ from perfect trigonal pyramidal geometry = 29.85°} and {N31-K2-C3A 138.46(11)°, Δ = 18.46°}]. The angles from the K centre to the apical C atom range from [C2A-K2-C3A 91.47(12)°] to [{N41-K2-C2A 127.06(11)°, Δ = 37.06°} and {N31-K2-C2A 68.36(10)°, Δ = 21.64°}]. The K-N distances are approximately equal [K2-N31 2.968(4) Å and K2-N41 2.943(4) Å], short in comparison to the more distended K-C bonds, which can almost be considered electrostatic interactions rather than formal bonds [K2-C2A 3.287(5) Å and

K2-C3A 3.145(5) Å] (Typical K-C bond distances around 3.1Å).[24b] Interestingly, if we turn the helix and look directly down its centre, we see that the TMP ligands are all arranged around the outside, with the butyl groups all pointing towards the centre (**Figure 5.15**). This poly-amido outer scaffold with central alkyl (or aryl) units is a direct mimic of the hexameric benzene-encapsulated inverse crown species.
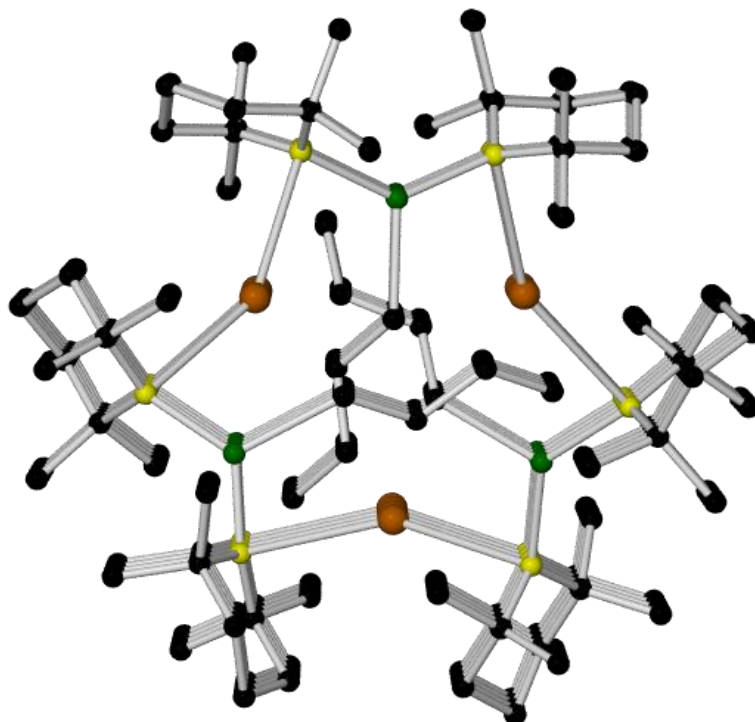
Fig. 5.15: "Down the middle" view of **5f**.

5.10   Rational synthesis of [KMg(TMP)$_2$(C$_6$H$_5$)]$_6$ 5e

In the original paper, three equivalents of TMP(H) and a vast excess of benzene are employed in the arene monometallation. In order to test whether the bis-amido species **5f** was in fact the active agent of deprotonation, it was formed *in situ* ["KMg(TMP)$_2$Bu" (in methyl-cyclohexane)], followed by addition of either a single equivalent of benzene or toluene. This was then allowed to stir for one hour at room temperature in order to react fully, and allowed to rest on the bench overnight. Analysis of the crystalline material obtained revealed the structures in both instances as the monometallated benzene and toluene inverse crowns respectively (**Scheme 5.5**).
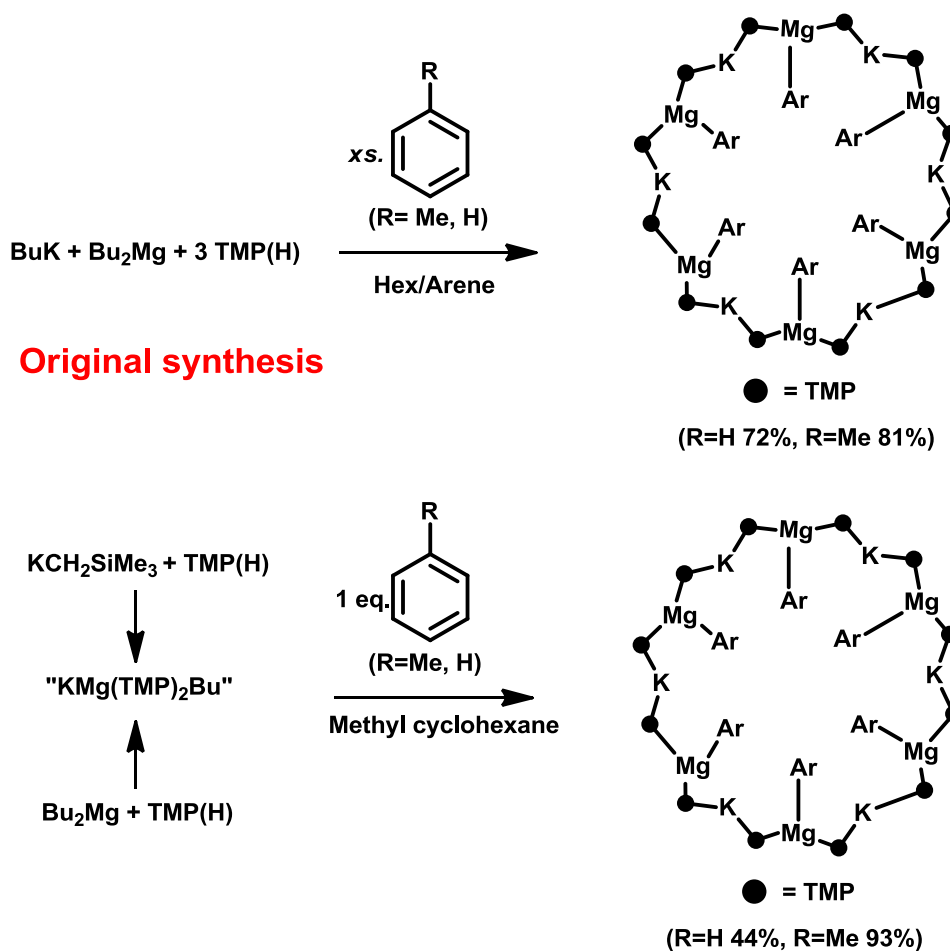
Scheme 5.5: Comparison of both routes to form hexapotassium inverse crowns (original synthesis-top, new synthesis-bottom).

By rational synthesis, both species were isolated in good to excellent yields, even surpassing that quoted in the original paper for the toluene example. This was also achived with stoichiometric arene addition and only two equivalents of the parent amine. These reactions were also undertaken at room temperature, with the original synthesis requiring heating to 60°C, and filtering prior to arene addition. These results served as a good model for a more efficient synthesis, as well as compelling evidence that a bis-amido species is indeed the active species in these reactions.

The next step was to discover if these potassium magnesiates could be used to form new or potentially different deprotonative metallation products or structural architectures, and also what potential active basic species could exist in solution.

5.11   Preparation of [KMg(TMP)$_2$Bu]$_4$ 5g

In our first of several substrates tested with this magnesiate mixture, the bulky and very weakly acidic hydrocarbon adamantane (C$_{10}$H$_{16}$) was chosen. This was indeed an ambitious choice, as no "alkane" had ever before been deprotonated using magnesiate chemistry. It was reasoned however that although still unlikely, the potassium magnesiate could possibly deprotonate this species, due to both the high reactivity of the base and relative acidity of the bridgehead C-H bond within the adamantane unit. The base was formed by combination of BuMgTMP (in methyl-cyclohexane) solution and KTMP (in methyl-cyclohexane) suspension, forming an overall red/orange solution, followed by addition of one equivalent of adamantane added via a solid addition tube. Though highly crystalline, the adamantane dissolved within minutes, at which point the solution was heated to reflux temperature. After cooling and concentration *in vacuo*, further heating redissolved the solid material formed, which was then cooled slowly overnight. What had in fact been crystallized was a tetrameric aggregate, of the same bis-amido mono-alkyl form exhibited by the polymer. The structure is a 16-membered polymetallic ring, of alternating K-N-Mg atoms, with potassium (unusually) two coordinate, forming a near linear bridge between the N atoms of its adjoining TMP anions. The Mg atom is distorted trigonal planar as observed previously, bound in a σ-fashion to the first carbon of the *n*-butyl group. Akin to the polymer **5f** (**Figure 5.13**), the butyl groups all tend towards the centre of the molecule, yet alternately point in opposite directions away from the plane of the K-N-Mg ring. It was originally believed that the adamantane may have played a part in formation of **5f**, although it was later proved that within the Schlenk tube, this tetrameric species could be isolated many times just by variation of concentration and temperature, in the absence of adamantane. Frustratingly however, not one of the numerous sets of crystals obtained, all unit-cell checked and deemed invariably to be this same tetramer, was of sufficient quality to allow detailed discussion on bond lengths and angles, allowing only connectivity to be concluded definitively.
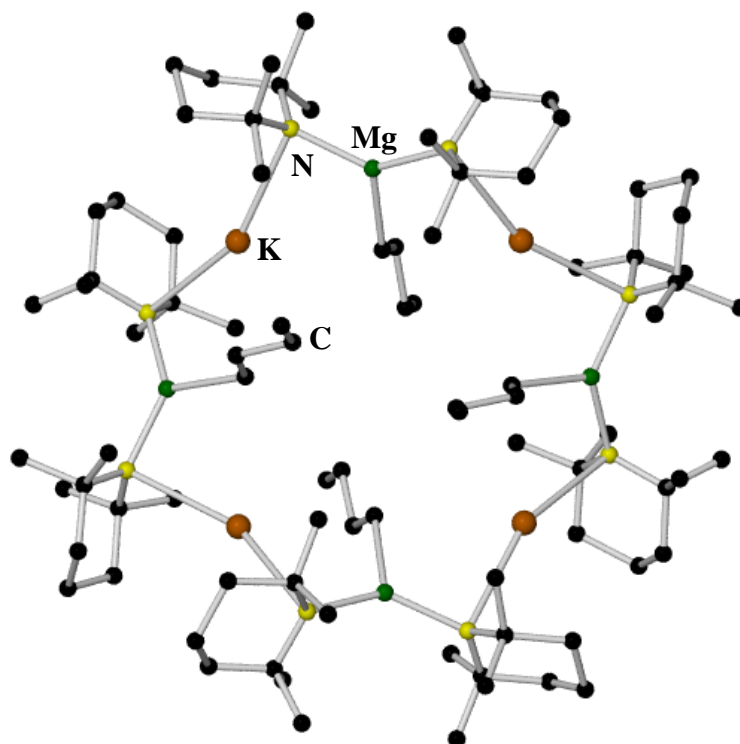
Fig. 5.16: Structure of tetrameric aggregate [KMg(TMP)$_2$Bu]$_4$ **5g**.

This structure represented for the first time what could essentially be considered an "empty" inverse crown species, inasmuch as it embodies the familiar macrocyclic metal amide crown, but the alkyl groups which act as the overall basic units remain intact in its centre. The only other structure previously published which is comparable was elucidated in 2003, a trimetallic lithium-potassium-(bis) magnesium N-metallated/N, C –dimetallated amide, described as an inverse crown species with an "atomless cavity" at its heart.[171] This serendipitous species was generated by reaction of ^{n}BuK, Bu$_2$Mg and the three equivalents of the amine *tert*-butyltrimethylsilylamine (^{t}Bu)(SiMe$_3$)N(H), with the lithium an unwanted by-product of the reaction to form the *n*-butyl potassium starting material. This species they then synthesised rationally, this time utilising the more stable benzylpotassium (**Figure 5.17**).
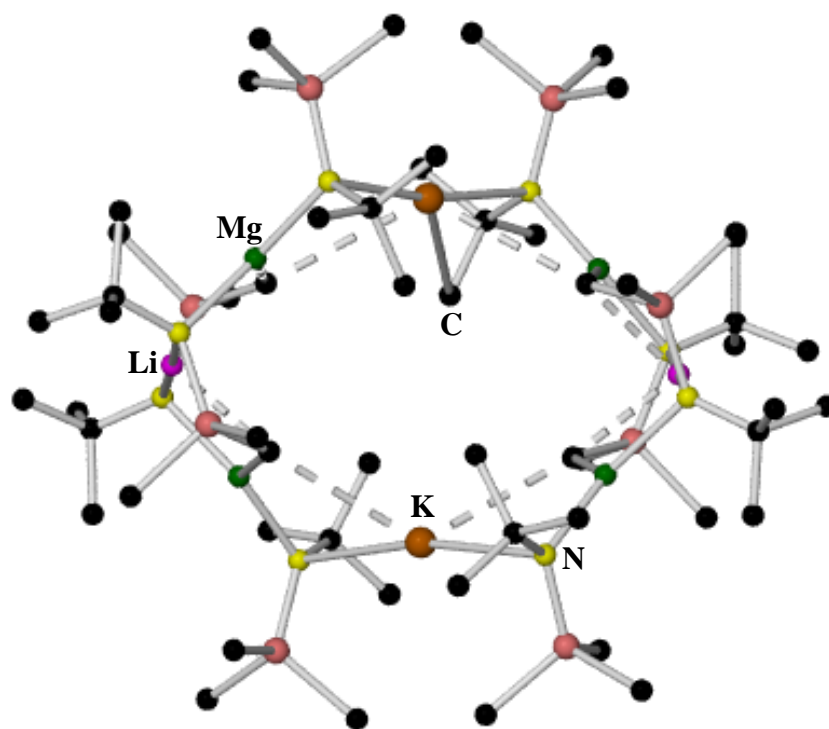
Fig. 5.17: Molecular structure of [Li$_2$K$_2$Mg$_4${^{t}Bu(Me$_3$Si)N}$_4${^{t}Bu[Me$_2$(CH$_2$)Si]N}$_4$] with omission of solvent molecules present in the crystal lattice.

This structure is also, essentially, a 16-membered ring (KNMgNLiNMgN)$_2$, with four equivalents of the unsymmetrical amine deprotonated singly at the N-H, and four units dimetallated, at both the N-H position and a single methyl group of the SiMe$_3$ portion of the amine. The (CH$_3$)$_2$SiCH$_2^-$ moiety can essentially be considered an "alkyl group" mimic of the *n*-butyl groups in **5g**. Whilst this original structure represents the only other structure, prior to characterisation of tetrameric **5g** which could be called an "empty" inverse crown, its disadvantage is that it is only a model structure, not a potential precursor to a real metallation system or legitimate inverse crown complex that appears to be inviting a substrate to occupy its cavity.

5.11.1 NMR analysis of 5g

Even though the quality of the X-ray structure was not ideal, the crystalline material was of more than sufficient quality to allow a detailed NMR study. Again the non-polar C$_6$D$_{12}$ was selected as an NMR solvent, as attempts to characterise the species in both C$_6$D$_6$ and d$_8$-THF proved fruitless, both reacting with the base quickly at room temperature. Furthest upfield in the ^{1}H NMR spectrum is the C*H$_2$* of the *n*-butyl group bound to the magnesium, observed as a triplet at -0.84 ppm. At a value of 0.78 ppm is the triplet associated with the terminal CH$_3$ portion of the n-butyl group, with the

remaining two resonances associated with the CH_2CH_3 and CH_2CH_2-M obscured by the TMP signals, yet visible in the ^{1}H-^{13}C HSQC spectrum, at values of 1.35 and 1.26 ppm respectively. With twice the number of TMP ligands present in this complex compared to *n*-butyl groups, the resonances associated with the former are understandably dominant. The methyl groups of the TMP appear as a single resonance at 1.27 ppm, corresponding to 24 H atoms. The β-CH_2 signals most unusually fall upfield of the methyl resonance at 1.19 ppm, whereas ordinarily these TMP β signals are observed downfield of this same signal. The final resonance, attributed to the γ-CH_2 of the TMP, appears as a broad multiplet at 1.80 ppm, exhibiting a more usual downfield shift with respect to the methyl group (**Figure 5.18**).

Fig. 5.18: ^{1}H NMR spectrum (400.13 MHz, 298K, C_6D_{12}) of **5g**.

Study of the ^{13}C NMR spectrum (**Figure 5.19**) of **5g** reveals seven distinct signals matching nicely with those observed in the corresponding ^{1}H NMR spectrum. Furthest upfield is the Bu-CH_3 resonance, at a shift of 14.9 ppm, followed by the CH_2 attached to the metal at 18.8 ppm. The remaining two *n*-Bu signals appear close together at values of 34.2 (CH_2CH_3) and 34.4 (CH_2CH_2M) respectively. A broad resonance at 36.3 ppm is indicative of the TMP methyl groups, with the β and γ resonances appearing at values of 42.3 and 20.1 ppm respectively.

Fig. 5.19: ^{13}C NMR spectrum (100.62 MHz, 298K, C$_6$D$_{12}$) of **5g**.

5.12   Preparation of [KMg(TMP)Bu]$_6$

In an attempt to repeat the synthesis of the original polymeric aggregate, "KMg(TMP)$_2$Bu" was formed again *in situ* by the same previously adopted methodology, then concentrated the solution massively *in vacuo*, such that a 2 mM solution, originally in 10 ml methyl cyclohexane, was now at a volume of ~ 1 ml. Half this volume was transferred via syringe to a Young's NMR tube, and left overnight at a temperature of   3 °C. The following day a large amount of crystalline material was forthcoming, which a simple unit cell check revealed as neither the original polymer nor the tetrameric aggregate. What had in fact been happened upon, was a hexameric species of the same composition as the previous structures. This at last was a true and faithful representation of an empty inverse crown, of a type near identical to the original mono-metallated benzene and toluene containing species, directly comparable in aggregation state, with all its butyl arms still intact. It requires only a small leap of the imagination to envisage the empty hexamer replacing its reactive butyl anions with phenyl anions directly, showing unequivocally the propensity of this magnesiate system to form these novel hexameric units in the solid state, even without the significant extra stability imparted by the K-arene π interactions detailed in the original paper.

5.12.1 X-ray crystallographic studies of 5h
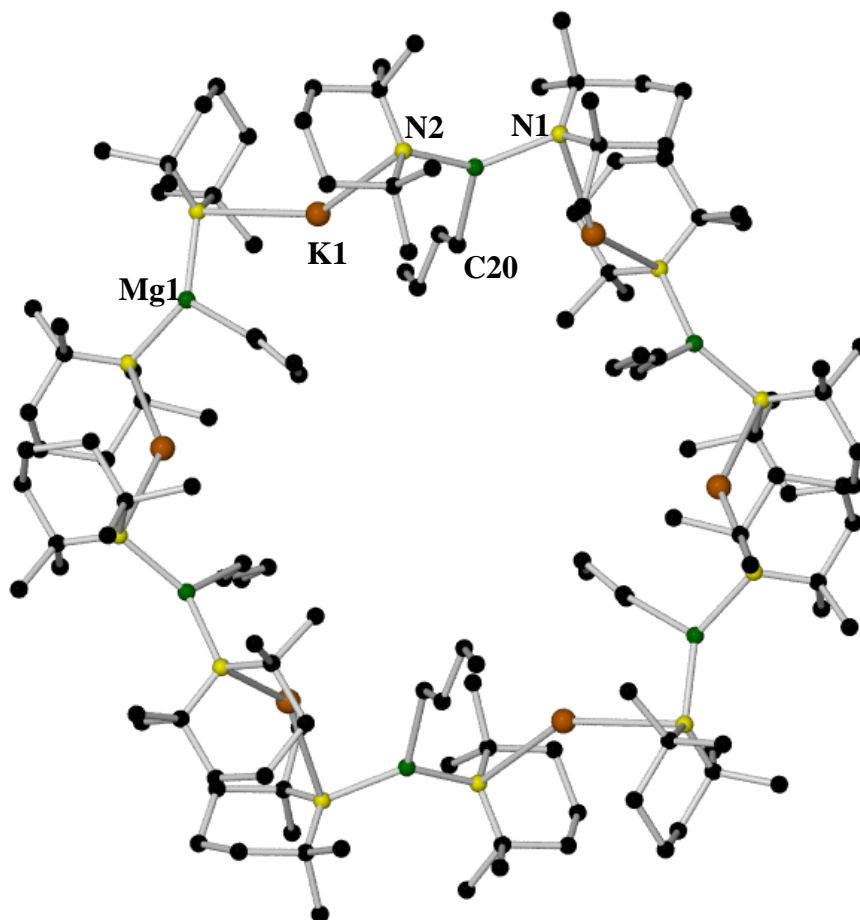
Fig. 5.20: Structure of $[KMg(TMP)_2Bu]_6$ **5h**. Key bond distances (Å) and angles (°): K1-N1 3.052(2), K1-N2 3.053(2), K1-C20 3.143(5), Mg1-C20 2.192(4), Mg1-N1 2.036(2), Mg1-N2 2.043(2), N1-K1-N2 146.72(6), N1-K1-C20 70.55(9), N2-K1-C20 130.39(9), N1-Mg1-C20 115.57(14), N1-Mg1-N2 133.63(9), N2-Mg1-C20 110.28(14), Mg1-N1-K1 89.43(7), Mg1-N2-K1 92.03(7).

The structure of **5h** is essentially a 24-membered $(KNMgN)_6$ ring, with formally two and three coordinate K and Mg centres respectively, although the K finds itself in relatively close proximity to the first carbon atom of its neighbouring *n*-butyl groups [K1-C20 3.143(5) Å and K1-C20* 3.243(5) Å]. Note that these two distances in this tighter, more sterically congested hexameric arrangement are practically unchanged from the corresponding K-C distances in the helical polymer [*cf*. K2-C2A 3.287(5) Å and K2-C3A 3.145(5) Å]. The K atom bridges between two TMP units, forming strong K-N contacts [K1-N1 3.052(2) and K1-N2 3.053(2) Å], with a bridging N1-K1-N2 angle of 146.72(6)°. By comparison, the Mg centre, bearing a third strong, formal σ bond to the carbon atom of the butyl group, is pushed towards the centre, resulting in a more constrained bridging N1-Mg1-N2 angle of 133.63(9)°. The remaining bridging

angles present within the 24-membered ring are the Mg1-N1-K1 and Mg1-N2-K1 angles of the bridging TMP units, experiencing a far greater degree of strain [Mg1-N1-K1 89.43(7) and Mg1-N2-K1 92.03(7)°]. The Mg atom is in a distorted trigonal planar arrangement, the sum of its angles totalling 359.48°, the greatest deviation from true trigonal planar exhibited by the N1-Mg1-N2 angle (Δ from perfect tetrahedral = 13.63 °). The butyl appendages point alternately in then out of the plane of the ring (which is severely puckered), in a similar fashion to that observed in the related tetramer.
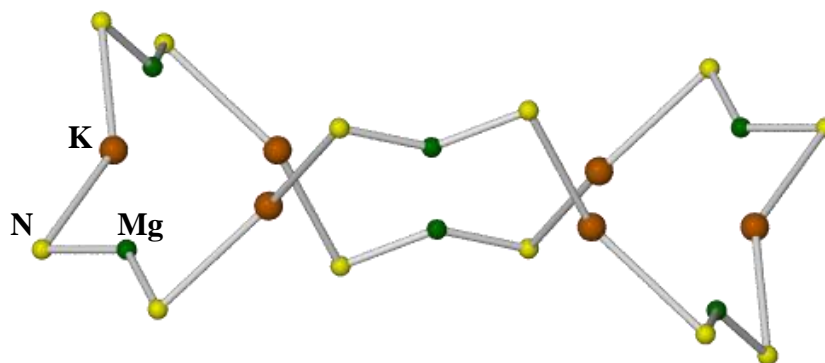
Fig. 5.21: Horizontal view of the puckered $[KMg(TMP)_2Bu]_6$ ring, with all C and H atoms omitted for clarity.

5.13 Comparitive NMR spectroscopic studies of 5g and 5h

This hexameric species was subjected to an in-depth study by both ^{1}H and ^{13}C NMR spectroscopy, the respective peaks of both the TMP and *n*-butyl anions in correct proportions, that is, 2:1. Curiously however, when stacked with the ^{1}H NMR spectrum of the corresponding tetrameric aggregate (both species dissolved in carefully dried C_6D_{12} due to their extremely reactive nature and consequently unfortunate tendency to succumb to unwanted hydrolysis), their spectra were found to be practically identical (**Figure 5.22**).

Fig. 5.22: Stacked plot of both tetramer **5g** and hexamer **5h** ^{1}H NMR spectra.

The stacked plot of the potentially more enlightening ^{13}C NMR spectrum also attests to their total spectroscopic equivalence (**Figure 5.23**).

Fig. 5.23: Stacked plot of both tetramer **5g** (bottom) and hexamer **5h** (top) ^{13}C NMR spectra.

It was then theorised that this could be a great coincidence, so mixed identical quantities of crystalline samples of both tetrameric and hexameric species, to observe whether in collusion each of these species could affect the shift of the other, or consequently give rise to new shifts. This mixing however showed only a single CH_2-M resonance, leading us to conclude that in solution these species were in fact one single entity. In order to ascertain the identity of this species, DOSY NMR studies were undertaken.

5.14   DOSY NMR analysis of 5g

Prior to these NMR studies we had attempted using **5g**, to form monometallated species in a tetrameric framework, but addition of substrates to solutions of dissolved **5g** had yielded thus far only intractable mixtures. It was later discovered that by adding only slight excess of benzene and toluene to this solution, we actually crystallized time and again the same hexameric inverse crowns, despite beginning initially with a tetrameric species in the solid state. These findings bolstered our revised theory that tetrameric species of the type [KMg(TMP)$_2$Bu]$_4$ may not in fact be present in solution. So in order to pin down the nature of the active species, we turned to DOSY NMR spectroscopy. This technique works by separating component parts of a solution mixture, then estimating their "size", a quantity inversely proportional to their diffusion coefficient (D).[173] In this regard, DOSY can be described as chromatography for NMR spectroscopy. Recently, Mulvey *et al* have utilised DOSY NMR to great effect, studying the system of the basic species "LiZn(TMP)$_3$", to decipher whether this reagent is in fact the contact ion-pair complex inferred by its empirical formula, or a different entity entirely.[174]   They discovered that instead of a base of the sort TMEDA.LiZn(TMP)$_3$, it seemed that LiTMP .LiCl $\pm$ TMEDA performs the initial metallation of the organic substrate, followed by transmetallation with Zn(TMP)$_2$, resulting in an overall zincation.

In order to characterize a chemical compound by DOSY NMR, ordinarily it is studied in the presence of a number of internal standards of increasing size. The standards typically employed (in order of decreasing molecular weight) are tetraphenylnaphthalene (TPhN) > phenylnaphthalene (PhN) > tetramethylsilane (TMS), which separate easily in the diffusion dimension of the spectrum, all dissolved within the same sample as the organometallic mixture. It was found in our own DOSY studies of the **5g** material in C$_6$D$_{12}$, that a combination of both the uniquely aggressive nature of

the base reacting quickly with the aromatic standards, and poor solubility of both the TPhN and PhN in C_6D_{12} solution precluded any useful insight into the nature of the base in the presence of these standards, much to our frustration. Having repeatedly attempted this analysis to no avail, two separate NMR samples were prepared, one containing only the standards in carefully measured concentrations, neatly separated according to their increasing diffusion coefficients [D(TPhN) = 6.69 × 10^{-10} < D(PhN) = 1.17 × 10^{-9} < D(TMS) = 1.64 × 10^{-9} m^2s^{-1}], and a second containing only a dissolved sample of known quantity of [KMg(TMP)$_2$Bu]$_4$. The DOSY processing was carried out separately on both species, and the diffusion coefficient of the magnesiate plotted on the same graph as the separate standards, with the relationship between log D and log FW of the standards producing a trend-line of reasonably good fit. Placement of the magnesiate species on this trend line provided by the standards proved possible as its diffusion coefficient fell only slightly outwith the range of molecular weights exhibited by the standards, thus allowing that of the unknown species to be reasonably estimated. It was discovered that, allowing for the considerable overlap of signals present in the ^{1}H NMR spectrum, three distinct data points gave an average diffusion coefficient for the magnesiate species of 6.11 × 10^{-10} m^2s^{-1}, and consequently a predicted molecular weight of 552.32 gmol^{-1}.

A diffusion coefficient of this value suggests definitively that no larger aggregates such as those observed in the solid state can be present in solution, even in a non-coordinating solvent such as C_6D_{12}. The molecular weight of the monomeric species, naked and uncoordinated is 401.0 g, a species with an associated error of -37.7% when compared to the predicted value. This is unsurprising, as even the act of breaking down the crystalline material i.e. dissolving it, is physical proof that deaggregation and solvation must be occurring. Dimeric, unsolvated species as the next largest aggregate would also have a very large error of 31.2% associated with it, rendering its existence in solution also very unlikely. In fact, the most plausible species associated with the predicted MW value of 552.32 gmol^{-1} would be a monomeric species solvated by one or more molecules of C_6D_{12}, although the binding of this alkane to the K centre would be expected to be weak. When we consider both the most likely active species in solution KMg(TMP)$_2$Bu·(C_6D_{12}) and KMg(TMP)$_2$Bu·(C_6D_{12})$_2$, the errors associated with each of these are -11.02 and 6.95 % respectively, both in relatively good agreement with the predicted value.
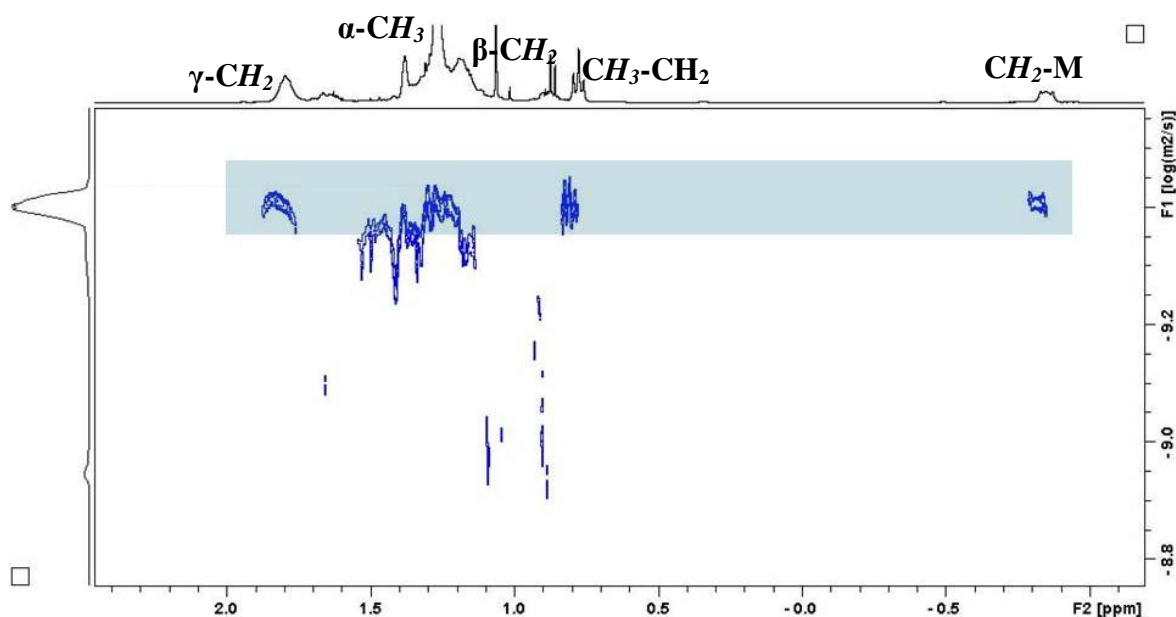
Fig. 5.24: ^{1}H DOSY NMR spectrum of **5g** in C_6D_{12} solution without standards.

It can be concluded then, at least tentatively, that the bis-amido potassium magnesiate [KMg(TMP)$_2$Bu]$_n$, whether beginning with any pre-formed crystalline aggregate or *in situ* mixture, its resonances appear all as spectroscopically equivalent in studies by both ^{1}H and ^{13}C NMR, exhibit identical reactivity towards both benzene and toluene, and by DOSY NMR, it appears as though the active species in solution is the highly reactive monomeric unit, coordinated to either one or two molecules of C_6D_{12}, a good solvent mimic for non-polar methyl-cyclohexane utilised in reactions.

5.15 DFT calculations

Having studied these "KMg(TMP)$_2$Bu" aggregates in both solid and solution state, we next investigated the relative stabilities of the different aggregates by DFT calculations, in order to establish any reason for preferential crystallization of one aggregation over another, and also if we can elucidate the reason for the remarkable hexameric ring systems invariably isolated after metallation of an aromatic substrate in terms of the energy involved in the reaction.

All transition states and reaction intermediates were optimised at the M06L level[175] of theory, utilising the basis set 6-311 ++ G(d, p).[176] Geometry optimizations were carried out with standard procedures based on analytical energy gradients. Frequency calculations were performed to characterize the optimized structures as minima or transition states, where the transition states were found to each have a single imaginary frequency. In addition, the vibrational frequencies were used to obtain temperature

corrected energies, enthalpies, entropies and free energies. All calculations were carried out using the Gaussian 09 package.[177] In order to begin our DFT studies, we required a base model for the bis-amido magnesiate species, so selected the monomeric unit. In modelling this species, the energy barriers of three monomeric units containing two bridging TMP units were calculated, and likewise three monomeric units containing a single bridging TMP and a single *n*-butyl group also modelled, with the lowest energy conformations shown below (**Figure 5.25**).

0.00 kcal mol⁻¹   **0.00 kcal mol⁻¹**
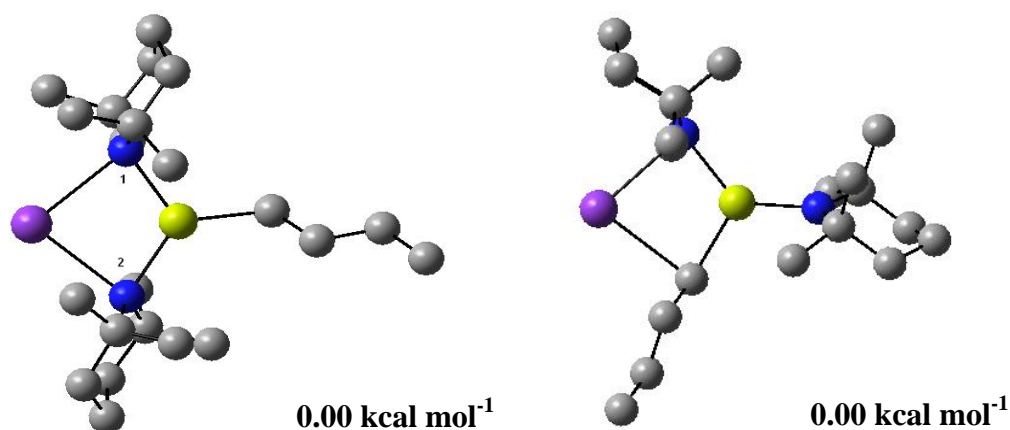
Fig. 5.25: Modelled energy minima of monomeric units with two (Left) or one (Right) bridging TMP groups.

Next, the energy of solvation by a single molecule of methyl cyclohexane was calculated, and the greatest energy minima found on solvation of the monomeric unit containing two bridging TMP units (ΔE = -2.07 kcal mol^{-1}). Note that this cumulative energy of solvation for both tetramer and hexamer are -8.28 and -12.42 kcal mol^{-1} respectively.

The energy of the potential dimeric species was then calculated, the first model as a closed ring structure (K-N-Mg-N-K-N-Mg-N), with each Mg centre bearing an ^{n}Bu group, pointing away from the centre of the molecule. Owing to the huge steric strain present in such a structure, a commensurately high relative energy is associated with it, calculated at a value of + 9.40 kcal mol^{-1}. The second dimeric model appears as a very loosely associated species, essentially two monomeric units, held together by very long range K-N interactions [interannular K-N distance 5.17 Å cf. intraannular K-N distance 2.84 Å]. The model is represented by an open dimer structure, featuring two four membered K-N-Mg-C rings, the Mg centres each bearing a terminal TMP unit, joined through K-N interactions far shorter than in the second model (interannular K-N distance = 3.272 Å). The relative energies of each of these modelled dimeric species are

+9.40, +3.09 and 0.00 kcal mol^{-1} respectively, with the overall energy of dimerization calculated as -4.57 kcal mol^{-1} (**Figure 5.26**).

Model 1: + 9.40 kcal mol^{-1}   **Model 2: + 3.09 kcal mol^{-1}**

Model 3: 0.00 kcal mol^{-1}
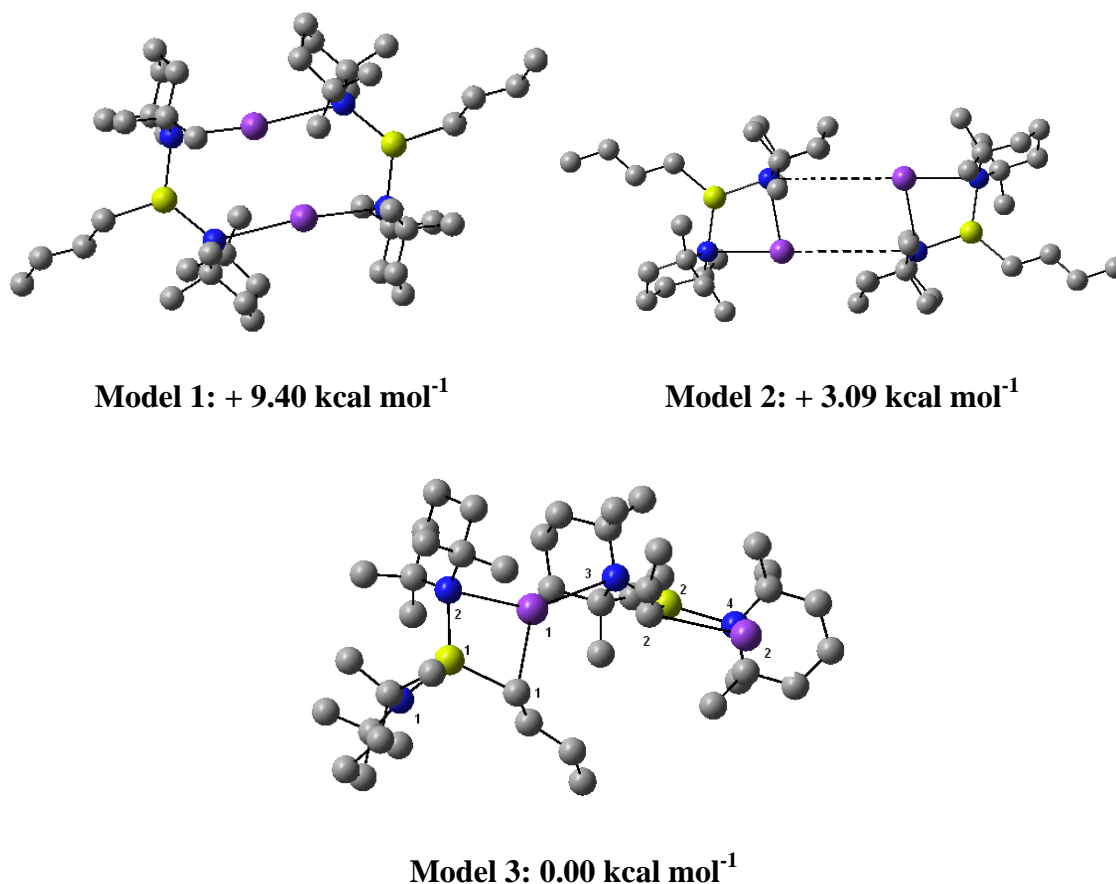
Fig. 5.26: Three dimeric models and their relative energies.

The open dimer species represents the lowest energy model for this aggregation, perhaps unsurpsrising on one hand due to the diminished steric strain, and on the other due to a number of publications giving precedent for open dimer structures of this type.[178] Moving to a higher degree of aggregation, the trimeric potassium magnesiate was modelled, and found to have again a proportionally higher energy of association (ΔE = -10.42 kcal mol^{-1}). Whilst interesting, none of these smaller aggregates have ever been isolated crystallographically, so moving to the experimentally observed tetrameric and hexameric species. Interestingly, the DFT calculations nicely mirror our experimental observations, with the tetramer and hexamer almost identical in energy (-13.83 kcal mol^{-1}), hence their propensity to crystallize preferentially before any other aggregates, yet require only the subtlest of changes in concentrations or solvents to crystallize one over the other (**Figure 5.27**).

KMg(TMP)₂Bu → **1/x [KMg(TMP)₂Bu]ₓ**

x = 2, 3, 4 and 6
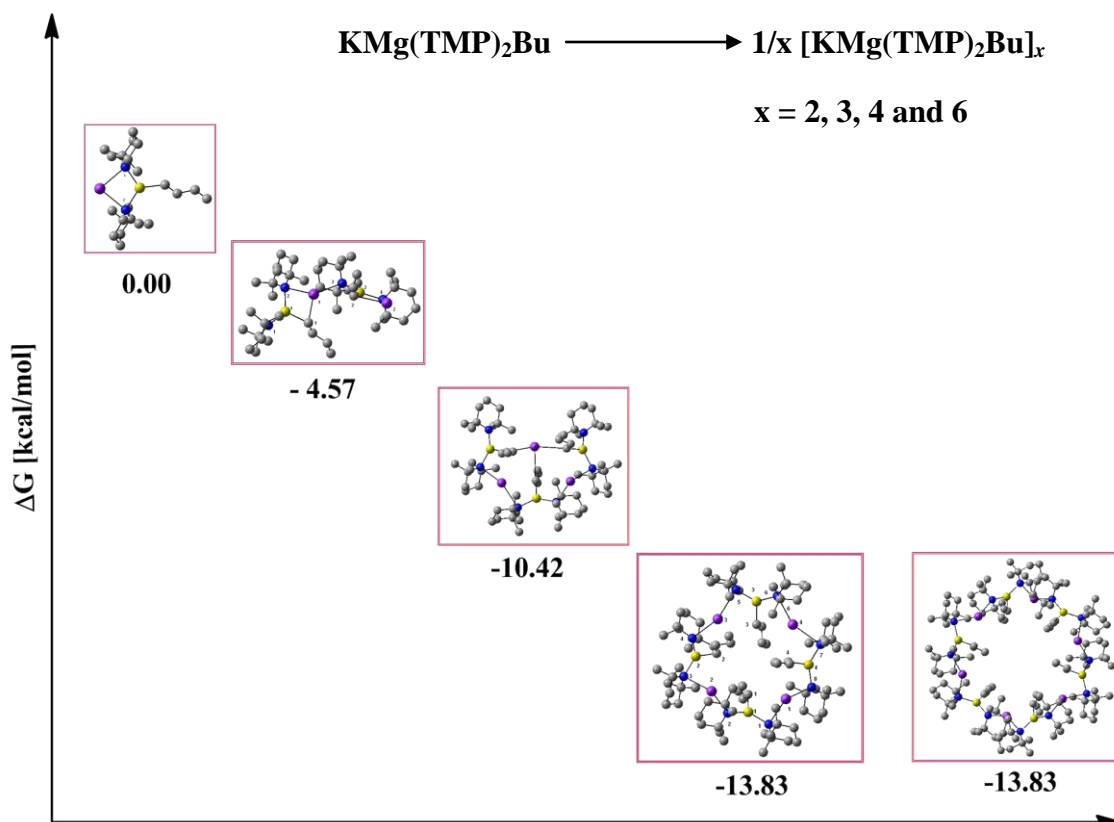
Fig. 5.27: Relative free energy (ΔG) profile of aggregates from monomer to hexamer of "KMg(TMP)$_2$Bu" in the gas phase (Left to right: monomer, dimer, trimer, tetramer, hexamer).

Also of considerable interest is the calculated energy of reaction when the *n*-butyl groups are replaced by Ph⁻ *i.e.* the potassium magnesiate deprotonates benzene. The cumulative energy of benzene deprotonation by six monomeric units and subsequent hexameric formation is -81.18 kcal mol^{-1}, showing that the hexameric benzene containing species is remarkably more stable than the initial precursor. This corroborates the situation observed experimentally, inasmuch as the tetramer and hexamer with alkyl groups still intact are easily dissolved in deuterated cyclohexane solution, experiencing only a minimal energy deficit in energy of solvation, whereas by comparison, the benzene inverse crown's greatly enhanced stability (a consequence of its high number of complimentary σ/π interactions) means that it is dissolved in only the most polar of solvents.

5.16   Reactivity of "KMg(TMP)$_2$Bu" towards ferrocene

Having systematically studied the base in isolation (both in solution and its multi-varied solid state aggregates) and its subsequent reaction with benzene and toluene to produce two known products, it came time to explore the activity of this basic mixture in the presence of new substrates and test whether formation of these hexameric inverse crowns was a coincidental motif, or a general reaction mode for encapsulation of deprotonated anions.

The first foray into the territory of new substrates began with the commonly utilised metallocene ferrocene. This substrate was intriguing due to its propensity to undergo multiple modes of deprotonation. It can for instance be deprotonated once, twice or indeed four times within a single reaction. This tetrametallation (detailed in the introduction) was the possibility that reignited an interest in the possibility of a tetrameric inverse crown incorporating TMP as the parent amide, as one can imagine quite easily the ferrocenyl unit being incorporated into the cavity now occupied by the *n*-butyl anions, poised for attack.

The base was formed by the method previously described, and one equivalent of ferrocene added *via* a solid addition tube. Vigorous heating produced after only several minutes an intense colour change from orange to deep red, a change ascribed in previous reports to the deprotonation of the ferrocene unit. Continued heating in methyl cyclohexane gave a suspension which no further heating was able to dissolve. Removal of all solvent *in vacuo* followed by addition of 10 ml toluene again gave a product only sparingly soluble. Further addition of 2 ml THF gave instant dissolution of all remaining solid material, with subsequent cooling of this bright red solution at 3°C for two weeks yielding a modest amount of deep-red crystals. Analysis by X-ray crystallography revealed neither a tetrameric nor hexameric aggregate, but instead the trinuclear ferrocenophane complex **5i**.
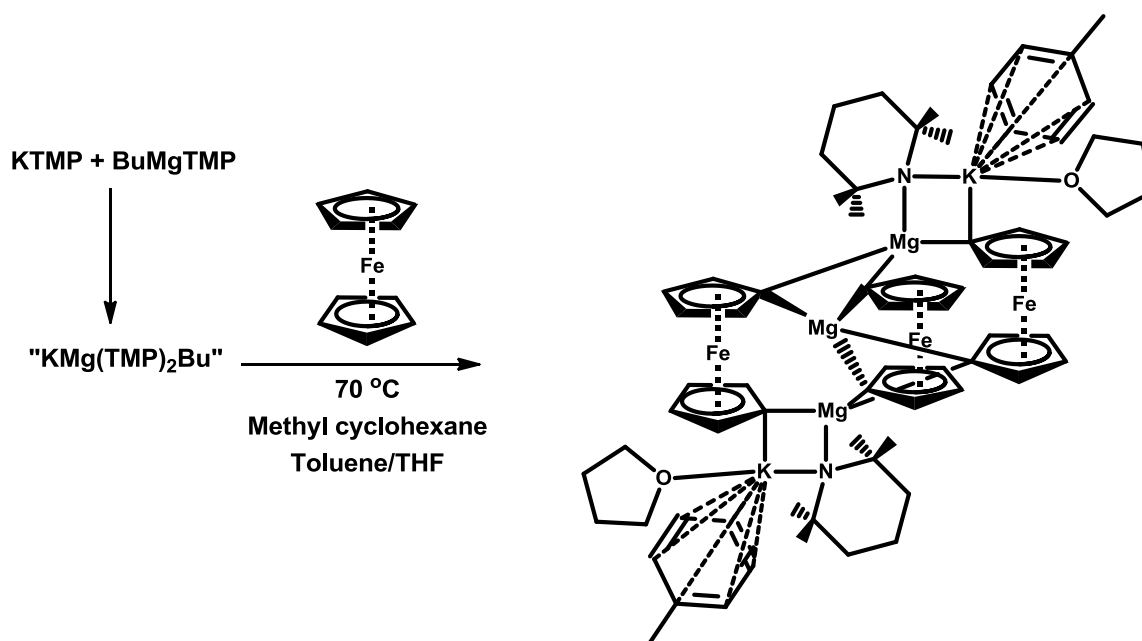
Scheme 5.7: Ferrocene deprotonation by "KMg(TMP)$_2$Bu" to form a trinuclear ferrocenophane **5i**.

Traditionally, the expression ferrocenophane is used to denote two ferrocenyl units bridged by a carbon atom, but in this case the magnesium atom acts as this bridging centre. This motif has been noted previously within our research group, with analogous Na-Mg[179] and Na-Mn[180] complexes of this type synthesised. A lighter lithium congener of the same type has also been elucidated,[179] marking **5i** as the first potassium example of these unusual hetero tri-metallic structures.

5.16.1 Crystallographic studies of [{Fe-(C$_5$H$_4$)}$_2${K$_2$Mg$_3$(TMP)$_2$(THF)$_2$(Toluene)$_2$}] 5i

The structure comprises three central magnesium atoms, stitching together three dideprotonated ferrocene units, once one each cyclopentadienyl ring. The two outer magnesium centres are bridged each to a single K atom through one N atom of a TMP anion, forming an overall neutral molecule. The K centres are then bound datively each to a single THF unit and η^6 to the π face of a single toluene molecule. The larger coordination sphere of K requires the extra interactions afforded by two coordinating ligands, notably different to the analogous sodium species in which the Na centres coordinate to only a single molecule of either pyridine or TMP(H). In our potassium complex, the solid state structure is redolent of the situation observed experimentally, inasmuch as the toluene provides a sparingly soluble compound, with the final THF

addition occupying the vacant coordination site, deaggregating the magnesiate and providing solubility.
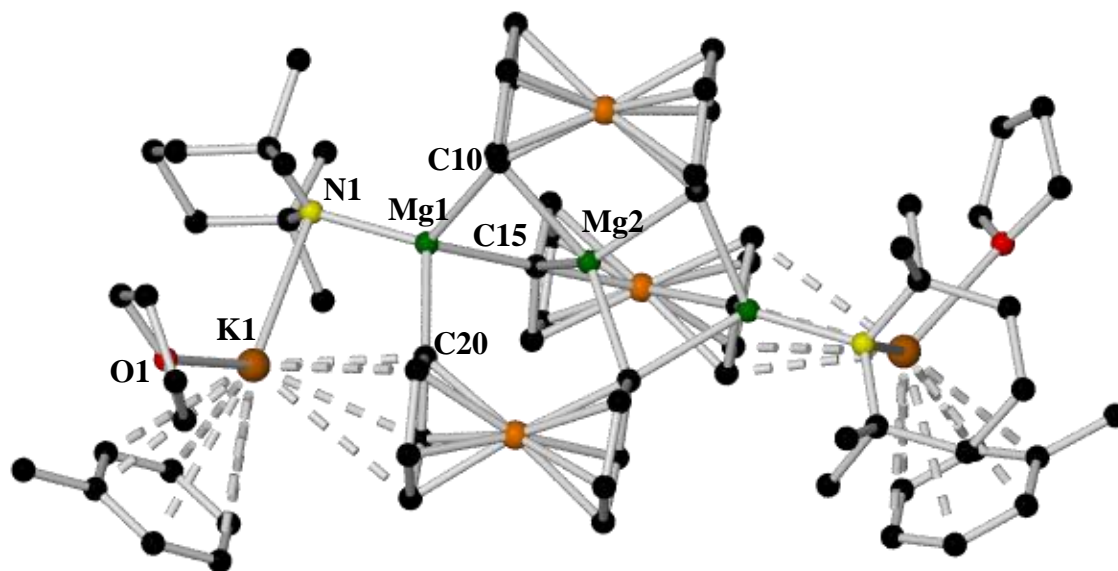
Fig. 5.28: Structure of [{Fe-(C$_5$H$_4$)}$_2${K$_2$Mg$_3$(TMP)$_2$(THF)$_2$(Toluene)$_2$}] **5i**. Key bond distances (Å) and angles (°): K1-O1 2.655(4), K1-N1 3.020(2), Mg1-N1 2.055(2), Mg1-C10 2.158(3), Mg1-C20 2.240(3), Mg1-C15 2.245(3), Mg2-C15 2.223(3), Mg2-C20 2.338(3), O1-K1-N1 121.16(11), N1-Mg1-C10 110.41(10), N1-Mg1-C20 120.37(10), C10-Mg1-C20 103.35(10), N1-Mg1-C15 125.82(9), C10-Mg1-C15 100.04(9), C20-Mg1-C15 93.02(10), C15-Mg2-C20 133.62(9).

The shortest distance K-heteroatom distance is that exhibited by the K-O dative bond to the THF ligand, at a value of 2.655(4) Å. The distance to the bridging N of the TMP anion is 3.02(2) Å, with a corresponding K-N-Mg bridging angle of 87.52(7) Å. The toluene molecules capping either end of the ferrocenophane demonstrate very significant π engagements with the K atom [K1-C26 3.341(4), K1-C27 3.312(4), K1-C28 3.323(4), K1-C29 3.342(4), K1-C30 3.373(4) and K1-C31 3.363(4) Å] which sits almost immediately above the centre of the π face, evidenced by the small degree of disparity between K-C$_{tol}$ bond distances. The coordination sphere of potassium is satisfied even further by the strong electrostatic interactions provided by the Cp face of a ferrocenyl unit to which it is bound η^4. The shortest distance form this Cp face to the potassium centre is in face 2.855(3) Å, shorter even than the K-N distance to the TMP. The K centre this time is more skewed in its orientation above the Cp ring, sitting not dead centre as above the toluene, doubtless a consequence of the ferrocenyl unit being part of a more rigid fixed system, bereft of the freedom of movement enjoyed by the toluene molecule. These close K-C$_{cp}$ distances are perhaps not so unsurprising, when we

consider past examples of the ferrocene unit acting as a strongly π bonding agent, having acted effectively as a ditopic linker to form organometallic polymers.[181] A consequence of this spacial bias towards one edge of the Cp face is that in having these shorter bonds, by necessity, more protracted K-C interactions exist [Range of 2.855(3) – 3.581Å], resulting in a greater range of K-C distances than exist with toluene π-interactions. Considering the abundance of contributing π bonds to the potassium, we can simplify our understanding of its geometry by taking only the centroid of each π face, thereby limiting its total number of bonds to only four, since the bonds K-C bonds from each unit are roughly equidistant [C_{ferr} = centroid of Cp face, C_{tol} = centroid of toluene face]. The average K-C distance to the centre to each face is 3.046 and 3.002 Å for the toluene and ferrocenyl faces respectively. In this simplified description of its bonding interactions, each K atom can be described as exhibiting a distorted tetrahedral geometry, its terminal position and abundance of softer interactions accounting for its distortion being experienced to a lesser degree than that of its magnesium counterparts, also four coordinate [C_{ferr}-K1-N1 96.97 °, C_{ferr}r-K1-Ctol 108.77 °, C_{ferr}-K1-O1 104.08 °, C_{tol}-K1-O1 96.16 °, C_{tol}-K1-N1 127.63 ° and N1-K1-O1 121.16(11) °].

There are two different magnesium environments within this structure, the two terminal centres, singly bound to each of the three ferrocenyl units, and also to the N atom of a single bridging TMP molecule. Owing to the symmetry within this structure, both Mg-N bond distances are equal, at a value of 2.055(2) Å, with each of the remaining Mg-C distances experiencing a slight incremental increase [Mg1-C10 2.158(3), Mg1-C20 2.240(3) and Mg1-C15* 2.345(3) Å]. Being four-coordinate, their geometries can be considered distorted tetrahedral, with the sum of these internal angles totalling 653.01 °, the greatest deviation from true tetrahedral occurring in the C20-Mg1-C15* angle [93.02(10) °, Δ = 15.98 °]. Focusing now on the central Mg atom, pinioned between three bulky ferrocenyl units, it exists in a markedly different environment to those end-capping this trinuclear arrangement. For instance, each Mg centre is bound to C atoms only. It also shows preference for one particular ferrocenyl unit, forming two Mg-C bonds, one to each Cp face, yet bonding only once to a single face of the remaining two ferrocenyl moeities. There is no disparity between the bond distances to each face of the top metallocene, each at a value of 2.223(3) Å, mirroring the situation experienced in its remaining bonds, which, although belonging to two separate ferrocenyl groups, are nonetheless equal [Mg2-C20 2.338(3) and Mg2-C20* 2.338(3) Å], a consequence of the symmetry generated nature of the structure. This central Mg atom is also four

coordinate, with the more rigid environment engendered by the encapsulating metallocenes exerting a larger degree of strain, thus distorting the tetrahedral environment to a greater degree [C15-Mg2-C15* 115.53(14), C15*-Mg2-C20 93.63(9), C15-Mg2-C20 133.62(9), C15*-Mg2-C20* 133.62(9), C15-Mg2-C20* 93.63(9), C20-Mg2-C20* 90.19(13) Å], the sum of these internal angles totalling 660.22°.

5.12.2 NMR analysis of 5i

In order to characterize this species fully in solution, the highly polar d_8-THF was employed, the crystalline material insoluble in both benzene and toluene. Gratifyingly, both ^{1}H and ^{13}C NMR spectra strongly support structural retention in solution, with exception of the solvent molecules (THF and toluene) bound to the K centre. The main body of the ferrocenophane is represented by two Cp signals, indicating that the two Cp rings of the dideprotonated ferrocene moieties are spectroscopically different, but each H atom within each particular ring spectroscopically equivalent. These resonances appear as singlets at 4.32 and 4.19 ppm respectively. The other anionic portion of the molecule i.e. TMP anion appears in the usual arrangement, with three sets of signals corresponding to the methyl, β-CH_2 and γ-CH_2 protons [0.60 ppm, 0.77 ppm and 1.40 ppm respectively], integrating to the expected ratio of 24:8:4. The now abundant deuterated THF solvent displaces the previously bound THF and toluene molecules, such that in solution we see evidence of free toluene and two different types of THF (bound deuterated THF and free "normal" THF). The toluene exhibits signals at 2.31 ppm (CH_3) and a series of overlapping aromatic signals, corresponding to the *ortho*, *meta* and *para* positions (7.1-7.2 ppm). The remaining signals attributed to the free THF appear as multiplets at 3.62 ppm (O-CH_2) and 1.78 ppm (CH$_2$CH_2).

Fig. 5.29: ^{1}H NMR spectrum of **5i** in d^8-THF solution.

The ^{13}C NMR spectrum neatly compliments that observed in the ^{1}H NMR spectrum (**Figure 5.30**), exhibiting two distinct resonances associated with the ferrocenyl anions at values of 80.2 ppm and 71.8 ppm. The TMP again exhibits three main signals, moving upfield from 42.6 (*C*H$_3$) through to 35.3 (β-*C*H$_2$) and finally to 20.7 ppm (γ-*C*H$_2$). The spectrum is sharp enough even to observe the quaternary TMP C atom at a value of 21.2 ppm. The free THF signals again appear in two environments [O-*C*H$_2$ 77.0 ppm and CH$_2$*C*H$_2$ 52.0 ppm], significantly downfield of the coordinating THF solvent signals [O-*C*H$_2$ 68.3 ppm and CH$_2$*C*H$_2$ 26.4 ppm]. The free toluene signals are also observed at 26.7 ppm (*C*H$_3$) and 129.8, 129.1 and 125.9 ppm (*o*, *m* and *p* respectively).

Fig. 5.30: ^{13}C NMR of **5i** in d^8-THF solution

Since this species is clearly a disproportionation product attempts at its reproduction utilising both rational stoichiometries and our original approach so far proved unsuccessful within the course of the project, but the unique ability of our mixed metal systems to fashion these unique architectures should suggest future attempts could be both possible and worthwhile.

5.17   Generation of a new naphthalene inverse crown

The different motif obtained in the deprotonation of ferrocene in perhaps understandable, owing to the drastically increased bulk when compared to the smaller substrates previously deprotonated by this base. Having successfully modified and optimized the conditions required for potassium mediated magnesiation of both benzene and toluene and their subsequent capture within an inverse crown framework, the next logical step in selecting a substrate was to move to the larger but more closely related fused ring system naphthalene. Naphthalene has been extensively studied in the field of metallation chemistry, both in terms of their reactivity with traditional alkyllithium reagents and more complex synergic metallators. For instance, it has been shown that the Lochmann-Schlosser superbase can effectively di-deprotonate naphthalene at cryogenic temperatures. Unfortunately it performs this so well that ten different

disubstituted isomers are formed.[182] A far higher degree of selectivity is obtained when utilising the sodium zincate **2a**, previously described as a highly effective Brønsted base, among its many other qualities.[183] It was found that reaction of naphthalene with this zincate at room temperature, produced a monometallated product of reaction at the two position, but that employment of two equivalents of base combined with more aggressive conditions of 5 hours heating at reflux temperature gave a di-zincated species, reacting at both the 2 and 6 positions (**Scheme 5.8**).
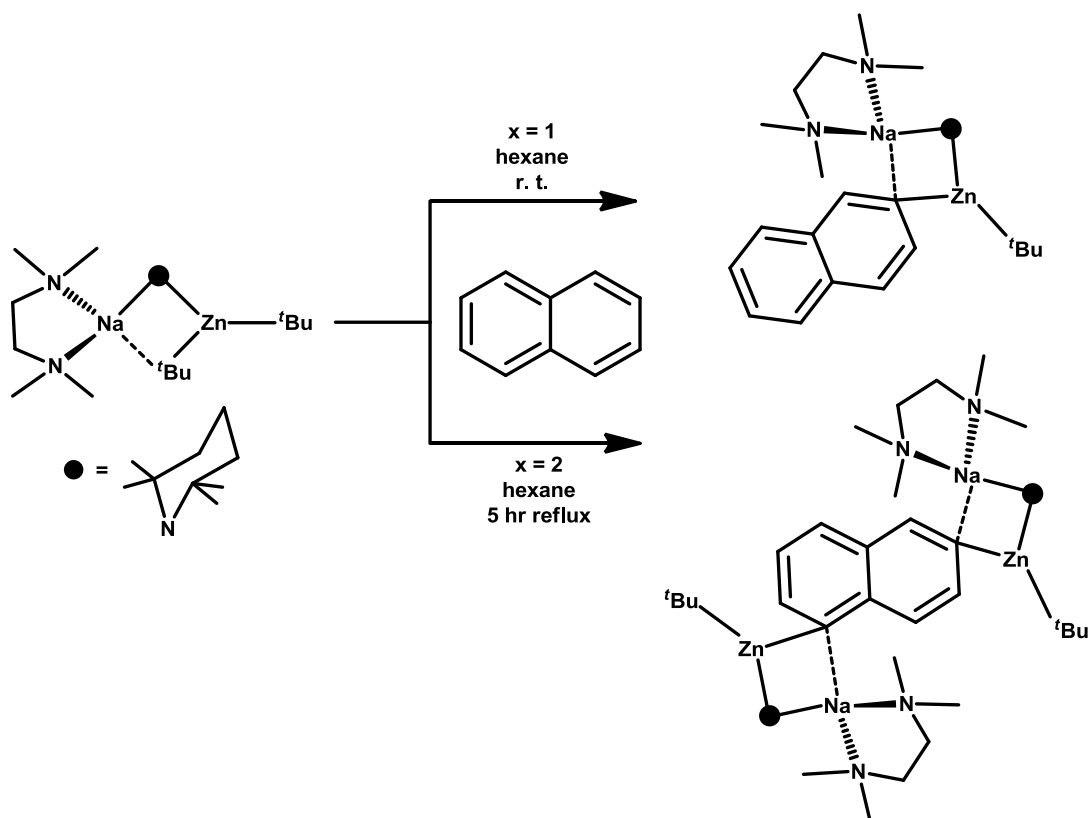
Scheme 5.8: Mono- and dizincation of naphthalene.

Since high levels of selectivity had been observed towards naphthalene in these related mixed-metal systems, it followed in this project to see what influence the second fused ring system and consequent positions of enhanced acidity would have on both the structure of the final product and reactivity of the base in general. To this end, the base was first prepared *in situ* by combination of KTMP and BuMgTMP in methyl cyclohexane solution. A single equivalent of naphthalene was then added via a solid addition tube, which after several minutes had fully dissolved. At this point, the solution was heated to reflux temperature, resulting in an off-white suspension within a red solution. Refluxing continued for another hour, allowing the reaction to achieve completion. Most of the methyl-cyclohexane was removed *in vacuo*, whereon 10 ml

toluene was added. Vigorous heating of this suspension after several minutes produced a red solution, at which point heating had to be immediately ceased, otherwise precipitation again occurred, producing a solid which no amount of heating could return to solution. If removed from heating at the point of initial dissolution and placed in a hot dewar to cool slowly overnight, a large amount of crystalline material was formed.

Upon X-ray analysis, this species was found to be the new inverse crown which was the ultimate goal of this study, containing six monometallated naphthalene species, each deprotonated at the 2 position (**Scheme 5.9**).
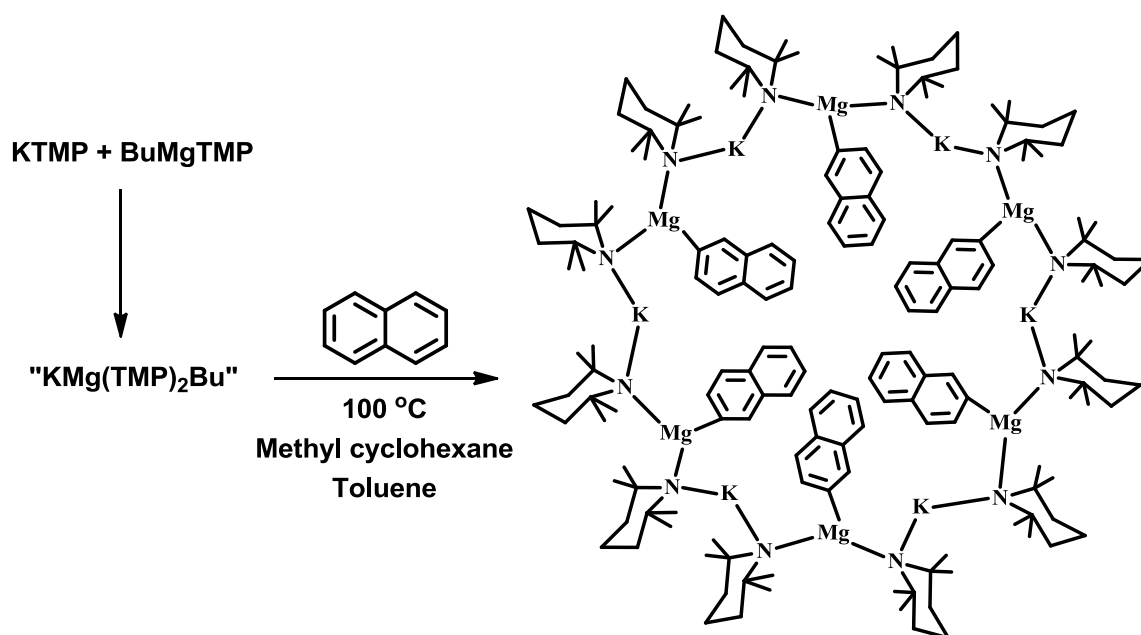
Scheme 5.9: Reaction of "KMg(TMP)$_2$Bu" with naphthalene.

5.17.1 Crystallographic studies of [KMg(TMP)$_2$(C$_{10}$H$_7$)]$_6$ 5j

This structure consists of a central 24 membered [K-N-Mg-N]$_6$ ring, with significant K-π interactions resulting in a series of smaller doubly fused four-membered ring appendages, mirroring the situation experienced in the polymeric precursor. These K-C interactions also describe two elegant internal structures, a twelve membered hexagonal arrangement propagating through the C2 position of the naphthalene, and a complimentary 12 membered, six-pointed star structure born solely of K-C3 interactions. When viewed side on, the [K-N-Mg-N]$_6$ ring is extremely puckered, almost identical to that of the hexamer **5h**. By comparison, if the naphthalene structure is viewed from the same sidelong orientation viewing only the significant K-π

interactions, these smaller secondary rings are almost entirely planar, revealing a doubly sided "paddle wheel" motif (**Figure 5.31**).
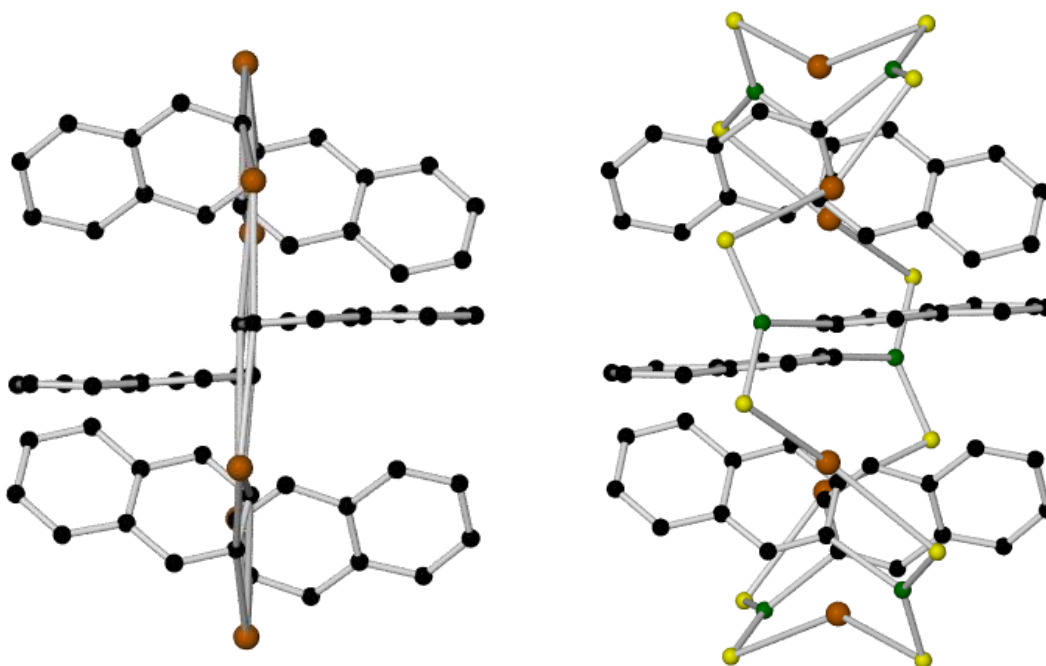
Fig. 5.31: Left figure: side-on image of **5j** showing only K and C atoms (all bonds solid); right figure: side-on image of **5j** with omission of TMP C atoms and K-C bonds.

The Mg centres are trigonal planar as in all previous inverse crown complexes, σ bound to the C2 position of the naphthalene ring system, bound also to two bridging TMP N atoms. The short Mg1-C30 bond is 2.248(2) Å, with both Mg-N bonds roughly equidistant [Mg1-N1 2.028(3) and Mg1-N2 2.029(3) Å]. The sum of the angles around the Mg total 359.84 °, with the greatest deviation from true trigonal planar found in the N1-Mg1-N2 angle [136.08(12)°, Δ from perfect trigonal planar = 16.08°]. These Mg-N bond distances are virtually coincident with those reported in the analogous deprotonated benzene structure [Mg1-N1 2.016(4) and Mg1-N2 2.022(4)], as are the corresponding angles around the same Mg centres [N1-Mg-N2 136.7(2), N1-Mg-C19 110.3(2) and N2-Mg-C19 113.0(2)°]. Within the main central ring system, each of the metals points in towards the centre of the molecule, exhibiting obtuse exocyclic bridging angles [N1-Mg1-N2 136.08(12) and N1-K1-N2 140.92(8)°], with concommitant projection of the N atoms outwards away from the core, with these exocyclic bond angles almost acute in nature (mean angle = 90.33°).
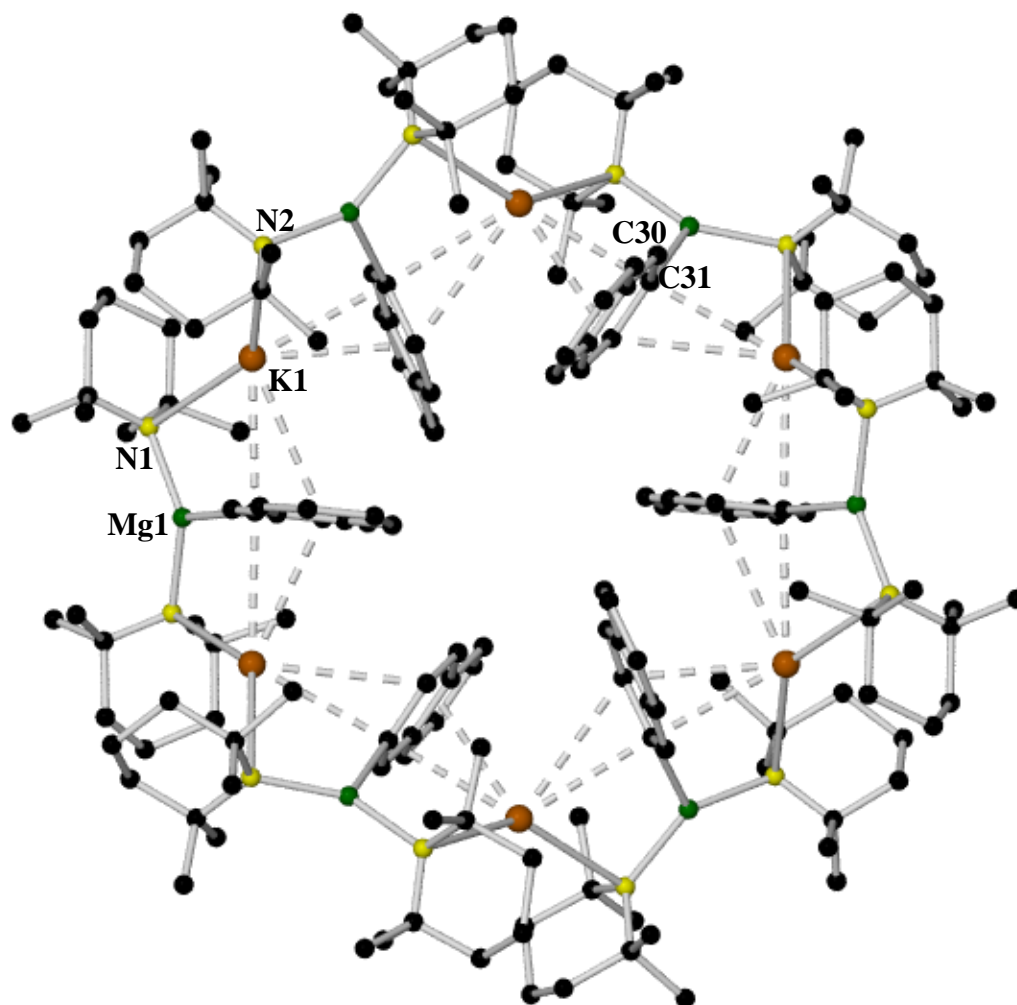
Fig. 5.32: Structure of $[KMg(TMP)_2(C_{10}H_7)]_6$ **5j**. Key bond distances (Å) and angles (°): K1-N2 3.072(3), K1-N1 3.174(3), K1-C30 3.128(4), K1-C31 3.318(12), Mg1-N1 2.028(3), Mg1-N2 2.029(3), Mg1-C30 2.248(2), C30-K1-N2 70.50(7), N1-K1-N2 140.92(8), N1-Mg1-N2 136.08(12), N1-Mg1-C30 110.30(14), N2-Mg1-C30 113.46(14).

The K centres are all identical, owing to the symmetry generated nature of the molecule, allowing each to be described as octahedral in terms of its bonding environment. Each K centre is bound to two TMP anions, forming near identical K-N bonds of 3.174(3) and 3.072(3) Å respectively. The faces of each naphthalene unit are orientated in such a way as to maximize the number of contributing π interaction with the nearest K atom, but since each naphthalene is wedged between a K centre of each side, each inclines slightly to favour one side. As a consequence, each K forms four π interations in total, with each naphthalene anion binding η^2 through the C30 and C31 positions to a K centre on either side. The K forms two contacts of 3.064(4) and 3.318(12) Å to positions C30 and C31 respectively, with the further stabilising interactions to positions

C30* and C31* marginally elongated at respective distances of 3.128(4) and 3.318(12) Å. Due to the large number of bonds associated with the K in **5j**, an array of surrounding angles are observed, from the obtuse C31*-K1-N2 [141.24(7) Å] to the extremely acute C30-K1-C31 [24.75(14) Å] angles.

The strength of this hexameric complex has imbued upon it, much as with the earlier metallated benzene and toluene inverse crowns, the uniquely frustrating property of being almost totally insoluble in any NMR solvent except the most polar, whilst simultaneously being so reactive in the presence of these polar solvents, it reacts with them almost immediately. This harks back to the previous assertions that the metallated species are "true" hexamers, the energy of solubility imparted by the weakly coordinating solvent C_6D_{12} not enough to deaggregate them, due to the cumulative energy of the complimentary Mg-σ and K-π interactions. The tetrameric and hexameric precursors do not enjoy the benefit of these interactions and can thus be broken down with comparative ease by even non-polar cyclohexane. As a consequence, characterisation of **5j** by NMR proved difficult but not impossible. By necessity, the polar d_8-THF had to be employed, with this donor solvent ultimately breaking the structure down, changing its nature in solution. Provided the sample was placed quickly on the instrument, satisfactory ^{1}H and ^{13}C NMR spectra could be obtained.

5.17.2 NMR spectroscopic analysis of 5j

The aromatic region shows seven separate signals, indicating that each C-H position within the deprotonated naphthalene unit is spectroscopically inequivalent. Most downfield of these is the single pertaining to the C-H of the C1 position adjacent to the Mg-C bond, at a value of 8.37 ppm. Doublets at 8.21 and 7.31 ppm are indicative of both the C_3-*H* and C_4-*H* positions respectively. The non-deprotonated second ring of the naphthalene fragment gives rise to four distinct resonances, with doublets at 7.57 (C_6-*H*) and 7.49 (C_9-*H*) ppm and triplets at values of 7.09 (C_7-*H*) and 7.01 (C_8-*H*). Since this species exists with toluene inclusive within the crystal lattice, toluene signals appear in both regions of the spectrum [(C*H*$_{(3, 5,)}$, m, 7.19 ppm), (C*H*$_{(2, 4, 6)}$, m, 7.10 ppm) and (C*H*$_3$, s, 2.31 ppm)]. In the aliphatic region we have again three distinct signal sets corresponding to the TMP anion. Furthest upfield (as expected) is a large singlet indicative of the C*H*$_3$ position, at a value of 1.26 ppm, with the remaining β and γ signals appearing at values of 1.29 and 1.71 ppm respectively. It is worthy of note that on utilising d_8-THF as our NMR solvent, the TMP signals are in the usually observed

order (*i.e.* γ < β < α), notably different to the order in C_6D_{12} experienced for the species $[KMg(TMP)_2Bu]_x$ (i.e. γ < α < β).

Fig. 5.33: ^{1}H NMR spectrum of naphthalene complex **5j** in d^8-THF solution.

The situation in the ^{13}C NMR spectrum mirrors that observed above, with seven distinct resonances in the aromatic region representative of the seven unique *C*-H environments, joined by several resonances which can be attributed to free toluene [($C_{(1)}$, 138.2 ppm), ($CH_{(2, 6)}$, 129.5 ppm), ($CH_{(3, 5)}$, 128.7 ppm), ($CH_{(4)}$, 125.8 ppm) and (CH_3, 21.3 ppm)]. The most downfield of these represents the C_3 position, at a value of 141.2 ppm, followed closely by the C_1 resonance at 140.6 ppm. The remaining resonance on this ring (C_4) falls immediately coincident with the C_8 resonance, such that the two are distinguishable by the HSQC spectrum, falling at a value of 121.9 ppm. The remaining resonaces associated with the second, untouched ring of the naphthalene appear at values of 128.0 (C_6), 127.8 (C_9) and 122.8 (C_7) ppm. The three main signals of the TMP anion appear at increasingly upfield values of 42.5 (β-CH_2), 36.2 (α-CH_3) and 21.7 (γ-CH_2) ppm.

Fig. 5.34: ^{13}C NMR spectrum of naphthalene complex **5j** in d^8-THF solution.

5.17.3 Quenching studies of 5j with I$_2$

In an attempt to quench this metallated intermediate, the commonly utilised electrophile I$_2$ was selected. The base was reacted with naphthalene as before, until an insoluble off-white suspension had been produced. This time, instead of removing the methyl cyclohexane and replacing it with toluene, the solid was filtered and washed with several portions of methyl cyclohexane. This powder was then dried under vaccum and stored in the dry box as a crude sample (83%). Prior attempts to quench this metallated species in the past with I$_2$ and a number of other electrophiles had proved fruitless, owing, it is believed, to the aggressive species reacting more rapidly with the THF in which the I$_2$ was dissolved than the halogen itself. Returning after overnight stirring and aqueous work-up only small amounts of the desired iodinated product were recovered, with the naphthalene starting material as the major product. Previous NMR spectroscopic studies had proved that physical cooling of the sample in THF solution could drastically increase its stability, but that spectra of samples conducted at room temperature often showed what appeared to be complete hydrolysis, with only free naphthalene and TMP(H) visible.

These observations mirrored in part what was believed to be the problem in the proceeding electrophilic quench studies. In order to combat this competitive reaction

with the solvent, 2 mmol of unrefined inverse-crown powder was placed within a Schlenk tube, and this mixture suspended in 10 ml methyl cyclohexane. In a second Schlenk tube, 20mmol I_2 was dissolved in 10 ml THF solution. Both samples were then cooled to -80°C and stirred for 15 minutes, at which time the cold suspension was taken up in a syringe and added dropwise to a stirring iodine solution. Ordinarily, when quenching reactions of this type are carried out, the iodine solution is stoichiometric and added to the metallated intermediate. Our rationale for both the vast excess and opposite order of addition was thus: had the I_2 been added to the metallated naphthalene, the highly reactive nature of this species when deaggregated by THF could have induced immediate reaction of any number of anions with the newly iodinated species, resulting in potentially unwanted side reactions. Adding the metallated naphthalene to the excess iodine solution would ensure, in a physical sense, that each molecule of metallated naphthalene would be immediately surrounded and swamped by I_2 molecules, forming the iodinated products immediately. After I_2 addition, the reactions were allowed to stir at -80°C for three hours, followed by stirring at room temperature for five hours more. After aqueous work-up, the crude product was analysed by NMR spectroscopy, revealing that iodination had occurred exclusively at the 2-position, with only trace amounts of free naphthalene in the aromatic region (**Figure 5.35**).
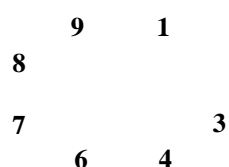
Fig. 5.35: ^{1}H NMR spectrum (400.13 MHz, 298K, CDCl$_3$) of 2-iodonaphthalene (close-up of aromatic region).

5.18   Preparation of a potassium bis-alkyl amido magnesiate

Until this point, past research and our own corroborative projects have revealed a definite pattern in the composition of both zincates and magnesiates. In general, the most effective and successful bases in zincate chemistry have contained one amido and two alkyl groups, whereas in the case of magnesiates a bis-amido monoalkyl system has proven both the most prevalent arrangement and the most potent system for substrate metallation. In fact, the only notable exceptions to this rule are a small number of zincates.[152c, 184] In attempting to exploit the apparent paucity of magnesiates deviating from the type [(donor)·M(NR$_2$)$_2$Mg(R)], an investigation was undertaken to decide whether or not bis-alkyl amido magnesiates could be generated, and if this proved possible, could they be used as effective Brønsted bases?

Firstly, an attempt was made to produce a bis-alkyl mono-amido analogue of the potassium magnesiate which has thus far been the main protagonist of the chapter, namely [KMg(TMP)$_2$Bu]$_x$. To achieve this, commercially available ^{n}Bu$_2$Mg (1M in heptane) solution was added to a suspension of KTMP in methyl cyclohexane. Repeated attempts unfortunately produced only a viscous brown oil, which no variety of solvents, concentrations, or combined efforts with prior filtering through Celite and glass wool could dispel. Even NMR spectroscopic evidence showed a mixture of n-butyl signals in the aliphatic region, indicating a number of species present in solution. With repeated failure to produced our desired magnesiate containing the n-butyl group, the related monosyl ligand instead ($^-$CH$_2$SiMe$_3$) was utilised in its stead. This alkyl group had been successfully utilised in the past, most notably in the deprotonation of THF, with either subsequent trapping of the sensitive α-metallated anion by [(TMEDA).Na(μ-TMP)(μ-CH$_2$SiMe$_3$)Zn(CH$_2$SiMe$_3$)][90] or alternative trapping of the same ether, totally fragmented, by the more aggressive [(TMEDA).Na(μ-TMP)(μ-CH$_2$SiMe$_3$)Mg(TMP)].[88] However, a remarkable example of the monosyl anion in metallation chemistry, far more pertinent to our own work, was discovered again in the absence of donor solvent, when the related species "NaMg(TMP)$_2$(CH$_2$SiMe$_3$)" was used to metallate toluene.

Remembering the earlier example, when the basic mixture "NaMg(TMP)$_2$^{n}Bu" was reacted with an excess of toluene, a twofold metallation occurred at both the 2 and 5 positions of the ring, trapping this anion at the centre of an inverse crown framework. It was discovered however, that on making the superficially minor change of replacing the

n-butyl ligand with ⁻CH_2SiMe_3, a remarkable change in selectivity was observed. The two units differ only slightly in bulk and even less in terms of basicity, so it was a matter of much surprise when double deprotonation had again occurred, except this time at the 3 and 5 positions of the ring (**Figure 5.36**).
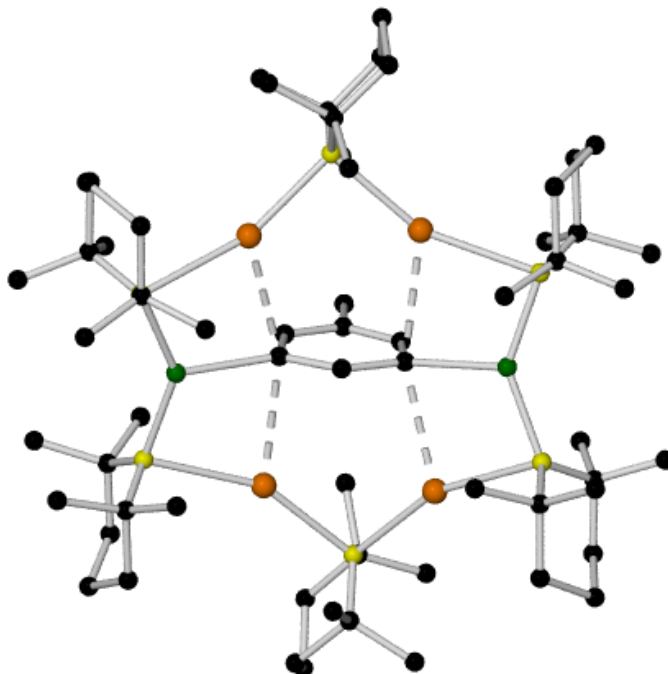
Figure 5.36: Molecular structure of 3, 5 − dimetallated toluene inverse crown.

This remarkable difference in reactivity prompted an investigation into the potentially different structures and reactivities in these new systems, changing not only the alkyl group but also doubling the number present in the parent base. To achieve this, the previously employed $^{n}Bu_2Mg$ solution was exchanged with solid $Mg(CH_2SiMe_3)_2$, which was purified by sublimation. Using this solid provided several advantages, inasmuch as its concentration and freedom from oxygen contamination could never be called into question or doubted, a worry ever present in the use of a bottled solution. To prepare what we hoped would be our bis-alkyl magnesiate species, we added solid $Mg(CH_2SiMe_3)_2$ (via a solid addition tube) to a KTMP suspension (in methylcyclohexane) in a 1:1 ratio. Immediate dissolution gave rise to a suspension several minutes later, which gentle heating reversed. Cooling of the hot solution overnight gave a large crop of block-like crystals, which proved to be the desired compound (**Figure 5.37**).

5.18.1 Crystallographic studies of [KMg(TMP)(CH₂SiMe₃)₂]∞ 5k
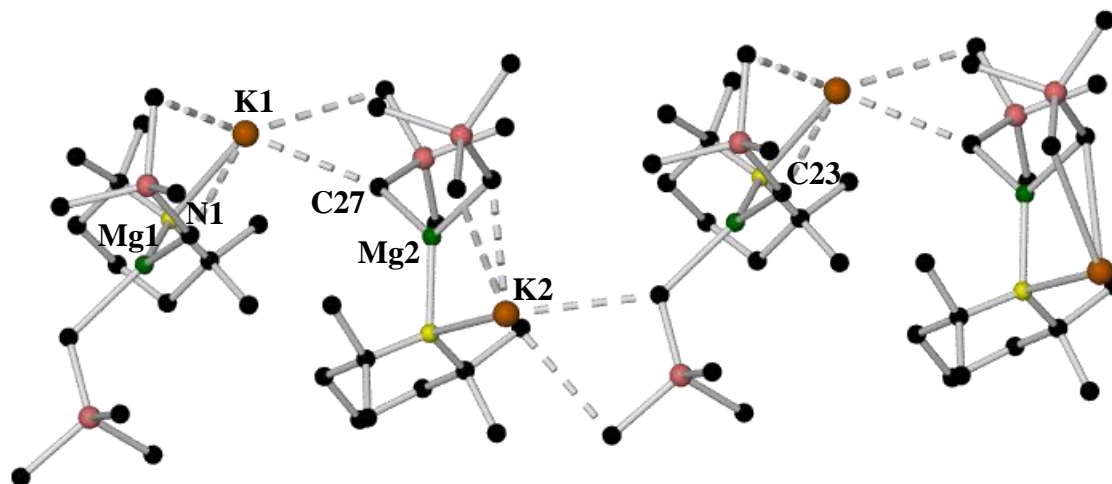
Fig. 5.37: Molecular structure of **5k**. Key bond distances (Å) and angles (°): K1-N1 2.820(2), K1-C23 3.148(3), K1-C27 3.186(3), K1-H27A 2.79(2), K1-H23A 2.77(2), K2-N2 2.79(2), K2-C31 3.093(3), K2-H31A 2.74(2), Mg1-N1 2.026(2), Mg1-C23 2.160(3), Mg1-C19 2.186(3), Mg2-N2 2.040(2), Mg2-C31 2.162(3), Mg2-C27 2.174(3), N1-K1-C23 73.47(7), N1-K1-C27 116.43(8), C23-K1-C27 82.53(8), N2-K2-C31 74.73(7), N2-K2-C19 127.18(8), C31-K2-C19 89.81(8), N1-Mg1-C23 117.51(11), N1-Mg1-C19 124.43(12), C23-Mg1-C19 117.94(14), Mg1-N1-K1 89.62(8), Mg2-N2-K2 89.02(8).

This structure was again polymeric in nature, though this time different in a great number of aspects to the bis-amido polymer detailed earlier. Instead of describing a helical path of propagation, this species, consisting of one TMP and two CH₂SiMe₃ anions, forms a two dimensional zig-zag arrangement, made up of essentially four membered K-N-Mg-C rings, bridging to each successive unit through a single C atom of a monosyl anion. In addition to being bound to three formally anionic centres (N, C, C), each K atom also forms strong electrostatic interactions to two additional methyl groups present in the monosyl moieties, thus allowing its geometry to be described as distorted trigonal bipyramidal. As in all precursor species alluded to, the larger coordination sphere of potassium allows a great number of differing bonding modes and geometries dependant on the nature of its surrounding anions, whereas the smaller Mg centre is far more contented to maintain its highly reactive trigonal planar environment, a situation which is unchanged within this complex.

Compared with all previous magnesiates, the K-N bond distance here is markedly more protracted, at a value of 2.820(2) Å, compared with an average K-N distance of 2.981 in **5f**. The K-C distances to the bridging C atoms are almost equivalent, at values of 3.148(3) and 3.186(3) Å for the K1-C23 and K1-C27 bonds respectively. Compare this again with the case in **5f**, where the K experiences significantly less interactions with one butyl group compared to the other, exhibiting notably different bond lengths of K1-C1A 3.331(6) and K1-C2A 3.126(6) Å. This can be attributed to the pulling in of the potassium by the extra electrostatic contacts made available by the monosyl group. Attached as it is to two formal C anions in a σ fashion, one bridiging within the four-membered K-N-Mg-C ring and the other bridiging each of these rings to form the polymer, the K centre comes in close proximity to a second methyl group of the propagating monosyl group, at a value of 3.148(3) Å, with a longer contact made to the corresponding methyl group of the ring anion [K1-C19 3.475(3) Å]. These electrostatic contacts are more clearly visible in **Figure 5.38**. This discrepancy in distances can be tentatively attributed to the increase in steric bulk within the more constrained ring system.
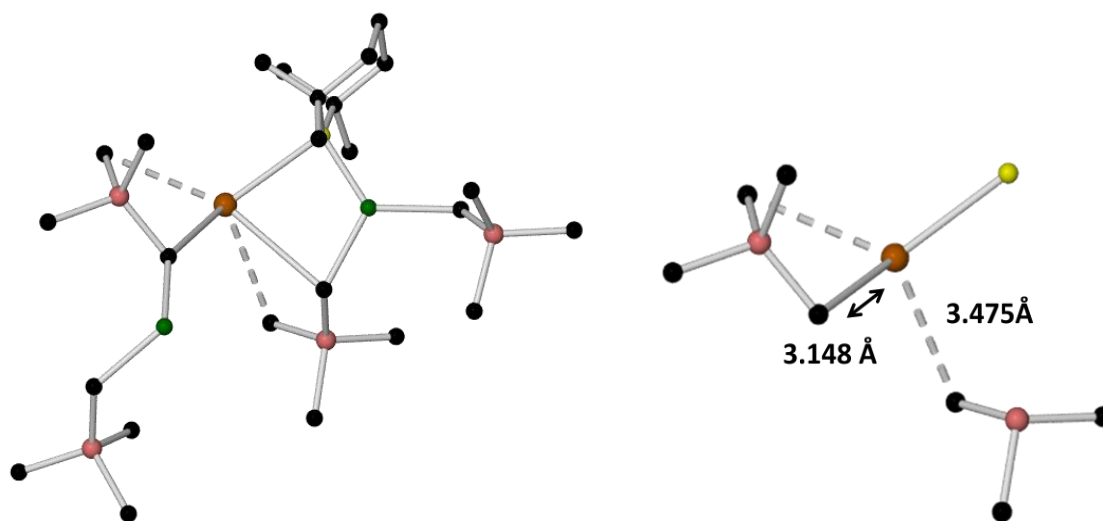
Fig. 5.38: Close up of K bonding situation in **5k**.

By comparison, the bonding situation with the Mg is far simpler, adopting a distorted trigonal planar geometry as before, forming short, strong σ bonds to two C atoms (of both ring and bridging monosyl ligands) and another to the N atom of the TMP. These distances come at values of 2.160(3), 2.186(3) and 2.026(2) Å for the bonds Mg1-C23, Mg1-C19 and Mg1-N1 respectively. Since this polymer contains only one bulky TMP anion, the Mg experiences a diminished degree of steric strain compared with in **5f**, most readily apparent in the angles around it. The angles denote only very little

deviation from true trigonal planar [N1-Mg1-C23 117.51(11), N1-Mg1-C19 124.43(12) and C23-Mg1-C19 117.94(14)°], the greatest of which occurs in the N1-Mg1-C19 angle (Δ from perfect trigonal planar = 4.43°). When we compare this to the bis-amido magnesiate polymer [N21-Mg2-N31 133.4(2), N31-Mg2-C2A 114.3(2) and N21-Mg2-C2A 112.1(2)°], enhanced deviation is apparent in each analogous angle, the most severe with a Δ value of 13.4°.

5.18.2 NMR spectroscopic studies of 5k

This species proved to be soluble in C_6D_{12}, allowing in depth NMR spectroscopic analysis to be conducted. The ^{1}H NMR spectrum shows evidence of only TMP and CH_2SiMe_3 anions, in the correct 1:2 ratio. Most downfield is the γ-CH_2 resonance of the TMP at a shift of 1.71 ppm, moving upfield to the β-CH_2 and the α-CH_3, exhibiting respective resonances of 1.27 and 1.14 ppm. Compared to the *n*-butyl ligand, the signals generated by CH_2SiMe_3 are much simpler, appearing as two singlets at 0.00 (Si*Me₃*) ppm, and the markedly upfield CH_2-M resonance at a value of -1.77 ppm (**Figure 5.39**).
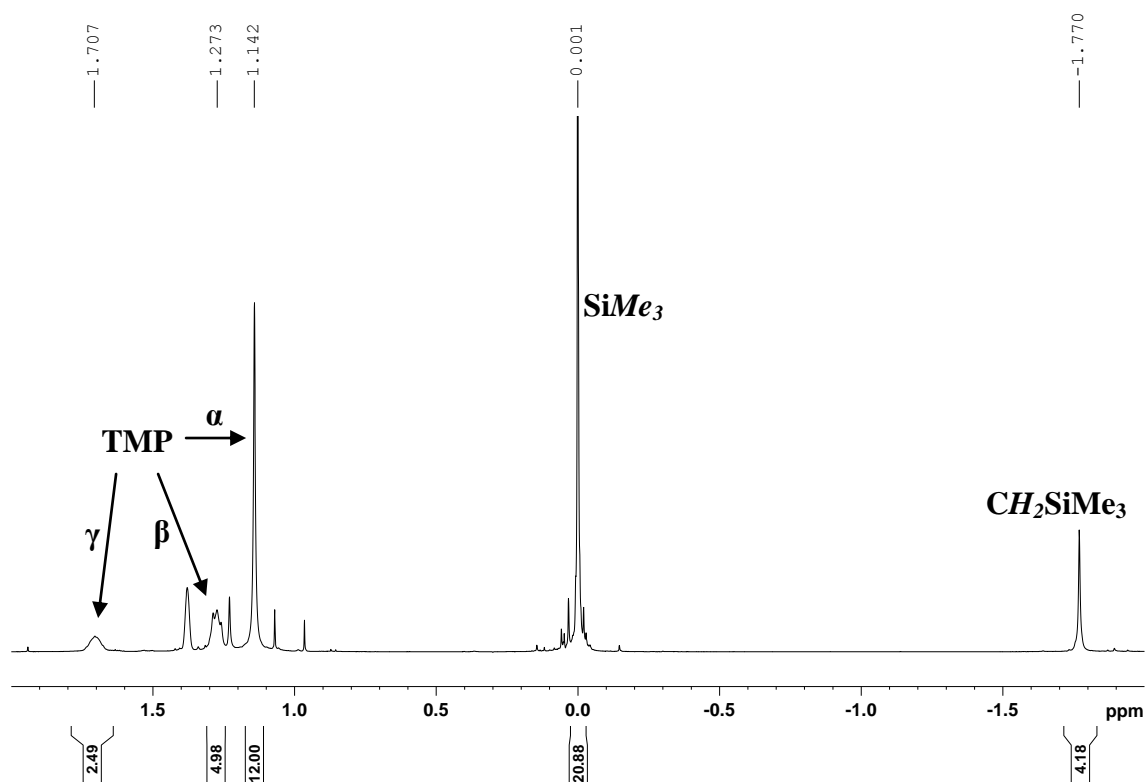
Fig. 5.39: ^{1}H NMR spectrum of **5k** in C_6D_{12}.

The ^{13}C NMR spectrum of **5k** is also both simple and illuminating, with three downfield signals which can be ascribed to the TMP anion (β-CH_2 41.7, α-CH_3 35 and γ-CH_2 20.4

ppm). Upfield of these, the two remaining resonances appear at 4.94 and 0.76 ppm, denoting the Si*Me₃* and *C*H₂-M groups respectively.
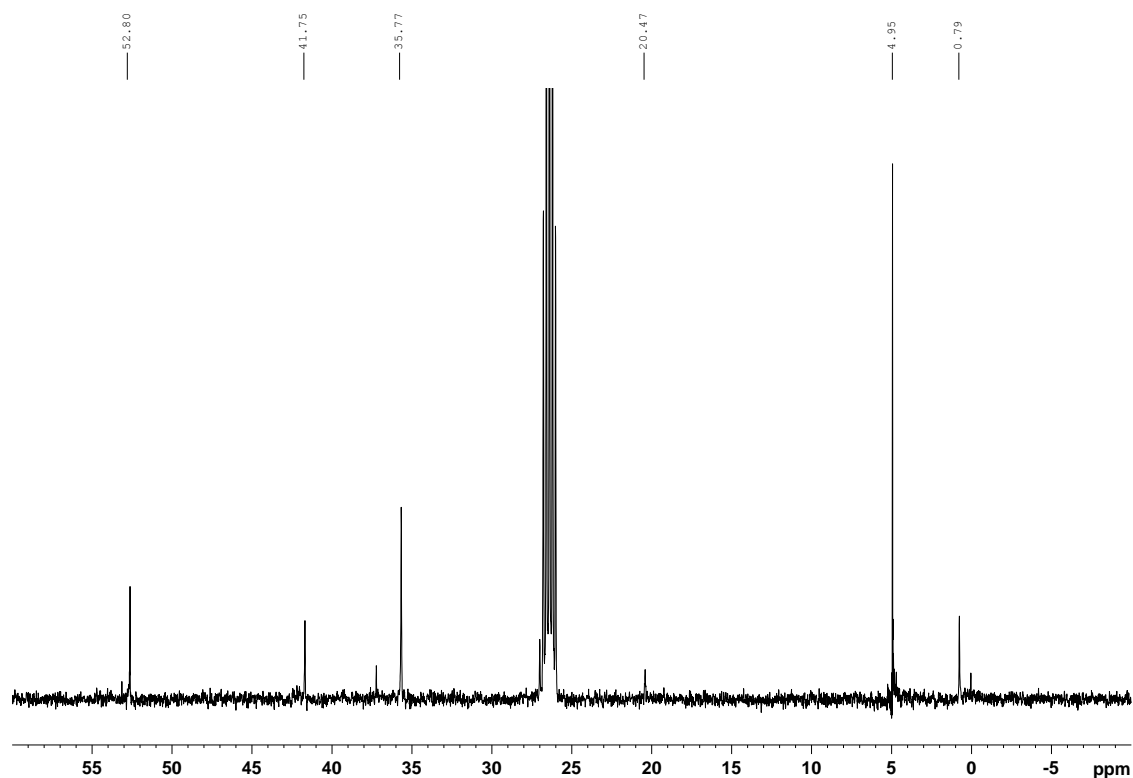
Fig. 5.40: ^{13}C NMR of **5k** in C_6D_{12}.

5.18 Preparation of a putative complex [(PMDETA)·K(μ-TMP)(μ-CH₂SiMe₃)Mg(μ-CH₂SiMe₃)]

Earlier it was described how the intermediate [(TMEDA)·Na(μ-TMP)(μ-^{n}Bu)Mg(TMP)] was trapped by addition of a single equivalent of the bidentate donor TMEDA to the inverse crown mixture "NaMg(TMP)₂Bu" forming a monomeric sodium magnesiate base subsequently utilised to perform selective metallations on a number of substrates. Some years later, the related potassium complex was synthesised, with the monosyl ligand replacing the *n*-butyl group as the alkyl component of the base (**Scheme 5.10**), which was then found to *ortho* metallate anisole smoothly at room temperature.
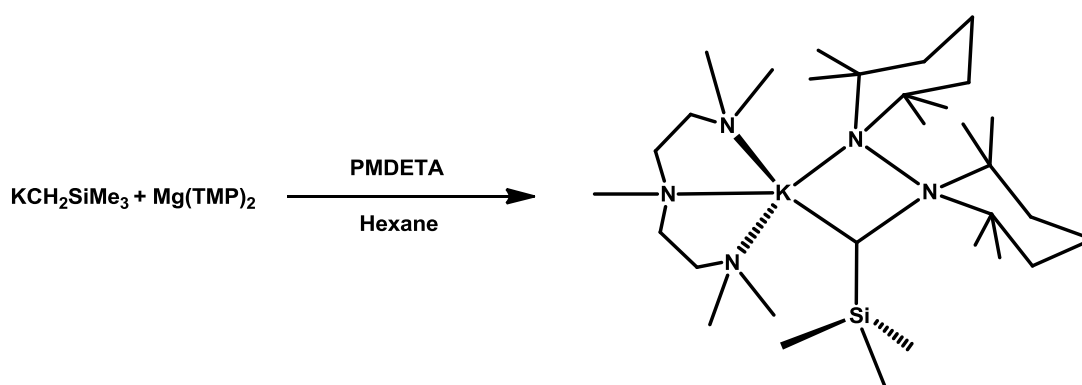
Scheme 5.10: Formation of [(PMDETA)·K(μ-TMP)(μ-CH$_2$SiMe$_3$)Mg(TMP)].

The activating effect of adding donor solvents to organometallic species is well known, so we wondered as to the feasibility of generating a (presumably monomeric) PMEDA solvate of our own [KMgTMPR$_2$]$_\infty$ in methyl cyclohexane. To achieve this the same suspension as before was generated containing the polymeric potassium magnesiate, though instead this time of heating to induce solubility, one molar equivalent of PMDETA was added, bringing about instant dissolution. Overnight cooling at -27°C afforded a crop of colourless crystals, which unfortunately, were not of sufficient quality to generate a useful diffraction pattern. Convinced of the likelihood that the desired putative intermediate had been formed, this material was subjected to study by ^{1}H NMR spectroscopy, and whilst not as definitive a result as one supported by the corresponding crystal structure, the spectrum showed all the expected resonances in the correct ratios (**Figure 5.41**). A correct ratio is immediately observed of the number of monosyl to TMP anions, namely 2:1. Beginning with the most downfield shift, the γ-CH_2 resonance appears as a multiplet at 1.90 ppm, the remaining TMP signals at 1.54 (β-CH_2) and 1.26 (α-CH_3) ppm. Since this crystalline material was dissolved in only weakly coordinating C$_6$D$_6$, the PMDETA remains intact in solution. All terminal methyl groups within the PMDETA are seen as spectroscopically equivalent, evidenced by one singlet appearing at 1.81 ppm, corresponding to 12 H atoms. The central methyl group also appears as a sharp singlet, upfield of the previous signal at a value of 1.71 ppm. The CH_2 positions of the ethyl backbone are represented by one broad intermediate signal at 1.73 ppm. The remaining two signals are attributed to the monosyl anions, appearing as sharp singlets, representing the SiMe_3 portion at 0.5 ppm, and the significantly upfield CH_2-M resonance at -1.25 ppm. Whilst this evidence allows only tentative identification of a PMDETA solvated species, it can be claimed with some confidence that this is in fact the desired species.

Fig. 5.41: ^{1}H NMR spectrum of putative complex [(PMDETA)·K(μ-TMP)(μ-CH$_2$SiMe$_3$)Mg(μ-CH$_2$SiMe$_3$] in C$_6$D$_6$.

5.19 Formation of a toluene solvate of 5k

Having generated a previously unseen potassium magnesiate motif with two alkyl groups and only a single amido anion, a final preliminary study into its reactivity was undertaken. **5k** was again generated *in situ* as before by combination of KTMP and Mg(CH$_2$SiMe$_3$)$_2$ in methyl-cyclohexane, and beginning with the simplest arene of sufficiently weak acidity, added benzene in a slight excess. Addition of the benzene failed to dissolve the suspension, even after stirring for several hours. Hoping that if the base had proved sufficiently reactive, it would by now have achieved full conversion to a metallated benzene intermediate, 3 ml of toluene were added, prompting immediate dissolution. Subsequent overnight cooling at -27°C afforded a modest amount of colourless crystalline material, of sufficient quality for X-ray analysis. Prior to this analysis, the potential reactivity of this new magnesiate was uncertain, since without the possibility of an entirely metal-amido framework, an inverse crown of the type to which we had become accustomed could not be possible. This led to the conclusion that even if the magnesiate with two alkyl groups was of sufficient reactivity to metallate benzene, its structure would likely be very different. Surprisingly, the structure elucidated was neither an inverse crown nor a metallated benzene containing species.

The polymer had in fact been retained, but in this instance, each K centre was coordinated η^3 to a molecule of toluene, added in excess to achieve solubility (**Figure 5.42**).

5.19.1 Crystallographic studies of [KMg(TMP)R$_2$·Toluene]$_\infty$ 5l
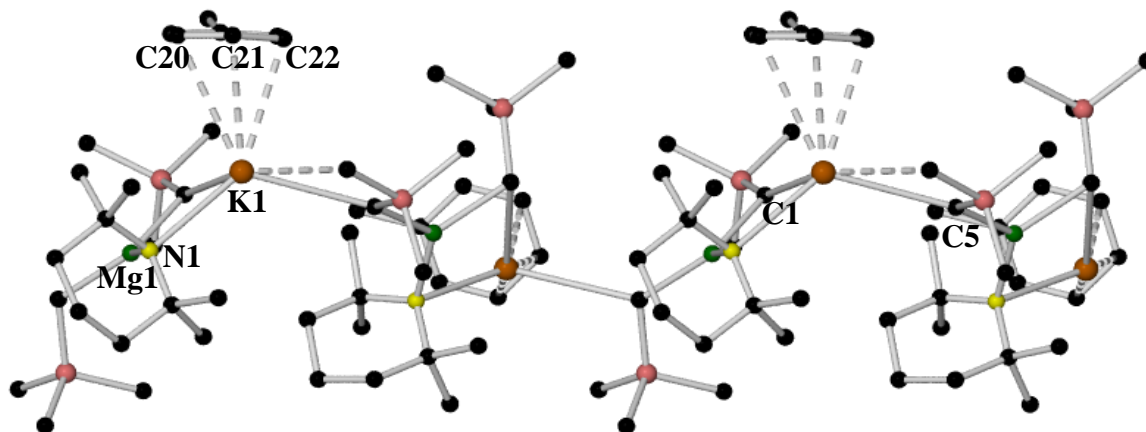
Fig. 5.42: Molecular structure of [KMg(TMP)R$_2$·Toluene]$_\infty$ **5l**. Key bond distances (Å) and angles (°): Mg1-N1 2.033(15), Mg1-C1 2.158(18), Mg1-C5 2.169(18), Mg1-C15 2.855(2), K1-N1 2.808(13), K1-C1 3.236(2), K1-C20 3.499(2), K1-C21 3.274(2), K1-C22 3.360(2), K1-C29 3.246(18), C1-Mg1-C5 119.44(8), C1-Mg1-N1 117.63(7), C5-Mg1-N1 122.76(7),

The same zig-zag arrangement present in the starting polymer is maintained here, the coordination sphere of each K centre widened to accommodate a molecule of toluene, which coordinates through its two *meta* and one *para* positions on the ring. This bias in coordination to favour π-interactions through these positions is perhaps telling of both the selectivity observed in the inverse crown generated by the bis amido potassium magnesiate, showing preferential *meta* selectivity, and the inverse crown produced by the related sodium species "NaMg(TMP)$_2$(CH$_2$SiMe$_3$)", which engenders twofold meta deprotonation. This toluene solvate could almost be considered a "pre-metallation" complex, showing how the toluene comes in close proximity to the electron deficient metal centre, primed for subsequent deprotonation. We are perhaps able to achive this coordination complex due to the apparently diminished Brønsted basicity of a potassium magnesiate bearing two alkyl groups.
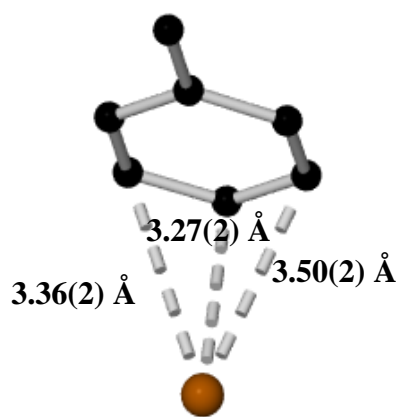
Fig. 5.43: Close-up of toluene binding η^3 to the K centre.

The bonding situation around the Mg centre is relatively unchanged, as it adopts the familiar distorted trigonal planar geometry ubiquitous in nearly all our previously described structures. The Mg forms short bonds to all three surrounding atoms [Mg1-N1 2.033(15), Mg1-C1 2.158(18) and Mg1-C5 2.169(18) Å], these distances practically unchanged from the unsolvated polymer **5l**. The lesser degree of steric congestion afforded by having only one bulky TMP anion again means that there is very little deviation from true trigonal planar experienced in the angles surrounding the Mg centre [C1-Mg1-C5 119.44(8), C1-Mg1-N1 117.63(7) and C5-Mg1-N1 122.76(7)°].

As a consequence of the coordinating toluene molecule, the bonding situation is different in each alternating K centre, making the bonds around centres K1 and K2 inequivalent. The K1 centre mirrors more closely matches that of the original polymer, binding through a single TMP N atom and two anionic C centres [K1-N1 2.808(13), K1-C1 3.236(2) and K1-C29 3.246(18) Å], whilst simultaneously forming two stabilising, though albeit distended, electrostatic interactions to two separate methyl groups [K1-C31 3.716 Å and K1-C2 3.762 Å]. This K1 centre also binds η^3 to the 3, 4 and 5 ring positions of the toluene molecule, at values of 3.36(2), 3.27(2) and 3.50(2) Å respectively. The situation with the K2 centre is very similar, the main difference being that now only a single secondary methyl interaction is experienced [K2-C7 3.42 Å], the closest K-C$_{methyl}$ distance on the second monosyl ligand elongated at 5.571 Å, far outwith any appreciable bonding distance.

The final chapter focuses on a large body of work that can be viewed as a direct progression of research carried out more than a decade ago. In 1999, the reaction of BuNa, Bu$_2$Mg and TMP(H) in a 1:1:3 ratio, when reacted in a vast excess of either benzene or toluene, resulted in a dideprotonation of the arene, 1,4 in the case of benzene

and 2,5 with toluene, these dianions encapsulated by a 12-membered metal amide crown. By contrast, when the analogous reaction with BuK was carried out, only monodeprotonation had occurred, resulting in a massive ring expansion, forming a 24-membered [K-N-Mg-N]$_6$ macrocycle. These early reactions suffered several drawbacks, in that vast excess of the arene solvent had to be employed, and that the parent base could not be identified. This active species was originally postulated as "MMg(TMP)3" (M=Na or K), but this was cast into doubt when we fortuitously synthesized the polymeric sodium magnesiate [NaMg(μ-HMDS)$_2$(^{n}Bu)]$_\infty$ from a reaction mixture containing this original 1:1:3 stoichiometry. Further studies led to isolation of the potassium analogue [KMg(μ-HMDS)$_2$(^{n}Bu)]$_\infty$ and more pertinent to our own investigations, the bis amido magnesiate [KMg(TMP)$_2$(^{n}Bu)]$_\infty$. Rational reaction of both this and the sodium analogue with stoichiometric benzene and toluene at room temperature resulted in these same inverse crown structures, indicating that a bis-amido magnesiate of this type is indeed the active species. Further investigation using a variety of solvents and concentrations also allowed characterization of two further aggregates of the potassium magnesiate, namely tetrameric [KMg(TMP)$_2$(^{n}Bu)]$_4$ and hexameric [KMg(TMP)$_2$(^{n}Bu)]$_6$. DOSY NMR studies indicated that the active species in solution was in all likelihood the monomer, solvated by either one or two molecules of deuterated cyclohexane, both possibilities within reasonable experimental error.

In order to ascertain whether this potassium magnesiate system could be used to produce new inverse crown species, the *in situ* mixture "KMg(TMP)$_2$Bu" was reacted with an equimolar amount of ferrocene. Incidentally, inverse crown formation was disfavoured, the actual complex isolated being a trinuclear ferrocenophane [{Fe-(C$_5$H$_4$)}$_2${K$_2$Mg$_3$(TMP)$_2$(THF)$_2$(toluene)$_2$}], the first of its kind containing potassium within its scaffold. Turning to naphthalene, reaction at reflux temperature and subsequent dissolution in toluene afforded a hexameric species, analogous with the original benzene/toluene examples, deprotonated at the C-2 position [KMg(TMP)$_2$(C$_{10}$H$_7$)]$_6$. This compound represented for the first time a rationally synthesised hexameric potassium inverse crown, the culmination of these bis-amido magnesiate studies. Next, investigation was undertaken to ascertain whether or not a potassium magnesiate bearing only a single amido group and two alkyl groups could be produced, and if so would it prove itself a synthetically useful material? Combination of KTMP and Mg(CH$_2$SiMe$_3$)$_2$ produced the polymeric species [KMg(TMP)(CH$_2$SiMe$_3$)$_2$]$_\infty$, which when reacted with toluene, did not produce an

inverse crown but in fact a toluene solvate, with the polymeric nature of the molecule maintained. This lack of metallation and preference for coordination instead, lead us to believe that this "alkyl-rich" magnesiate species may not be as basic as the previous "TMP-rich" species which acts as an aggressive Brønsted base. As a future avenue of study, a parallel can be drawn between our own reagents and those utilised to great effect by Knochel *et al.*[113, 185] His most effective magnesiate reagents have fallen into two categories, either turbo-Grgnard (RMgX.LiCl)[186] or turbo-Hauser (NR$_2$MgX.LiCl),[187] the former used primarily in lithium-halogen exchange reactions and the latter in deprotonative metallations. The comparison we can draw with the work in this chapter is most apparent when the basic species are represented in similar salt-like formula *i.e.,* (TMPMgR.KTMP) and (MgR$_2$.KTMP). The former species here is "TMP rich" and readily carries out a number of metallations at room temperature which preliminary studies suggest the "alkyl-rich" (MgR$_2$.KTMP) mixture cannot replicate. An interesting future study would be to investigate whether this mixture, with comparatively diminished deprotonative metallation capabilities could function as a strong agent of metal-halogen exchange.

It is clear from these studies into sodium and potassium magnesiates, that future studies could bring about a number of intriguing possibilities. Could these sodium magnesiates be used to dimetallate more electronically challenging arenes or heteroarenes in positions unachievable by any other method? And could the analogous potassium magnesiate species engender selective deprotonations of aromatic substrates, also unobtainable when utilising traditional organometallic reagents? Finally, could substrates of varying steric demand, when reacted in combination with these bis-amido magnesiate methodologies create new and exciting structural architectures, larger ring systems and shapes? This particular field is ripe for future studies, owing to the abundance of available avenues for exploration, as even a single variable change could bring about structural and reactivity changes which could only be imagined at. Finally, with such a paucity of bis-alkyl mono-amido sodium and potassium magnesiates, these rare bimetallic combinates are thus far unstudies in terms of reactivity. Even if they exhibit diminished capacity for deprotonative metallation, could they be used in metal-halogen exchange, or any number of other demanding synthetic transformations? These questions can only be answered in time and with perserverance.

6. <u>Conclusions and further work</u>

Each project detailed within this thesis can be considered a separate area of research in its own right, though all fall under the increasingly general umbrella description of synergic bimetallic chemistry. Though disparate in their content, each serves to further our understanding of this area, not simply in terms of alkali-metal mediated metallation, but also in the host of unique reactivities which are the preserve of our own particular brand of mixed metal chemistry.

Having seen how the zincate [(TMEDA)·Na(μ-TMP)(μ-^{t}Bu)Zn(^{t}Bu)] could anomalously add a ^{t}Bu group to the six position of benzophenone (with respect to the oxygen atom) in hexane at room temperature, we deemed this result an ideal starting point to probe the generality of this type of alkylation, otherwise unachievable unless carried out by the more aggressive ^{t}BuLi in THF at -100°C. We first selected the tricyclic ketone anthrone, containing a position of enhanced acidity (*i.e.* sp^3 centre between phenyl rings) and reacted it with the same sodium zincate. The dimeric species [(TMEDA)$_2$·Na$_2$(C$_{14}$H$_9$O)$_2$] was isolated invariably, containing only sodium, a product we deduced to occur via a CH$_2$ deprotonation and subsequent fragmentation pathway, and which could be produced rationally by the reaction of (TMEDA)·BuNa with anthrone. We then reacted a number of different sodium zincate and magnesiate combinations with our ketone, but discovered in every instance only the homometallic sodium dimer could be crystallographically characterized. We then turned our attentions to the analogous lithium and potassium zincates [(TMEDA)·Li(μ-TMP)(μ-Et)Zn(Et)] and [(PMDETA)·K(μ-TMP)(μ-^{t}Bu)Zn(^{t}Bu)], but found the sodium situation to be directly mimicked, forming time and again the respective homodimers [(TMEDA)$_2$·Li$_2$(C$_{14}$H$_9$O)$_2$] and [(PMDETA)$_2$·K$_2$(C$_{14}$H$_9$O)$_2$]. In order to ascertain whether zinc or magnesium containing anthracenolates were achievable, we reacted the comparitively weak monometallic bases (TMEDA)·Mg^{n}Bu$_2$ and (TMEDA)·ZnEt$_2$ and noted that deprotonation in the same position by a single basic arm had occurred, allowing us to isolate the monomeric species [(TMEDA)·Mg(C$_{14}$H$_9$O)(^{n}Bu)] and [(TMEDA)·Zn(C$_{14}$H$_9$O)(Et)]. In the duration of this project, we were unable to obtain a mixed metal species containing the anthracenolate anion, but the complexes produced have provided a platform for further studies, which could include reactions of different stoichiometries, different temperatures, or even indirect formation of mixed metal species by addition of a homometallic alkali metal reagent (*e.g.* BuLi, NaTMP) to either a magnesium or zinc monomer. Since a position of such enhanced acidity exists with

anthrone, it is perhaps unlikely that addition could take place preferentially over deprotonation in a 1:1 reaction, but a systematic study of different stoichiometries could reveal either polymetallation or dual addition/metallation modes of reactivity as plausible outcomes, both of which these bimetallic reagents have shown themselves able to carry out in the past.

Undeterred by the inability of our zincate [(TMEDA)·Na(μ-TMP)(μ-^{t}Bu)Zn(^{t}Bu)] to carry out addition on anthrone, we forged ahead in search of related and important and pharmaceutically releveant organic molecules, hitting upon the idea to utilize the ketones fluorenone and 2-benzoylpyridine. On reaction with fluorenone in hexane at room temperature, we gratifyingly achieved addition of a ^{t}Bu group to the six position of a single ring, allowing us to isolate the stable crystalline complex [(TMEDA)·Na{μ-OC(Ph)(4-^{t}Bu-C$_6$H$_4$)}(μ-TMP)Zn(^{t}Bu)]. We then reacted this species with D$_2$O and recorded its ^{1}H and ^{13}C NMR spectra over several days, noting that initially an enolate species was observed, but that after three days aerobic oxidation had eliminated DH from the molecule, giving us exclusively the ring substituted ketone. We then quenched the reaction media *in situ* (without prior isolation of our intermediate) with water, and found that although the 1, 6- addition product was indeed the predominant species, a substantial amount of the tertiary alcohol was also present, both of which could be separated and isolated by silica gel column. We could also improve the yield of tert-butylated ketone by oxidation of the metallo intermediate with SOCl$_2$ prior to aqueous workup. We then investigated whether changing the parent amine of the zincate to the less sterically demanding HMDS(H) would still allow us to observe similar reactivity. We discovered this was indeed the case, allowing us to achieve the same 1, 6- and 1, 2-addition products by quenching with water, albeit with a slightly higher observable quantity of the tertiary alcohol produced. On turning to the pyridyl ketone 2-benzoylpyridine, reaction with [(TMEDA)·Na(μ-TMP)(μ-^{t}Bu)Zn(^{t}Bu)] again facilitated ^{t}Bu addition in the 6 position, this time occurring on the electron deficient pyridine ring, an addition tantamount to a C-3 addition with respect to the N heteroatom, unachievable by any conventional means. NMR monitoring of D$_2$O quenched crystalline material revealed an analogous enolate to ketone formation occurring with elimination of DH. We also conducted *in situ* quenching studies, revealing this time (surprisingly) the tertiary alcohol to be the major product, a situation we could happily reverse by oxidation, again with SOCl$_2$, prior to aqueous workup. Changing the parent amine to HMDS also allowed us to isolate a stable crystalline intermediate, unusually containing

both 1, 6 and 1, 2 addition products within a single crystal. Changing the alkyl group seemed like the next logical progression, resulting in the reaction of the related zincate [(PMDETA)·Na(μ-TMP)(μ-Et)Zn(Et)] with fluorenone. We formed what we believe to be a disproportionation product, a homometallic hexamer and 1, 2 addition product [(Na-9-Et-9*H*-Fluoren-9-olate)$_6$]. This work has allowed us to show that the zincate [(TMEDA)·Na(μ-TMP)(μ-*t*Bu)Zn(*t*Bu)], most lauded in the past for its Brønsted basic capabilities, can perform a general 1, 6 addition of a single *t*Bu group towards several biaryl ketones, a class of organic molecules which enjoys considerable biological relevance. The next logical step in work of this type would be to probe whether different alkyl groups could also be added in a similar fashion. Even more interestingly, if were able to preform zincates containing aryl or substituted aryl groups, if reaction of these with fluorenone etc. showed these same anomalous substitution pattern, we could achieve what would be tantamount to a transition-metal free cross-coupling, and a unique method of C-C bond formation. To this end we have already prepared the biaryl sodium zincate [(TMEDA)·Na(μ-Ph)(μ-TMP)Zn(Ph)] which could be used in future potentially for this purpose.

In the chapter of this report discussing selected other results which have potential for further PhD projects, we also detail a third reactivity type which the selfsame zincate [(TMEDA)·Na(μ-TMP)(μ-*t*Bu)Zn(*t*Bu)] can exhibit, namely its ability to act as a single electron transfer reagent. It was shown by a previous group member that when reacted with a single molar equivalent of TEMPO, a *t*Bu· radical is liberated, reacting with another radical to form isobutene and isobutene, whilst simultaneously generating the TEMPO anion, which is trapped within the zincate, the structural integrity of which is obtained. The reaction of two molar equivalents of TEMPO results in twofold activation of the zincate, producing both TMP· and *t*Bu· radicals and subsequent replacement of these with two TEMPO anions within the bimetallic motif. We next reacted this zincate with the highly conjugated organic molecule chalcone, originally as part of the addition project, owing to the numerous different positions of reactivity within it. To our surprise two of SET had again occurred, resulting in homocoupling of two chalcone fragments, made stable and isolable by the stable zincate moieties capping each end ([(TMEDA)·{Na(μ-TMP)Zn(*t*Bu)}$_2$(μ-OCPhCH=CHPhCHPhCH=CPh-μ-O)]).

Isolation of a molecule of this type was unprecedented, representing a synthetically useful example of the zincate acting as an agent of SET, providing a solid foundation for further reactions of this type. Since these reactions can be carried out in non-polar

solvents at room temperature, they could represent another new method of transition-metal free C-C coupling.

Within this same chapter, we delved into the as yet unexplored territory of closo-carboranes reactivity with synergic bimetallic reagents, and found that the reaction of [(TMEDA)·Na(μ-^{n}Bu)(μ-TMP)Mg(TMP)] with the *ortho* isomer resulted in a solvent separated structure on dissolution by THF, commonly encountered when utilising this polar solvent. The cation was a familiar Na$^+$, sequestered by six THF molecules, whereas the more interesting anionic portion consisted of a Mg centre surrounded by three monodeprotonated carborane anions and a single THF molecule [{(THF)$_6$·Na}$^+${(THF)·Mg(o-carborane)$_3$}$^-$]. This structure was unfortunately of insufficient quality to infer even definitive connectivity, the main drawback of the carborane substrates being their apparent inability to give high quality crystalline material. Turning to the related lithium zincate [(THF)·Li(μ-^{t}Bu)(μ-TMP)Zn(^{t}Bu)], which we reacted with the *meta* isomer, followed by dissolution with THF. Again we achieved a solvent separated species of poor quality, consisiting of three cationic [(THF)$_6$·Li$^+$] moieties, the anionic portion consisting of a cyclic structure, with three dideprotonated carborane units, and each Zn centre bearing a third anion, a single ^{t}Bu group. As with the previous structure, poor quality has precluded any useful insight into key structural features. Although these structures regrettably did not diffract well, they serve to highlight the unusual modes of reactivity which carboranes can undergo in the presence of our complex metallators, and in future a more in-depth study would undoubtedly reveal both novel structural motifs and even unusual reactivity types such as potential polymetallation, with carboranes presenting themselves as an untapped vein in the field of metallation chemistry.

Focusing next on an unusual potassium tris-amido magnesiate, we reacted PhCH$_2$K, Bu$_2$Mg and Ph$_2$N(H) in a 1:1:3 ratio in the presence of THF and PMDETA to produce the contacted ion-pair structure [(PMDETA)·K(μ-NPh$_2$)Mg(THF)(NPh$_2$)$_2$]. As a consequence of the less sterically demanding amide employed, both metal centres exhibit unusual bonding modes, the potassium bound only to a single N atom of the diphenylamide, its coordination sphere satisfied by the tridentate PMDETA ligand and only through π-aryl contacts of a second amine. The Mg centre is, unusually, four coordinate, bound to the N atoms of each diphenylamide, its coordination sphere requiring a single THF molecule to achieve satisfaction. This unusual structure serves to highlight the paucity of potassium magnesiate structures bearing non-bulky substituents,

and how the structures can be altered to produce new and interesting bonding modes thought unachievable in other systems.

The final chapter focuses on a large body of work that can be viewed as a direct progression of research carried out more than a decade ago. In 1999, the reaction of BuNa, Bu_2Mg and TMP(H) in a 1:1:3 ratio, when reacted in a vast excess of either benzene or toluene, resulted in a dideprotonation of the arene, 1,4 in the case of benzene and 2,5 with toluene, these dianions encapsulated by a 12-membered metal amide crown. By contrast, when the analogous reaction with BuK was carried out, only monodeprotonation had occurred, resulting in a massive ring expansion, forming a 24-membered $[K-N-Mg-N]_6$ macrocycle. These early reactions suffered several drawbacks, in that vast excess of the arene solvent had to be employed, and that the parent base could not be identified. This active species was originally postulated as "$MMg(TMP)3$" (M=Na or K), but this was cast into doubt when we fortuitously synthesized the polymeric sodium magnesiate $[NaMg(\mu\text{-}HMDS)_2(^nBu)]_\infty$ from a reaction mixture containing this original 1:1:3 stoichiometry. Further studies led us to isolate the potassium analogue $[KMg(\mu\text{-}HMDS)_2(^nBu)]_\infty$ and more pertinent to our own investigations, the bis amido magnesiate $[KMg(TMP)_2(^nBu)]_\infty$. Rational reaction of both this and the sodium analogue with stoichiometric benzene and toluene at room temperature resulted in these same inverse crown structures, indicating that a bis-amido magnesiate of this type is indeed the active species. Further investigation using a variety of solvents and concentrations also allowed us to crystallographically characterize two further aggregates of the potassium magnesiate, namely tetrameric $[KMg(TMP)_2(^nBu)]_4$ and hexameric $[KMg(TMP)_2(^nBu)]_6$. DOSY NMR studies indicated that the active species in solution was in all likelihood the monomer, solvated by either one or two molecules of deuterated cyclohexane, both possibilities within reasonable experimental error.

In order to ascertain whether this potassium magnesiate system could be used to produce new inverse crown species, we first reacted the *in situ* mixture with an equimolar amount of ferrocene. Incidentally, inverse crown formation was disfavoured, the actual complex isolated being a trinuclear ferrocenophane $[\{Fe\text{-}(C_5H_4)\}_2\{K_2Mg_3(TMP)_2(THF)_2(toluene)_2\}]$, the first of its kind containing potassium within its scaffold. Turning to naphthalene, reaction at reflux temperature and subsequent dissolution in toluene afforded a hexameric species, analogous with the original benzene/toluene examples, deprotonated at the C-2 position

$[KMg(TMP)_2(C_{10}H_7)]_6$. This compound represented for the first time a rationally synthesised hexameric potassium inverse crown, the culmination of these bis-amido magnesiate studies. We next pondered as to whether or not a potassium magnesiate bearing only a single amido group and two alkyl groups could be produced, and if so would it prove itself a synthetically useful material? Combination of KTMP and $Mg(CH_2SiMe_3)_2$ produced the polymeric species $[KMg(TMP)(CH_2SiMe_3)_2]_\infty$, which when reacted with toluene, did not produce an inverse crown but in fact a toluene solvate, with the polymeric nature of the molecule maintained. This lack of metallation and preference for coordination instead, lead us to believe that this "alkyl-rich" magnesiate species may not be as basic as the previous "TMP-rich" species which acts as an aggressive Brønsted base. As a future avenue of study, we can draw a parallel between our own reagents and those utilised to great effect by Knochel *et al.*[113, 185] His most effective magnesiate reagents have fallen into two categories, either turbo-Grgnard $(RMgX.LiCl)$[186] or turbo-Hauser $(NR_2MgX.LiCl)$,[187] the former used primarily in lithium-halogen exchange reactions and the latter in deprotonative metallations. The comparison we can draw with our own work is most apparent when represent them in similar salt-like formula *i.e.,* $(TMPMgR.KTMP)$ and $(MgR_2.KTMP)$. Our former species here is "TMP rich" and readily carries out a number of metallations at room temperature which preliminary studies suggest the "alkyl-rich" $(MgR_2.KTMP)$ mixture cannot replicate. An interesting future study would be to investigate whether this mixture, with comparatively diminished deprotonative metallation capabilities could function as a strong agent of metal-halogen exchange.

It is clear from these studies into sodium and potassium magnesiates, that future studies could bring about a number of intriguing possibilities. Could these sodium magnesiates be used to dimetallate more electronically challenging arenes or heteroarenes in positions unachievable by any other method? And could the analogous potassium magnesiate species engender selective deprotonations of aromatic substrates, also unobtainable when utilising traditional organometallic reagents? Finally, could substrates of varying steric demand, when reacted in combination with these bis-amido magnesiate methodologies create new and exciting structural architectures, larger ring systems and shapes? This particular field is ripe for future studies, owing to the abundance of available avenues for exploration, as even a single variable change could bring about structural and reactivity changes which could only be imagined at. Finally, with such a paucity of bis-alkyl mono-amido sodium and potassium magnesiates, these

rare bimetallic combinates are thus far unstudies in terms of reactivity. Even if they exhibit diminished capacity for deprotonative metallation, could they be used in metal-halogen exchange, or any number of other demanding synthetic transformations? These questions can only be answered in time and with perserverance.

7. <u>General Experimental Techniques</u>

7. 1 Schlenk techniques

The majority of reagents employed throughout these projects were air-sensitive. Indeed, many compounds (such as *tert*-butyllithium) were pyrophoric, their reaction with moisture giving rise to flammable hydrocarbons:

$$^{t}\text{BuLi} \quad + \quad \text{H}_2\text{O} \quad \longrightarrow \quad ^{t}\text{BuH} \quad + \quad \text{LiOH}$$

Consequently, all reactions were carried out in a dry, inert atmosphere, utilising standard Schlenk techniques *i.e.*, the use of a Schlenk line, and Schlenk glassware (**Figures 7.1 and 7.2**). Among the most common types of glassware used were the Schlenk tube, the vessel in which all reactions were carried out, and the Schlenk filter stick, used in both isolating solid products for further use and in trapping and removal of unwanted solid impurities.

The Schlenk line itself is is made up of double manifold, containing two separate pathways: one pathway connected to a vacuum pump, and another connected a source of dry argon gas. Each Schlenk line also contains five connectors (**Figure 7.**1 shows only three), each of which can in turn be connected to the desired apparatus, most commonly a Schlenk tube. Each connector has a tap which can operate in two ways, either turned to vacuum or to a supply of argon gas. By connecting a Schlenk tube to the vacuum source, all air within can be evacuated, whereupon it can be re-filled with argon gas. Repeating this process three times (each separate evacuation for ten minutes) was practised each time prior to a reaction, ensuring that a dry, inert atmosphere was present in each instance. Whenever solvents or reagents were added to a Schlenk tube, it was done under a positive pressure of argon, preventing any air from entering the system.

At the end of each Schlenk line was a solvent trap, cooled by liquid nitrogen, condensing any volatile substances before they could reach the vacuum pump and cause potential damage. Incorporated within the Schlenk line was a pressure release bubbler, partially filled with silicon oil, to prevent a build up of pressure within the system. All

Schlenk glassware also contained ground-glass joints, each of which was greased before connecting, sealing the joints, and preventing their sticking together.
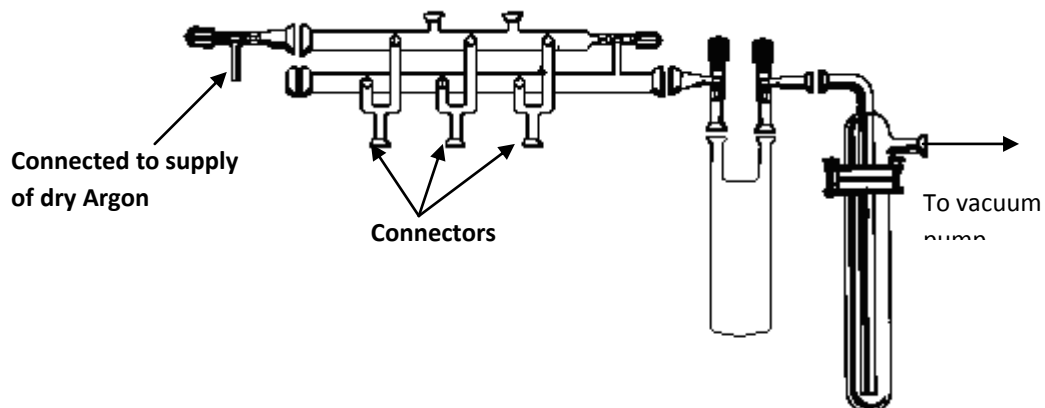
Fig. 7.1: Standard Schlenk line (three connectors shown).
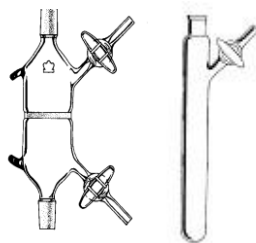
Fig. 7.2: Standard Schlenk filter stick (left) and Schlenk tube (right).

7.2 Glove box

Since all isolated solid materials had to be weighed out, both reactants and products, under inert atmosphere, and likewise NMR samples prepared, a glove box (or dry box) had to be used, providing a sealed, inert atmosphere to carry out this work in (**Figure 7.3**).
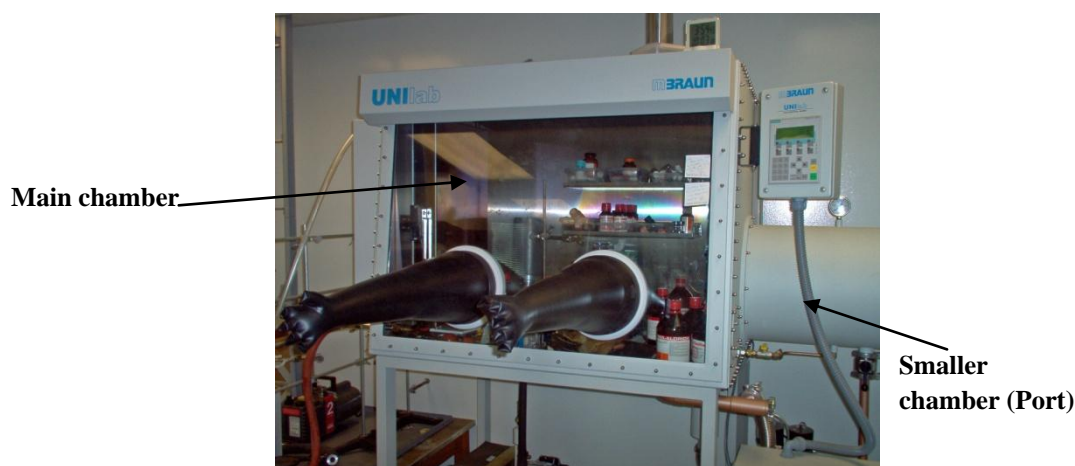
Fig. 7.3: Standard glove box.

Each glove box generally consists of two main chambers. The first contains both a large plastic window and two neoprene gloves, constituting the working area of the box. This chamber is filled with dry argon, allowing manipulation of chemicals to be carried out (e.g., weighing and isolating solids, NMR sample preparation). The second, smaller chamber on the right hand side (**Figure 7.3**) is referred to as the port, which has both an outer door and inner door, the latter connected to the main chamber. This port allows the transfer of both apparatus and chemicals to and from the glove box. Mirroring the evacuation/argon flushing process detailed previously, items are placed within the port, which is then placed under vacuum, ensuring removal of both air and moisture, followed by re-filling with argon gas. This process is repeated three times, at which point the inner port door can be opened, allowing the contents of the port to be transferred to the main chamber. Circulation takes place constantly within the glove box, the gas moving over a "scrubber", which removes any air and moisture which may be present.

7.3   Solvent Purification

Owing to the extreme sensitivity of most of our reactants towards air and moisture, all solvents used were dried and de-gassed prior to use. All standard solvents within this report were distilled over nitrogen, on the presence of sodium and benzophenone.[188] These substances act as self-indicators for ensuring the removal of oxygen and water from the solvent, with the reaction giving rise to the formation of a ketyl radical, which in turn produces an intense blue colour. Since this radical species is highly reactive in the presence of oxygen and/or water, if any is present, formation of yellow and

colourless products is the consequence. As such, this dramatic colour change presents a simple test for the presence of air or moisture. This dried solvent is collected in a small reservoir prior to use, and removed via a glass syringe and needle, also flushed three times with argon. When adding these solvents to a Schlenk tube, a positive pressure of argon is utilised, ensuring no air or moisture enters the system.

7.4   Hygroscopic liquid purification

Owing to the highly hygroscopic nature of many of the liquids used within these projects, particularly amines and alcohols, these had to be distilled before use in order to remove any traces of moisture which could be present and cause unwanted contamination. In order to achieve this, the desired liquid was placed into a round bottomed flask, and distilled in the presence of the necessary dessicant (most usually calcium hydride) for several hours under an atmosphere of nitrogen gas. After sufficient time had elapsed to ensure purification and elimination of advantageous moisture, the liquids were collected in a round bottom flask, charged with argon, and secured carefully with a Subaseal®, ready for later use.

7.5   Analytical Procedures

All ^{1}H NMR spectroscopic analysis were carried out on a Bruker DPX400 spectrometer, which operates at 400.13 MHz. The ^{13}C NMR spectra were carried out on the same instrument, operating at 100.62 MHz, and all were proton decoupled.

Abbreviations of NMR patterns are as follows: s (singlet), d (doublet), t (triplet), m (multiplet), and b (broad peak).

The X-ray crystallographic data were obtained on Bruker SMART and Nonius Kappa CCD diffractometers at 150K, with graphite monochromated Mo-Kα radiation (λ = 0.71073).

7.6   Standardisation of ^{n}BuLi and ^{n}Bu$_2$Mg

In order to ensure that the correct molarities of commercial organometallic solutions of ^{n}BuLi in hexane and ^{n}Bu$_2$Mg in heptane were employed in our reactions, standardisation of these had to be carried out on a regular basis. This process is vital owing to the highly reactive nature of these solutions, and thus their invariable decomposition due to unwanted O$_2$, and also more simply just to ensure correct concentrations due to unwanted solvent evaporation within the bottles.

Beginning first with ^{n}BuLi, salicylaldehyde phenylhydrazone (0.6 g) was dissolved in 10 ml THF, forming yellow solution. Titration with ^{n}BuLi gave eventual persistent red colouration, indicating the end of the reaction (**Scheme 7.1**).[189]
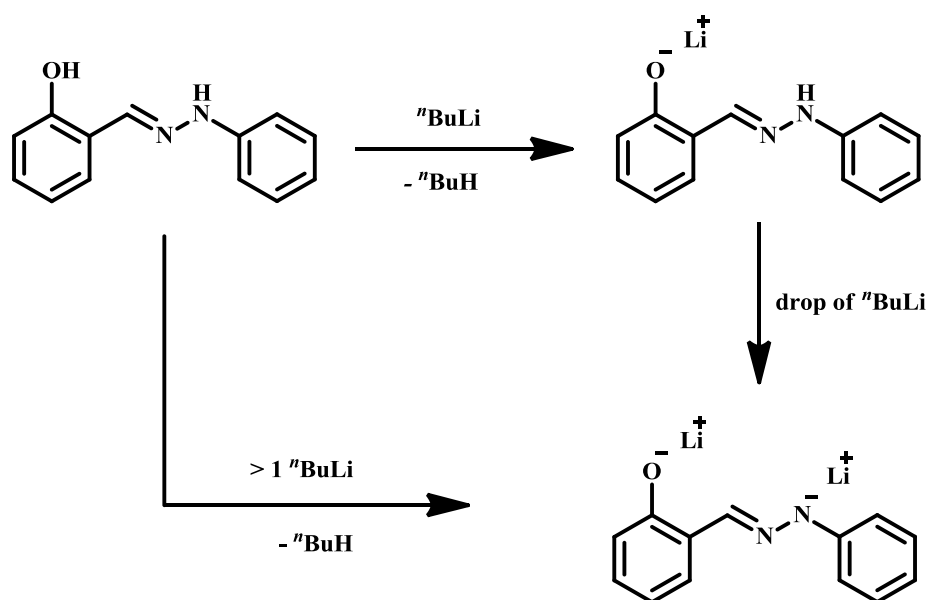
Scheme 7.1: Standardisation of ^{n}BuLi.

The molarity of the ^{n}BuLi solution can then by calculated by the following method:

X= Weight of salicaldehyde phenylhydrazone (g); Y= Volume of ^{n}BuLi required to reach reaction end (i.e. persistent red colour) (mL); Z= X/212.5 (molecular weight of salicaldehyde phenylhydrazone is 212.5 g)

Concentration of ^{n}BuLi solution = (Z/Y) x 1000

The method used for standardising ^{n}Bu$_2$Mg called for initial dilution of 2 ml organomagnesium solution in 10 ml THF. A small amount of 1, 10-phenanthroline was

then added, producing a red colour. Titration of this solution with *sec*-butanol in dry xylene gave rise to a colourless solution as indication of its end point.[190]

8 Experimental

8.1 Preparation of starting materials

8.1.1 Preparation of BuNa

3.84g of ^{t}BuONa (40 mmol) was placed in a Schlenk tube (complete with stirrer bar), within the argon atmosphere of a glove box. 60 ml of hexane was added to this, and the resulting mixture cooled to 0 ° C, and 25ml (40 mmol) n-BuLi (1.6M solution in hexane) added drop-wise for a period of approximately thirty minutes. This solution was left to stir overnight, and on the following day filtered and washed with hexane (~50 ml). The white solid collected was then dried under vacuum and placed in the glove-box for further use.

8.1.2 Preparation of ^{t}Bu$_2$Zn

ZnCl$_2$ (40 mmol, 40 ml in ether soln.) added to 30 ml of Et$_2$O within a Schlenk tube previously evacuated and flushed with argon. This was then cooled to 0°C in an ice bath, and 48 ml of ^{t}BuLi (40 mmol) added dropwise, forming a white precipitate. The Schlenk tube was then covered in a black plastic bag (owing to the light sensitive nature of the solution) and allowed to stir for approx. 2-3 hours. Subsequent filtration through Celite and glass wool gave a colourless solution, which was reduced in volume considerably. This was then transferred to a sublimer, also evacuated and flushed with argon. Under vacuum, the solvent was removed before the volatile ^{t}Bu$_2$Zn material, the latter being allowed to condense and solidify on the cold finger of the sublimer, cooled via an *iso*-propanol/liquid N$_2$ mixture to ~ -30°C. After approximately 1 hour had elapsed the coolant was removed and the sublimer transferred under vacuum to the glove box where the white crystalline ^{t}Bu$_2$Zn material was scraped from the cold finger into the Schlenk tube.

8.1.3 Preparation of K(CH$_2$SiMe$_3$)

2.75 g (25 mmol) of potassium *tert*-butoxide was placed in a Schlenk tube within the inert atmosphere of the glove box. Following removal from the glove box, 50 ml hexane was added to this, followed by 25 ml of (trimethylsilylmethyl)lithium (25 mmol). The resultant mixture was then allowed to stir overnight at room temperature. The solid product obtained was isolated via standard Schlenk filtration techniques and washed

with hexane. Finally, the product was dried *in vacuo* for upwards of an hour before being transferred to the glove box.

8.1.4   Preparation of $Mg(CH_2SiMe_3)_2$

A 500 mL round bottom flask (fitted with a condenser and addition funnel) was evacuated and thrice flushed with argon, followed by addition of magnesium turnings (4 g, 165 mmol) and dried diethylether (100 ml). A solution of $ClCH_2SiMe_3$ (136 mmol (19 m) in 50 ml Et_2O) was added slowly, dropwise via the addition funnel. After the mixture had been refluxed for 2 hours, dried dioxane (9 ml, 106 mmol) in 50 ml Et_2O was added via the same addition funnel. The resulting thick grey suspension was then allowed to stir at room temperature for three days. After this time, the suspension was filtered under gravity through Celite and glass wool, then washed with two portions of Et_2O (2 x 40 ml), producing a clear solution. The solvent was then removed *in vacuo*, yielding a pale yellow solid, which was then heated, washed with a further 2 ml Et_2O, then placed under vacuum to dryness again. The washed off-white solid was then purified by sublimation (170°C), resulting in a large amount of white crystalline powder, which was subsequently transferred under vacuum to the glove box.

Preparation of $[\{^nBuMg(\mu\text{-}TMP)_2\}]$

A Schlenk tube was charged with BuNa (30 mM, 2.4 g), and this suspended in 40 ml hexane. To this was added 30 mM TMP(H) (5.1 ml), and the suspension allowed to stir for 1 hour until pale yellow. At this point, ^nBuMgCl (15 ml, 2M soln. in Et_2O) was added, and the reaction mixture allowed to stir at room temperature overnight. The following day the mixture was filtered through Celite, removing the insoluble NaCl precipitate, and leaving the desired orange solution. This solution was then concentrated *in vacuo*, then placed in the freezer, operating at -28°C, overnight, whereon a large deposition of huge colourless block crystals were observed the following day.

8.2 Preparation of compounds

8.2.1   Preparation of [(TMEDA)$_2$.Li$_2$(C$_{14}$H$_9$O)$_2$] (2c)
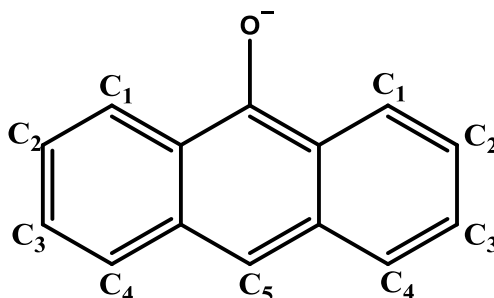
^{n}BuLi (1 mmol, 0.625 ml (1.6M Hex. Solution)) added to 10ml hexane, followed by TMEDA (1 mmol, 0.15 ml), forming pale yellow solution. Anthrone (C$_{14}$H$_{10}$O)(1 mmol, 0.194 g) added, turning solution bright yellow. This was then placed in the freezer at-27°C, yielding a small amount of crystals (0.13 g, 34%). ^{1}**H NMR** (400.13 MHz, 298K, C$_6$D$_6$):- δ 9.06 (2H, d, C$_1$), 8.06 (2H, d, C$_4$), 7.76 (1H, s, C$_5$), 7.47 (2H, t, C$_2$), 7.40 (2H, t, C$_3$), 1.72 (12H, s, TMEDA-CH$_3$), 1.37 (4H, s, TMEDA-CH$_2$). ^{13}**C NMR** (400.13 MHz, 298K, C$_6$D$_6$):- δ 128.9 (C$_4$), 125.8 (C$_1$), 125.6 (C$_2$), 120.1 (C$_3$), 108.3 (C$_5$), 59.8 (TMEDA-CH$_2$), 46.1 (TMEDA-CH$_3$).

8.2.2   Preparation of [(TMEDA)$_2$.Na$_2$(C$_{14}$H$_9$O)$_2$] (2b)

BuNa (1 mmol, 0.08 g) added to 10 ml hexane, and ^{t}Bu$_2$Zn (1 mmol, 0.18g)cannulated into this Schlenk tube followed by TMEDA (1 mmol, 0.15 ml), forming pale yellow solution. Anthrone (C$_{14}$H$_{10}$O)(1 mmol, 0.194g) added, turning solution bright green. This was then placed in the freezer at-27°C, yielding a small amount of crystals (0.210 g, 55%). ^{1}**H NMR** (400.13 MHz, 298K, C$_6$D$_6$):- δ 9.04 (2H, d, C$_1$), 8.05 (2H, d, C$_4$), 7.67 (1H, s, C$_5$), 7.47 (2H, t, C$_3$), 7.42 (2H, t, C$_2$), 1.43 (12H, s, TMEDA-CH$_3$), 1.29 (4H, s, TMEDA-CH$_2$). ^{13}**C NMR** (400.13 MHz, 298K, C$_6$D$_6$):- δ 129.0 (C$_4$), 125.6 (C$_3$), 124.6 (C$_1$), 120.0 (C$_2$), 106.3 (C$_5$), 56.5 (TMEDA-CH$_2$), 44.9 (TMEDA-CH$_3$).

8.2.3   Preparation of [(PMDETA)$_2$.K$_2$(C$_{14}$H$_9$O)$_2$] (2d)

K(CH$_2$SiMe$_3$) added to a Schlenk under argon (1 mmol, 0.12 g) and suspended in 10ml hexane. To this TMP(H) added (1 mmol, 0.17ml) and this left stirring for ~ 1 hour, forming KTMP. ^{t}Bu$_2$Zn (1 mmol, 0.18 g) added via cannula, followed by PMDETA (1 mmol, 0.21 ml), forming a yellow/brown solution. Addition of anthrone (1 mmol, 0.194 g) turned solution bright yellow. Solution filtered through Celite and glass wool to

remove impurities. Resultant filtrate placed in freezer at -27°C, resulting in formation of a crop of yellow crystals (0.21g, 51%). **^{1}H NMR** (400.13 MHz, 298K, C_6D_6):- δ 8.99 (2H, d, C_1), 8.03 (2H, d, C_4), 7.51 (1H, s, C_5), 7.51 (2H, t, C_2), 7.45 (2H, t, C_3), 2.31 (4H, t, CH_2-PMDETA), 2.23 (4H, t, CH_2-PMDETA), 2.05 (12H, s, CH_3-PMDETA(outer)), 1.99 (3H, s, CH_3-PMDETA(central)).**^{13}C NMR** (400.13 MHz, 298K, C_6D_6):- δ 128.5 (C_4), 125.7 (C_3), 125.4 (C_1), 118.8 (C_5), 103.3 (C_2), 58.0 (PMDETA Et_1), 56.7 (PMDETA Et_2), 45.8 (PMDETA Me (outer)), 42.7 (PMDETA Me (central)). **^{1}H NMR** (400.13 MHz, 298K, d^8-THF):- δ 8.66 (2H, d, C_1), 7.58 (2H, d, C_4), 7.13 (1H, s, C_3), 6.94 (2H, t, C_2), 6.91 (2H, t, C_5), 2.42 (4H, t, CH_2-PMDETA), 2.30 (4H, t, CH_2-PMDETA), 2.15 (12H, s, CH_3-PMDETA(outer)), 2.19 (3H, s, CH_3-PMDETA(central)).**^{13}C NMR** (400.13 MHz, 298K, d^8-THF):- δ 128.0 (C_4), 126.5 (C_1), 125.5 (C_3), 117.9 (C_2), 101.7 (C_5), 59.0 (PMDETA Et_1), 57.4 (PMDETA Et_2), 46.2 (PMDETA Me (outer)), 43.3 (PMDETA Me (central)).

8.2.4 Preparation of [(TMEDA)·Mg(^{n}Bu)($C_{14}H_9O$)] (2e)

^{n}Bu$_2$Mg (1 mmol, 1 ml (1M pentane solution)) added via syringe to a Schlenk under argon atmosphere, containing 10 ml dried hexane. TMEDA added to this (1 mmol, 0.15 ml), followed by anthrone (1 mmol, 0.194 g), turning solution bright yellow. This was transferred to the freezer at -27°C, depositing yellow crystals (0.18 g, 47%). **^{1}H NMR** (400.13 MHz, 298K, C_6D_6):- δ 8.79 (2H, d, C_1), 8.03 (2H, d, C_4), 7.80 (1H, s, C_5), 7.44 (2H, t, C_2), 7.42 (2H, t, C_3), 2.18 (2H, m, CH_2 nBu), 1.86 (2H, m, CH_2 nBu), 1.73 (12H, bs, TMEDA-CH_3), 1.51 (4H, bs, TMEDA-CH_2), 1.33 (3H, m, CH_3 nBu), 0.14 (2H, t, CH_2-Mg). **^{13}C NMR** (400.13 MHz, 298K, C_6D_6):- δ 128.9 (C_4), 125.4 (C_2), 124.9 (C_1), 120.9 (C_3), 110.1 (C_5), 55.9 (TMEDA-CH_2), 45.6 (TMEDA-CH_3), 33.5 (β-CH_2 nBu), 32.6 (γ-CH_2 nBu), 14.7 (CH_3 nBu), 7.1 (α-CH_2 nBu).

8.2.5 Preparation of [(TMEDA)·Zn(Et)($C_{14}H_9O$)] (2f)

Et$_2$Zn (1 mmol, 1 ml(1M solution)) added via syringe to a Schlenk tube containing 10ml hexane under inert atmosphere, followed by TMEDA (1 mmol, 0.15ml), resulting in a clear solution. Upon addition of anthrone (1 mmol, 0.194 g), solution turned bright yellow. This was then placed in the freezer at -27°C where crystals were formed (0.25 g, 61%). **^{1}H NMR** (400.13 MHz, 298K, C_6D_6):- δ 8.86 (2H, d, C_1), 8.01 (2H, d, C_4), 7.74 (1H, s, C_5), 7.42 (2H, t, C_2), 7.40 (2H, t, C_3), 1.78 (16H, bs, TMEDA), 1.65 (3H, t, Et-CH_3), 0.54 (2H, q, Et-CH_2). **^{13}C NMR** (400.13 MHz, 298K, C_6D_6):- δ 128.8 (C_4), 125.3

(C$_2$), 125.2 (C$_1$), 120.4 (C$_3$), 109.5 (C$_5$), 46.4 (TMEDA(r. t.)), 13.8 (Et-CH_3), -1.3 (Et-CH_2).

8.2.6 Preparation of [(TMEDA)·Na{μ-OC(Ph)(4-^{t}Bu-C$_6$H$_4$)}(μ-TMP)Zn(^{t}Bu)] (3b)

BuNa (1 mmol, 0.08 g) suspended in 10ml hexane, to which was added TMP(H) (1 mmol, 0.17 ml) via syringe. The resultant creamy white mixture was allowed to stir for 1 hour, after which time a solution of ^{t}Bu$_2$Zn in 10 ml hexane, previously prepared in a second Schlenk, was added via cannula to it. Subsequent addition of TMEDA (1 mmol, 0.15 ml) formed a clear, yellow solution. After being allowed to stir for some time, 1 molar equivalent of 9-Fluorenone (0.180 g) was added via solid addition tube, turning the solution a deep red almost. This solution when placed in the freezer at -27°C deposited a crop of yellow crystals (0.422 g, 66%).**^{1}H NMR** (400.13 MHz, 298K, C$_6$D$_6$):- δ 7.66 (1H, bd, C$_2$(Ph)), 7.51 (1H, bd, C$_5$(Ph)), 7.34 (1H, bt, C$_3$(Ph)), 7.21 (1H, bt, C$_4$(Ph)), 7.10 (1H, bs, H**a**), 6.50 (1H, bs, H**d**), 5.78 (1H, bs, H**b**), 3.10 (1H, bs, H**c**), 1.87 (12H, s, TMEDA-CH$_3$), 1.80 (4H, s, TMEDA-CH$_2$), 1.09 (9H, s, ^{t}Bu). **^{13}C NMR** (400.13 MHz, 298K, C$_6$D$_6$):- δ 127.0 (C$_3$(Ph)), 124.7 (C$_4$(Ph)), 122.3 (C**a**), 119.9 (C**b**), 118.8 (C$_2$(Ph)), 117.1 (C$_5$(Ph)), 116.7 (C**d**), 57.1 (TMEDA-CH$_2$), 47.3 (TMEDA-CH$_3$), 50.7 (C**c**), 27.1 (^{t}Bu).

8.2.7 Preparation of [(TMEDA)·Na{μ-OC(Ph)(4-^{t}Bu-C$_5$NH$_4$)}(μ-TMP)Zn(^{t}Bu)] (3c)
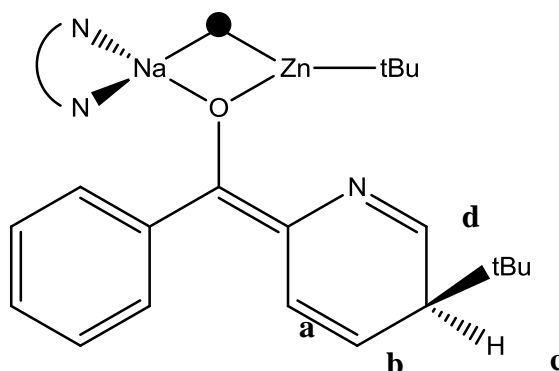
BuNa (1 mmol, 0.08 g) suspended in 10ml hexane, to which was added TMP(H) (1 mmol, 0.17 ml) via syringe. The resultant creamy white mixture was allowed to stir for 1 hour, after which time a solution of ^{t}Bu$_2$Zn in 10 ml hexane, previously prepared in a second Schlenk, was added via cannula to it. Subsequent addition of TMEDA (1 mmol, 0.15 ml) formed a clear, yellow solution. After being allowed to stir for some time, 1 molar equivalent of 2-Benzoylpyridine (0.183 g) was added via solid addition tube, turning the solution a deep red. After placing this solution in the freezer at -27°C, a small amount of yellow crystals were collected (0.359 g, 56%). **^{1}H NMR** (400.13 MHz, 298K, C$_6$D$_6$):- δ 7.69 (1H, bs, C$_2$(Ph)), 7.63 (1H, bs, C$_4$(Ph)), 7.39 (1H, bs, H**d**), 7.26 (1H, bs, C$_3$), 7.12 (2H, bs, C$_{1/5}$(Ph)), 6.64 (1H, bs, H**a**), 4.97 (1H, bs, H**b**), 2.87 (1H, bs, H**c**), 1.90 (16H, bs, TMEDA), 1.01(9H, s, ^{t}Bu). **^{13}C NMR** (400.13 MHz, 298K, C$_6$D$_6$):- δ 128.5 (2H, C$_2$/C$_4$), 149.9 (C$_6$), 126.9 (C$_3$), 126.7 (2H, C$_1$/C$_5$), 125.6 (C$_9$), 109.3(C$_8$), 49.5 (C$_7$), 33.3 [4H, TMP(H)(β-CH$_2$)], 31.1 [12H, TMP(H)(α-CH$_3$)], 1.01(9H,(^{t}Bu)).

8.2.8 Preparation of [(TMEDA)·Na{μ-OC(Ph)(4-^{t}Bu-C$_6$H$_4$)}(μ-HMDS)Zn(^{t}Bu)] (3d)

NaHMDS (1 mM, 0.183 g) was suspended in 10 ml heaxane, to which was added 1mM ^{t}Bu$_2$Zn (1mM in 5ml hexane), followed by TMEDA (1mM, 0.15ml), resulting in a colourless solution. After being allowed to stir for some time, 1 molar equivalent of 9-Fluorenone (0.180 g) was added via solid addition tube, turning the solution a deep red almost. This solution when placed in the freezer at -27°C deposited a crop of yellow crystals.

8.2.9   Preparation of [(TMEDA)·Na{μ-OC(Ph)(4-^{t}Bu-C$_5$NH$_4$)}(μ-HMDS)Zn(^{t}Bu)] (3e)

NaHMDS (1 mM, 0.183 g) was suspended in 10 ml heaxane, to which was added 1mM ^{t}Bu$_2$Zn (1mM in 5ml hexane), followed by TMEDA (1mM, 0.15ml), resulting in a colourless solution. After being allowed to stir for some time, 1 molar equivalent of 2-Benzoylpyridine (0.183 g) was added via solid addition tube, turning the solution a dark green. After placing this solution in the freezer at -27°C, a small amount of yellow crystals were collected.

8.2.10 Preparation of [(Na-9-Et-9H-Fluoren-9-olate)$_6$] (3f)

BuNa (1 mmol, 0.08 g) suspended in 10ml hexane, to which was added TMP(H) (1 mmol, 0.17 ml) via syringe. The resultant creamy white mixture was allowed to stir for 1 hour, after which time a solution of Et$_2$Zn (1M, 1ml in hexane) was added to it. Subsequent addition of TMEDA (1 mmol, 0.15 ml) formed a clear, yellow solution. After being allowed to stir for some time, 1 molar equivalent of 9-Fluorenone (0.180 g) was added via solid addition tube, turning the solution a deep blue. This solution when placed in the freezer at -27°C deposited a crop of yellow crystals (0.044 g, 17%). **^{1}H NMR** (400.13 MHz, 293 K, C$_6$D$_6$): 7.53 (*ortho* CH, bs, 2H), 7.14 (*meta* CH, bs, 4H), 6.91 (*para* CH, bs, 2H), 1.09 (CH_2CH$_3$, bq, 2H), 0.25 (CH_3CH$_2$, bt 3H) 2.42 (4H, t, CH$_2$-PMDETA), 2.30 (4H, t, CH$_2$-PMDETA), 2.15 (12H, s, CH$_3$-PMDETA(outer)), 2.19 (3H, s, CH$_3$-PMDETA(central)).**^{13}C NMR** (100.62 MHz, 293 K, C$_6$D$_6$): 140.0 (*C*-O), 128.8 (*meta* CH), 121.4 (*para* CH), 120.5 (*ortho* CH), 37.0 (CH_2), 9.3 (CH_3).

8.2.11 Preparation of [{(THF)$_6$Na}$^+${(THF)·Mg(o-carborane)$_3$}$^-$] (4b)

BuNa (1 mmol, 0.08 g) suspended in 10ml hexane, followed by addition of ^{n}Bu$_2$Mg (1 mmol, 1ml). Addition of TMP(H) (2 mmol, 0.34 ml) and TMEDA (1 mmol, 0.15 ml) formed straw coloured solution. Addition of o-carborane (3 mmol, 0.426 g) yielded a creamy white suspension. Solvent was then removed, and the mixture dissolved in 10ml THF, in addition to 3ml hexane, aiding recrystallization. This was then placed in the freezer at -27°C, where colourless crystals were deposited.

8.2.12 Preparation of [{(^{t}Bu)$_3$Zn$_3$(m-carborane)$_3$}$^{3-}${(THF)$_6$·Li}$_3^+$] (4c)

n-BuLi (1 mmol, 0.625ml (1.6M Hex. Solution)) added to 5ml hexane, followed by ^{t}Bu$_2$Zn (1 mmol in 5 ml hexane), added via a cannula. 2eq. TMP(H) (0.34 ml) added,

and the resulting mixture left to stir for a few minutes. Via a solid addition tube, meta-carborane was introduced (1 mmol, 0.142 g), turning the previously yellow solution into a creamy white suspension. All solvent was then removed, and the mixture dissolved in THF/hexane in the ratio 9ml : 1ml. After being placed in the freezer at -27°C, a crop of colourless crystals was isolated.

8.2.12 Preparation of [(TMEDA)·{Na(μ-TMP)Zn(^{t}Bu)}$_2$(μ-OCPhCH=CHPhCHPhCH=CPh-μ-O)] (4f)

BuNa (1 mmol, 0.08 g) suspended in 10ml hexane, to which was added TMP(H) (1 mmol, 0.17 ml) via syringe. The resultant creamy white mixture was allowed to stir for 1 hour, after which time a solution of ^{t}Bu$_2$Zn in 10 ml hexane, previously prepared in a second Schlenk, was added via cannula to it. Subsequent addition of TMEDA (1 mmol, 0.15 ml) formed a clear, yellow solution. After being allowed to stir for some time, chalcone was added (1 mmol, 0.21g), causing an immediate colour change to bright orange. The solution was reduced in volume *in vacuo* and placed in a freezer operating at -28°C, yielding a crop of yellow crystals (0.23 g, 38%). **^{1}H NMR** (400.13 MHz, d^8-THF, 300K): δ (ppm) = 7.74 (d, 4H, ortho), 7.33 (d, 4H, ortho), 7.13 (t, 8H, meta), 6.99 (m, 4H, para), 4.96 (d, 2H, allylic), 3.82 (d, 2H, benzylic), 2.30 (s, 8H, TMEDA CH$_2$), 2.15 (s, 24H, TMEDA CH$_3$), 1.63 (m, 4H, TMP-γ), 1.29 (t, 8H, TMP-β), 1.06 (s, 24H, TMP-CH$_3$), 0.94 (s, 18H, ^{t}Bu). **^{13}C NMR** (100.62 MHz, d^8-THF, 300K): δ (ppm) = 130.9 (CH, ortho), 127.7 (CH, meta), 126.1 (CH, ortho), 125.4 (CH, para), 91.4 (CH, allylic), 58.9 (CH$_2$, TMEDA), 53.9 (CH, benzylic), 46.2 (CH$_3$, TMEDA), 32.3 (CH$_3$, TMP), 30.6 (β-CH$_2$, TMP), 29.0 (CH$_3$, ^{t}Bu), 19.3 (γ-CH$_2$, TMP).

8.2.14 Preparation of [(TMEDA)·Na(μ-DTBN)$_2$Zn(^{t}Bu)] (4g)

BuNa (1 mmol, 0.08 g) suspended in 10ml hexane, to which was added TMP(H) (1 mmol, 0.17 ml) via syringe. The resultant creamy white mixture was allowed to stir for 1 hour, after which time a solution of ^{t}Bu$_2$Zn in 10 ml hexane, previously prepared in a second Schlenk, was added via cannula to it. Subsequent addition of TMEDA (1 mmol, 0.15 ml) formed a clear, yellow solution. After being allowed to stir for some time, 1 mmol DTBN was added, turning the solution slightly orange/red. This was then allowed to rest overnight at room temperature, yielding a crop of very large colourless block crystals (0.159 g, 29 %). **^{1}H NMR** (400.13 MHz, 293 K, d^8-THF): 2.30 (s, 4H,

TMEDA-CH_2), 2.15 (s, 12H, TMEDA-CH_3), 1.19 (s, 36H, ^{t}Bu-DTBN), 1.14 (s, 9H, ^{t}Bu).

8.2.15 Preparation of [(PMDETA)·K(μ-NPh$_2$)Mg(THF)(NPh)$_2$] (4h)

Benzylpotassium (0.26 g, 2 mmol) was suspended in 10 mL of dried hexane and place in an ultrasonic bath for 5 min. Di-n-butylmagnesium(2 mL of a 1 M solution in hexanes, 2 mmol) was added dropwise with constant stirring yielding an orange-red precipitate. Diphenylamine (1.01 mL, 6 mmol) was introduced followed by PMDETA (0.42 mL, 2 mmol) and THF (5 mL). Gentle heating of this mixture produced a yellow solution which on leaving at 5 °C for 24 h resulted in the precipitation of a crop of highly soluble, colourless cubic crystals (0.68 g, 42%). **^{1}H NMR** (400.13 MHz, 293 K, C$_6$D$_6$): 7.52 (*ortho*-H, 12H, d), 7.13 (*meta*-H, 12H, m), 6.60 (*para*-H, 6H, m), 3.22 (THF α-CH$_2$, 4H, br s), 1.77 (CH$_2$, 8H, s), 1.69 (CH$_3$, 12H, s), 1.55 (CH3, 3H, s), 0.91 (THF β-CH2, 4H, br s). **^{13}C NMR** (100.62 MHz, 293 K, C$_6$D$_6$): 157.3 (*ipso*-C), 129.5 (*meta*-C), 121.3 (*ortho*-C), 116.5 (*para*-C), 69.1 (THF α-CH2), 57.3 (NCH$_2$), 55.7 (NCH$_2$), 45.3 [N(CH$_3$)$_2$], 42.4 (NCH$_3$), 25.1 (THF β-CH$_2$).

8.2.16 Preparation of [(TMEDA)·Na(μ-Ph)(μ-TMP)Zn(Ph)] (4i)

BuNa (1 mmol, 0.08 g) suspended in 10ml hexane, to which was added TMP(H) (1 mmol, 0.17 ml) via syringe. The resultant creamy white mixture was allowed to stir for 1 hour, after which time Ph$_2$Zn (1 mmol, 0.219 g) was added via a solid addition tube, followed by 1 mmol TMEDA (0.15 ml), resulting in a colourless solution. This was placed in a freezer operating at -28°C overnight, depositing colourless needle crystals, suitable for X-ray analysis (0.13 g, 27%). **^{1}H NMR** (400.13 MHz, 293 K, C$_6$D$_6$): 8.04 (d, *ortho* CH, 4H), 7.36 (t, *meta* CH, 4H), 7.24 (t, *para* CH, 2H), 1.93 (m, TMP-γ CH_2, 2H), 1.50 (s, TMEDA-CH_3, 12H), 1.43 (s, TMEDA-CH_2, 4H), 1.36 (bs, TMP-CH_3 and TMP β-CH_2). **^{13}C NMR** (100.62 MHz, 293 K, C$_6$D$_6$): 139.5 (*ortho* CH), 127.5 (*meta* CH), 125.6 (*para* CH), 56.7 (TMEDA CH_2), 45.6 (TMEDA CH_3), 40.8 (TMP β-CH_2), 35.4 (TMP α-CH_3), 20.3 (TMP γ-CH_2).

8.2.17 Preparation of [NaMg(μ-HMDS)$_2$(^{n}Bu)]$_\infty$ (5a)

BuNa (2 mmol, 0.16 g) was added to a Schlenk tube under inert atmosphere, and suspended in 8 ml hexane, followed by 4 mmol HMDS(H) and allowed to stir for 1

hour. To this was added 2 ml (1M, in heptane) ^{n}Bu$_2$Mg, forming a slight white suspension after stirring. Gentle heating and subsequent cooling slowly overnight in a hot water dewar afforded a large amount of colourless crystalline material (0.732 g, 81%). ^{1}**H NMR** (400.13 MHz, 293 K, C$_6$D$_6$): ^{13}**C NMR** (100.62 MHz, 298K, C$_6$D$_6$): 2.05 (2H, m, n-Bu CH_2), 1.79 (2H, m, n-Bu CH_2), 1.26 (3H, t, n-Bu CH_3), 0.21 (36H, s, HMDS-CH_3), 0.08 (2H, t, M-CH_2). ^{13}**C NMR** (100.62 MHz, 298K, C$_6$D$_6$): 33.2 (CH_2-Bu), 32.2 (CH_2-Bu), 14.6 (CH_2-M), 12.1 (CH_3-Bu), 6.1 (HMDS-CH_3).

8.2.18 Preparation of [KMg(μ-HMDS)$_2$(^{n}Bu)]$_∞$ (5d)

KCH$_2$SiMe$_3$ (2 mmol, 0.24 g) was added to a Schlenk tube under inert atmosphere, and suspended in 8 ml hexane, followed by 4 mmol HMDS(H) and allowed to stir for 1 hour. To this was added 2 ml (1M, in heptane) ^{n}Bu$_2$Mg, forming a white suspension after stirring. 2 ml mesitylene was added to aid solubility. Cooling this colourless solution at -27°C overnight gave a crop of colourless crystals (0.317 g, 72%). ^{1}**H NMR** (400.13 MHz, 293 K, C$_6$D$_6$): 2.02 (2H, m, n-Bu CH_2), 1.76 (2H, m, n-Bu CH_2), 1.26 (3H, t, n-Bu CH_3), 0.48 (18H, s, HMDS-CH_3), 0.26 (18H, s, HMDS-CH_3), -0.35 (2H, t, M-CH_2). ^{13}**C NMR** (100.62 MHz, 298K, C$_6$D$_6$): 33.2 (CH_2-Bu), 33.0 (CH_2-Bu), 14.6 (CH_3-Bu), 14.2 (CH_2-M), 7.4 (HMDS-CH_3), 6.3 (HMDS-CH_3).

Preparation of [KMg(TMP)$_2$Bu]$_∞$ (5f)

A Schlenk tube was charged with 2 mM (0.24 g) KCH$_2$SiMe$_3$ in 8 ml cyclohexane , then reacted with 2 mM TMP(H) for 1 hour, forming a yellow suspension. In a second Schlenk tube, 2 ml ^{n}Bu$_2$Mg (1M solution in heptane) was reacted with 2 mM TMP(H) for 1 hour in 3 ml cyclohexane, forming a pale yellow solution. This BuMgTMP solution was cannulated into the newly formed KTMP, forming a yellow/orange solution. The cyclohexane was then replaced by deuterated cyclohexane and a quantity transferred via syringe to a Young's NMR tube. This was then left at 4°C, and after 2 days a small quantity of colourless needle crystals were deposited.

8.2.20 Preparation of [KMg(TMP)$_2$Bu]$_4$ (5g)

A first Schlenk tube was charged with 2 mmol (0.24g) KCH$_2$SiMe$_3$, and suspended in 8 ml methyl cyclohexane. This was then reacted with TMP(H) (2 mmol, 0.34 ml) for one hour, forming a yellow suspension. In a second Schlenk tube, ^{n}Bu$_2$Mg (2 mmol, 2 ml (1M soln. in heptane) was added to 2 ml methylcyclohexane and reacted with TMP(H)

(2 mmol, 0.34 ml) for one hour, forming BuMgTMP *in situ*. This BuMgTMP was then transferred via cannula to the Schlenk tube containing KTMP, forming a yellow/orange solution. After 2 days on the bench at room temperature, a crop of colourless crystals, suitable for X-ray, were deposited (0.401 g, 50%). **^{1}H NMR** (400.13 MHz, 293 K, C_6D_{12}): 1.80 (4H, m, TMP-γ CH_2), 1.35 (2H, m, *n*-Bu-CH_2), 1.27 (24H, s, TMP-CH$_3$), 1.26 (2H, M, *n*-Bu-CH$_2$), 1.19 (8H, t, TMP-β CH$_2$), 0.78 (3H, t, *n*-Bu CH_3), -0.84 (2H, t, M-CH_2). **^{13}C NMR** (100.62 MHz, 298K, C_6D_{12}): 42.3 (TMP-β), 36.3 (TMP-*CH$_3$*), 34.41 (*n*-Bu *C*H$_2$), 34.15 (*n*-Bu *C*H$_2$), 20.1 (TMP-γ), 18.8 (M-*C*H$_2$), 14.9 (*n*-Bu *C*H$_3$).

Preparation of [KMg(TMP)$_2$Bu]$_6$ (5h)

A first Schlenk tube was charged with 2 mmol (0.24g) KCH$_2$SiMe$_3$, and suspended in 8 ml methyl cyclohexane. This was then reacted with TMP(H) (2 mmol, 0.34 ml) for one hour, forming a yellow suspension. In a second Schlenk tube, ^{n}Bu$_2$Mg (2 mmol, 2ml (1M soln. in heptane) was added to 2 ml methylcyclohexane and reacted with TMP(H) (2 mmol, 0.34 ml) for one hour, forming BuMgTMP *in situ*. This BuMgTMP was then transferred via cannula to the Schlenk tube containing KTMP, forming a yellow/orange solution. This solution was then concentrated (*in vacuo*) to a volume of ~ 1ml, and then transferred via syringe to an NMR tube. After 2 days at 3°C, an amount of colourless crystalline material was deposited within the tube. **^{1}H NMR** (400.13 MHz, 293 K, C_6D_{12}): 1.80 (4H, m, TMP-γ CH_2), 1.35 (2H, m, *n*-Bu-CH_2), 1.27 (24H, s, TMP-CH$_3$), 1.26 (2H, M, *n*-Bu-CH$_2$), 1.19 (8H, t, TMP-β CH$_2$), 0.78 (3H, t, *n*-Bu CH_3), -0.84 (2H, t, M-CH_2). **^{13}C NMR** (100.62 MHz, 298K, C_6D_{12}): 42.3 (TMP-β), 36.3 (TMP-*CH$_3$*), 34.41 (*n*-Bu *C*H$_2$), 34.15 (*n*-Bu *C*H$_2$), 20.1 (TMP-γ), 18.8 (M-*C*H$_2$), 14.9 (*n*-Bu *C*H$_3$).

8.2.22 Preparation of [{Fe-(C$_5$H$_4$)}$_2${K$_2$Mg$_3$(TMP)$_2$(THF)$_2$(Toluene)$_2$}] (5i)

A Schlenk tube was charged with 2 mmol (0.24 g) KCH$_2$SiMe$_3$, and to this added 4 mmol TMP(H) (0.68 ml) in 10 ml methylcyclohexane, which was then allowed to stir for 1 hour. After this time, 2 mmol ^{n}Bu$_2$Mg (1M, in heptane) was added, forming a yellow/orange solution. 2 mmol of ferrocene were then added (0.372 g), and upon heating for 10 minutes gave a deep red suspension. 5ml toluene were added in an attempt to aid solubility, followed by 1ml THF, which gave almost immediately a clear, deep red solution. The solution was concentrated *in vacuo*, then placed in the fridge at 5°C. After two weeks, a small amount of crystalline material, suitable for X-ray analysis, was observed (0.069 g, 15 %). **^{1}H NMR** (400.13 MHz, 293 K, d^8-THF): 7.0-7.2 (10H, *o*, *m*, *p* toluene C$H's$), 4.32 (12H, s, Ferrocene$_1$ C$H's$), 4.12 (12H, s,

Ferrocene$_2$ CH's), 3.62 (8H, t, THF α-CH_2's), 1.78 (8H, m, THF β-CH_2's), 1.40 (4H, m, TMP γ-H's), 0.77 (8H, t, TMP β-H's), 0.60 (24H, s, TMP CH_3). ^{13}C NMR (100.62 MHz, 298K, d^8-THF): 125-131 (o, m, p toluene C's), 80.2 (Ferrocene$_1$-C's), 77.0 (THF α-C's), 71.8 (Ferrocene$_2$, -C's), 52.0 (THF β-C's), 43.6 (TMP-β), 35.3 (TMP-CH$_3$), 20.5 (TMP-γ).

8.2.23 Preparation of [KMg(TMP)$_2$(C$_{10}$H$_7$)]$_6$ (5j)
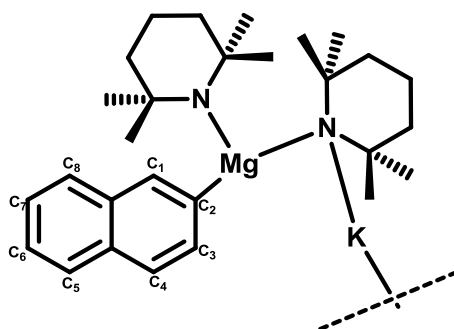
A first Schlenk tube was charged with 2 mmol (0.24g) KCH$_2$SiMe$_3$, and suspended in 8 ml methyl cyclohexane. This was then reacted with TMP(H) (2 mmol, 0.34 ml) for one hour, forming a yellow suspension. In a second Schlenk tube, ^{n}Bu$_2$Mg (2 mmol, 2 ml (1M soln. in heptane) was added to 2 ml methylcyclohexane and reacted with TMP(H) (2 mmol, 0.34 ml) for one hour, forming BuMgTMP *in situ*. This BuMgTMP was then transferred via cannula to the Schlenk tube containing KTMP, forming a yellow/orange solution. Napthalene was added (2 mmol, 0.256 g), and this mixture then allowed to reflux for 1 hour, having formed a yellow precipitate. Most of the solvent was removed *in vacuo*, and replaced with 10 ml toluene. After vigorous heating, an orange solution was achieved, and this immediately placed in a dewar of hot water overnight. The following day, an amount of crystals, suitable for X-ray, were deposited (0.414 g, 41 %). ^{1}H NMR (400.13 MHz, 293 K, d^8-THF): 8.37 (1H, s, C$_1$-H), 8.20 (1H, d, C$_3$-H), 7.57 (1H, d, C$_5$-H), 7.49 (1H, d, C$_8$-H), 7.31 (1H, d, C$_4$-H), 7.09 (1H, t, C$_6$-H), 7.01 (1H, t, C$_7$-H), 1.71 (4H, m, TMP γ-H's), 1.29 (8H, m, TMP β-H's), 1.26 (24H, s, TMP CH_3). ^{13}C NMR (100.62 MHz, 298K, d^8-THF): 142.1 (C3), 140.6 (C1), 128.0 (C5), 127.8 (C8), 122.8 (C6), 121.9 (C7, C4), 42.5 (TMP-β), 36.2 (TMP-CH$_3$), 21.7 (TMP-γ).

8.2.24 Preparation of [KMg(TMP)(CH$_2$SiMe$_3$)$_2$]$_∞$ (5k)

A Schlenk tube was charged with 2 mmol (0.24 g) KCH$_2$SiMe$_3$, and to this added 2 mmol TMP(H) (0.34 ml) in 10 ml methylcyclohexane, which was then allowed to stir for 1 hour. After this time, 2 mmol Mg(CH$_2$SiMe$_3$)$_2$ was added, forming after 5 minutes

a yellow/orange solution, which if allowed to stir a while longer became a suspension. Heating of this suspension reformed the solution, which was then allowed to rest overnight in a hot water dewar, giving an amount of crystalline material (0.468 g, 62%). **^{1}H NMR** (400.13 MHz, 293 K, C_6D_{12}): 1.71 (m, 2H, TMP γ-*H's*), 1.28 (m, 4H, TMP β-*H's*), 1.14 (s, 12H, TMP C*H$_3$*), 0.00 (s, 18H, Si*Me$_3$*), -1.77 (s, 4H, M-C*H$_2$*). **^{13}C NMR** (100.62 MHz, 298K, C_6D_{12}): 41.7 (TMP-β), 35.7 (TMP-CH$_3$), 20.4 (TMP-γ), 4.94 (SiMe$_3$), 0.76 (M-*C*H$_2$). **^{1}H NMR** (400.13 MHz, 293 K, C_6D_6): 1.78 (m, 2H, TMP γ-*H's*), 1.40 (m, 4H, TMP β-*H's*), 0.99 (s, 12H, TMP C*H$_3$*), 0.38 (s, 18H, Si*Me$_3$*), -1.44 (s, 4H, M-C*H$_2$*). **^{13}C NMR** (100.62 MHz, 298K, C_6D_6): 40.6 (TMP-β), 35.00 (TMP-CH$_3$), 20.22 (TMP-γ), 5.07 (SiMe$_3$), -1.01 (M-*C*H$_2$).

8.2.25 Preparation of [KMg(TMP)(CH$_2$SiMe$_3$)$_2$·(Toluene)]$_∞$ (5l)

A Schlenk tube was charged with 2 mmol (0.24 g) KCH$_2$SiMe$_3$, and to this added 2 mmol TMP(H) (0.34 ml) in 10 ml methylcyclohexane, which was then allowed to stir for 1 hour. After this time, 2 mmol Mg(CH$_2$SiMe$_3$)$_2$ was added, forming after 5 minutes a yellow/orange solution, which if allowed to stir a while longer became a suspension. 5ml toluene added, turning the mixture again into a solution. This was then allowed to rest overnight on the bench, depositing a crop of large block crystals (0.151 g, 16 %).

8.2.26 Preparation of 3-(*tert*-butyl)-9*H*-fluoren-9-one

Repeat preparation of **3b** until after addition of fluorenone. Deisonised water was then added, followed by extraction using Et$_2$O. The crude product was then dried with MgSO$_4$ and filtered to remove solid impurities, before being dried *in vacuo*. Separation by silica gel column chromatography afforded the desired product as a yellow oil (59% isolated product, 0.139 g). The eluent used in the chromatography was 100 % hexane. Note, if SOCl$_2$ was used to first oxidise the *in situ* mixture before aqueous workup, this yield could be increased to 71% isolated yield (0.167 g). **^{1}H NMR** (400.13 MHz, 293 K, CDCl$_3$): 7.64 (d, 1H, C$_8$-H), 7.59 (d, 1H, C$_1$-H), 7.55 (s, 1H, C$_4$-H), 7.54 (d, 1H, C$_5$-H), 7.47 (t, 1H, C$_7$-H), (d, 1H, C$_2$-H), (t, 1H, C$_6$-H), 1.38 (s, 9H, *^{t}*Bu).

8.2.27 Preparation of 9-(*tert*-butyl)-9*H*-fluoren-9-ol

Repeat preparation of **3b** until after addition of fluorenone. Deisonised water was then added, followed by extraction using Et$_2$O. The crude product was then dried with MgSO$_4$ and filtered to remove solid impurities, before being dried *in vacuo*. Separation by silica gel column chromatography afforded the desired product as a colourless solid (17% isolated product, 0.041 g). The eluent used in the chromatography was 100 % hexane. Note, if SOCl$_2$ was used to first oxidise the *in situ* mixture before aqueous workup, this yield was decreased. **^{1}H NMR** (400.13 MHz, 293 K, CDCl$_3$): 7.60 (d, 2H, C$_{1/8}$-H's), 7.58 (d, 2H, C$_{4/5}$-H's), 7.34 (t, 2H, C$_{2/7}$-H's), 7.23 (t, 2H, C$_{3/6}$-H's), 1.98 (bs, 1H, O*H*), 1.02 (s, 9H, ^{t}Bu).

8.2.28 Preparation of (5-(*tert*-butyl)pyridine-2-yl)(phenyl)methanone

Repeat preparation of **3d** until after addition of 2-benzoylpyridine. Deisonised water was then added, followed by extraction using Et$_2$O. The crude product was then dried with MgSO$_4$ and filtered to remove solid impurities, before being dried *in vacuo*. Separation by silica gel column chromatography afforded the desired product as a yellow/orange oil (37% isolated product, 0.088 g). The eluent used in the chromatography was 100 % hexane. Note, if SOCl$_2$ was used to first oxidise the *in situ* mixture before aqueous workup, this yield could be increased to 69% isolated yield (0.165 g). **^{1}H NMR** (400.13 MHz, 293 K, CDCl$_3$): 8.81 (s, 1H, C$_6$-H), 8.12 (d, 2H, C$_{8/12}$-H), 8.03 (d, 1H, C$_2$-H), 7.90 (d, 1H, C$_3$-H), 7.62 (t, 1H, C$_{10}$-H), 7.51 (t, 2H, C$_{9/11}$-H), 1.43 (s, 9H, ^{t}Bu). **^{13}C NMR** (100.62 MHz, 298K, CDCl$_3$): 193.3 (C=O), 133.3 (C$_3$), 132.2 (C$_{10}$), 130.5 (C$_{8/12}$), 127.5 (C$_{9/11}$), 123.7 (C$_2$), 30.4 (^{t}Bu).

8.2.29 Preparation of 2, 2-dimethyl-1-phenyl-1-(pyridine-2-yl)propan-1-ol

Repeat preparation of **3d** until after addition of 2-benzoylpyridine. Deisonised water was then added, followed by extraction using Et$_2$O. The crude product was then dried with MgSO$_4$ and filtered to remove solid impurities, before being dried *in vacuo*. Separation by silica gel column chromatography afforded the desired product as a colourless solid (48% isolated product, 0.116 g). The eluent used in the chromatography was 100 % hexane. Note, if SOCl$_2$ was used to first oxidise the *in situ* mixture before aqueous workup, this yield was decreased to 18% isolated yield (0.043 g). **^{1}H NMR**

(400.13 MHz, 293 K, CDCl$_3$): 8.52 (d, 1H, C$_6$-H), 7.81 (d, 1H, C$_3$-H), 7.76 (d, 2H, C$_{8/12}$-H), 7.70 (t, 1H, C$_{10}$-H), 7.29 (t, 2H, C$_{9/11}$-H), 7.21 (t, 1H, C$_5$-H), 7.20 (t, 1H, C$_4$-H), 6.42 (bs, 1H, OH), 1.11 (s, 9H, ^{t}Bu). **^{13}C NMR** (100.62 MHz, 298K, CDCl$_3$): 161.9 (C-O), 146.2 (C$_6$), 135.5 (C$_{10}$), 127.7 (C$_{8/12}$), 126.7 (C$_{9/11}$), 126.0 (C$_4$), 122.3 (C$_3$), 121.5 (C$_5$), 26.4 (^{t}Bu).

8.2.30 Preparation of 2-iodonaphthalene

Product **5j** was isolated as powder in methyl-cyclohexane (2 mmol, 1.034 g). We placed 2 mmol of our unrefined inverse-crown powder in a Schlenk tube, suspending this mixture in 10 ml methyl cyclohexane. In a second Schlenk tube, we dissolved 20 mmol I$_2$ in 10 ml THF solution. Both samples were then cooled to -80°C and stirred for 15 minutes, at which time the cold suspension was taken up in a syringe and added dropwise to a stirring iodine solution. After I$_2$ addition, the reactions were allowed to stir at -80°C for three hours, followed by stirring at room temperature for five hours more. After this time Na$_2$S$_2$O$_3$ was added, followed by de-ionised water, whereon this crude mixture was extracted by Et$_2$O, dried by MgSO$_4$ and dried *in vacuo*, producing a red/brown solid (0.206g, 81% crude). **^{1}H NMR** (400.13 MHz, 293 K, CDCl$_3$): 8.26 (s, 1H, C$_1$-H), 7.81 (1H, d, C$_6$-H), 7.74 (1H, d, C$_9$-H), 7.73 (1H, d, C$_3$-H), 7.59 (1H, d, C$_4$-H), 7.51 (1H, d, C$_7$), 7.49 (1H, d, C$_8$).

Crystal Data For [(TMEDA)$_2$·Li$_2$(C$_{14}$H$_9$O)$_2$] (2c)

Empirical formula	C49 H58 Li2 N4 O2
Formula weight	748.87
Temperature	123(2) K
Wavelength	0.71073 Å
Crystal system	Triclinic
Space group	P-1
Unit cell dimensions	a = 12.2149(10) Å α= 66.429(8)°.
	b = 12.9366(12) Å β= 81.568(7)°.
	c = 15.0500(12) Å γ = 75.877(8)°.
Volume	2110.7(3) Å^3
Z	2
Density (calculated)	1.178 Mg/m^3
Absorption coefficient	0.071 mm^{-1}
F(000)	804
Crystal size	0.5 x 0.4 x 0.3 mm^3
Theta range for data collection	2.79 to 27.00°.
Index ranges	-15<=h<=15, -16<=k<=16, -19<=l<=19
Reflections collected	25300
Independent reflections	9215 [R(int) = 0.0336]
Completeness to theta = 27.00°	99.9 %
Absorption correction	Semi-empirical from equivalents
Max. and min. transmission	1.00000 and 0.77705
Refinement method	Full-matrix least-squares on F^2
Data / restraints / parameters	9215 / 32 / 464
Goodness-of-fit on F^2	1.275
Final R indices [I>2sigma(I)]	R1 = 0.1097, wR2 = 0.3289
R indices (all data)	R1 = 0.1531, wR2 = 0.3599
Largest diff. peak and hole	0.639 and -0.825 e.Å^{-3}

Crystal Data For [(TMEDA)$_2$.Na$_2$(C$_{14}$H$_9$O)$_2$] (2b)

Chemical formula (total)	C$_{47}$H$_{58}$N$_4$Na$_2$O$_2$
Formula weight	756.95
Temperature	150(2) K
Radiation, wavelength	MoKα, 0.71073 Å
Crystal system, space group	monoclinic, P2$_1$/c
Unit cell parameters	a = 13.873(5) Å α = 90°
	b = 17.818(10) Å β = 104.96(2)°
	c = 18.828(6) Å γ = 90°
Cell volume	4496(3) Å^3
Z	4
Calculated density	1.118 g/cm^3
Absorption coefficient μ	0.085 mm^{-1}
F(000)	1624
Crystal colour and size	colourless, 0.39 × 0.28 × 0.10 mm^3
Reflections for cell refinement	8552 (θ range 4.0 to 27.5°)
Data collection method	Nonius KappaCCD diffractometer
	φ and ω scans
θ range for data collection	5.1 to 25.0°
Index ranges	h −16 to 16, k −21 to 21, l −22 to 22
Completeness to θ = 25.0°	98.3 %
Reflections collected	37051
Independent reflections	7791 (R$_{int}$ = 0.0647)
Reflections with F^2>2σ	3895
Absorption correction	semi-empirical from equivalents
Min. and max. transmission	0.9677 and 0.9916
Structure solution	direct methods
Refinement method	Full-matrix least-squares on F^2
Weighting parameters a, b	0.0421, 5.3919
Data / restraints / parameters	7791 / 1358 / 646
Final R indices [F^2>2σ]	R1 = 0.0755, wR2 = 0.1405
R indices (all data)	R1 = 0.1695, wR2 = 0.1843
Goodness-of-fit on F^2	1.051
Largest and mean shift/su	0.000 and 0.000
Largest diff. peak and hole	0.59 and −0.26 e Å^{-3}

Crystal Data For [(PMDETA)$_2$K$_2$(C$_{14}$H$_9$O)$_2$] (2d)

Empirical formula	C46 H64 K2 N6 O2
Formula weight	811.23
Temperature	123(2) K
Wavelength	0.71073 Å
Crystal system	Monoclinic
Space group	P21/c
Unit cell dimensions	a = 10.4500(3) Å α= 90°.
	b = 17.6550(4) Å β= 111.112(3)°.
	c = 13.5543(4) Å γ= 90°.
Volume	2332.84(11) Å^3
Z	2
Density (calculated)	1.155 Mg/m^3
Absorption coefficient	0.244 mm^{-1}
F(000)	872
Crystal size	0.25 x 0.20 x 0.18 mm^3
Theta range for data collection	2.81 to 28.50°.
Index ranges	-12<=h<=14, -23<=k<=21, -18<=l<=17
Reflections collected	14911
Independent reflections	5899 [R(int) = 0.0274]
Completeness to theta = 28.00°	99.9 %
Absorption correction	Semi-empirical from equivalents
Max. and min. transmission	1.00000 and 0.98061
Refinement method	Full-matrix least-squares on F^2
Data / restraints / parameters	5899 / 14 / 277
Goodness-of-fit on F^2	0.964
Final R indices [I>2sigma(I)]	R1 = 0.0439, wR2 = 0.1057
R indices (all data)	R1 = 0.0718, wR2 = 0.1120
Largest diff. peak and hole	0.399 and -0.231 e.Å^{-3}

Crystal Data For [(TMEDA)(^{n}Bu)Mg(C$_{14}$H$_{9}$O)] (2e)

Empirical formula	C24 H34 Mg N2 O
Formula weight	390.84
Temperature	123(2) K
Wavelength	1.54180 Å
Crystal system	Monoclinic
Space group	P2(1)/c
Unit cell dimensions	a = 14.6935(8) Å $\quad$ α= 90°.
	b = 12.3086(6) Å $\quad$ β= 100.338(4)°.
	c = 12.5596(5) Å $\quad$ γ = 90°.
Volume	2234.61(19) Å^3
Z	4
Density (calculated)	1.162 Mg/m^3
Absorption coefficient	0.795 mm^{-1}
F(000)	848
Crystal size	0.5 x 0.4 x 0.03 mm^3
Theta range for data collection	4.72 to 45.04°.
Index ranges	-11<=h<=13, -11<=k<=6, -11<=l<=7
Reflections collected	3571
Independent reflections	1791 [R(int) = 0.0356]
Completeness to theta = 45.04°	98.4 %
Absorption correction	Semi-empirical from equivalents
Max. and min. transmission	1.00000 and 0.81096
Refinement method	Full-matrix least-squares on F^2
Data / restraints / parameters	1791 / 0 / 258
Goodness-of-fit on F^2	1.109
Final R indices [I>2sigma(I)]	R1 = 0.0648, wR2 = 0.1823
R indices (all data)	R1 = 0.0733, wR2 = 0.1878
Largest diff. peak and hole	0.371 and -0.226 e.Å^{-3}

Crystal Data For [(TMEDA)·(Et)Zn(C$_{14}$H$_9$O)] (2f)

Empirical formula	C22 H30 N2 O Zn
Formula weight	403.85
Temperature	123(2) K
Wavelength	0.71073 Å
Crystal system	Monoclinic
Space group	P2(1)/c
Unit cell dimensions	a = 12.2484(9) Å α= 90°.
	b = 13.6732(7) Å β= 108.087(8)°.
	c = 12.7425(9) Å γ= 90°.
Volume	2028.6(2) Å^3
Z	4
Density (calculated)	1.322 Mg/m^3
Absorption coefficient	1.223 mm^{-1}
F(000)	856
Crystal size	0.5 x 0.1 x 0.1 mm^3
Theta range for data collection	2.98 to 28.99°.
Index ranges	-16<=h<=16, -18<=k<=18, -17<=l<=17
Reflections collected	21632
Independent reflections	5387 [R(int) = 0.0426]
Completeness to theta = 28.99°	99.7 %
Absorption correction	Semi-empirical from equivalents
Max. and min. transmission	1.00000 and 0.81696
Refinement method	Full-matrix least-squares on F^2
Data / restraints / parameters	5387 / 0 / 248
Goodness-of-fit on F^2	0.908
Final R indices [I>2sigma(I)]	R1 = 0.0296, wR2 = 0.0628
R indices (all data)	R1 = 0.0519, wR2 = 0.0657
Largest diff. peak and hole	0.390 and -0.351 e.Å^{-3}

Crystal Data For [TMEDA.Na{μ-OC(Ph)(4-^{t}Bu-C$_6$H$_4$)}(μ-TMP)Zn(^{t}Bu)]] (3b)

Empirical formula	C36 H60 N3 Na O Zn
Formula weight	639.23
Temperature	123(2) K
Wavelength	0.71073 Å
Crystal system	Monoclinic
Space group	P2(1)/c
Unit cell dimensions	a = 10.2426(6) Å α= 90°.
	b = 19.6573(15) Å β= 94.903(6)°.
	c = 36.846(3) Å γ= 90°.
Volume	7391.5(9) Å^3
Z	8
Density (calculated)	1.149 Mg/m^3
Absorption coefficient	0.706 mm^{-1}
F(000)	2768
Crystal size	0.3 x 0.1 x 0.1 mm^3
Theta range for data collection	3.14 to 26.00°.
Index ranges	-11<=h<=12, -24<=k<=24, -45<=l<=45
Reflections collected	49503
Independent reflections	14502 [R(int) = 0.0842]
Completeness to theta = 26.00°	99.8 %
Absorption correction	Semi-empirical from equivalents
Max. and min. transmission	1.00000 and 0.50172
Refinement method	Full-matrix least-squares on F^2
Data / restraints / parameters	14502 / 22 / 780
Goodness-of-fit on F^2	0.765
Final R indices [I>2sigma(I)]	R1 = 0.0494, wR2 = 0.0820
R indices (all data)	R1 = 0.1368, wR2 = 0.0930
Largest diff. peak and hole	0.506 and -0.615 e.Å^{-3}

Crystal Data For [TMEDA.Na{μ-OC(Ph)(4-^{t}Bu-C$_5$NH$_4$)}(μ-TMP)Zn(^{t}Bu)] (3c)

Empirical formula	C35 H61 N4 Na O Zn
Formula weight	642.24
Temperature	123(2) K
Wavelength	0.71073 Å
Crystal system	Monoclinic
Space group	P2(1)/n
Unit cell dimensions	a = 12.4016(4) Å $\quad$ α= 90°.
	b = 17.0724(5) Å $\quad$ β= 92.959(3)°.
	c = 17.6812(5) Å $\quad$ γ = 90°.
Volume	3738.56(19) Å^3
Z	4
Density (calculated)	1.141 Mg/m^3
Absorption coefficient	0.698 mm^{-1}
F(000)	1392
Crystal size	0.2 x 0.2 x 0.1 mm^3
Theta range for data collection	2.65 to 27.00°.
Index ranges	-15<=h<=15, -21<=k<=15, -22<=l<=22
Reflections collected	22100
Independent reflections	8152 [R(int) = 0.0338]
Completeness to theta = 27.00°	99.9 %
Absorption correction	Semi-empirical from equivalents
Max. and min. transmission	1.00000 and 0.95703
Refinement method	Full-matrix least-squares on F^2
Data / restraints / parameters	8152 / 14 / 395
Goodness-of-fit on F^2	0.896
Final R indices [I>2sigma(I)]	R1 = 0.0348, wR2 = 0.0683
R indices (all data)	R1 = 0.0607, wR2 = 0.0718
Largest diff. peak and hole	0.361 and -0.284 e.Å^{-3}

Crystal Data For [TMEDA.Na{μ-OC(Ph)(4-^{t}Bu-C$_5$NH$_4$)}(μ-HMDS)Zn(^{t}Bu)] 1, 2 and 1, 6 adducts (3e)

Empirical formula	C33.50 H64.50 N4 Na O Si2 Zn
Formula weight	683.93
Temperature	123(2) K
Wavelength	0.71073 Å
Crystal system	Monoclinic
Space group	P2(1)/n
Unit cell dimensions	a = 22.9311(9) Å α= 90°.
	b = 11.3886(5) Å β= 98.568(4)°.
	c = 30.8966(13) Å γ = 90°.
Volume	7978.7(6) Å^3
Z	8
Density (calculated)	1.139 Mg/m^3
Absorption coefficient	0.715 mm^{-1}
F(000)	2964
Crystal size	0.2 x 0.2 x 0.2 mm^3
Theta range for data collection	2.68 to 27.00°.
Index ranges	-29<=h<=29, -13<=k<=14, -39<=l<=38
Reflections collected	49191
Independent reflections	17410 [R(int) = 0.0631]
Completeness to theta = 27.00°	99.9 %
Absorption correction	Semi-empirical from equivalents
Max. and min. transmission	1.00000 and 0.98972
Refinement method	Full-matrix least-squares on F^2
Data / restraints / parameters	17410 / 0 / 799
Goodness-of-fit on F^2	0.852
Final R indices [I>2sigma(I)]	R1 = 0.0432, wR2 = 0.0713
R indices (all data)	R1 = 0.0938, wR2 = 0.0782
Largest diff. peak and hole	0.601 and -0.429 e.Å^{-3}

Crystal Data for [(Na-9-Et-9*H*-Fluoren-9-olate)$_6$] (3f)

Empirical formula	C104 H94 Na6 O6
Formula weight	1577.73
Temperature	123(2) K
Wavelength	0.71073 Å
Crystal system	Triclinic
Space group	P-1
Unit cell dimensions	a = 11.9267(5) Å $\quad$ α= 62.180(5)°.
	b = 14.1821(7) Å $\quad$ β= 85.983(4)°.
	c = 14.6604(7) Å $\quad$ γ = 79.242(4)°.
Volume	2154.17(20) Å^3
Z	1
Density (calculated)	1.216 Mg/m^3
Absorption coefficient	0.100 mm^{-1}
F(000)	832
Crystal size	0.14 x 0.10 x 0.08 mm^3
Theta range for data collection	2.92 to 26.00°.
Index ranges	-14<=h<=14, -17<=k<=16, -18<=l<=17
Reflections collected	19659
Independent reflections	8451 [R(int) = 0.0468]
Completeness to theta = 26.00°	99.8 %
Absorption correction	Semi-empirical from equivalents
Max. and min. transmission	1.00000 and 0.79956
Refinement method	Full-matrix least-squares on F^2
Data / restraints / parameters	8451 / 0 / 509
Goodness-of-fit on F^2	0.866
Final R indices [I>2sigma(I)]	R1 = 0.0447, wR2 = 0.0987
R indices (all data)	R1 = 0.0946, wR2 = 0.1080
Largest diff. peak and hole	0.248 and -0.290 e.Å^{-3}

Crystal Data for of [(TMEDA)·{Na(μ-TMP)Zn(ᵗBu)}₂(μ-OCPhCH=CHPhCHPhCH=CPh-μ-O)] (4f)

Empirical formula	C68 H110 N6 Na2 O2 Zn2
Formula weight	1220.34
Temperature	123(2) K
Wavelength	0.71073 Å
Crystal system	Triclinic
Space group	P-1
Unit cell dimensions	a = 11.9774(7) Å α= 102.420(7)°.
	b = 15.1883(13) Å β= 105.102(6)°.
	c = 20.8913(16) Å γ = 91.831(6)°.
Volume	3567.7(5) Å^3
Z	2
Density (calculated)	1.136 Mg/m^3
Absorption coefficient	0.728 mm^{-1}
F(000)	1316
Crystal size	0.15 x 0.15 x 0.05 mm^3
Theta range for data collection	2.86 to 25.00°.
Index ranges	-14<=h<=14, -18<=k<=18, -24<=l<=24
Reflections collected	31018
Independent reflections	12537 [R(int) = 0.0917]
Completeness to theta = 25.00°	99.8 %
Absorption correction	Semi-empirical from equivalents
Max. and min. transmission	1.00000 and 0.81246
Refinement method	Full-matrix least-squares on F^2
Data / restraints / parameters	12537 / 270 / 790
Goodness-of-fit on F^2	0.725
Final R indices [I>2sigma(I)]	R1 = 0.0575, wR2 = 0.1195
R indices (all data)	R1 = 0.1577, wR2 = 0.1323
Largest diff. peak and hole	0.642 and -0.637 e.Å^{-3}

Crystal Data for [(TMEDA)·Na(μ-DTBN)$_2$Zn(^{t}Bu)] (4g)

Empirical formula	C26 H61 N4 Na O2 Zn
Formula weight	550.15
Temperature	123(2) K
Wavelength	0.71073 Å
Crystal system	Monoclinic
Space group	P21/m
Unit cell dimensions	a = 8.5075(2) Å α= 90°.
	b = 17.8113(3) Å β= 99.796(2)°.
	c = 10.9333(2) Å γ = 90°.
Volume	1632.56(6) Å^3
Z	2
Density (calculated)	1.119 Mg/m^3
Absorption coefficient	0.791 mm^{-1}
F(000)	604
Crystal size	0.4 x 0.3 x 0.3 mm^3
Theta range for data collection	2.81 to 29.00°.
Index ranges	-11<=h<=11, -21<=k<=24, -14<=l<=14
Reflections collected	9906
Independent reflections	4456 [R(int) = 0.0241]
Completeness to theta = 27.00°	99.9 %
Absorption correction	Semi-empirical from equivalents
Max. and min. transmission	1.00000 and 0.98478
Refinement method	Full-matrix least-squares on F^2
Data / restraints / parameters	4456 / 7 / 208
Goodness-of-fit on F^2	1.032
Final R indices [I>2sigma(I)]	R1 = 0.0327, wR2 = 0.0769
R indices (all data)	R1 = 0.0397, wR2 = 0.0806
Largest diff. peak and hole	0.386 and -0.320 e.Å^{-3}

Crystal Data For [(TMEDA)Na·(μ-TMP)(μ-Ph)Zn(Ph)] (4i)

Empirical formula	C27 H44 N3 Na Zn
Formula weight	499.01
Temperature	123(2) K
Wavelength	0.71073 Å
Crystal system	Orthorhombic
Space group	Pna2$_1$
Unit cell dimensions	a = 36.7199(16) Å α= 90°.
	b = 10.2414(6) Å β= 90°.
	c = 43.751(3) Å γ = 90°.
Volume	16453.2(15) Å^3
Z	24
Density (calculated)	1.209 Mg/m^3
Absorption coefficient	0.930 mm^{-1}
F(000)	6432
Crystal size	? x ? x ? mm^3
Theta range for data collection	2.78 to 27.00°.
Index ranges	-27<=h<=46, -13<=k<=12, -55<=l<=55
Reflections collected	60304
Independent reflections	29822 [R(int) = 0.0457]
Completeness to theta = 27.00°	99.8 %
Absorption correction	Semi-empirical from equivalents
Max. and min. transmission	1.00000 and 0.88732
Refinement method	Full-matrix least-squares on F^2
Data / restraints / parameters	29822 / 285 / 1867
Goodness-of-fit on F^2	1.030
Final R indices [I>2sigma(I)]	R1 = 0.0611, wR2 = 0.0975
R indices (all data)	R1 = 0.0925, wR2 = 0.1114
Absolute structure parameter	0.475(7)
Largest diff. peak and hole	0.946 and -0.469 e.Å^{-3}

Crystal Data For [KMg(TMP)$_2$Bu]$_\infty$ (5f)

Empirical formula	C22 H45 K Mg N2
Formula weight	401.01
Temperature	123(2) K
Wavelength	1.54180 Å
Crystal system	Monoclinic
Space group	P2(1)
Unit cell dimensions	a = 12.8807(5) Å $\quad\quad$ α= 90°.
	b = 26.5173(9) Å $\quad\quad$ β= 105.997(4)°.
	c = 16.1073(6) Å $\quad\quad$ γ = 90°.
Volume	5288.6(3) Å^3
Z	6
Density (calculated)	0.755 Mg/m^3
Absorption coefficient	1.516 mm^{-1}
F(000)	1332
Crystal size	0.2 x 0.1 x 0.1 mm^3
Theta range for data collection	6.36 to 55.74°.
Index ranges	-12<=h<=13, -28<=k<=28, -17<=l<=16
Reflections collected	20246
Independent reflections	11462 [R(int) = 0.0499]
Completeness to theta = 55.74°	98.7 %
Absorption correction	Semi-empirical from equivalents
Max. and min. transmission	1.00000 and 0.84562
Refinement method	Full-matrix least-squares on F^2
Data / restraints / parameters	11462 / 1 / 731
Goodness-of-fit on F^2	0.805
Final R indices [I>2sigma(I)]	R1 = 0.0468, wR2 = 0.0923
R indices (all data)	R1 = 0.0729, wR2 = 0.0975
Absolute structure parameter	0.151(9)
Largest diff. peak and hole	0.244 and -0.157 e.Å^{-3}

Crystal Data For [KMg(TMP)$_2$(C$_{10}$H$_7$)]$_6$ (5j)

Empirical formula	C189 H282 K6 Mg6 N12
Formula weight	3102.73
Temperature	123(2) K
Wavelength	1.54180 Å
Crystal system	Trigonal
Space group	R -3
Unit cell dimensions	a = 37.8751(15) Å α= 90°.
	b = 37.8751(15) Å β= 90°.
	c = 11.7865(4) Å γ = 120°.
Volume	14642.8(10) Å^3
Z	3
Density (calculated)	1.056 Mg/m^3
Absorption coefficient	1.748 mm^{-1}
F(000)	5058
Crystal size	0.14 x 0.04 x 0.02 mm^3
Theta range for data collection	7.64 to 69.97°.
Index ranges	-45<=h<=44, -46<=k<=39, -10<=l<=14
Reflections collected	20485
Independent reflections	6129 [R(int) = 0.0297]
Completeness to theta = 69.97°	99.3 %
Absorption correction	Semi-empirical from equivalents
Max. and min. transmission	1.00000 and 0.62580
Refinement method	Full-matrix least-squares on F^2
Data / restraints / parameters	6129 / 252 / 367
Goodness-of-fit on F^2	1.057
Final R indices [I>2sigma(I)]	R1 = 0.0842, wR2 = 0.2430
R indices (all data)	R1 = 0.0991, wR2 = 0.2627
Largest diff. peak and hole	0.756 and -0.402 e.Å^{-3}

Crystal Data For [KMg(TMP)$_2$Bu]$_6$ (5h)

Empirical formula	C168 H342 K6 Mg6 N12
Formula weight	2911.00
Temperature	123(2) K
Wavelength	0.71073 Å
Crystal system	Hexagonal
Space group	R-3
Unit cell dimensions	a = 37.852(2) Å $\quad$ α= 90°.
	b = 37.852(2) Å $\quad$ β= 90°.
	c = 11.5850(6) Å $\quad$ γ= 120°.
Volume	14374.9(13) Å^3
Z	3
Density (calculated)	1.009 Mg/m^3
Absorption coefficient	0.202 mm^{-1}
F(000)	4860
Crystal size	0.24 x 0.22 x 0.16 mm^3
Theta range for data collection	4.17 to 26.99°.
Index ranges	-29<=h<=48, -48<=k<=47, -14<=l<=13
Reflections collected	14300
Independent reflections	6852 [R(int) = 0.0314]
Completeness to theta = 26.99°	98.1 %
Absorption correction	Semi-empirical from equivalents
Max. and min. transmission	1.00000 and 0.98736
Refinement method	Full-matrix least-squares on F^2
Data / restraints / parameters	6852 / 3 / 312
Goodness-of-fit on F^2	1.021
Final R indices [I>2sigma(I)]	R1 = 0.0621, wR2 = 0.1475
R indices (all data)	R1 = 0.1005, wR2 = 0.1734
Largest diff. peak and hole	0.548 and -0.565 e.Å^{-3}

Crystal Data for [KMg(TMP)(CH₂SiMe₃)₂] ∞ (5k)

Empirical formula	C17 H40 K Mg N Si2
Formula weight	378.09
Temperature	123(2) K
Wavelength	0.71073 Å
Crystal system	Monoclinic
Space group	P 21/a
Unit cell dimensions	a = 11.9623(10) Å $\alpha= 90°$.
	b = 36.608(3) Å $\alpha= 112.640(9)°$.
	c = 12.0390(9) Å $\gamma= 90°$.
Volume	4865.8(6) Å^3
Z	8
Density (calculated)	1.032 Mg/m^3
Absorption coefficient	0.341 mm^{-1}
F(000)	1664
Crystal size	0.16 x 0.08 x 0.06 mm^3
Theta range for data collection	3.11 to 28.29°.
Index ranges	-15<=h<=15, -48<=k<=48, -15<=l<=15
Reflections collected	19763
Independent reflections	19765 [R(int) = 0.0000]
Completeness to theta = 26.00°	92.2 %
Absorption correction	Semi-empirical from equivalents
Max. and min. transmission	1.00000 and 0.95016
Refinement method	Full-matrix least-squares on F^2
Data / restraints / parameters	19765 / 0 / 450
Goodness-of-fit on F^2	1.025
Final R indices [I>2sigma(I)]	R1 = 0.0480, wR2 = 0.1028
R indices (all data)	R1 = 0.0624, wR2 = 0.1131
Largest diff. peak and hole	0.506 and -0.344 e.Å^{-3}

Crystal Data for [KMg(TMP)(CH$_2$SiMe$_3$)$_2$·(Tol.)] ∞ (5l)

Empirical formula	C48 H96 K2 Mg2 N2 Si4
Formula weight	940.45
Temperature	123(2) K
Wavelength	0.71073 Å
Crystal system	Triclinic
Space group	P -1
Unit cell dimensions	a = 11.7270(4) Å α= 72.849(2)°.
	b = 13.2699(3) Å β= 74.708(3)°.
	c = 20.7661(6) Å γ = 85.361(2)°.
Volume	2978.49(15) Å^3
Z	2
Density (calculated)	1.049 Mg/m^3
Absorption coefficient	0.290 mm^{-1}
F(000)	1032
Crystal size	0.6 x 0.5 x 0.5 mm^3
Theta range for data collection	3.22 to 29.00°.
Index ranges	-15<=h<=15, -17<=k<=18, -28<=l<=28
Reflections collected	34441
Independent reflections	15234 [R(int) = 0.0298]
Completeness to theta = 27.00°	99.8 %
Absorption correction	Semi-empirical from equivalents
Max. and min. transmission	1.00000 and 0.84534
Refinement method	Full-matrix least-squares on F^2
Data / restraints / parameters	15234 / 0 / 619
Goodness-of-fit on F^2	1.027
Final R indices [I>2sigma(I)]	R1 = 0.0454, wR2 = 0.0957
R indices (all data)	R1 = 0.0739, wR2 = 0.1106
Largest diff. peak and hole	0.425 and -0.377 e.Å^{-3}

Crystal Data for [NaMg(HMDS)₂Bu] ∞ (5a)

Empirical formula	C16 H45 Mg N2 Na Si4
Formula weight	425.20
Temperature	123(2) K
Wavelength	0.71073 Å
Crystal system	Monoclinic
Space group	P 21/n
Unit cell dimensions	a = 9.2943(2) Å $\alpha = 90°$.
	b = 20.5586(5) Å $\beta = 96.463(2)°$.
	c = 13.8977(3) Å $\gamma = 90°$.
Volume	2638.67(10) Å^3
Z	4
Density (calculated)	1.070 Mg/m^3
Absorption coefficient	0.269 mm^{-1}
F(000)	936
Crystal size	0.26 x 0.10 x 0.10 mm^3
Theta range for data collection	3.89 to 29.71°.
Index ranges	-9<=h<=12, -25<=k<=27, -18<=l<=18
Reflections collected	16297
Independent reflections	6593 [R(int) = 0.0271]
Completeness to theta = 27.50°	99.5 %
Absorption correction	Semi-empirical from equivalents
Max. and min. transmission	1.00000 and 0.91953
Refinement method	Full-matrix least-squares on F^2
Data / restraints / parameters	6593 / 0 / 238
Goodness-of-fit on F^2	1.087
Final R indices [I>2sigma(I)]	R1 = 0.0486, wR2 = 0.1126
R indices (all data)	R1 = 0.0671, wR2 = 0.1217
Largest diff. peak and hole	0.896 and -0.527 e.Å^{-3}

Crystal Data for [KMg(HMDS)$_2$Bu] ∞ (5d)

Empirical formula	C16 H45 K Mg N2 Si4
Formula weight	441.31
Temperature	123(2) K
Wavelength	0.71073 Å
Crystal system	Monoclinic
Space group	P2(1)/n
Unit cell dimensions	a = 9.2256(3) Å $\quad$ α= 90°.
	b = 20.4442(7) Å $\quad$ β= 93.263(3)°.
	c = 14.6828(5) Å $\quad$ γ = 90°.
Volume	2764.83(16) Å^3
Z	4
Density (calculated)	1.060 Mg/m^3
Absorption coefficient	0.392 mm^{-1}
F(000)	968
Crystal size	0.18 x 0.12 x 0.12 mm^3
Theta range for data collection	2.95 to 28.00°.
Index ranges	-11<=h<=12, -23<=k<=26, -18<=l<=19
Reflections collected	15547
Independent reflections	6496 [R(int) = 0.0356]
Completeness to theta = 27.00°	99.8 %
Absorption correction	Semi-empirical from equivalents
Max. and min. transmission	1.00000 and 0.95411
Refinement method	Full-matrix least-squares on F^2
Data / restraints / parameters	6496 / 69 / 250
Goodness-of-fit on F^2	1.152
Final R indices [I>2sigma(I)]	R1 = 0.1564, wR2 = 0.3536
R indices (all data)	R1 = 0.1703, wR2 = 0.3600
Largest diff. peak and hole	0.932 and -0.926 e.Å^{-3}

Crystal Data for [{Fe-(C$_5$H$_4$)}$_2${K$_2$Mg$_3$(TMP)$_2$(THF)$_2$(Toluene)$_2$}] (5i)

Empirical formula	C74 H100 Fe3 K2 Mg3 N2 O3
Formula weight	1384.24
Temperature	123(2) K
Wavelength	1.54180 Å
Crystal system	Monoclinic
Space group	C 2/c
Unit cell dimensions	a = 31.5029(4) Å α= 90°.
	b = 10.2642(1) Å β= 93.9320(10)°.
	c = 21.6666(2) Å γ = 90°.
Volume	6989.45(13) Å^3
Z	4
Density (calculated)	1.315 Mg/m^3
Absorption coefficient	6.616 mm^{-1}
F(000)	2936
Crystal size	0.26 x 0.24 x 0.04 mm^3
Theta range for data collection	8.88 to 73.03°.
Index ranges	-38<=h<=38, -11<=k<=12, -24<=l<=26
Reflections collected	33806
Independent reflections	6960 [R(int) = 0.0490]
Completeness to theta = 70.00°	99.6 %
Absorption correction	Semi-empirical from equivalents
Max. and min. transmission	1.00000 and 0.31386
Refinement method	Full-matrix least-squares on F^2
Data / restraints / parameters	6960 / 165 / 437
Goodness-of-fit on F^2	1.039
Final R indices [I>2sigma(I)]	R1 = 0.0479, wR2 = 0.1251
R indices (all data)	R1 = 0.0547, wR2 = 0.1313
Largest diff. peak and hole	0.775 and -0.563 e.Å^{-3}

[1] J. Clayden, *Organolithiums: Selectivity for Synthesis*, Pergamon, Oxford, **2002**, p.

[2] a) H. Gilman and B. J. Gaj, *J. Org. Chem.* **1957**, *22*, 1165; b) S. Honeycutt, *J. Organomet. Chem.* **1971**, *29*, 1.

[3] W. Schlenk and J. Holtz, *Ber. Dtsc. Chem. Ger.* **1917**, *47*, 473.

[4] K. Zeigler and H. Colonius, *Liebigs Ann. Chem.* **1930**, *476*, 135.

[5] T. L. Brown, *Acc. Chem. Res.* **1968**, *1*, 23.

[6] P. West and R. Waack, *J. Am. Chem. Soc.* **1967**, *69*, 4395.

[7] D. J. Ciappenelli and M. D. Rausch, *J. Organomet. Chem.* **1967**, *10*, 127.

[8] P. Beak, M. L. Boys and Y. S. Park, *J. Am. Chem. Soc.* **1996**, *118*, 3757.

[9] a) G. B. Buckton, *Proc. R. Soc. London* **1859**, *9*, 309; b) G. B. Buckton, *Proc. R. Soc. London* **1859**, *9*, 685; c) G. B. Buckton, *Ann.* **1859**, *112*, 220; d) G. B. Buckton, *Ann.* **1859**, *109*, 122, 222.

[10] P. Schorigin, *Ber. Dtsch. Chem. Ges.* **1908**, *41*, 2717.

[11] P. Schorigin, *Ber. Dtsch. Chem. Ges.* **1908**, *41*.

[12] a) H. Gilman and H. A. Pacevitz, *J. Am. Chem. Soc.* **1940**, *62*, 673; b) H. Gilman and H. A. Pacevitz, *J. Am. Chem. Soc.* **1940**, *62*, 1301.

[13] a) A. A. Morton and C. E. Claff, *J. Org. Chem.* **1956**, *21*, 736; b) A. A. Morton, J. T. Massengale and M. L. Brown, *J. Am. Chem. Soc.* **1945**, *67*, 1620.

[14] R. A. Benkeser, D. J. Foster, D. M. Sauve and J. F. Nobis, *Chem. Rev.* **1957**, *57*, 867-894.

[15] a) E. Weiss, S. Corbelin, J. K. Cockroft and A. N. Fitch, *Angew. Chem. Int. Ed.* **1990**, *29*, 650; b) E. Weiss and G. Sauermann, *J. Organomet. Chem.* **1970**, *21*, 1; c) M. Niemeyer and P. P. Power, *Organometallics* **1997**, *16*, 3258.

[16] a) S. Corbelin, N. P. Lorenzen, J. Kopf and E. Weiss, *J. Organomet. Chem.* **1991**, *415*, 293; b) U. Schumann and E. Weiss in *Vol.* **1987**.

[17] S. E. Baillie, W. Clegg, P. Garcia-Alvarez, E. Hevia, A. R. Kennedy, J. Klett and L. Russo, *Chem. Commun.* **2011**, *47*, 388-390.

[18] D. Stalke and T. Kottke, *Angew. Chem. Int. Ed.* **1993**, *32*, 580.

[19] B. Gehrhus, P. H. Hitchcock, A. R. Kennedy, M. F. Lappert, R. E. Mulvey and P. J. A. Rodger, *J. Organomet. Chem.* **1999**, *587*, 88.

[20] R. Gruning and J. L. Atwood, *J. Organomet. Chem.* **1977**, *137*, 101.

[21] M. Dreiss, H. Pritzkow, M. Skipinski and U. Winkler, *Organometallics* **1997**, *16*, 5108.

[22] D. R. Armstrong, D. V. Graham, A. R. Kennedy, R. E. Mulvey and C. T. O'Hara, *Chem. Eur. J.* **2008**, *14*, 8025.

[23] a) I. Coldham, *J. Chem. Soc. Perkin Trans. 1* **1998**, 1343-1364; b) J. Hartman and M. Schlosser, *Helv. Chim. Acta* **1976**, *59*, 453-464.

[24] a) P. B. Hitchcock, M. F. Lappert, W.-P. Leung, L. Diangsheng and T. Shun, *Chem. Commun.* **1993**, *18*, 1386-1387; b) C. Eaborn, P. B. Hitchcock, K. Izod, A. J. Jaggar and J. D. Smith, *Organometallics* **1994**, *13*, 753.

[25] a) B. Conway, A. R. Kennedy, R. E. Mulvey, S. D. Robertson and J. Garcia-Alvarez, *Angew. Chem. Int. Ed.* **2010**, *49*, 3182-3184; b) B. Conway, D. V. Graham, E. Hevia, A. R. Kennedy, J. Klett and R. E. Mulvey, *Chem. Commun.* **2008**, 2638.

[26] W. Clegg, B. Conway, A. R. Kennedy, J. Klett, R. E. Mulvey and L. Russo, *Eur. J. Inorg. Chem.* **2011**, 721-726.

[27] L. S. Hegedus, B. H. Lipshutz, J. A. Marshall, E. Nakamura, E. Negishi, M. T. Reetz, M. Schlosser, M. F. Semmelhack, K. Smith and H. Yamamoto, *Organometallics in Synthesis: A Manual (Second Edition)*, Wiley, **2001**, p.

[28] R. A. Finnegan, *Tetrahedron Lett.* **1963**, *4*, 429-433.

[29] R. Lehmann and M. Schlosser, *Tetrahedron Lett.* **1984**, *225*.

[30] T. P. Hanusa, J. C. Huffman and K. F. Tesh, *Inorg. Chem.* **1990**, *29*, 1584.

[31] a) K. W. Henderson, J. J. Morris and B. C. Noll, *Acta Cryst. E* **2007**, *63*, 2477; b) G. C. Forbes, A. R. Kennedy, R. E. Mulvey, B. A. Roberts and R. B. Rowlings, *Organometallics* **2002**, *21*, 5115; c) F. Feil and S. Harder, *Organometallics* **2000**, *19*, 5010.

[32] E. Frankland, *J. Chem. Soc.* **1850**, *2*, 263.

[33] J. Basca, F. Hanke, S. Hindley, R. Odedra, G. R. Darling, A. C. Jones and A. Steiner, *Angew. Chem. Int. Ed.* **2011**, *50*, 1-4.

[34] a) M. Moskowitz and C. Wolf, *J. Org. Chem.* **2011**, *76*, 6372; b) P. G. Cozzi, *Angew. Chem. Int. Ed.* **2006**, *45*, 2951; c) C. C. C. Johansson and T. J. Colacot, *Angew. Chem. Int. Ed.* **2010**, *49*, 676.

[35] a) E.-i. Negishi, *Angew. Chem. Int. Ed.* **2011**, *50*, 6738; b) B. Haag, E. Hartmann, A. Gavryushin, R. M. Gschwind, P. Knochel, P. Mayer, K. Schober, T. Thaler and H. Zipse, *Nat. Chem.* **2010**, *2*, 125.

[36] C. Garban and F. M. Rabagliati, *J. Polym. Sci.* **1985**, *23*, 895.

[37] a) B. T. Cho and S. H. Shin, *Bull. Korean Chem. Soc.* **2006**, *27*, 1283; b) K. Itoh, Y. Miyagi and N. Oguni, *Tetrahedron Lett.* **1998**, *39*, 9023.

[38] P. Barbier, *Compt. Rend. Acad. Sci.* **1899**, *128*, 111.

[39] V. Grignard, *Compt. Rend. Acad. Sci.* **1900**, *130*, 1322.

[40] R. Abegg, *Chem. Ber.* **1905**, *38*, 4112.

[41] J. T. B. H. Jastrzebski, J. Boersma and G. v. Koten in *Vol.* Eds.: Z. Rappoport and I. Marek), Wiley, **2008**.

[42] a) G. D. Stucky and R. E. Rundle, *J. Am. Chem. Soc.* **1963**, *85*, 1002; b) L. J. Guggenberger and R. E. Rundle, *J. Am. Chem. Soc.* **1964**, *86*, 5344.

[43] A. Baeyer and V. Villiger, *Chem. Ber.* **1902**, *35*, 1201.

[44] a) L. Boymond, M. Rottlander, G. Cahiez and P. Knochel, *Angewandte Chemie-International Edition* **1998**, *37*, 1701-1703; b) M. Kienle, A. Unsinn and P. Knochel, *Angewandte Chemie-International Edition* **2010**, *49*, 4751-4754.

[45] a) A. Krasovskiy, A. Tishkov, V. del Amo, H. Mayr and P. Knochel, *Angewandte Chemie-International Edition* **2006**, *45*, 5010-5014; b) H. J. Ren and P. Knochel, *Angewandte Chemie-International Edition* **2006**, *45*, 3462-3465; c) L. Melzig, C. B. Rauhut and P. Knochel, *Chem. Commun.* **2009**, 3536-3538.

[46] a) D. R. Armstrong, P. Garcia-Alvarez, A. R. Kennedy, R. E. Mulvey and J. A. Parkinson, *Angew. Chem. Int. Ed.* **2010**, *49*, 3185-3188; b) P. Garcia-Alvarez, D. V. Graham, E. Hevia, A. R. Kennedy, J. Klett, R. E. Mulvey, C. T. O'Hara and S. Weatherstone, *Angew. Chem. Int. Ed.* **2008**, *120*, 8199.

[47] P. E. Eaton, C.-H. Lee and Y. Xiong, *J. Am. Chem. Soc.* **1989**, *111*, 8017.

[48] O. Harada, A. Kawachi, S. Nagae, Y. Onoue and Y. Yamamoto, *Chem. Eur. J.* **2011**, *17*, 8005.

[49] O. Just, W. S. Rees Jr., H. Schumann and R. Weimann, *Polyhedron* **1998**, *17*, 1001.

[50] D. R. Armstrong, A. R. Kennedy, R. E. Mulvey, J. A. Parkinson and S. D. Robertson, *Chem. Sci.* **2012**, *3*, 2700.

[51] P. Caubere, *Chem. Rev.* **1993**, *93*, 2317.

[52] P. Gros, P. Fort and P. Caubere, *J. Chem. Soc. Perkin Trans. 1* **1997**, 3071.

[53] E. W. Thomas, *J. Org. Chem.* **1986**, *51*, 2184.

[54] D. Lim, L. Lochmann and J. Pospisil, *Tetrahedron Lett.* **1965**, *2*, 257.

[55] M. Schlosser, *J. Organomet. Chem.* **1967**, *8*, 9.

[56] A. W. Langer, *Adv. Chem. Ser.* **1974**, *No. 130*.

[57] J. Hartmann and M. Schlosser, *Synthesis* **1975**, 888.

[58] H. Bosshardt, M. Schlosser, M. Stahle and A. Walde, *Angew. Chem. Int. Ed.* **1980**, *18*, 489.

[59] J. Hartmann, R. Muthukrishnan and M. Schlosser, *Helv. Chim. Acta* **1974**, *57*, 2261.

[60] F. Faigl and M. Schlosser, *Tetrahedron Lett.* **1991**, *32*, 3369.

[61] a) J. Cotter, P. Fleming, V. H. Gessner, A.-M. L. Hogan, D. F. O'Shea, C. Strohmann and T. Tricotet, *J. Am. Chem. Soc.* **2009**, *131*, 3142; b) J. Cotter, A.-M. L. Hogan and D. F. O'Shea, *Org. Lett.* **2007**, *9*, 1493.

[62] P. Fleming and D. R. O'Shea, *J. Am. Chem. Soc.* **2011**, *133*, 1698.

[63] A. R. Kennedy, J. G. MacLellan and R. E. Mulvey, *Angew. Chem. Int. Ed.* **2001**, *40*, 3245.

[64] L. Lochmann and J. Trekoval, *J. Organomet. Chem.* **1979**, *179*, 123.

[65] J. A. Wanklyn, *Liebigs Ann. Chem.* **1858**, *107*, 125.

[66] P. Knochel and P. Jones, *Organozinc Reagents: A Practical Approach*, Hardwood, L. H. and Moody, C. J., Oxford University Press, Oxford, **1999**, p.

[67] a) Y. Kameda, M. Koike, Y. Kondo, T. Sakamoto and M. Uchiyama, *J. Am. Chem. Soc.* **1996**, *118*, 8733; b) Y. Kameda, M. Koike, Y. Kondo, N. Mishima, T. Sakamoto, M. Uchiyama and M. Yokoyam, *J. Am. Chem. Soc.* **1998**, *120*, 4934; c) Y. Kondo, T. Sakamoto, A. Takazawa and T. Yoshida, *J. Chem. Soc. Perkin Trans.* **1995**, *1*, 1207.

[68] R. E. Mulvey, F. Mongin, M. Uchiyama and Y. Kondo, *Angew. Chem. Int. Ed.* **2007**, *46*, 3802.

[69] Y. Kameda, M. Koike, Y. Kondo, N. Mishima, T. Sakamoto, M. Uchiyama and M. Yokohama, *J. Am. Chem. Soc.* **1998**, *120*, 4934.

[70] A. E. H. Wheatley, *New J. Chem.* **2004**, *28*, 435.

[71] R. E. Mulvey, *Organometallics* **2006**, *25*, 1060.

[72] E. Weiss and R. Wolfrum, *Chem. Ber.* **1968**, *101*, 35.

[73] D. R. Armstrong, L. Balloch, L. Drummond, D. V. Graham, E. Hevia and A. R. Kennedy, *Organometallics* **2008**, *27*, 5860.

[74] a) Y. Kondo, T. Sakamoto, M. Shilai and M. Uchiyama, *J. Am. Chem. Soc.* **1999**, *121*, 3539; b) K. Furuyama, D. Matsumoto, K. Morokuma, D. Nobuto, M. Uchiyama and K. Yamaguchi, *J. Am. Chem. Soc.* **2006**, *128*, 8748.

[75] G. Lange, F. J. Meyer and G. Wittig, *Liebigs Ann. Chem.* **1951**, *571*, 167.

[76] G. Wittig, *Angew. Chem. Int. Ed.* **1958**, *70*, 65.

[77] E. Bellamy, O. Bayh, C. Hoarau, F. Marsais, G. Queguiner and F. Trecourt, *Chem. Commun.* **2010**, *46*, 7043.

[78] A. R. Kennedy, R. E. Mulvey and R. B. Rowlings, *J. Am. Chem. Soc.* **1998**, *120*, 7816.

[79] R. E. Mulvey, *Chem. Commun.* **2001**, 1049.

[80] a) G. Gokel, *Crown Ethers and Cryptands*, The Royal Society of Chemistry, Cambridge, **1991**, p; b) G. Gokel, *Large Ring Molecules*, ed. J. A. Semlyen, John Wiley and Sons Ltd., Chichester, **1996**, p.

[81] A. R. Kennedy, R. E. Mulvey and R. B. Rowlings, *Angew. Chem. Int. Ed.* **1998**, *37*, 3180.

[82] A. R. Kennedy, R. E. Mulvey, C. L. Raston, B. A. Roberts and R. B. Rowlings, *Chem. Commun.* **1999**, 353.

[83] W. Clegg, K. W. Henderson, A. R. Kennedy, R. E. Mulvey, C. T. O'Hara, R. B. Rowlings and D. M. Tooke, *Angew. Chem. Int. Ed.* **2001**, *40*, 3902.

[84] a) M. D. Rausch and D. J. Ciappenelli, *J. Organomet. Chem.* **1967**, *10*, 127; b) M. Walczak, K. Walczak, R. Mink, M. D. Rausch and G. D. Stucky, *J. Am. Chem. Soc.* **1978**, *100*, 6382; c) A. F. Halasa and D. P. Tate, *J. Organomet. Chem.* **1970**, *24*, 769.

[85] D. R. Armstrong, A. R. Kennedy, R. E. Mulvey and R. B. Rowlings, *Angew. Chem. Int. Ed.* **1999**, *38*, 131.

[86] P. C. Andrikopolous, D. R. Armstrong, W. Clegg, C. J. Gilfillan, E. Hevia, A. R. Kennedy, R. E. Mulvey, C. T. O'Hara, J. A. Parkinson and D. M. Tooke, *J. Am. Chem. Soc.* **2004**, *126*, 11612.

[87] D. J. Gallagher, K. W. Henderson, A. R. Kennedy, C. T. O'Hara, R. E. Mulvey and R. B. Rowlings, *Chem. Commun.* **2002**, 376.

[88] V. L. Blair, W. Clegg, A. R. Kennedy, J. Klett, R. E. Mulvey and L. Russo, *Nat. Chem.* **2010**, *2*, 588.

[89] R. B. Bates, L. M. Kroposki and D. E. Potter, *J. Org. Chem.* **1972**, *37*, 560.

[90] A. R. Kennedy, J. Klett, R. E. Mulvey and D. S. Wright, *Science* **2009**, *326*, 706.

[91] A. Dermarderosian, J. A. Beutler, C. Grauds, D. S. Tatro, M. Cirigliano and D. DeSilva, *Review of Natural Products*, A & C Black Publishers Ltd., **2008**, p.

[92] a) J. M. Jiang, G. Li and C. Y. Wang, *Polymer* **2009**, *50*, 1709; b) D. Jiang, C. Y. Ma, S. L. Zhang, Y. H. Yang and Z. H. Jiang, *J. Polymer. Eng.* **2010**, *30*, 207; c) W. L. Archer and N. P. Cheremisinoff, *Industrial Solvents Handbook*, **2003**, p.

[93] S. N. Srivastava, *Acta Crystallogr.* **1964**, *17*, 851.

[94] a) Y. Koyama, K. Suzuki and R. Yamaguchi, *Angew. Chem. Int. Ed.* **2008**, *47*, 1084; b) J. M. Crawford, E. A. Hill, O. Kamari-Bidkorpeh, T. P. Korman, J. W. Labonte, C. A. Townsend, S. C. Tsai and A. L. Vagstad, *Nature* **2009**, *461*, 1139; c) F. Diaz, H.-B. Chai, Q. Mi, B. Su, J. S. Vigo, J. G. Graham, F. Cabieses, N. R. Farnsworth, G. A. Cordell, J. M. Pezzuto, S. M. Swanson and A. D. Kinghorn, *J. Nat.*

Prod. **2004**, *67*, 352; d) K. C. Ehlrich, P. Li, L. Scharfenstein and P. Chang, *Appl. Environ. Microbiol.* **2010**, *76*, 3374.

[95] J. M. Crawford, T. P. Korman, J. W. Labonte, A. G. Newman, C. A. Townsend, S. C. Tsai and J. Wong, *Proc. Natl. Acad. Sci. U. S. A.* **2010**, *107*, 6246.

[96] R. G. Arumugham, T. Gore, S. Singh and T. E. Turula, *Anal. Chem.* **2010**, *82*, 1786.

[97] P. C. Andrikopolous, D. R. Armstrong, H. R. L. Barley, W. Clegg, S. H. Dale, E. Hevia, G. W. Honeyman, A. R. Kennedy and R. E. Mulvey, *J. Am. Chem. Soc.* **2005**, *127*, 6184.

[98] G. M. McCann, C. M. McDonnell, L. Magris and R. A. More O'Ferrall, *J. Chem. Soc. Perkin Trans.* **2002**, *2*, 784.

[99] J. March and M. B. Smith, *Advanced Organic Chemistry: Reactions, Mechanism and Structure*, Wiley-VCH, New York, **2007**, p.

[100] E. Hevia, D. J. Gallagher, A. R. Kennedy, R. E. Mulvey, C. T. O'Hara and C. Talmard, *Chem. Commun.* **2004**, 2422.

[101] H. R. L. Barley, W. Clegg, S. H. Dale, E. Hevia, G. W. Honeyman, A. R. Kennedy and R. E. Mulvey, *Angew. Chem. Int. Ed.* **2005**, *44*, 6018.

[102] M. Gartner, H. Gorls and M. Westerhausen, *Acta Cryst. E* **2007**, *63*, m2287.

[103] a) R. E. Mulvey, *Chem. Commun.* **2001**, *12*, 1049; b) W. Clegg, B. Conway, P. Garcia-Alvarez, A. R. Kennedy, J. Klett, R. E. Mulvey and L. Russo, *Dalton Trans.* **2010**, *39*, 62; c) J. Hu, L. J. Barbour and G. W. Gokel, *Proc. Natl. Acad. Sci. U. S. A.* **2002**, *99*, 5121; d) E. S. Meadows, S. L. De Wall, L. J. Barbour and G. W. Gokel, *J. Am. Chem. Soc.* **2001**, *123*, 3092.

[104] M. G. Davidson, D. Garcia-Vivo, A. R. Kennedy, R. E. Mulvey and S. D. Robertson, *Chem. Eur. J.* **2011**, *17*, 3364.

[105] G. J. P. Britovsek, J. England and A. J. P. White, *Inorg. Chem.* **2005**, *44*, 8125.

[106] a) R. E. Mulvey, *Acc. Chem. Res.* **2009**, *42*, 743; b) F. Feil and S. Harder, *Organometallics* **2001**, *20*, 4616.

[107] E. Hevia, A. R. Kennedy, J. Klett, Z. Livingstone and M. D. McCall, *Dalton Trans.* **2010**, *39*, 520-526.

[108] a) J. Cadet and B. Morin, *Photochemistry and Photobiology* **1994**, *60*, 102; b) L. J. Mathias and J. Wang, *Polym. Int.* **2005**, *54*, 1537.

[109] X. Jiang, X. Luo and J. Yin, *Photochemistry and Photobiology* **2005**, *174*, 165.

[110] K. M. Maclin and H. G. Richey, *J. Org. Chem.* **2002**, *10*, 3915.

[111] C. Wolf and K. Yearick, *Org. Lett.* **2008**, *10*, 3915.

[112] K. Ishihara, M. Hatano and S. Suzuki, *J. Am. Chem. Soc.* **2006**, *128*, 9998.

[113] B. Haag, M. Mosrin, I. Hiriyakkanavar, V. Malakhov and P. Knochel, *Angew. Chem. Int. Ed.* **2011**, *50*, 9794.

[114] E. Hevia, G. W. Honeyman, A. R. Kennedy and R. E. Mulvey, *J. Am. Chem. Soc.* **2005**, *127*, 13106.

[115] a) K. Asok, S. Bose, B. Talapatra and S. K. Talapatra, *Tetrahedron* **1985**, *41*, 2765; b) M. V. Sargent, *J. Chem. Soc. Perkin Trans.* **1987**, 2553; c) C. Fan, G. Qin, W. Wang, Y. Wang and W. Zhao, *Phytochemistry* **2001**, *57*, 1255; d) C. Fan, G. Qin, X. Y. Wu and R. S. Xu, *Phytochemistry* **1994**, *36*, 477.

[116] U. Beutler, P. C. Fuenfschilling and A. Steinkemper, *Org. Process Res. Dev.* **2007**, *11*, 341.

[117] R. T. Davies, S. M. Gowan, L. R. Kelland, S. Neidle, P. J. Perry, M. A. Read, A. P. Reszka and A. A. Wood, *J. Med. Chem.* **1999**, *42*, 2679.

[118] a) A. Facchetti, T. J. Marks and H. Usta, *Org. Lett.* **2008**, *10*, 1385; b) E. P. Gosselink, D. M. Lemal and S. D. McGregor, *J. Am. Chem. Soc.* **1966**, *88*, 582; c) K. L. Hummert, J. A. Katzenellenbogen, P. R. Kym, M. Lubin and A. G. Nilsson, *J. Med. Chem.* **1996**, *39*, 4897.

[119] a) R. P. Lemieux, J. A. McCubbin, V. Snieckus, X. Tong, R. Wang and Y. Zhao, *J. Am. Chem. Soc.* **2004**, *126*, 1161; b) J.-M. Fu, M. J. Sharp, V. Snieckus and B.-P. Zhao, *J. Org. Chem.* **1991**, *56*, 1683.

[120] E. Hevia, A. R. Kennedy and M. D. McCall, *Dalton Trans.* **2012**, *41*, 98.

[121] I. Crossland and T. Holm, *Acta Chem. Scand.* **1971**, *25*, 59.

[122] O. Farooq, G. A. Olah and A.-h. Wu, *Synthesis* **1991**, *12*, 1179.

[123] E. G. Akgemci, H. Bingol, M. Ersoz and M. Ozcelik, *Acta Physico-Chimica Sinica* **2007**, *24*, 619.

[124] H. Beraldo, D. Carrilho, L. Ferandes, K. S. Ferraz, M. F. Leite, I. C. Mendes, E. M. Souza-Fagundez and N. L. Speziali, *Bioorg. Med. Chem.* **2009**, *17*, 7138.

[125] a) L. Hao, J.-J. Hong, J. Zhu and Z.-P. Zhan, *Chem. Eur. J.* **2013**, *19*, 5715; b) B. Miller, *J. Am. Chem. Soc.* **1970**, *92*, 432; c) A. S. Dudnik and V. Gevorgyan, *Angew. Chem. Int. Ed.* **2007**, *46*, 5195; d) W. R. Dolbier Jr., K. E. Anapolle, L. McCullagh, K. Matsui, J. M. Riemann and D. Rolison, *J. Org. Chem.* **1979**, *44*, 2485.

[126] J. Geier, H. Ruegger and H. Grutzmacher, *Dalton Trans.* **2006**, 129.

[127] A. K. Bhattacharjee, *J. Mol. Struct.* **2000**, *529*, 193.

[128] a) J. W. Ager, S. L. Clark, H. L. Goldstein, T. L. Heying, M. Hillman, D. J. Mangold, R. J. Polak and J. W. Szymanski, *Inorg. Chem.* **1963**, *2*, 1089; b) T. L.

Heying, H. Schroeder and J. R. Reiner, *Inorg. Chem.* **1963**, *2*, 1092; c) J. W. Ager, S. L. Clark, R. P. Alexander, T. L. Heying, S. Papetti, J. A. Reid and S. I. Trotz, *Inorg. Chem.* **1963**, *2*, 1097; d) T. L. Heying and S. Papetti, *Inorg. Chem.* **1963**, *2*, 1105.

[129] a) J. D. Eluvathingal, *J. Am. Chem. Soc.* **1982**, *104*, 7017; b) C. R. Kutal, D. A. Owen and L. J. Todd, *Inorg. Syn.* **1968**, *11*, 19.

[130] B. A. Barnum, R. E. Barth, I. M. Codogni, F. G. Rong, A. H. Soloway, W. Tjarks and J. G. Wilson, *Chem. Rev.* **1998**, *98*, 1515.

[131] a) A. P. Petrova, *J. Pol. Sci. Ser. C.* **2007**, *49*, 251; b) K. F. Jackson, R. E. Kesting and J. M. Newman, *Appl. Pol. Sci.* **1971**, *15*, 2645.

[132] F. Hoffman, M. Juhasz, K. C. Kim, C. A. Reed and E. Stoyanov, *Angew. Chem. Int. Ed.* **2004**, *43*, 5352.

[133] S. R. Wang, Z. Z. Qiu and Z. W. Xie, *J. Am. Chem. Soc.* **2010**, *132*, 9988.

[134] L. Deng, H. S. Chan, S. Ren and Z. W. Xie, *Organometallics* **2009**, *28*, 5749.

[135] R. N. Grimes, *Carboranes*, Academic Press, **1970**, p.

[136] D. A. Brown, S. J. Bryan, W. Clegg and K. Wade, *J. Organomet. Chem.* **1987**, *325*, 39.

[137] M. F. Hawthorne, C. B. Knobler, X. Yang and Z. Zheng, *J. Am. Chem. Soc.* **1993**, *115*, 193.

[138] C. Blomberg, R. Salinger and H. S. Mosher, *J. Org. Chem.* **1969**, *34*, 2385.

[139] G. A. Olah, A.-h. Wu and O. Farooq, *Synthesis* **1991**, *12*, 1179.

[140] L. Tebben and A. Struder, *Angew. Chem. Int. Ed.* **2011**, *50*, 5034.

[141] M. S. Maji, S. Murarka and A. Studer, *Org. Lett.* **2010**, *12*, 3878.

[142] a) L. Balloch, A. M. Drummond, P. Garcia-Alvarez, D. V. Graham, A. R. Kennedy, J. Klett, R. E. Mulvey, C. T. O'Hara, P. J. A. Rodger and I. D. Rushworth, *Inorg. Chem.* **2009**, *48*, 6934; b) G. C. Forbes, A. R. Kennedy, R. E. Mulvey and P. J. A. Rodger, *Chem. Commun.* **2001**, 1400.

[143] a) J. E. Anderson, D. Casarini, J. E. T. Corrie and L. Lunazzi, *J. Chem. Soc. Perkin Trans. 2* **1993**, 1299; b) G. Sorin, R. M. Mallorquin, Y. Contie, A. Baralle, M. Malacria, J.-P. Goddard and L. Fensterbank, *Angew. Chem. Int. Ed.* **2010**, *49*, 8721.

[144] M. Satyanarayana, P. Tiwari, B. K. Tripathi, A. K. Srivastava and R. Pratap, *Bioorg. Med. Chem.* **2004**, *12*, 883.

[145] a) A. Modzelewska, C. Pettit, G. Achanta, N. E. Davidson, P. Huang and S. R. Khan, *Bioorg. Med. Chem.* **2006**, *14*, 3491; b) V. Sharma, V. Kumar and P. Kumar, *Anticancer Agents Med. Chem.* **2013**, *13*, 422.

[146] D. H. Evans, *Chem. Rev.* **2008**, *108*, 2113.

[147] G. C. Forbes, F. R. Kenley, A. R. Kennedy, R. E. Mulvey, C. T. O'Hara and J. A. Parkinson, *Chem. Commun.* **2003**, 1140.

[148] A. Onistschenko, A. Sommer, H. Stamm and A. Woderer, *J. Org. Chem.* **1986**, *51*, 4979.

[149] D. R. Anderson, J. S. Keute, T. H. Koch and R. H. Moseley, *J. Am. Chem. Soc.* **1977**, *99*, 6332.

[150] P. T. Emmerson and P. Howard-Flanders, *Nature* **1964**, *204*, 1005.

[151] a) C. H. Galka, D. J. M. Trosch, I. Rudenauer, L. H. Gade, I. Scowen and M. McPartlin, *Inorg. Chem.* **2000**, *39*, 4615; b) G. C. Forbes, A. R. Kennedy, R. E. Mulvey, P. J. A. Rodger and R. B. Rowlings, *J. Chem. Soc., Dalton Trans.* **2001**, 1477; c) L. Barr, J. G. MacLellan, J. H. Moir, R. E. Mulvey and P. J. A. Rodger, *Chem. Commun.* **2000**, 1757.

[152] a) E. Hevia, F. R. Kenley, A. R. Kennedy, R. E. Mulvey and R. B. Rowlings, *Eur. J. Inorg. Chem.* **2003**, 3347; b) A. R. Kennedy and C. T. O'Hara, *Dalton Trans.* **2008**, 4975; c) R. Campbell, B. Conway, G. S. Fairweather, P. Garcia-Alvarez, A. R. Kennedy, J. Klett, R. E. Mulvey, C. T. O'Hara and G. M. Robertson, *Dalton Trans.* **2010**, *39*, 511.

[153] W. Clegg, B. Conway, P. Garcia-Alvarez, A. R. Kennedy, R. E. Mulvey, L. Russo, J. Sassmannshausen and T. Tuttle, *Chem. Eur. J.* **2009**, *15*, 10702.

[154] a) P. C. Andrews, A. R. Kennedy, R. E. Mulvey, C. L. Raston, B. A. Roberts and R. B. Rowlings, *Angew. Chem. Int. Ed.* **2000**, *39*, 1960; b) E. Hevia, G. W. Honeyman, A. R. Kennedy, R. E. Mulvey and D. C. Sherrington, *Angew. Chem. Int. Ed.* **2005**, *44*, 68; c) P. C. Andrikopolous, D. R. Armstrong, A. R. Kennedy, R. E. Mulvey, C. T. O'Hara and R. B. Rowlings, *Eur. J. Inorg. Chem.* **2003**, 3354.

[155] P. B. Hitchcock, A. V. Khvostov, M. F. Lappert and A. V. Protchenko, *J. Organomet. Chem.* **2002**, *647*, 198.

[156] M. Gartner, H. Gorls and M. Westerhausen, *Acta Cryst. E* **2007**, *63*, m2289.

[157] A. R. Kennedy, J. Klett, C. T. O'Hara, R. E. Mulvey and G. M. Robertson, *Eur. J. Inorg. Chem.* **2009**, 5029.

[158] K. Issleib and H. J. Deylig, *Chem. Ber.* **1964**, *97*, 946.

[159] H. O. Frohlich, *Z. Chem.* **1975**, *15*, 316.

[160] M. Gartner, R. Fischer, J. Langer, H. Gorls, D. Walther and M. Westerhausen, *Inorg. Chem.* **2007**, *46*, 5118.

[161] G. Gokel, L. J. Barbour, S. L. De Wall and E. S. Meadows, *Chem. Rev.* **2001**, *222*, 127.

[162] a) L. S. Bennie, W. J. Kerr, M. Middleditch and A. J. B. Watson, *Chem. Commun.* **2011**, *47*, 2264; b) V. L. Blair, A. R. Kennedy, J. Klett and R. E. Mulvey, *Chem. Commun. (Camb)* **2008**, *42*, 5426.

[163] a) V. L. Blair, A. R. Kennedy, R. E. Mulvey and C. T. O'Hara, *Chem. Eur. J.* **2010**, *29*, 8600; b) R. E. Mulvey, A. R. Kennedy and E. Hevia, *Chem. Commun.* **2007**, *27*, 2864.

[164] G. Monzon, I. Tirotta and P. Knochel, *Angew. Chem. Int. Ed.* **2012**, *51*, 10624.

[165] T. Bresser and P. Knochel, *Angew. Chem. Int. Ed.* **2011**, *50*, 1914.

[166] A. J. Chalk and T. J. Hoogeboom, *J. Organomet. Chem.* **1968**, *11*, 615.

[167] C. D. Broaddus, *J. Am. Chem. Soc.* **1966**, *88*, 4174.

[168] P. C. Andrikopolous, D. R. Armstrong, D. V. Graham, E. Hevia, A. R. Kennedy, R. E. Mulvey, C. T. O'Hara and C. Talmard, *Angew. Chem. Int. Ed.* **2005**, *44*, 3459.

[169] K. J. Drewette, K. W. Henderson, A. R. Kennedy, R. E. Mulvey, C. T. O'Hara and R. B. Rowlings, *Chem. Commun.* **2002**, 1176.

[170] a) Y. Sarazin, D. L. Hughes, N. Kaltsoyannis, J. A. Wright and M. Bochmann, *J. Am. Chem. Soc.* **2007**, *129*, 881; b) H. A. Skinner and J. A. Connor, *Pure & Appl. Chem.* **1985**, *57*, 79.

[171] G. C. Forbes, F. R. Kenley, A. R. Kennedy, R. E. Mulvey, C. T. O'Hara and J. A. Parkinson, *Chem. Commun.* **2003**, 1140.

[172] E. Hevia, A. R. Kennedy, R. E. Mulvey and S. Weatherstone, *Angew. Chem. Int. Ed.* **2004**, *43*, 1709.

[173] D. Li, I. Keresztes, R. Hopson and P. Williard, *Acc. Chem. Res.* **2009**, *42*, 270.

[174] P. Garcia-Alvarez, R. E. Mulvey and J. A. Parkinson, *Angew. Chem. Int. Ed.* **2011**, *50*, 9668.

[175] Y. Zhao and D. G. Truhlar, *J. Chem. Phys.* **2006**, *125*, 194101.

[176] a) P. C. Hariharan and J. A. Pople, *Theor. Chim. Acta* **1973**, *58*, 1200; b) R. Krishnan, J. S. Binkley, R. Seeger and J. A. Pople, *J. Chem. Phys.* **1980**, *72*, 650.

[177] M. J. Frisch, G. W. Trucks, H. B. Schlegel, G. E. Scuseria, M. A. Robb, J. R. Cheeseman, G. Scalmani, V. Barone, B. Mennucci, G. A. Petersson, H. Nakatsuji, M. Caricato, X. Li, H. P. Hratchian, A. F. Izmaylov, J. Bloino, G. Zheng, J. L. Sonnenberg, M. Hada, M. Ehara, K. Toyota, R. Fukuda, J. Hasegawa, M. Ishida, T. Nakajima, Y. Honda, O. Kitao, H. Nakai, T. Vreven, J. Montgomery, J. A. J. E. Peralta, F. Ogliaro, M. Bearpark, J. J. Heyd, E. Brothers, K. N. Kudin, V. N. Staroverov, R. Kobayashi, J. Normand, K. Raghavachari, A. Rendell, J. C. Burant, S. S. Iyengar, J. Tomasi, M. Cossi, N. Rega, J. M. Millam, M. Klene, J. E. Knox, J. B. Cross, V. Bakken, C. Adamo,

J. Jaramillo, R. Gomperts, R. E. Stratmann, O. Yazyev, A. J. Austin, R. Cammi, C. Pomelli, J. W. Octherski, R. L. Martin, K. Morokuma, V. G. Zakrzewski, G. A. Voth, P. Salvador, J. J. Dannenberg, S. Dapprich, A. D. Daniels, O. Farkas, J. B. Foresman, J. V. Ortiz, J. Cioslowski and D. J. Fox, *Gaussian, Inc.*, Wallingford, CT, **2009**, p.

[178] a) D. R. Armstrong, A. R. Kennedy, R. E. Mulvey and S. D. Robertson, *Chem. Eur. J.* **2011**, *17*, 8820; b) P. G. Williard and Q.-Y. Liu, *J. Am. Chem. Soc.* **1993**, *115*, 3380.

[179] K. W. Henderson, A. R. Kennedy, R. E. Mulvey, C. T. O'Hara and R. B. Rowlings, *Chem. Commun.* **2001**, 1678.

[180] V. L. Blair, L. M. Carrella, W. Clegg, J. Klett, R. E. Mulvey, E. Rentschler and L. Russo, *Chem. Eur. J.* **2009**, *15*, 856.

[181] J. J. Morris, B. C. Noll, G. W. Honeyman, C. T. O'Hara, A. R. Kennedy, R. E. Mulvey and K. W. Henderson, *Chem. Eur. J.* **2007**, *13*, 4418.

[182] M. Schlosser, J. H. Choi and S. Takagishi, *Tetrahedron* **1990**, *46*, 5633.

[183] W. Clegg, S. H. Dale, E. Hevia, L. M. Hogg, G. W. Honeyman, R. E. Mulvey and C. T. O'Hara, *Angew. Chem. Int. Ed.* **2006**, *45*, 6548.

[184] a) D. R. Armstrong, W. Clegg, S. H. Dale, J. Garcia-Alvarez, R. W. Harrington, E. Hevia, G. W. Honeyman, A. R. Kennedy, R. E. Mulvey and C. T. O'Hara, *Chem. Commun.* **2008**, 187; b) D. R. Armstrong, C. Dougan, D. V. Graham, E. Hevia and A. R. Kennedy, *Organometallics* **2008**, *27*, 6063; c) G. C. Forbes, A. R. Kennedy, R. B. Rowlings, W. Clegg, S. T. Liddle and C. C. Wilson, *Chem. Commun.* **2000**, 1759.

[185] A. Krasovskiy and P. Knochel, *Angew. Chem. Int. Ed.* **2004**, *43*, 3333.

[186] a) L. Shi, Y. Chu, P. Knochel and H. Mayr, *Org. Lett.* **2012**, *14*, 2602; b) C.-Y. Liu, H. Ren and P. Knochel, *Org. Lett.* **2006**, *8*, 617.

[187] a) C. Dunst and P. Knochel, *J. Org. Chem.* **2011**, *76*, 6972; b) W. Lin, O. Baron and P. Knochel, *Org. Lett.* **2006**, *8*, 5673.

[188] W. L. F. Armarego and C. Chai, *Purification of Laboratory Chemicals*, Butterworth-Heinemann, Oxford, **2003**, p.

[189] B. E. Love and E. G. Jones, *J. Org. Chem.* **1999**, *64*, 3755.

[190] Y. Aso, H. Yamashita, T. Otsubo and F. Ogura, *J. Org. Chem.* **1989**, *54*, 5627.